QUANTUM GRAVITY PHENOMENOLOGY: FROM ATOMS TO THE COSMOS

MITJA FRIDMAN
Master of Science, University of Ljubljana, 2018

A thesis submitted
in partial fulfilment of
the requirements for the degree of

DOCTOR OF PHILOSOPHY

in

THEORETICAL AND COMPUTATIONAL SCIENCE

Department of Physics and Astronomy
University of Lethbridge
LETHBRIDGE, ALBERTA, CANADA

QUANTUM GRAVITY PHENOMENOLOGY: FROM ATOMS TO THE COSMOS

MITJA FRIDMAN

Date of Defence: May 24, 2023

Dr. Saurya Das Thesis Supervisor	Professor	Ph.D.
Dr. Mark Walton Thesis Examination Committee Member	Professor	Ph.D.
Dr. Pasquale Bosso Thesis Examination Committee Member	Adjunct Professor	Ph.D.
Dr. Ken J. E. Vos Internal External Examiner Department of Physics and Astronomy Faculty of Arts and Science	Associate Professor	Ph.D.
Dr. Douglas Singleton External Examiner California State University Fresno, California	Professor	Ph.D.
Dr. Locke Spencer Chair, Thesis Examination Committee	Associate Professor	Ph.D.

Dedication

I dedicate this work to my wonderful fiancée Nancy Graciela Barajas Jaimes.

Abstract

Quantum Theory and General Relativity are two of the most successful theories of Nature in their respective regimes. In situations where effects from both are non-negligible, the regime of Quantum Gravity emerges. Many theories, such as String Theory, Loop Quantum Gravity and Doubly Special Relativity, attempt to address the high-energy regime of Quantum Gravity. The structures of such theories suggest the existence of a minimum measurable length. This in turn modifies the Heisenberg Uncertainty Principle, to the so-called Generalized Uncertainty Principle (GUP). In this work, GUP is used to construct phenomenological models, which can be used to verify the existence of a minimum measurable length. Specifically, in Earth-based experiments, the magnetometer experiment and Bose-Einstein condensation are considered, and in cosmology, explanations of the baryon asymmetry in the Universe and the EDGES anomaly are provided. Furthermore, a novel conceptual approach to Quantum Gravity, namely the Quantum Equivalence Principle, is explored.

Acknowledgments

I have conducted my Ph.D. studies at the University of Lethbridge, which is located in the traditional Blackfoot Confederacy territory. The Blackfoot name of the University of Lethbridge is Iniskim, which means Sacred Buffalo Stone. I am grateful to have resided in this land, as well as to its Indigenous Peoples. I am also very fortunate to have made friends in their communities, and to have had the opportunity to talk to their Elders. They taught me about their culture and their ways of knowing, which sparked a deep appreciation of their history and land. This appreciation will forever remain a part of me.

It takes a significant amount of courage and sacrifice to start a new chapter of life far away from home. It was not easy, but I was very fortunate to have found an amazing community of people, which made me feel like at home and made me a better person, one way or another. I am thankful to every single one them, especially the following.

First, I would first like to thank my supervisor Dr. Saurya Das for his guidance and support throughout my Ph.D. program. He was delightful to work with, and his constructive feedback greatly shaped the way I think about and perform scientific research. Above all, he was kind and genuinely cared about my personal well-being. I truly feel grateful to have had the opportunity to meet him and to work with him.

I would like to thank my collaborators Dr. Gaetano Lambiase, Dr. Gil Porat, Dr. Antonio Stabile and Dr. Elias C. Vagenas for their useful discussions, comments and ideas, which helped in improving the works covered in this thesis.

I would like to thank my wonderful fiancée Nancy Graciela Barajas Jaimes, whom I met during my Ph.D. studies in Lethbridge, for all her support and invaluable help with creating several figures for Chapters 1 and 2. She has been a beacon of light in my darkest moments,

throughout the daunting process of obtaining a Ph.D. degree.

I would like to thank my parents Marija and Darko, my sister Andreja, and my niece and nephew, Danaja Tea and Anej Ian, for inspiring and encouraging me throughout my journey of learning physics.

Lastly, I would like to thank my four-legged, one-eyed companion Loki. A small dog, with a big personality. He travelled the world with me and is the only friend who has been by my side in my best and my worst times throughout my entire 11-year journey of learning physics. I hope he will continue bringing joy to my life for many more years.

Contents

List of Figures

List of Abbreviations

Chapter 1

Introduction

> "If you wish to make an apple pie from scratch, you must first invent the Universe."
>
> *Carl Sagan*

The workings of Nature have been studied and contemplated since ancient times by philosophers such as Democritus, Aristotle, Pythagoras, Archimedes and many others. Their descriptions and explanations of observed phenomena were based mostly on geometric principles. The modern picture of physics started forming after the discoveries of Copernicus, Galileo and Newton between the 15th and 17th centuries. More specifically, physics took a more modern form after the publication of *Philosophiae Naturalis Principia Mathematica* by Isaac Newton [1]. However, physics has developed significantly throughout the last hundred-fifty years, compared to the rest of its long history. Quantum Theory (QT) changed the classical concepts of position and velocity of a particle and the theory of General Relativity (GR) identified space-time as a dynamic variable, which changes in response to mass. These two theories are very successful in explaining and predicting observable phenomena to a high degree of precision at microscopic and macroscopic length scales, respectively [2, 3]. They are also considered to be fundamental theories of Nature, since their descriptions include the most basic known building blocks of the Universe and they both reduce to the well known standard Newtonian physics of everyday life in the classical and non-relativistic limits.

Physics at the small scale and non-relativistic speeds is described within the framework of Quantum Mechanics (QM) and is governed by the Schrödinger equation

$$i\hbar\frac{\partial\psi(\mathbf{x},t)}{\partial t}=\left(-\frac{\hbar^2}{2m}\nabla^2+V(\mathbf{x})\right)\psi(\mathbf{x},t)\ , \tag{1.1}$$

where $\hbar=h/2\pi$ is the reduced Planck constant (h is the Planck constant), m is the particle mass, $\psi(\mathbf{x},t)$ is the wave function describing the particle in consideration and $V(\mathbf{x})$ is the classical potential. It introduces the concept that one cannot measure the position and momentum of a particle simultaneously. This concept is described by the Heisenberg Uncertainty Principle

$$\Delta x\Delta p\geq\frac{\hbar}{2}\ , \tag{1.2}$$

where Δx is the uncertainty in position and Δp the uncertainty in momentum. The product of these two uncertainties has a constant lower bound. This means that the more one knows about the position of a particle, the less one knows about the momentum of that particle, and vice versa.

On the other hand, physics at the large scale and relativistic regimes is described within the framework of GR, and is governed by the Einstein equations

$$R_{\mu\nu}-\frac{1}{2}Rg_{\mu\nu}+\Lambda g_{\mu\nu}=\frac{8\pi G}{c^4}T_{\mu\nu}\ , \tag{1.3}$$

where $R_{\mu\nu}=\partial_\rho\Gamma^\rho_{\mu\nu}-\partial_\mu\Gamma^\rho_{\nu\rho}+\Gamma^\rho_{\rho\sigma}\Gamma^\sigma_{\mu\nu}-\Gamma^\rho_{\mu\sigma}\Gamma^\sigma_{\rho\nu}$ is the Ricci tensor,

$$\Gamma^\rho_{\mu\nu}=\frac{1}{2}g^{\rho\sigma}\left(\partial_\mu g_{\nu\sigma}+\partial_\nu g_{\mu\sigma}-\partial_\sigma g_{\mu\nu}\right) \tag{1.4}$$

are the Christoffel symbols, $R=g^{\mu\nu}R_{\mu\nu}=R^\mu_\mu$ is the Ricci scalar, $g_{\mu\nu}$ is the space-time metric, Λ is the cosmological constant, G is the universal gravitational constant, c is the speed of light and $T_{\mu\nu}$ is the energy momentum tensor. In the above, the Einstein summation

rule is used

$$\sum_{\mu=0}^{3} a_\mu b^\mu \equiv a_\mu b^\mu \,, \tag{1.5}$$

for any two same indices in the above configuration. This rule is used for all relativistic considerations in this work. The Greek indices denote space-time components, which can take values $\mu,\nu = 0,1,2,3$, with 0 representing the time component and $1,2,3$ the spatial components, denoted with Latin indices i, j, when considered separately. The Einstein equations, presented in Eq. (1.3) describe dynamics of a space-time $(\mathcal{M}, g_{\mu\nu})$, defined on a manifold $\mathcal{M}$, as a response to the energy content $T_{\mu\nu}$ within that space-time.

QM has also been modified to include special-relativistic effects on a flat Minkowski space-time, neglecting gravitational interactions. The resulting theory is called relativistic Quantum Field Theory (QFT), which successfully quantizes three out of four fundamental forces of Nature, namely the Electromagnetic, Weak nuclear and Strong nuclear forces. In the formulation of relativistic QFTs, the spin of the considered particle becomes relevant. It is relevant to the extent that the equations of motion for particles with different spin will take different forms. The Klein-Gordon equation describes relativistic spin-0 particles (bosons), and can be generalized in an arbitrary curved space-time, described by a metric $g_{\mu\nu}$ as [4]

$$\left(g^{\mu\nu} \nabla_\mu \nabla_\nu + \frac{m^2 c^2}{\hbar^2} \right) \Phi(\mathbf{x},t) = 0 \,, \tag{1.6}$$

where ∇_μ is the covariant derivative, related to $g_{\mu\nu}$, and $\Phi(\mathbf{x},t)$ is the Klein-Gordon field. The Dirac equation describes relativistic spin-$1/2$ particles (fermions), and can also be generalized in an arbitrary curved space-time, described by a metric $g_{\mu\nu}$ as [5]

$$\left(i\hbar \underline{\gamma}^\mu D_\mu - mc \right) \Psi(\mathbf{x},t) = 0 \,, \tag{1.7}$$

where $\underline{\gamma}^\mu$ are the space-time dependent Dirac gamma matrices, $D_\mu = \partial_\mu + \Gamma_\mu$, in which Γ_μ

is the spinor affine connection (see Section 5.1 for details on $\underline{\gamma}^{\mu}$ and Γ_{μ}), and $\Psi(\mathbf{x},t)$ is the Dirac spinor field. Note that Eqs. (1.6) and (1.7) include gravity in a classical sense, as a background geometry, and do not imply a quantization of the force of gravity. Therefore, gravity is the remaining fundamental force, which still lacks a quantum description, and a consistent theory which bridges the two regimes is still up for debate [6].

Despite their success, QT and GR are incomplete theories. They both display inconsistencies at small distance and time scales (Planck length $\ell_P = \sqrt{\hbar G/c^3} = 1.62 \times 10^{-35}\,\mathrm{m}$ and Planck time $t_P = \sqrt{\hbar G/c^5} = 5.39 \times 10^{-44}\,\mathrm{s}$, respectively), i.e., very high energies (around the Planck energy $E_P = \sqrt{\hbar c^5/G} = 1.22 \times 10^{28}\,\mathrm{eV}$), where contributions from each regime are expected. At those scales QT becomes inconsistent, because it does not explain effects of high energy particles on space-time, which become prominent, while GR displays singularities when studying black holes and the origin of the Universe [7]. In this context, space-time is expected to no longer be a passive background, but an active and interacting physical object.

The predictions of QT work remarkably well within the range of current highest experimentally achievable energies in particle colliders, which reach $E_{exp} \lesssim 10^{13}\,\mathrm{eV}$ in the specific case of the Large Hadron Collider (LHC). However, around E_p gravitational effects can no longer be neglected. Since such high energies are experimentally not achievable now or in the near future, such effects cannot be directly observed [7]. Such high energy scenarios may also take place near black holes, cosmological singularities, and perhaps at large distances as well, where dark components and/or modifications of GR are invoked to explain Dark Matter effects and the accelerated phase of the present Universe. It is expected that the inconsistencies at small scales (high energies) can be resolved within the framework of Quantum Gravity (QG), which must incorporate the principles of QT and GR, and must provide a description of the microstructure of space-time at the Planck scale. However, there is no simple way of combining the two theories to describe phenomena in high energy scenarios, where effects of both domains are applicable simultaneously. It can be seen

that Eqs. (1.1) and (1.3) are not compatible, since only Eq. (1.3) is relativistic. Although QM can be generalized to a relativistic QFT, as discussed above, the two are still incompatible, since Eqs. (1.1), (1.6) and (1.7) use a probabilistic approach to describe particles using wavefunctions or fields, while Eq. (1.3) treats particles in a completely deterministic way. QT and GR have some concepts in common, such as the notion of space-time, but they consider them in a different way. In QT the space-time metric is considered to be a passive static background, while the space-time metric in GR is a dynamic variable.

The above reasons prevent a straightforward unification of the two theories, although both have relativistic descriptions [7]. It is expected that space-time should not have a classical geometry such as in GR, but that it should be quantized. Candidate theories of QG aim to accomplish this. Among the existing candidate theories of QG, String Theory and Loop Quantum Gravity are the two of the best studied. However, there has not been a single experiment or observation which support or refute any theory of QG, due to the currently unattainable immensity of the Planck energy scale. Therefore, it is important to look for indirect signatures of these theories in accessible, low energy laboratory-based experiments [7, 8].

1.1 Quantum Gravity Theories and Approaches

In the well established QFTs which describe the fundamental forces of Nature, except gravity, one is often lead to infinite scattering amplitudes, which can be mitigated by using standard renormalization procedures. The same process of quantization and renormalization can be attempted with gravity, but one quickly realizes that the infinities do not disappear due to the dimensionful coupling constant G. One way out could be a higher-derivative theory of gravity where renormalization works to obtain finite results, but gives rise to other issues, such as non-physical ghost fields [9]. Therefore, a novel theory of QG is required. There are several candidate theories of QG, which could explain phenomena at or near the Planck scale. They attempt to reconcile the probabilistic nature of QT with

the geometrical interpretation of GR. As QT and GR both reduce to Newtonian physics in the classical and non-relativistic limits, also a theory of QG must reduce to QT and GR in their respective regimes. As is the case in other areas of physics, a successful theory should explain previously unexplained observable phenomena and predict new effects. In the following, several candidate theories of QG and approaches to QG are briefly summarized, namely String Theory, Loop Quantum Gravity and Doubly Special Relativity.

1.1.1 String Theory

One of the best studied candidate theories of QG is String Theory (ST) [10, 11, 12, 13]. In ST, one hopes to resolve the problem of classical singularities and removing quantum infinities, by describing fundamental building blocks of matter as tiny strings. It was initially developed to describe the strong nuclear force, but a more consistent Yang-Mills theory was adapted for that interaction instead. ST was revived when attempts were made to unify gravity with the other fundamental forces of Nature. Several, apparently different STs were proposed in the mid 1980's, during the so-called *first superstring revolution* [13]:

- Type I: formulated in 10 dimensions, and contains unoriented open and closed strings.
- Type IIA: formulated in 10 dimensions, contains oriented closed strings and is a non-chiral theory.
- Type IIB: similar to type IIA, with the difference that it is a chiral theory.
- $SO(32)$ heterotic: left moving excitations propagate in 26 dimensions, while right moving excitations propagate in 10 dimensions. Contains closed strings and implements the gauge group $SO(32)$.
- $E_8 \times E_8$ heterotic: similar to $SO(32)$ heterotic, with the difference that it implements the gauge group $E_8 \times E_8$.

It was later discovered, that they are all equivalent and are different limits of one underlying theory, known as M-Theory [6, 13]. At low energies it can describe gauge interactions,

using stringy Feynman diagrams, and gravity, where it predicts a massless spin-2 particle (graviton), whose dynamics effectively describe GR at large distances. ST uses Supersymmetry [14] and compactified extra dimensions [10, 11, 12, 13] in its formulation. The required extra dimensions, which are suggested to be of the size of ℓ_P, lead to QG effects. Therefore, since the stringy behaviour is supposed to manifest at energies of the order of E_P [15], ST cannot predict directly measurable effects at relatively low energies, currently achievable in accelerators, which is also the case with many other candidate theories of QG. The theory is also formulated on a fixed, as opposed to a dynamical curved space-time background, and therefore cannot address all aspects of QG.

Strings

In standard QFT, world lines are graphical representations, used to describe a path of a point particle in space-time. The main idea of ST is to replace point-like particles which have no size, with string-like objects which have a non-zero length, as the fundamental building blocks of matter in the Universe. This effectively replaces a one-dimensional world line of a particle with a two-dimensional world sheet of a string in a space-time diagram (see Fig. 1.1). A world line of a point particle is described by a single parameter, while for a world sheet, a second parameter needs to be introduced to describe the path of a string in space-time (see Eq. (1.9)). The size of a string is assumed to be no smaller than the Planck length ℓ_P, but can be larger. Therefore, it is considered as a free parameter of the theory.

To transition from classical to quantum mechanics, one needs to introduce Planck's constant $\hbar$, and to transition from classical to relativistic mechanics, one needs to introduce the speed of light c. Similarly, one needs to introduce a fundamental constant α', called string tension, when a transition to ST is made. This approach has several advantages. For example, when regular 4-point Feynman diagrams are considered (see figure 1.2 **a)**), infinities appear in such calculations, which arise from interactions taking place in infinitely

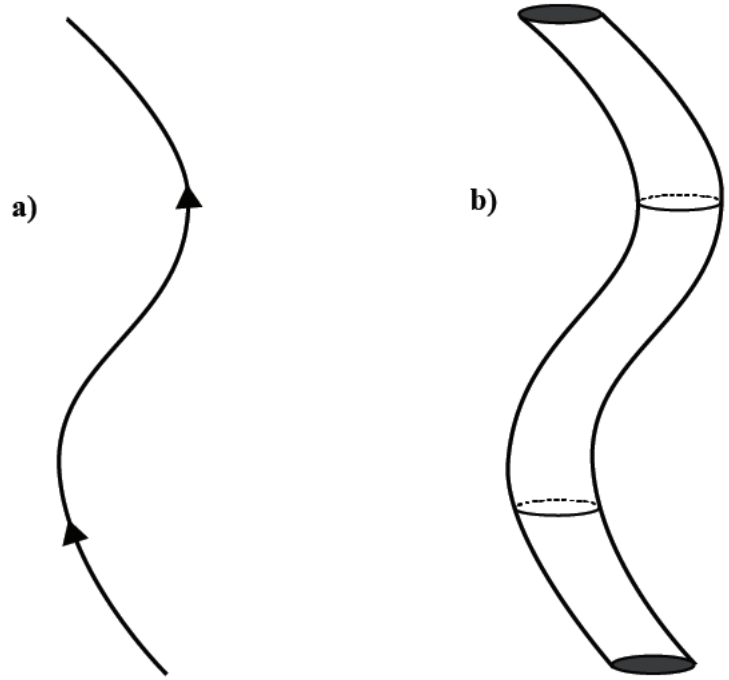

Figure 1.1: Replacing a world line **a)** with a world sheet **b)**. Adapted from Ref. [6]. Credit of Nancy Barajas.

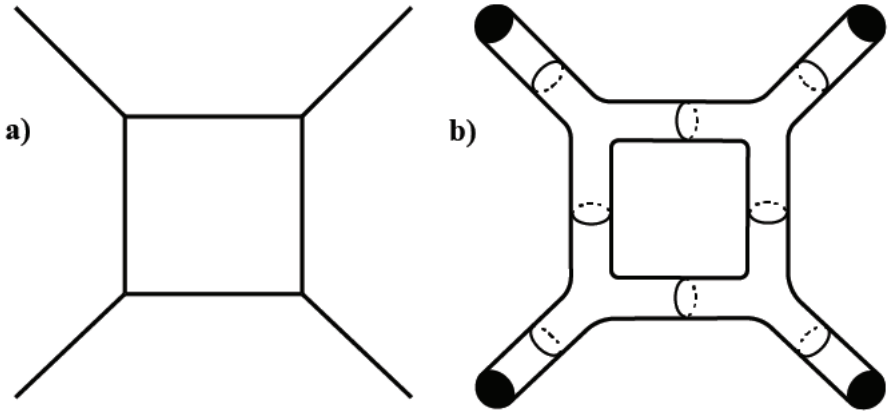

Figure 1.2: Replacing a regular 4-point Feynman diagram **a)** with a stringy Feynman diagram **b)**. Adapted from Ref. [6]. Credit of Nancy Barajas.

small volumes, and have to be mitigated by renormalization. However, when ST is applied to such processes (see figure 1.2 **b)**), the singular vertex interaction points are no longer present and the infinities do not appear. Therefore, renormalization is not required.

The following review of ST is based on Ref. [12]. The action for a relativistic point particle in curved space-time, parameterized with proper time τ can be written as

$$S_{pp} = \frac{1}{2}\int \mathrm{d}\tau \left(\eta^{-1} g_{\mu\nu}(X) \frac{\mathrm{d}X^{\mu}}{\mathrm{d}\tau} \frac{\mathrm{d}X^{\nu}}{\mathrm{d}\tau} - \eta\, m^2 \right) , \tag{1.8}$$

where η is the world line tetrad and X^{μ} the space-time coordinate. As mentioned earlier, to consider an action for a string, a second parameter must be introduced. This new parameter, labeled as σ, is called proper position. The set of parameters for a string can then be written as $\sigma^a = (\sigma, \tau)$ and the position in space-time as $X^{\mu}(\sigma^a)$. This formulation is used to describe the dynamics of a string. The action for the string is called the Polyakov action and reads as

$$S = \frac{1}{4\pi\alpha'}\int \mathrm{d}\sigma\, \mathrm{d}\tau\, h^{1/2} h^{ab} \eta_{\mu\nu} \frac{\mathrm{d}X^{\mu}}{\mathrm{d}\sigma^a} \frac{\mathrm{d}X^{\nu}}{\mathrm{d}\sigma^b} , \tag{1.9}$$

where h^{ab} is the Euclidian world sheet metric with signature $(+,+)$, $h = \det(h^{ab})$ and $\eta_{\mu\nu}$ is the Minkowski metric, describing flat space-time. Note that the entire expression is divided by the string tension α'. One can see that Eq. (1.8) has an explicit term for mass, which is a free parameter of the theory, while Eq. (1.9) does not. In ST, particle masses depend on α' and are not free parameters themselves. The masses of particles in ST read as

$$m^2 = \frac{1}{\alpha'}\left(N + \frac{2-D}{24} \right) , \tag{1.10}$$

where N is the level of excitation of the string and D the space-time dimensionality. For an arbitrary classical space-time metric $g_{\mu\nu}$, the action (1.9) can be rewritten as

$$S = \frac{1}{4\pi\alpha'}\int \mathrm{d}\sigma\, \mathrm{d}\tau\, h^{1/2} h^{ab} g_{\mu\nu}(X) \frac{\mathrm{d}X^{\mu}}{\mathrm{d}\sigma^a} \frac{\mathrm{d}X^{\nu}}{\mathrm{d}\sigma^b} . \tag{1.11}$$

It turns out that Eq. (1.11) is all one needs to compute stringy Feynman diagrams. Quantizing a string, described by the above action, gives rise to interesting new results. One of the most important results, which appears in such considerations is the emergence of a quantized gravity.

To demonstrate how gravity emerges from ST, one introduces a slowly evolving scalar dilaton field Φ_D, coupled to the Ricci curvature scalar R in the action from Eq. (1.11) as

$$S = \frac{1}{4\pi\alpha'} \int \mathrm{d}\sigma\, \mathrm{d}\tau\, h^{1/2} \left(h^{ab}\, g_{\mu\nu}(X)\, \frac{\mathrm{d}X^\mu}{\mathrm{d}\sigma^a}\, \frac{\mathrm{d}X^\nu}{\mathrm{d}\sigma^b} + \alpha' R\, \Phi_D(X) \right) . \tag{1.12}$$

From the above, one can compute the renormalization group $\beta-$functions, which appear as

$$\beta^g_{\mu\nu} + 8\pi^2 g_{\mu\nu}\, \frac{\beta^{\Phi_D}}{\alpha'} = \alpha' \left(R_{\mu\nu} - \frac{1}{2}\, g_{\mu\nu} R \right) + \alpha'\, f_{\mu\nu}(\nabla^2 \Phi_D) + O(\alpha'^2) , \tag{1.13}$$

where $f_{\mu\nu}(\nabla^2\Phi_D)$ is a tensor function of second derivatives of Φ_D and represents the source terms. The requirement of ST to be Weyl invariant ensures that $\beta^g_{\mu\nu} = \beta^{\Phi_D} = 0$. From Eq. (1.13) one can see that the Einstein equations, coupled to the dilaton field Φ_D are obtained.

When ST, formulated on a fixed flat or curved space-time is quantized, one obtains excitations of various masses and spins, which includes, interestingly, a massless spin-2 particle, which can be identified with the perturbative graviton, which is the force carrier in a quantized theory of gravity. To quantize ST, one can use the standard quantization methods, such as Feynman path integrals or canonical quantization [10, 11, 12, 13]. The canonical quantization is briefly summarized below, following Ref. [10].

For a specific class of a world sheet parameterization, the equations of motion for both open and closed strings turn out to be wave equations $\ddot{X}^\mu - X^{\mu\prime\prime} = 0$, where $\dot{}$ denotes the derivative over τ and $'$ the derivative over σ. The canonically conjugate momentum densities in this case turn out as

$$P^{\tau\mu} = \frac{1}{2\pi\alpha'} \dot{X}^\mu \quad \text{and} \quad P^{\sigma\mu} = -\frac{1}{2\pi\alpha'} X^{\mu\prime} . \tag{1.14}$$

The above conjugate momentum densities hold for any gauge of the considered class. The canonical quantization turns out to be identical for open and closed strings, and is expressed by the equal-time canonical commutation relations

$$\begin{aligned} \left[X^{\mu}(\tau,\sigma), P^{\tau\nu}(\tau,\sigma')\right] &= i\hbar\eta^{\mu\nu}\,\delta(\sigma-\sigma')\ , \\ \left[X^{\mu}(\tau,\sigma), X^{\nu}(\tau,\sigma')\right] = \left[P^{\tau\mu}(\tau,\sigma), P^{\tau\nu}(\tau,\sigma')\right] &= 0, \\ \left[x^{-}(\tau), p^{+}(\tau)\right] &= -i\hbar\ , \end{aligned} \tag{1.15}$$

where $\delta(\sigma-\sigma')$ is the Dirac delta function, and x^- and p^+ are the $0-$th components of position and momentum vectors in the light-cone coordinate system. The solutions of $X^{\mu}(\tau,\sigma)$ for open and closed strings turn out to be different. On one hand, the solution for an open string is expressed in terms of open string oscillation modes $\alpha_n^{o\mu}$, where $n \in \mathbb{N}\cup\{0\}$. Given the commutation relations in Eq. (1.15), the open string oscillation modes, which are now quantum operators, obey

$$[\alpha_m^{o\mu}, \alpha_n^{o\nu}] = -n\,\eta^{\mu\nu}\,\delta_{m+n,0}\ . \tag{1.16}$$

On the other hand, the solution for a closed string is expressed in terms of closed string oscillation modes $\alpha_n^{c\mu}$ and $\overline{\alpha}_n^{c\mu}$. Given the commutation relations in Eq. (1.15), the closed string oscillation modes, which are now quantum operators obey

$$[\alpha_m^{c\mu}, \alpha_n^{c\nu}] = -n\,\eta^{\mu\nu}\,\delta_{m+n,0}\ ,\quad [\overline{\alpha}_m^{c\mu}, \overline{\alpha}_n^{c\nu}] = -n\,\eta^{\mu\nu}\,\delta_{m+n,0}\ \text{ and }\ [\alpha_m^{c\mu}, \overline{\alpha}_n^{c\nu}] = 0\ . \tag{1.17}$$

The commutation relations in Eqs. (1.16) and (1.17) govern the quantum behaviour of strings and are a fundamental feature in ST. They are used as ladder operators to construct quantum states, and quantum operators for physical observables, such as number operators, momentum operators, Hamiltonians and others.

Summary

As promising as ST appears, it still has several issues which need to be addressed to be considered as a consistent theory of QG. One such issue is the requirement for Supersymmetry [14]. Supersymmetry states that all bosons and fermions from the Standard Model of particle interactions have supersymmetric counterparts with opposite particle statistics and equal masses, if the symmetry is to be preserved. Supersymmetric particles have not been detected so far, which suggests that such particles do not exist, or that Supersymmetry is broken and the supersymmetric particles are much heavier. Also, ST assumes the existence of compact dimensions, which lack experimental confirmation. The compact dimensions can form different topologies, depending on the number of compact dimensions, and are described by Calabi-Yau manifolds [13]. For two compact dimensions there are only two cases, $\mathbb{C}$ and a two-torus T^2. For four compact dimensions there are two cases, $K3$ and a four-torus T^4 (there are also two non-compact cases, $\mathbb{C}^2$ and $\mathbb{C} \times T^2$ in four dimensions). For six compact dimensions, which is the most interesting case, found in superstring models, there is a large number $\sim 10^{100}$ of possible Calabi-Yau three-folds. This introduces an ambiguity, called the vacuum selection problem.

1.1.2 Loop Quantum Gravity

The next candidate theory of QG is Loop Quantum Gravity (LQG) [16, 17, 18, 19, 20, 21, 22], which provides a novel theoretical framework for a quantum description of space-time and attempts to quantize GR in a non-perturbative way. It considers GR in four space-time dimensions as the starting point for its formulation, as opposed to ST, which considers GR to be a low energy approximation of a more fundamental theory in higher dimensions. LQG uses a background independent Hamiltonian approach. In other words, no background is assumed. It introduces several new techniques and concepts, of which the Ashtekar variables and the formulation of space-time in terms of finite loops incorporated into a network, are the most important. Networks of such loops are called spin networks or

spin foam, and require the introduction of non-separable Hilbert spaces and representations of operators, compatible with such Hilbert spaces [22]. Time evolution in LQG systems takes place in increments of the size of ℓ_P, which indicates quantization of space-time. This can provide a viable explanation of the Planck scale departures from Lorentz symmetry and make predictions in early Universe cosmology [7].

Canonical General Relativity

The formalism of LQG is that of canonical GR. To transition to a canonical description, one needs to rely on the use of vierbeins (tetrads), labeled by e^a_μ and defined through $g_{\mu\nu} = e^a_\mu e^b_\nu \eta_{ab}$. Here, η_{ab} is the Minkowski space-time metric of the tangent space and a, b are the tangent space indices. The vierbeins are covariantly conserved, which means

$$D_\mu e^a_\nu \equiv \nabla_\mu e^a_\nu - \omega^{ab}_\mu e_{\nu b} = 0 \,, \tag{1.18}$$

where ω^{ab}_μ is the spin connection. According to the standard ADM prescription (named after R. Arnowitt, S. Deser and W. Misner), one takes a globally hyperbolic manifold $\mathcal{M}$, which can be foliated as $\mathcal{M} = \Sigma \times \mathbb{R}$, where Σ is a spatial manifold and $\mathbb{R}$ the temporal manifold. Usually, a triangular gauge is chosen for the vierbeins

$$e^a_\mu = \begin{bmatrix} N & N^A \\ 0 & e^A_m \end{bmatrix} \,, \tag{1.19}$$

where e^A_m is a spatial dreibein, m and A represent curved and flat indices, respectively, while N and N^A are the Lagrange multipliers, called *lapse* and *shift*, respectively. The space-time metric $g_{\mu\nu}$ then takes the form

$$g_{\mu\nu} = \begin{bmatrix} -N^2 + N_A N_A & N_n \\ N_m & g_{mn} \end{bmatrix} \,, \tag{1.20}$$

where $g_{mn} = e^A_m e_{nA}$ refers to the spatial part of the metric. Using the standard procedure, one can obtain the canonically conjugate momenta from the Einstein-Hilbert Lagrangian $\mathcal{L}_{EH}$ as

$$\Pi^m_A = \frac{\delta \mathcal{L}_{EH}}{\delta \partial_t e^A_m} = \frac{1}{2} e e^m_B (K_{AB} - \delta_{AB} K) \ , \tag{1.21}$$

where $K_{AB} = e^\mu_A e^\nu_B \nabla_\mu e_{\nu 0} = \omega_{AB0}$ and $K = K_{AA}$ are the extrinsic curvature tensor and scalar of Σ, respectively, $e = \det\left(e^A_m\right)$ and δ_{AB} the Kronecker delta. The conjugate momenta from Eq. (1.21) are used to construct the Hamiltonian density through a Legendre transformation

$$\mathcal{H} = \partial_t e^m_A \Pi^A_m - \mathcal{L}_{EH} = N H_0 + N_A H_A \ , \tag{1.22}$$

where $H_A = D_m \Pi^m_A$,

$$H_0 = e^{-1} \left(\Pi_{AB} \Pi_{AB} - \frac{1}{2} \Pi^2 \right) - e R^{(3)} \ , \tag{1.23}$$

$\Pi_{AB} = \Pi^m_A e^B_m$, $\Pi = \Pi_{AA}$ and $R^{(3)}$ the spatial Ricci scalar. Setting $H_0 \approx 0$ represents the classical Hamiltonian constraint. A standard canonical quantization of the above can be performed by promoting the dreibein e^A_m to a multiplication operator and writing the canonically conjugate momenta as a functional differential operator as

$$\Pi^m_A(x) = -i\hbar \frac{\delta}{\delta e^A_m(x)} \ . \tag{1.24}$$

By this substitution, the previously mentioned Hamiltonian constraint becomes a quantum equation, called the *Wheeler-DeWitt* equation, which generates dynamics in LQG and is given by

$$H_0(x) \Psi[e] = 0 \ , \tag{1.25}$$

where $\Psi[e]$ is a wave functional, which can in general depend on more variables. It is also known as the *wave function of the Universe*, since it is expected to contain all information about the Universe from its beginning to its end. However, by using the conjugate momentum operator from Eq. (1.24) to solve Eq. (1.25), one obtains a highly singular and ill-defined form of a functional differential equation. This creates a significant obstacle in constructing appropriate Hilbert spaces with befitting scalar products for wave functionals. Therefore, LQG approaches quantization of gravity by virtue of the Ashtekar variables, which complement the above canonical formalism of GR.

Loops

A new set of canonical variables was introduced by Abhay Ashtekar in 1986, which provide a connection representation in canonical GR. They present a novel way to write the metric canonical variables within slices Σ_t, using a $SU(2)$ gauge field. As shown in the following, LQG uses the Ashtekar variables to introduce loops, which comprise the spin network description of space-time. They are derived in detail in Refs. [23, 24] (see also Ref. [25]) where the first variable is the $SU(2)$ gauge field connection, which reads as

$$\mathcal{A}_{mA} = -\frac{1}{2}\,\varepsilon_{ABC}\,\omega_{mBC} + \gamma\,K_{mA}\ , \tag{1.26}$$

where ε_{ABC} is the Levi-Civita anti-symmetric tensor, γ is the Barbero-Immirzi parameter[1] and $K_{mA} = K_{BA}\,e^B_m$. In classical considerations γ has no physical interpretation. However, when the theory is quantized, γ sets the scale for fundamental areas and volumes. The second variable is the so-called *inverse densitized spatial dreibein* and is defined as $E^m_A =$

[1]The Barbero-Immirzi parameter γ was initially taken to be complex. More specifically, for $\gamma = \pm i$ the Hamiltonian constraint is expressed in terms of the new variables polynomially and simplifies the calculations significantly. However, this choice implies that the phase space of GR is complex, and turns out to be an issue when quantizing gravity. It poses a problem in defining suitable hermiticity conditions of states and operators, which has not been resolved so far. Therefore, to obtain the real phase space of GR and avoid quantization issues, the Barbero-Immirzi parameter is currently taken to be real, $\gamma \in \mathbb{R}$.

$e\,e_A^m$. It can be straightforwardly verified that the Ashtekar variables ($\mathcal{A}_{mA}$ from Eq. (1.26) and E_A^m) obey the Poisson algebra

$$\begin{aligned}
\{\mathcal{A}_{mA}(\mathbf{x}),\, \mathcal{A}_{nB}(\mathbf{y})\} &= 0\ , \\
\{E_A^m(\mathbf{x}),\, E_B^n(\mathbf{y})\} &= 0\ , \\
\left\{\mathcal{A}_m^A(\mathbf{x}),\, E_B^n(\mathbf{y})\right\} &= 8\,\pi\, G\,\gamma\,\delta_m^n\,\delta_B^A\,\delta^{(3)}(\mathbf{x}-\mathbf{y})\ ,
\end{aligned} \tag{1.27}$$

where $\delta^{(3)}(\mathbf{x}-\mathbf{y})$ is the spatial Dirac delta function. From the above one can see that γ renormalizes the universal gravitational constant G.

LQG is formulated using spin networks and spin foams, represented by loops. Description of such loops is based on *holonomies*. The loop representation is related to the connection from Eq. (1.26) by the loop transform, which is a functional analog to a Fourier transform. In contrast to using functionals, such as $\Psi[\mathcal{A}]$, which are defined on the entirety of Σ, it is more convenient to use holonomies, which are gauge covariant functionals, defined on one-dimensional curves within Σ and designated by e. A holonomy for a given curve inside Σ is a matrix valued functional, defined as

$$h_e[\mathcal{A}] = \mathcal{P}\exp\left(\int_e \mathcal{A}_m\,\mathrm{d}x^m\right)\ , \tag{1.28}$$

where $\mathcal{A}_m = \mathcal{A}_{mA}\,\tau^A$ with τ^A being the generators of $SU(2)$, i.e., the Pauli matrices, $\mathcal{A} = \mathcal{A}_m\,e_A^m\,\tau^A$ and $\mathcal{P}$ denotes path ordering from shortest paths on the left, to longest paths on the right. It turns out that the trace of a holonomy in Eq. (1.28) for a closed loop is gauge invariant and is called a *Wilson loop*, which reads as

$$W_e[\mathcal{A}] = \mathrm{Tr}\left[h_e[\mathcal{A}]\right]\ . \tag{1.29}$$

The Wilson loops can be used to quantize gravity non-perturbatively, since they form a basis for expansion of any gauge invariant functional $\Psi[\mathcal{A}] = \sum_e \Psi[e]\,W_e[\mathcal{A}]$. Since the size of the

curves, described by their individual e, can be arbitrarily small in Σ, the basis comprised of Wilson loops forms a so-called spin network space. However, such a space does not address all constraints of the theory. Therefore, a larger space is required. To obtain this larger space, LQG assumes quantization of the holonomy $h_e[\mathcal{A}]$ and its conjugate variable, the flux vector $F_S^A[E]$ through any surface S embedded in Σ, where $E = \det\left(E_A^m\right)$ (see Refs. [16, 17, 18, 19, 20, 21, 22] for details on $F_S^A[E]$ and the commutation relations between the quantized variables). The non-separable Hilbert space of LQG, denoted by $\mathcal{S}$, is then constructed by linear combinations of functionals $\Psi_{\Gamma,\psi}[\mathcal{A}] = \psi\left(h_{e_1}[\mathcal{A}], h_{e_2}[\mathcal{A}], \dots\right) \equiv |\Psi_\Gamma\rangle$ over all possible graphs $\Gamma \subset \Sigma$, containing edges $e_i \in \Gamma$ and vertices $v \in \Gamma$. Here, ψ is some function of holonomies.

Using $F_S^A[E]$, one can construct surface and volume operators, which have discrete spectra proportional to $\ell_P^2\gamma$ and $\ell_P^3\gamma^{3/2}$, respectively [26] (see Section 2.1.3 for an example). This implies that LQG predicts the existence of a minimal area and volume, parameterized by γ. In this context, the spin network quantizes space-time. Note that the spin network is embedded within a continuous manifold Σ and is considered to be a fundamental physical object of space-time.

Summary

LQG manifests a number of important features a theory of QG must have, such as background independence and quantization of space-time. However, it still has its shortcomings and open problems, which need to be addressed for it to be considered a consistent theory of QG. For example, it is unclear how to obtain the classical limit of LQG, where standard GR with a smooth space-time emerges. The reason for this is that the quantum states in LQG are significantly different than quantum states in the standard Fock space quantization. In addition, LQG cannot address the two-loop divergence, which is expected to appear when expanding the non-perturbative quantized gravity in Newton's constant. Such an expansion has not been performed, since the semi-classical state, which should manifest

this divergence, has not been found. There is also little justification for the Hamiltonian constraint operator, which is central in LQG, and it is not clear if the space-time covariance can be recovered. Including matter in LQG also raises some issues. It appears that LQG imposes no restrictions for types of matter and their interactions with themselves as well as with gravity. Therefore, it is not clear if the consistency requirements from perturbative relativistic QFTs on matter can be recovered.

1.1.3 Doubly Special Relativity

Doubly Special Relativity (DSR) [27, 28, 29, 30] is a theoretical framework, which aims to explore what happens to the Lorentz symmetry at or near the Planck scale ℓ_P. It is not considered as a candidate theory of QG, such as ST and LQG, but it is believed to emerge as a certain limit of QG. Despite the expected departures from Special Relativity (SR) at the Planck scale, the principle of relativity (equivalence of inertial frames) remains unmodified in the context of DSR. The *doubly* in DSR comes from the main assumption of the theory, which states that there are two observer-independent scales, in contrast to SR, which contains only one, the speed of light c. This gives rise to a modified set of postulates:

- Principle of relativity: all inertial frames are equivalent, which means that all laws of physics take the same form in all inertial frames.
- There exist two observer-independent scales: the speed of light c and the Planck length ℓ_P, parameterized by $\kappa \propto 1/\ell_P$, i.e., $\kappa \propto M_P$ and has units of mass, where $M_P = \sqrt{\hbar c/G}$.

Note that the standard SR is obtained by $\kappa \longrightarrow \infty$. The problem to incorporate both observer-independent scales in a theory is non-trivial, since from SR one expects to measure different lengths from different inertial frames. However, it is possible to incorporate both scales by introducing concepts, such as space-time non-commutativity and description of space-time symmetries using quantum groups [27, 28, 29, 30]. This results in a non-

classical description of space-time with properties somewhat similar to those of a phase space in standard QM.

Analogously as in SR, the postulates in DSR suggest that the symmetry group should be ten dimensional. However, because of the inclusion of a second observer-independent scale, the symmetry group cannot be the standard Poincaré group. This suggests a modification to the standard energy-momentum dispersion relation $E^2 = p^2c^2 + m^2c^4$ from SR. By considering the framework of SR, it does not permit an introduction of another observer-independent scale. However, a complete theory of QG must include further observer-independent constants $\hbar$, G and Λ. Therefore, one can argue that in limits of QG, where gravitational interactions and quantum effects are negligible, space-time becomes locally flat, and traces of QG persist in terms of the previously introduced scale κ.

The new scale κ then modifies the Poincaré algebra to the quantum κ-Poincaré algebra. Specifically, $SO(3,1) \longrightarrow SO_q(3,1)$ for three dimensions and $SO(3,2) \longrightarrow SO_q(3,2)$ for four dimensions, where $q = \exp\left(\Lambda\hbar^2/\kappa^2c^2\right)$ [30]. For $\kappa \longrightarrow \infty$, $q = 1$ and one obtains the standard Poincaré algebra. In DSR, a specific basis for the κ-Poincaré algebra is chosen, where only the translational sector is modified and the Lorentz sector remains unmodified [31]. However, in the four dimensional case, the generators of physical quantities need to be renormalized[2] to obtain finite results [32, 33]. Such renormalization introduces a family of contractions, parameterized by $r \in \mathbb{R}$. It turns out that only $r = 1$ returns the required four dimensional κ-Poincaré algebra, which reads as [30]

$$
\begin{aligned}
[J_i, J_j] &= i\varepsilon_{ijk}J_k \ , \\
[J_i, K_j] &= i\varepsilon_{ijk}K_k \ , \\
[K_i, K_j] &= -i\varepsilon_{ijk}J_k \ , \\
[J_i, p_j] &= i\varepsilon_{ijk}J_k \ ,
\end{aligned}
$$

[2]Note that renormalization in this context does not refer to the renormalization of the gravitational field, but ensuring that energy and momentum variables remain finite in the representation of $SO_q(3,2)$.

$$
\begin{aligned}
&[J_i, p_0] = 0 \,, \\
&[K_i, p_j] = i\delta_{ij}\left(\frac{\kappa c}{2}\left(1 - e^{-2p_0/\kappa c}\right) + \frac{\mathbf{p}^2}{2\kappa c}\right) - i\frac{p_i p_j}{\kappa c} \,, \\
&[K_i, p_0] = i\, p_i \,,
\end{aligned} \tag{1.30}
$$

where J_i are the rotation generators, K_i the boost generators and p_μ the translation operators, i.e., the four-momentum. The feature that the Lorentz sector remains unmodified shows that Lorentz symmetry is not broken. However, its action on momenta is non-linear. By computing the Casimir invariant, one arrives at the modified energy-momentum dispersion relation

$$
\kappa^2 c^4 \cosh\left(\frac{E}{\kappa c^2}\right) = \frac{1}{2}\,\mathbf{p}^2 c^2\, e^{E/\kappa c^2} + \kappa^2 c^4 \cosh\left(\frac{m}{\kappa}\right) \,, \tag{1.31}
$$

where $p_0 = E/c$ was used. From the above, one can see that by increasing the momentum to $p = |\mathbf{p}| \longrightarrow \kappa c$, the energy approaches infinity $p_0 \longrightarrow \infty$ for any observer. This confirms that κ is observer-independent and sets an upper bound to the possible physical momenta of particles in DSR. One can verify that Eq. (1.31) also implies a momentum-dependent speed of light for massless particles

$$
v = \frac{\partial E}{\partial p} = \frac{c}{1 - \frac{p}{\kappa c}} \,, \tag{1.32}
$$

where one can see that it diverges for $p \longrightarrow \kappa c$. This result will be subject to tests in the future [34].

The above formulation of DSR, based on the algebra from Eq. (1.30) is only one possible realization, often called DSR1. Another realization of DSR, explored in Refs. [28, 35], often called DSR2, uses a choice of a slightly different basis for the κ-Poincaré algebra. In the basis of DSR2, the algebra differs from the one in Eq. (1.30) only in the last two

expressions as

$$[K_i, p_j] = i\left(\delta_{ij}\, p_0 - \frac{p_i\, p_j}{\kappa c}\right) ,$$
$$[K_i, p_0] = i\left(1 - \frac{p_0}{\kappa c}\right) p_i , \tag{1.33}$$

while the rest remain unchanged. Therefore, the Lorentz sector remains unmodified in this formulation as well. By computing the Casimir invariant for this case, one arrives at the modified energy-momentum dispersion relation

$$\frac{E^2}{\left(1 - \frac{E}{\kappa c^2}\right)^2} = \frac{\mathbf{p}^2 c^2}{\left(1 - \frac{E}{\kappa c^2}\right)^2} + m^2 c^4 , \tag{1.34}$$

where again $p_0 = E/c$ was used. From the above, one can see that an upper limit on the energy $E < \kappa c^2$ is implied. One can verify that Eq. (1.34) does not suggest a varying speed of light. Note that there exists a third realization of DSR, explored in Refs. [36, 37, 38], but will not be discussed here, since it would provide no further insight into DSR.

One of the interesting features of DSR is that the four-momentum space is not described by a flat manifold, but a manifold with constant curvature κ^{-2}. A consequence of this is that space-time coordinates do not commute. Therefore, a space-time of DSR is a non-commutative manifold, the κ-Minkowski space-time [31, 39], where

$$[x_0, x_i] = -\frac{i}{\kappa} x_i , \quad \text{and} \quad [x_i, x_j] = 0 , \tag{1.35}$$

valid for all realizations of DSR. For comparison, in standard QM it is not possible to simultaneously measure the position and momentum of a particle. This feature is given in terms of non-commutativity of position and momentum. Similarly, for the above space-time non-commutativity, there exists a similar limitation of simultaneously measuring a time and a space coordinate [7].

As a final note, the authors in Ref. [40] proposed an extension of DSR to include space-

time curvature, known as Doubly General Relativity. One of the important results of this extension is that the geometry of space-time depends on the energy E of the particle used to probe it (*gravity's rainbow*) [41].

Summary

Since DSR is not formulated as a theory of QG, but as a limit of QG, it provides an insightful description of the space-time symmetries and relativistic dynamics of high energy particles in negligible gravitational fields. However, DSR still has several open problems which need to be addressed for it to be complete and consistent. While single particle dynamics are understood well, it has several issues describing multi-particle dynamics, manifesting as the so-called soccer-ball problem [42]. It is also not completely clear how DSR emerges from a limit of QG and what are its conservation laws. Justification of why Nature would choose the $SO_q(3,2)$ algebra as a limit of QG and $r = 1$ to renormalize physical quantities, also remain open questions. Finally, DSR is formulated on momentum space and there is still no consistent formulation in position space.

1.1.4 Other Approaches to Quantum Gravity

From the candidate theories of QG, reviewed in this work, ST quantizes the perturbations of the graviton field on a fixed background, LQG quantizes space-time itself, and DSR addresses the behaviour of space-time symmetries in limits of QG. In contrast to the above, there are several other candidate theories of QG and approaches to QG, which introduce new concepts to address the QG problem. However, they will not be discussed in this work, but will only be mentioned, including a reference for the interested reader:

- Discrete causal sets [43]: Lorentzian metric used as geometry and causal structure.
- Causal Dynamical Triangulations [44]: gravitational path integral on a differential manifold realized explicitly, non-perturbative and with no dependence on the background.

- Asymptotically safe QG [45]: non-perturbative construction of a QFT of the metric tensor.
- Non-commutative QFT [46]: Formulation of a QFT on a non-commutative space-time.

Chapter 2

Quantum Gravity Phenomenology

> "I have a naive trust in the Universe –
> that at some level it all makes sense,
> and we can get glimpses of that sense if
> we try."
>
> *Mihaly Csikszentmihalyi*

By taking a close look at competing candidate theories of QG (e.g., theories reviewed in Section 1.1), one notices that it is difficult to provide experimentally testable predictions within their frameworks. This difficulty is mainly attributed to technological limitations of contemporary experiments, which can be quantified in terms of energy. Currently, the highest experimentally achievable energies in particle colliders reach $E_{exp} \lesssim 10^{13}\,\text{eV}$, an upper bound set by the LHC experiments. As explained in Chapter 1, QG effects are believed to manifest at energies comparable to the Planck energy $E_P \sim 10^{28}\,\text{eV}$. This is 15 orders of magnitude greater than the energy, which can currently be achieved. Therefore, direct tests of candidate theories of QG are currently not possible. However, QG effects are shown to be universal [7, 8, 47], which implies they must also persist at low and accessible energies, where although their signatures are expected to be small, they may still be detectable in high precision experiments. In other words, by taking the low energy limit of a theory of QG, which must give rise in QT and GR, the QG effects are expected to appear as corrections to established results from QT and GR. These corrections are expected to be non-vanishing, even in the regime of Newtonian mechanics. Therefore, if precise enough experiments are

designed, signatures of such effects are expected to be observable. Endeavours to provide observable predictions and explanations of anomalous phenomena (observed phenomena, which have no explanation within the standard frameworks of QT and GR) in terms of these corrections, comprise the field of Quantum Gravity Phenomenology (QGP) [7].

In QGP, phenomenological models are constructed in order to test general properties, as well as specific predictions which a consistent theory of QG may exhibit (e.g. Refs. [48, 49, 50]). An abundance of research on QGP has been produced in the last 30 years, which is evident from this extensive (yet incomplete) sample of Refs. [15, 48, 49, 50, 51, 52, 53, 54, 55, 56, 57, 58, 59, 60, 61, 62, 63, 64, 65, 66, 67, 68, 69, 70, 71, 72, 73, 74, 75, 76, 77, 78, 79, 80, 81, 82, 83, 84], covering predictions and constraints of QG effects from atomic to cosmic scales. QGP does not assume any specific candidate theory of QG as the correct one. It considers the consequences of quantization of gravity and a quantized space-time, such as a minimum measurable length ℓ_{min}.

2.1 Motivation for Minimum Length

In QG considerations, the notion of space-time at Planck scales must be reconsidered, from which corrections to quantum principles are expected to follow. For example, one of the consequences of ST (as well as M-Theory) and DSR is space-time non-commutativity [85, 86, 87, 88, 89, 90]. It leads to modified dispersion relations [91] and in some situations, may also exhibit a varying speed of light [92, 93], which gives rise to non-local field theories and the modification of the standard canonical commutation relation of the Heisenberg Uncertainty Principle [62, 80, 94, 95, 96] (see also Refs. [8, 68, 97, 98]).

The above results imply the existence of a non-vanishing minimum measurable length. In general, most candidate theories of QG and the pertinent thought experiments agree on the existence of a minimum measurable length in one way or another [6, 7, 27, 41, 63, 69, 72, 99, 100, 101, 102, 103, 104, 105, 106, 107]. In the following, a handful of examples of the emergence of a minimum measurable length are discussed. Specifically, the black hole

thought experiment, ST, LQG and DSR.

2.1.1 A Thought Experiment with a Black Hole

In the region near the apparent horizon of a small black hole, both QT and GR effects become important. Therefore, it is reasonable to assume that QG effects can manifest there. This thought experiment implies QG effects by means of measuring the area of the apparent horizon of a black hole. In this approach, only model-independent QG properties are used. The main physical process underlying this thought experiment is Hawking radiation.

Hawking radiation is a nearly black body radiation, with a characteristic temperature, known as the Hawking temperature of the black hole, as seen by an asymptotic observer [108]. One of the consequences of Hawking radiation is loss of black hole mass, resulting in black hole evaporation. In this context, if a black hole does not gain mass by accretion or other mechanisms, it will shrink and eventually vanish.

The main idea is to perform the Heisenberg microscope thought experiment, where the observed quantum particle is replaced by a black hole with a non-vanishing area of the apparent horizon. For simplicity, a Reissner-Nordström black hole with mass M and charge Q is considered, given by the metric [109]

$$\mathrm{d}s^2 = -\left(1 - \frac{R_S}{r} + \frac{R_Q^2}{r^2}\right) c^2 \mathrm{d}t^2 + \left(1 - \frac{R_S}{r} + \frac{R_Q^2}{r^2}\right)^{-1} \mathrm{d}r^2 + r^2(\mathrm{d}\vartheta^2 + \sin^2\vartheta\, \mathrm{d}\varphi^2)\,, \quad (2.1)$$

where

$$R_S = \frac{2GM}{c^2} \quad \text{and} \quad R_Q^2 = \frac{Q^2 G}{4\pi\varepsilon_0 c^4}\,, \quad (2.2)$$

ε_0 the electric constant, s the invariant interval, t time, and r, ϑ and φ are the standard spherical coordinates. Note that for charge $Q = 0$, Eq. (2.1) reduces to the Schwarzschild metric.

A Reissner-Nordström black hole has two horizons. The outer apparent horizon and the inner horizon. The latter is in general located at a shorter radius than the former. The hori-

zons of any given black hole are found where the *rr* component of its metric in a spherical coordinate system diverges, i.e., $g_{rr}^{-1} = 0$. For a Reissner-Nordström black hole, described by Eq. (2.1), they turn out as

$$R_h^{\pm} = \frac{GM}{c^2}\left(1 \pm \sqrt{1 - \frac{Q^2}{4\pi\varepsilon_0 GM^2}}\right) , \tag{2.3}$$

where $+$ denotes the outer apparent horizon solution and $-$ the inner horizon solution. A Reissner-Nordström black hole is extremal when the above two horizons coincide $R_h^+ = R_h^-$. This equality is satisfied when $Q^2 = 4\pi\varepsilon_0 GM^2$. It turns out that an extremal black hole does not emit spontaneous Hawking radiation, because it has a vanishing Hawking temperature, and is therefore an ideal candidate for the Heisenberg microscope thought experiment. It is also assumed, that the black hole does not discharge. The goal of this thought experiment is to examine the limitations to the precision of measuring R_h^+ [58].

In classical GR, an observer cannot obtain information beyond the apparent horizon, which implies that nothing is emitted from the black hole. However, the area of a black hole can be measured indirectly, by observing the motion of test particles at infinity. In this way, the mass M and the charge Q of the black hole are obtained. By using the $+$ solution of Eq. (2.3), the area of the apparent horizon is $A = 4\pi R_h^{+\,2}$. However, a black hole can emit Hawking radiation due to quantum effects near its apparent horizon. Therefore, a stationary observer at $r > R_h^+$ can detect a signal, which allows for a direct measurement of the area of the apparent horizon.

By using the Heisenberg microscope thought experiment, one can measure the area of the apparent horizon. A photon with wavelength λ is sent from infinity towards an extremal Reissner-Nordström black hole, where it gets absorbed. The mass of the black hole after absorption is $M + \Delta M$, where

$$\Delta M = \frac{h}{\lambda c} \tag{2.4}$$

and follows from the conservation of energy $\Delta M c^2 = h\nu = hc/\lambda$. Due to this change

in mass, the black hole is not extremal anymore, and is expected to decay back to the extremal state through Hawking radiation. It is assumed that a single photon of the same wavelength λ is emitted from the black hole and detected by the microscope (see Fig. 2.1). The measurement is repeated many times, so a complete image of the black hole is obtained. From this, the radius of the apparent horizon R_h^+ can be determined.

If a Schwarzschild black hole was chosen instead, it would eventually evaporate through Hawking radiation and it would also not be possible to discriminate the re-emitted photon from the background Hawking radiation. If an extremal Kerr-Newman black hole was chosen instead, the flattening of the apparent horizon and frame dragging effects would need to be taken into account, when determining where the photon came from. However, the following results would not change [58].

In the standard Heisenberg microscope thought experiment, the resolving power of the microscope and the wavelength of the detected photon determine the uncertainty in measuring the position of a particle. The exact same factors determine the first contribution to the uncertainty of measuring the radius of an apparent horizon of a black hole, which reads as

$$\Delta x^{(1)} \simeq \frac{\lambda}{\sin\theta} \,, \tag{2.5}$$

where θ defines the angular size of the microscope as seen from the apparent horizon of the black hole. It is related to the resolving power of the microscope, given by its lens diameter D and focal length f as $\sin\theta = D/2f$. Also, the photon itself poses a limitation. It cannot resolve length scales smaller than its wavelength λ.

The uncertainty in measuring the momentum of the black hole after re-emitting the photon is also the same as in the standard case, which reads as

$$\Delta p \simeq \frac{h}{\lambda} \sin\theta \,. \tag{2.6}$$

Multiplying the above by Eq. (2.5), one obtains the standard form of the Heisenberg Un-

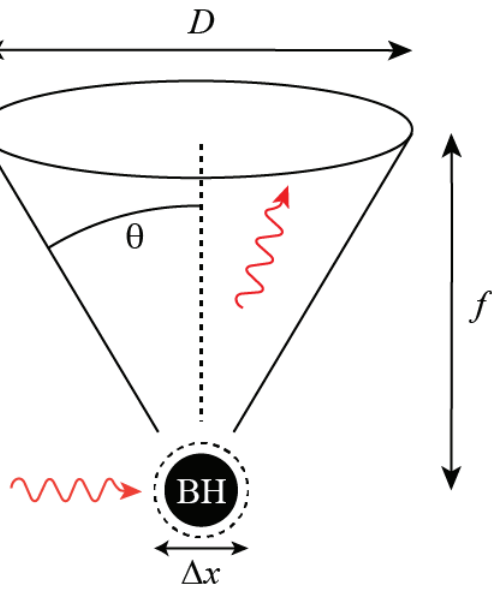

Figure 2.1: The Heisenberg microscope with a lens of diameter D and focal length f, observing a black hole (BH) through Hawking radiation. Credit of Nancy Barajas.

certainty Principle

$$\Delta x^{(1)} \Delta p \sim \hbar \, . \tag{2.7}$$

Note the interchange between the Planck constant h and the reduced Planck constant $\hbar$. In estimations such as here, one can safely assume $h \sim \hbar$.

For a black hole, there exists another contribution in determining the uncertainty of the radius of the apparent horizon. As the black hole emits the photon, its mass decreases from $M + \Delta M$ to M, and as a consequence, the apparent horizon radius also changes by $\Delta x^{(2)} = R_h^+(M + \Delta M) - R_h^+(M)$, which turns out as

$$\Delta x^{(2)} \simeq \frac{G\Delta M}{c^2} + \sqrt{\left(\frac{GM}{c^2} + \frac{G\Delta M}{c^2}\right)^2 - \frac{GQ^2}{4\pi\varepsilon_0}} - \sqrt{\left(\frac{GM}{c^2}\right)^2 - \frac{GQ^2}{4\pi\varepsilon_0}} \geq \frac{2G\Delta M}{c^2} \, . \tag{2.8}$$

By plugging Eq. (2.4) in the above, the second contribution to the uncertainty becomes

$$\Delta x^{(2)} \geq \frac{\hbar G}{c^3 \lambda} = \frac{\ell_P^2}{\lambda} \, . \tag{2.9}$$

By considering the inequality $\lambda/\sin\theta \geq \lambda$ the dependence on the microscope is eliminated. The terms $\Delta x^{(1)}$ and $\Delta x^{(2)}$ can then be linearly added to obtain

$$\Delta x \geq \lambda + B\frac{\ell_P^2}{\lambda} , \tag{2.10}$$

where B is a dimensionless constant, determining the magnitude of the second contribution. Elimination of the dependence on the microscope also implies considering the inequality $\Delta p/\sin\theta \geq \Delta p$. Using this with Eq. (2.6), one can rewrite Eq. (2.10) as

$$\Delta x \geq \frac{\hbar}{\Delta p} + B\ell_P^2\frac{\Delta p}{\hbar} = \frac{\hbar}{\Delta p} + \tilde{B}G\Delta p , \tag{2.11}$$

where $\tilde{B} = B/c^3$. The modified uncertainty relation from Eq. (2.11) can be written in a more familiar form as the modified Heisenberg Uncertainty Principle

$$\Delta x\Delta p \geq \hbar + B\frac{\ell_P^2}{\hbar}\Delta p^2 = \hbar + \tilde{B}G\Delta p^2 , \tag{2.12}$$

where it can be seen that an extra term appears, compared to the standard Heisenberg Uncertainty Principle. The term is squared in the uncertainty of momentum and it contains the gravitational constant G, which implies that the correction is of gravitational origin. As $\ell_P^2 \propto G$, the correction term is also related to minimum length. To estimate the minimum length, one finds the minimum of Eq. (2.11), which turns out as $\ell_{min} \equiv \Delta x_{min} = \sqrt{B}\,\ell_P$.

2.1.2 String Theory

From considerations of ST, discussed in Section 1.1.1, it can be concluded that there is no strict constraint on the string size. Therefore, ST allows the sizes of extra dimensions to be larger than the Planck scale. Specific choices of sizes and number of extra dimensions provide a range of observable effects. Other ST inspired phenomenological approaches introduce new fields, which give rise to new observable effects. Possible future reformu-

lations of ST could include a variety of space-time quantization, which could successfully predict measurable phenomena [7].

In ST the emergence of a minimum length can be demonstrated from considerations of dualities. A simple example, giving a general idea about dualities, comes from condensed matter physics [110]. A two-dimensional Ising model represents a dual spin system. The dual lattice has a $\mathbb{Z}_2$ symmetry, where spins on one lattice are oriented in one direction, while spins on the dual lattice are oriented in the opposite direction (see Fig. 2.2). Black and white dots represent opposite spins of the lattices, with temperatures T and $1/T$ respectively. There is one phase transition in such a system and it occurs at the critical temperature $T_c = 1$, at which the lattices switch roles and the system behaves the same at temperatures $T > T_c$ as at temperatures $T < T_c$. This is called T-duality [6].

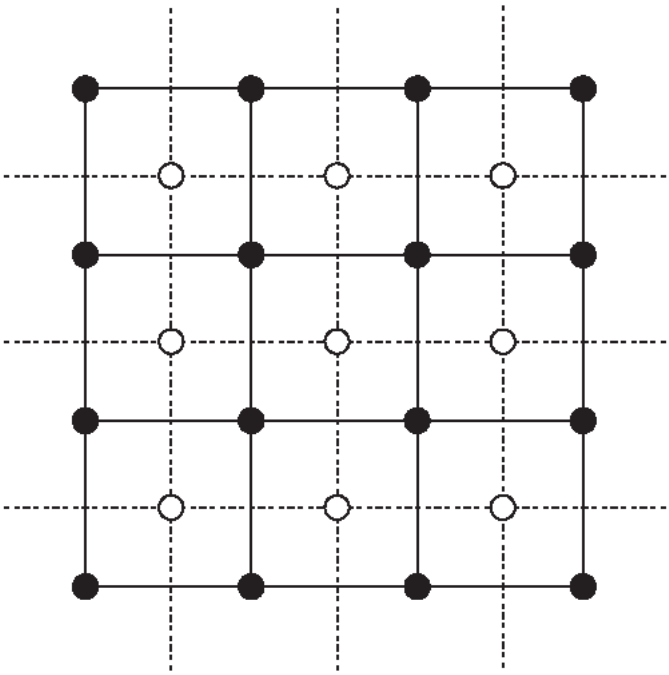

Figure 2.2: Dual lattice of a two-dimensional Ising model. Credit of Nancy Barajas.

T-duality is also found in ST and it implies the existence of a smallest circle, at which the radii R and α'/R of dual circles are equal. To see this, one considers a space, where at least one dimension is periodic with period $2\pi R$. One then proceeds to shrink R below

$\sqrt{\alpha'}$. It turns out that the circle will begin to expand again. This means that the circle radius can't get smaller than $\sqrt{\alpha'}$ [6]. On such a circle with radius R, a massless string (assumed for simplicity) has momentum and energy

$$p = \hbar \frac{n}{R} \quad \text{and} \quad E_n = \hbar c \frac{|n|}{R} \,, \tag{2.13}$$

where $n \in \mathbb{Z}$ are the excitation levels of the string (momentum modes). Strings can also be wrapped around the circle. If a string is wrapped m times around the circle (winding modes), their energy increases by

$$\tilde{E}_m = \hbar c \frac{mR}{\alpha'} \,. \tag{2.14}$$

Momentum modes and winding modes are analogous to the Ising dual spin system, where the symmetry $\mathbb{Z}_2$ is generalized to $\mathbb{Z}$. A scheme of a string on a circle with momentum and energy spectra at different values of R is shown on Fig. 2.3, from where one can see that the role of the string momentum modes and the winding modes interchange through the equivalence $R \iff \alpha'/R$, as the circle is shrunk below $\sqrt{\alpha'}$. This is how T-duality manifests in ST.

An immediate consequence of not being able to compress a circle below a certain size, is the existence of a minimum length. According to the Heisenberg Uncertainty Principle, distance scales are probed with momentum (energy) as $\Delta x \simeq \hbar/\Delta p$. However, this does not work for very large energies, since the strings begin to re-expand with increasing energy after a certain threshold, which is determined by the string tension α'. The smallest uncertainty in momentum is the difference between two neighbouring momentum modes

$$\Delta p = \hbar \frac{n}{R} - \hbar \frac{(n-1)}{R} = \frac{\hbar}{R} \quad \Longrightarrow \quad R = \frac{\hbar}{\Delta p} \,. \tag{2.15}$$

As the T-duality, $R \iff \alpha'/R$, and the above relation is taken into account, one can see

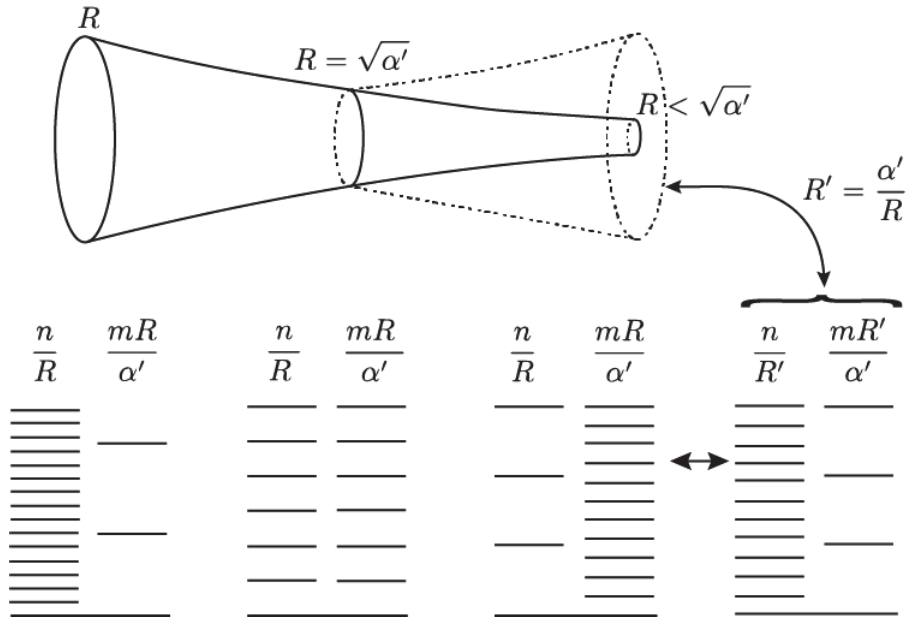

Figure 2.3: String on a circle for shrinking R with it's spectrum. Here $\hbar = c = 1$ is assumed. Adapted from [6]. Credit of Nancy Barajas.

that momenta in ST manifest T-duality as well

$$\frac{\hbar}{\Delta p} \iff \alpha' \frac{\Delta p}{\hbar} \,. \tag{2.16}$$

Since contributions of both of the above terms are present at all energies (momenta), the sum of these terms expresses the uncertainty in position of a particle, as a consequence of T-duality as

$$\Delta x \geq \frac{\hbar}{\Delta p} + \alpha' \frac{\Delta p}{\hbar} \,. \tag{2.17}$$

The above can be written in the form of a modified Heisenberg Uncertainty Principle

$$\Delta x \Delta p \geq \hbar + \frac{\alpha'}{\hbar} \Delta p^2 \,. \tag{2.18}$$

Using the same reasoning as for Eq. (2.11) at the end of Section 2.1.1, one finds the minimum length by calculating the minimum of Eq. (2.17). In the framework of ST, one can see that the minimum length is $\ell_{min} \equiv \Delta x_{min} = \sqrt{\alpha'} \propto \ell_P$. A similar result is obtained in a

study of scattering processes of strings at energies $\sim E_P$ [73].

2.1.3 Loop Quantum Gravity

One of the most important results, obtained within the framework of LQG, discussed in Section 1.1.2, is the discreteness of space-time, as seen by studying spin networks. This concept introduces fundamental discrete area and volume spectra [26], as well as a discrete length spectrum [111], implying the existence of a minimum measurable length. To see exactly how a minimum measurable length emerges within LQG, dimensional physical operators must be introduced.

In LQG one can construct length, area and volume operators. The simplest operator to construct is the area operator, defined on a two-dimensional surface $S \subset \Sigma$. This surface is then subdivided into N small surfaces S_I, where $I = 1,2,...,N$ and $S = \cup_I S_I$. The area operator is constructed using the flux vector operator $F_S^A[E]$ and the above division of S as

$$\hat{A}_S[E] = \lim_{N\to\infty} \sum_{I=1}^{N} \sqrt{F_{S_I}^A[E]\, F_{S_I}^A[E]}\ . \tag{2.19}$$

For simplicity, a simple wave functional $|\Psi_\Gamma\rangle$ of a single fixed graph Γ, which has $L(\Gamma)$ edges $e_p \in \Gamma$, is taken. In this case, every surface S_I is crossed by one edge of the spin network. The eigenvalue of the area operator from Eq. (2.19) on such a wave functional is

$$\hat{A}_S\,|\Psi_\Gamma\rangle = 8\pi\ell_P^2\hbar\gamma \sum_{p=1}^{L(\Gamma)} \sqrt{j_p(j_p+1)}\,|\Psi_\Gamma\rangle\ , \tag{2.20}$$

where $j_p \neq 0$ are the spins of the edges e_p. In the most minimalistic case, one considers a graph Γ_{min}, which contains only one edge e in the ground state with spin $j = 1/2$. In this case, the smallest possible area eigenvalue is

$$\hat{A}_S\,|\Psi_{\Gamma_{min}}\rangle = 4\sqrt{3}\pi\ell_P^2\hbar\gamma\,|\Psi_{\Gamma_{min}}\rangle\ , \tag{2.21}$$

which is called the area gap and is the smallest area an edge can carry. One can construct volume and length operators in a similar fashion, but it is a significantly more involved process, and will not be covered here. To understand in detail how the $F_S^A[E]$ operator works on holonomies, which are the main components of spin network wave functionals, and how they are used to construct volume and length operators, the reader can consult Refs. [16, 17, 18, 19, 20, 21, 111].

Within the framework of LQG, the area operator eigenvalue obtained in Eq. (2.21) is the smallest quantum of area, while the smallest eigenvalue of a length operator is $\ell_{min} = \sqrt[4]{3}\,\gamma^{1/2}\ell_P/\sqrt{2}$ [111], and implies the existence of a minimum measurable length. The Barbero-Immirzi parameter γ defines the magnitudes of the minimum area, minimum volume and minimum length in terms of ℓ_P, and remains a free parameter in LQG.

To probe such a space-time (spin network), described by LQG, one needs to introduce matter. For simplicity, a scalar field is considered. In LQG, matter must also be quantized in a background independent way. One way to approach a background independent quantization of scalar fields, is called *polymer quantization* [112, 113, 114, 115, 116]. Such quantization introduces a new length scale $\mu \propto \gamma^{1/2}\ell_P$, called *polymer length*. In this formulation, the scalar particle in consideration can be effectively described by the approximate position and momentum operators [115, 117]

$$x = x_0\ , \quad \text{and} \quad p = \frac{\hbar}{\mu}\sin\left(\frac{\mu}{\hbar}p_0\right)\ , \tag{2.22}$$

where x_0 and p_0 are the standard canonical operators from QM, and are given in one dimension for simplicity. Using the above, one can construct a commutation relation between x and p as

$$[x,p] = i\hbar\left(1 - \frac{\mu^2}{\hbar^2}p^2 + O(\mu^4)\right)\ , \tag{2.23}$$

which is the commutator form of the modified Heisenberg Uncertainty Principle. From

the above, one can see that the standard Heisenberg commutation relation is obtained in the limit $\mu \longrightarrow 0$. The modification of the above commutation relation, emerging from LQG, appears as a quadratic correction to the standard case in terms of the scalar particle momentum p, with its magnitude parameterized by μ.

2.1.4 Doubly Special Relativity

In a similar way as seen in the above considerations, DSR incorporates the existence of a minimum measurable length. The κ-Poincaré algebra, introduced in Section 1.1.3, suggests modifications of QT in terms of the canonical commutation relations. Such modifications arise as a consequence of the modification of energy-momentum dispersion relation. In general, a modified dispersion relation can be written as [35, 118]

$$E^2 f^2 - \mathbf{p}^2 c^2 g^2 = m^2 c^4 \,, \tag{2.24}$$

where $f = f(E/\kappa c^2, \mathbf{p}^2/\kappa^2 c^2)$ and $g = g(E/\kappa c^2, \mathbf{p}^2/\kappa^2 c^2)$ are model dependent modification functions of two variables, and can be used to define the auxiliary energy and momentum variables as $\varepsilon = E\, f(E/\kappa c^2, \mathbf{p}^2/\kappa^2 c^2)$ and $\pi_i = p_i\, g(E/\kappa c^2, \mathbf{p}^2/\kappa^2 c^2)$, for convenience.

To see how the above modifications affect QM, one can construct commutation relations between t, x_i, E and p_i, once promoted to quantum operators (see Ref. [118]). However, to demonstrate the emergence of a minimum measurable length, only the commutation relation between the position x_i and momentum p_i variables is relevant. Since DSR is formulated on momentum space (see Section 1.1.3), it is natural to choose a momentum representation to define quantum operators. This makes p_i the multiplication operator and $x_i = i\hbar\partial_{\pi_i}$ the translation operator in momentum space. Note that the x_i operator is defined in terms of the derivative over the variable π_i and not the physical momentum p_i. In momentum space, this can always be done, when $g \neq 1$ [35] (see also Ref. [63]). Using these definitions of x_i and p_i, when the energy-momentum dispersion relation is modified by f

and g, the resulting commutation relation reads as [118]

$$[x_i, p_j] = i\hbar \frac{\partial p_j}{\partial \pi_i} = \frac{i\hbar}{g} \left(\delta_{ij} - 2 \frac{p_i p_j}{\kappa^2 c^2} \frac{\mathcal{N}}{\mathcal{D}} \right) , \tag{2.25}$$

where

$$\mathcal{N} = f \, \partial_1 g + \frac{E}{\kappa c^2} \left(\partial_1 f \, \partial_2 g - \partial_2 f \, \partial_1 g \right) \tag{2.26}$$

and

$$\mathcal{D} = \left(f + \frac{E}{\kappa c^2} \partial_1 f \right) \left(g + 2 \frac{\mathbf{p}^2}{\kappa^2 c^2} \partial_2 g \right) - 2 \frac{\mathbf{p}^2}{\kappa^2 c^2} \partial_1 g \frac{E}{\kappa c^2} \partial_2 f \, . \tag{2.27}$$

In the above, ∂_1 and ∂_2 denote partial derivatives of the modification functions f and g, over their first and second arguments, respectively. The right-hand side of Eq. (2.25) is obtained by a straightforward, yet involved algebra of ε and π_i.

In the case of the DSR1 realization, where the modified energy-momentum dispersion relation is given by Eq. (1.31), the modification functions are given by

$$f(E/\kappa c^2, \mathbf{p}^2/\kappa^2 c^2) = \frac{1}{2} \left[\left(1 + \frac{\mathbf{p}^2}{\kappa^2 c^2} \right) \frac{e^{E/\kappa c^2}}{E/\kappa c^2} - \frac{e^{-E/\kappa c^2}}{E/\kappa c^2} \right] \tag{2.28}$$

and

$$g(E/\kappa c^2) = e^{E/\kappa c^2} \, , \tag{2.29}$$

where g turns out to not depend on $\mathbf{p}^2$. Plugging the above modification functions f and g in Eq. (2.25), the modified commutation relation reads as

$$[x_i, p_j] = i\hbar \left[e^{-E/\kappa c^2} \, \delta_{ij} + \frac{p_i p_j}{\kappa^2 c^2} \frac{1}{\cosh(m/\kappa)} \right] , \tag{2.30}$$

which can be rewritten in the phenomenologically relevant low particle mass limit, $m \ll \kappa$, as

$$[x_i, p_j] \simeq i\hbar \left[\left(1 - \frac{p}{\kappa c} - \frac{m^2 c^2}{2\kappa c\, p} + \frac{m^2}{2\kappa^2} \right) \delta_{ij} + \frac{p_i p_j}{\kappa^2 c^2} + O(\kappa^{-4}) \right] , \tag{2.31}$$

or in the massless case, $m = 0$, as

$$[x_i, p_j] = i\hbar \left[\left(1 - \frac{p}{\kappa c} \right) \delta_{ij} + \frac{p_i p_j}{\kappa^2 c^2} \right] . \tag{2.32}$$

From the above modification of the canonical commutation relations, one can see that the standard QM commutation relation is obtained in the limit $\kappa \longrightarrow \infty$. The modification in the DSR1 realization appears as linear and quadratic corrections to the standard case in terms of the particle momentum p, with their magnitude parameterized by κ.

In the case of the DSR2 realization, where the modified energy-momentum dispersion relation is given by Eq. (1.34), the modification functions are given by

$$f(E/\kappa c^2) = g(E/\kappa c^2) = \frac{1}{1 - \frac{E}{\kappa c^2}} , \tag{2.33}$$

where both take the same shape and neither of them depend on $\mathbf{p}^2$. Plugging the above modification functions f and g in Eq. (2.25), the modified commutation relation reads as

$$[x_i, p_j] = i\hbar\, \delta_{ij} \left(1 - \frac{E}{\kappa c^2} \right) . \tag{2.34}$$

From the above modification of the canonical commutation relations, one can also see that the standard QM commutation relation is obtained in the limit $\kappa \longrightarrow \infty$. The modification in the DSR2 realization appears only as a linear correction to the standard case in terms of the particle energy E, with its magnitude parameterized by κ.

Comparing Eqs. (2.30), (2.31) and (2.32) with Eq. (2.34), one can see that the DSR1 modification contains corrections up to second order in κ, while the DSR2 modification

contains corrections only up to first order in κ, and that the DSR1 modification is given in terms of the particle momentum p, while the DSR2 modification is given in terms of the particle energy E. However, the two realizations are equivalent, since there exists a mapping between the variables of DSR1 and DSR2 [37, 38].

Considerations in Sections 2.1.1 and 2.1.2 demonstrate that a modified Heisenberg Uncertainty Principle implies the existence of a minimum measurable length. The Heisenberg Uncertainty Principle, as well as an uncertainty relation between any two quantum operators, can also be expressed in terms of commutation relations (see Section 2.2). Therefore, Eqs. (2.30), (2.31), (2.32) and (2.34) represent modifications of the Heisenberg Uncertainty Principle. They imply the existence of a minimum measurable length, parameterized by $1/\kappa \propto \ell_P$, emerging from the framework of DSR. Furthermore, DSR imposes an addition of a linear correction term, while considerations in Sections 2.1.1 and 2.1.2 propose only a quadratic correction term. This addition implies the existence of a fundamental maximum energy-momentum scale, parameterized by $\kappa \propto M_P$.

2.2 Generalized Uncertainty Principle

Examples in Section 2.1 provide a strong motivation for the existence of a minimum measurable length ℓ_{min}, and suggest that a fully consistent theory of QG must provide a fundamental description of space-time in terms of ℓ_{min}. Given the variety of formulations in these approaches to QG, it is very interesting to note that they all share a common phenomenological feature; a modification of the Heisenberg Uncertainty Principle, parameterized by an unknown minimum length scale $\ell_{min} \propto \ell_P$. The Heisenberg Uncertainty Principle, modified in this manner, is known as the Generalized Uncertainty Principle (GUP). It can be used to probe QG signatures at low and accessible energies, as well as in the absence of strong gravity objects, such as black holes. Overall, this feature of QG is completely model independent. GUP shifts the focus from searching for QG effects in high energy experiments to searching for them in high precision experiments. Therefore, low

energy signatures of QG effects are expected to be discovered eventually, as the precision of experiments increases with time. However, higher experimental energies are still favorable, as they amplify the QG signatures. GUP and its implications have been studied extensively in the past [15, 48, 49, 50, 54, 58, 59, 60, 61, 62, 63, 64, 65, 66, 67, 68, 69, 70, 71, 72, 73, 74, 75, 76, 77, 78, 79, 80, 81, 82, 83, 84], and remain relevant in searching for signatures of QG in previously unexplored fields.

2.2.1 The GUP Model

For practical applications, a specific model of GUP needs to be introduced. There are several different realizations of GUP models used in QGP research. For example, some of the commonly used models, given in commutator form in one dimension, are [63, 69, 72]

$$[x,p] = i\hbar(1-\alpha p)\ , \tag{2.35}$$

$$[x,p] = i\hbar\left(1+\beta p^2\right)\ , \tag{2.36}$$

$$[x,p] = i\hbar\sqrt{1+2\beta\left(p^2+m^2c^2\right)}\ , \tag{2.37}$$

where α and β are the dimensionful GUP parameters, defined below Eq. (2.42). At phenomenologically relevant energies, the GUP model from Eq. (2.37) is equivalent to the GUP model from Eq. (2.36). In literature, the most widely used GUP model is the quadratic one, presented in Eq. (2.36), which was explored in detail by Kempf, Mangano and Mann (KMM) in Ref. [63]. Therefore, this model is referred to as the KMM model, for convenience. A short summary of its implications follows.

In a well defined Hilbert space representation, the wave functions must be normalizable, while the position and momentum operators should have finite expectation values and uncertainties. To demonstrate how the KMM model affects QM, two arbitrary wave functions, $\psi(p)$ and $\phi(p)$, defined in the momentum space representation, are introduced. The momentum operator is defined as $\hat{p}\,\psi(p) = p\,\psi(p)$ and the position operator as $\hat{x}\,\psi(p) = i\hbar(1+\beta p^2)\,\partial_p\psi(p)$ to satisfy the KMM model. The scalar product in momentum

space is then

$$\langle\psi|\phi\rangle = \int_{-\infty}^{\infty} \frac{\mathrm{d}p}{1+\beta p^2}\, \psi^*(p)\,\phi(p)\ , \tag{2.38}$$

and the identity operator takes the form

$$1 = \int_{-\infty}^{\infty} \frac{\mathrm{d}p}{1+\beta p^2}\, |p\rangle\langle p|\ . \tag{2.39}$$

Because a minimal position uncertainty is introduced, a physical state that corresponds to a position eigenstate cannot be retrieved. However, one can obtain a quasi position wave function $\psi(\xi)$ in the form

$$\psi(\xi) = \sqrt{\frac{2\sqrt{\beta}}{\pi}} \int_{-\infty}^{\infty} \frac{\mathrm{d}p}{(1+\beta p^2)^{3/2}}\, e^{i\frac{\xi \tan^{-1}(\sqrt{\beta}p)}{\hbar\sqrt{\beta}}}\, \psi(p)\ , \tag{2.40}$$

with the position and momentum operators represented in the quasi position space as

$$\hat{x}\,\psi(\xi) = \left(\xi + \hbar\beta \frac{\tan(-i\hbar\sqrt{\beta}\,\partial_\xi)}{\sqrt{\beta}}\right)\psi(\xi)\ , \quad \text{and} \quad \hat{p}\,\psi(\xi) = \frac{\tan(-i\hbar\sqrt{\beta}\,\partial_\xi)}{\sqrt{\beta}}\,\psi(\xi)\ . \tag{2.41}$$

One can see that the operators $\hat{x}$ and $\hat{p}$ are expressed as functions of ξ and $-i\hbar\,\partial_\xi$, for which the standard Heisenberg commutation relation $[\xi, -i\hbar\,\partial_\xi] = i\hbar$ holds. Furthermore, the above implies that the physical states are distinct from those in standard QM. The standard QM states and operators are retrieved when $\beta \longrightarrow 0$.

However, in this work the linear and quadratic form of the GUP, consistent with all approaches to QG, is considered, which was introduced and explored by Ali, Das and Vagenas (ADV) in Refs. [66, 68]. Therefore, this model is referred to as the ADV model, for convenience. For the ADV model, the above phase-space considerations are similar, but more involved (see Ref. [119]). In three dimensions, the ADV model is given by

$$[x_i, p_j] = i\hbar\left(\delta_{ij} - \alpha\left(p\,\delta_{ij} + \frac{p_i\,p_j}{p}\right) + \beta\left(p^2\,\delta_{ij} + 3\,p_i\,p_j\right)\right)\ , \tag{2.42}$$

where $\alpha \equiv \alpha_0/(M_P c)$ and $\beta \equiv \beta_0/(M_P c)^2$, with α_0 and β_0 the dimensionless linear and quadratic GUP parameters, respectively, and $p = \sqrt{p_i p_i}$. In general, α_0 and β_0 are different, which implies two length scales $\alpha_0 \ell_P$ and $\sqrt{\beta_0}\ell_P$. They correspond to a maximum measurable momentum $p_{max} \propto 1/\alpha_0 \ell_P \propto M_P c/\alpha_0$ and a minimum measurable length $\ell_{min} \propto \sqrt{\beta_0}\ell_P$, respectively. The upper bound on experimentally achievable energies E_{exp} determines the smallest experimentally achievable probing length scale $\ell_{EW} \sim 10^{-18}\,\mathrm{m}$, through the Heisenberg Uncertainty Principle. It is called the electroweak length scale, because it successfully probes the domain of the electroweak force. In terms of ℓ_P, it can be expressed as $\alpha_{EW} \equiv \ell_{EW}/\ell_P = 10^{17}$. Since no QG effects have been observed at this scale, the actual value of ℓ_{min} can be anywhere between $\ell_P < \ell_{min} < \ell_{EW}$. The only restrictions on GUP, imposed by this scale, are bounds $\alpha_0 < \alpha_{EW} = 10^{17}$ and $\beta_0 < \alpha_{EW}^2 = 10^{34}$.

The connection between the position-momentum commutator and the Heisenberg Uncertainty Principle is called the Robertson uncertainty relation. In general, this connection relates a commutator and the uncertainty relation between any two quantum operators A and B as

$$\Delta A\,\Delta B \geq \frac{1}{2}\left|\langle [A,B]\rangle\right| . \tag{2.43}$$

The Robertson relation for the position-momentum commutator in one dimension reads as $\Delta x \Delta p \geq \frac{1}{2}|\langle [x,p]\rangle|$, and returns

$$\begin{aligned}\Delta x \Delta p &\geq \frac{\hbar}{2}(1+\beta\langle p^2\rangle)\\ &= \frac{\hbar}{2}(1+\beta\Delta p^2+\beta\langle p\rangle^2)\\ &= \frac{\hbar}{2}(1+\beta\Delta p^2)\end{aligned} \tag{2.44}$$

in the case of the KMM model from Eq. (2.36), and

$$\Delta x \Delta p \geq \frac{\hbar}{2}(1-2\alpha\langle p\rangle+4\beta\langle p^2\rangle)$$

$$\geq \frac{\hbar}{2}\left[1+\left(\frac{\alpha}{\sqrt{\langle p^2\rangle}}+4\beta\right)\Delta p^2+4\beta\langle p\rangle^2-2\alpha\sqrt{\langle p^2\rangle}\right]$$
$$=\frac{\hbar}{2}\left[1-\alpha\Delta p+4\beta\Delta p^2\right] \tag{2.45}$$

in the case of the ADV model from Eq. (2.42), where the relation $\Delta p^2 = \langle p^2\rangle - \langle p\rangle^2$ and mirror symmetric states $\langle p\rangle = 0$ were considered.

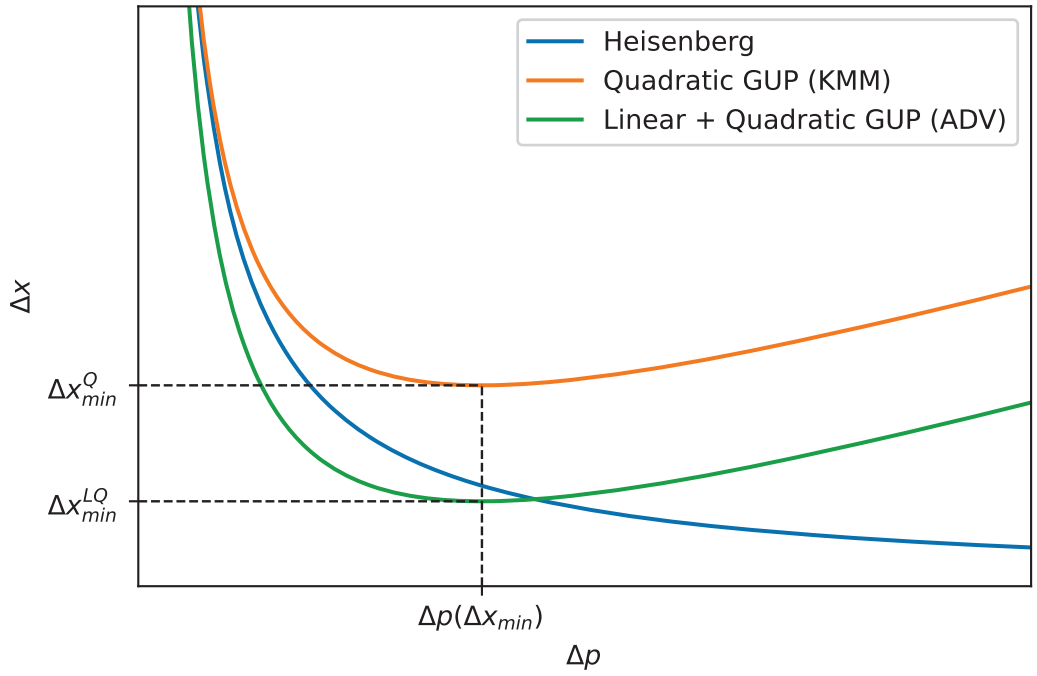

Figure 2.4: The Generalized Uncertainty Principle (KMM model (orange) and ADV model (green)), compared to the Heisenberg Uncertainty Principle (blue).

One can compare the KMM model from Eq. (2.44) and the ADV model from Eq. (2.45) with the standard Heisenberg Uncertainty Principle from Eq. (1.2) by plotting them alongside each other, as seen in Fig. 2.4. For simplicity, the prefactors ($\propto \beta$) of the quadratic terms Δp^2 are taken to be the same, neglecting the factor 4 in Eq. (2.45). One can notice that each of the modified cases deviate from the standard Heisenberg case and predict a different minimum length. In the phenomenologically relevant, low energy range of Δp, the magnitude of the deviation is greater for the ADV model, compared to the KMM model. Also, in the same energy range, the ADV model deviates to the left of the Heisenberg case

due to the presence of the p_{max} scale in the linear term, compared to the purely quadratic KMM model, which deviates to the right. The above observations suggest that the ADV model predicts stronger QG effects than the KMM model, and provides a way to verify the existence of a maximum measurable momentum scale p_{max}, once QG effects are observed for the first time. This reinforces the phenomenological relevance of the ADV model, and is therefore used throughout this work.

2.2.2 Challenges

GUP motivated QGP also faces some challenges, which need to be taken into consideration. For example, Newton's gravitational constant G, which determines the Planck length $\ell_P \propto \sqrt{G}$, is commonly assumed to be constant on all scales. However, this assumption has no solid verification. Therefore, one should carefully examine whether G is constant across the diverse energy scales, from the very small to the very big. This can have direct consequences on GUP, since it depends on ℓ_P.

GUP is used to provide simple phenomenological models. A limitation of this approach is that most of testable QG signatures, described by GUP, are based only on the minimum measurable length, and not on other QG features. However, this limitation is at the same time a strength of GUP, since it is model independent. A full test theory should be able to provide additional information, alongside the form of GUP and the corresponding dispersion relation (the two are related; see Section 2.1.4). It must also address the following issues [7]:

- Universality of GUP. Is the modification parameter always the same, or is it different for different particles?
- How is the soccer-ball problem addressed for multi-particle dynamics, described by GUP and the corresponding modified dispersion relation?
- Is the standard energy-momentum conservation law assumed valid in general, given a modified dispersion relation?

In the worst case scenario, the suppression factor $\propto E^n/E_P^n$, where $n \in \mathbb{N}$, may completely prevent observations of any QG effects in low energy experiments [7]. However, even in this scenario, the development of more detailed phenomenological models and the increasing precision of low energy experiments, may provide ever stronger bounds on ℓ_{min} (see Chapter 3). On the other hand, cosmological considerations do not only bound ℓ_{min}, but determine it (see Chapter 4). Both, improvements on the bound of ℓ_{min} in low energy experiments and measurements of ℓ_{min} in cosmological considerations, drive the progress of QGP, and encourage future research in this field. Furthermore, testing fundamental concepts, which are believed to lead towards a consistent theory of QG, such as the Quantum Equivalence Principle (see Chapter 5), proves to be an equally important branch of QGP.

Chapter 3

Earth-based Experiments

> "The beauty of a living thing is not the atoms that go into it, but the way those atoms are put together."
>
> *Carl Sagan*

Earth-based experiments provide a wide scope of tests, where the bulk of QGP research is applied [49, 15, 48, 51, 52, 53, 55, 56, 57, 62, 65, 66, 67, 68, 69, 72, 73, 79, 80, 120, 121, 122]. They are crucial in QGP, since it is possible to control the conditions and parameters of a given experimental setup. This allows for a dedicated search for QG effects in well defined conditions.

In this chapter, new results of QGP in Earth-based experiments are presented. Specifically, GUP motivated QG signatures in Bose-Einstein condensates and in magnetometer experiments, are explored in detail. Furthermore, QG signatures in a Bose-Einstein Condensate are also explored in terms of extra compact dimensions.

3.1 Bose-Einstein Condensate

The phenomenon of a Bose-Einstein Condensate (BEC) is explained within the framework of statistical mechanics [123]. Although, QG effects in statistical mechanics have not been studied extensively, some proposals suggest to search for QG signatures in BECs [120, 121, 122], and signatures of compact extra dimensions in BECs [124, 125, 126]. Work in this section explores QG signatures in BECs, where two novel approaches are

used. They provide a number of new results and are based on compact extra dimensions and GUP, respectively. They imply QG corrections to observables in BEC, such as the critical temperature T_c and fraction of bosons in the ground state f_0.

The aforementioned two approaches are considered independently of each other in the following. In the approach with extra compact dimensions, it is shown that the modifications of observables enter through the energy-momentum dispersion relation in a space-time with compact dimensions. In the approach with GUP, it is shown that GUP modifies the energy levels of a particle in a box, and hence the corresponding phase space volume. This directly modifies the density of states. When such a modification is applied to phase-space integrals of a BEC, modifications of observables follow. Supporting material for this section is found in Appendix A.

3.1.1 From Classical to Quantum Gases

Description of a classical gas at relatively high temperatures neglects the interactions between the constituent particles. This can be safely assumed, since the thermal de Broglie wavelength $\lambda_B = h/\sqrt{2\pi m k_B T}$, at high temperature, is much smaller than the mean free path between particles of the gas. Here k_B is the Boltzmann constant and T the temperature of the gas. This condition can be written as

$$n\lambda_B^3 = \frac{n h^3}{(2\pi m k_B T)^{3/2}} \ll 1 \,, \tag{3.1}$$

where n is the number density of the gas, related to the mean free path as $\overline{\ell}_{free} = 1/n^{1/3}$. When the temperature of the gas is lowered, the parameter $n\lambda_B^3$ approaches unity and all physical quantities of the system correspond to its classical properties. As the temperature decreases to a certain value, $n\lambda_B^3$ is still small, but becomes non-negligible. Therefore, the various physical quantities of the system can be expanded as a power series of this parameter. This implies that the condition in Eq. (3.1) can still be satisfied at low temperatures of the gas. However, the effects of quantum statistics, which arise from the spin of parti-

cles comprising the gas, become important. Such effects turn out to be different for bosons and fermions (see Eq. (A.4) in Appendix A.1). In general, for lower temperatures, higher particle densities and lower particle masses, quantum phenomena become more prominent [123].

3.1.2 Standard Bose-Einstein Condensation

The phenomenon of BEC occurs when a dilute gas of bosons is cooled below a certain temperature, where the bulk of these bosons occupy the ground state. This temperature is known as the critical temperature T_c. Since the Bose-Einstein (BE) statistics (see Eq. (A.4) in Appendix A.1) allows for an arbitrary number of bosons in any state, there could theoretically be an infinite number of bosons in the ground state. In the following, a few important results, related to a standard BEC, are reviewed. Note that the standard BEC observables T_c and f_0 are given in terms of an arbitrary number of Euclidean spatial dimensions d.

The critical temperature T_c is the threshold at which all of the bosons are still in the excited states. As soon as the gas temperature T drops below T_c, the bosons rapidly start to decay to their ground state. Furthermore, considering the non-relativistic case, the chemical potential vanishes $\mu \longrightarrow 0$ at $T < T_c$, in the thermodynamic limit $N_0 \longrightarrow \infty$, where N_0 is the number of bosons in the ground state. In d-dimensional space, with $d \geq 3$ (a non-relativistic BEC in $d = 1,2$ dimensions does not exist [125]), the critical temperature of a non-relativistic BEC (obtain by means of Eq. (A.11) from Appendix A.1) reads as

$$T_c = \frac{2\pi\hbar^2}{k_B m \zeta(\frac{d}{2})^{2/d}} n^{2/d} , \tag{3.2}$$

where $\zeta(d/2)$ is the Riemann zeta function, evaluated at $d/2$ (see Eq. (A.7) in Appendix A.1). From the above T_c, one can see that the critical temperature of a non-relativistic BEC will be higher for high boson densities and light boson masses. Note that Eq. (3.2) for $d = 3$, is identical to Eq. (3.1) up to an unimportant numerical factor when its right hand side is set to unity. From this, one can see that at T_c, the thermal de Broglie wavelength

λ_B equals the mean free path between particles $\overline{\ell}_{free}$, where the interactions between the constituent particles become significant. Furthermore, at temperatures lower than T_c, where $\lambda_B > \overline{\ell}_{free}$, the particles start to form a BEC for bosons, and a degenerate gas for fermions. The second important observable in BEC is the fraction of bosons in the ground state f_0. If n_0 is the number density of bosons in the ground state, $n(T)$ the number density of bosons in the excited states at temperature $T < T_c$ and n the total number density of bosons, one can relate these number densities as

$$n = n_0 + n(T) = n_0 + n\left(\frac{T}{T_c}\right)^{d/2} \implies f_0 = \frac{n_0}{n} = 1 - \left(\frac{T}{T_c}\right)^{d/2}, \tag{3.3}$$

where $n(T)$ is obtained by means of Eq. (A.11) from Appendix A.1. From the above f_0, one can see that at $T = T_c$ there are no bosons in the ground state, since $f_0 = 0$. The bosons start to occupy the ground state at $T < T_c$, where $f_0 > 0$, and completely occupy the ground state at $T = 0\,\mathrm{K}$, where $f_0 = 1$.

The critical temperature T_c and fraction of bosons in the ground state f_0 for the relativistic case can be found in a similar manner, by using the relativistic density of states instead (see Eq. (A.3) from Appendix A.1). There are two distinct cases of BECs for relativistic bosons. The first, when a gas of neutral bosons is considered, is associated with the following critical temperature

$$T_c = \frac{1}{k_B}\left(\frac{2^{d-1}\pi^{d/2}\hbar^d c^d \Gamma(\frac{d}{2})}{\Gamma(d)\,\zeta(d)}\right)^{1/d} n^{1/d}, \tag{3.4}$$

where $\Gamma(d)$ is the gamma function, evaluated at d. The above T_c is valid in arbitrary $d \geq 2$ spatial dimensions (a neutral relativistic BEC in $d = 1$ dimension does not exist [127, 128]). Note that it does not depend on boson mass, unlike the non-relativistic result given in Eq. (3.2). However, it continues to depend on the boson number density, albeit with a different (positive) power. The fraction of relativistic neutral bosons in the ground state turns out to

be

$$f_0 = 1 - \left(\frac{T}{T_c}\right)^d . \tag{3.5}$$

The reasoning behind the above f_0 is the same as for Eq. (3.3), but with a different power dependence of T/T_c. The second relativistic case considers a gas of charged particles, consisting of bosons and antibosons. The distribution function for such a gas is the total charge density n (in the previous two cases, n refers simply to the number density of bosons), obtained as the difference between the respective BE distributions. One subtracts the BE distribution of antibosons (where $\mu(T_c) = -mc^2$) from the BE distribution of bosons (where $\mu(T_c) = mc^2$). The relativistic boson-antiboson critical temperature, valid in arbitrary $d \geq 3$ spatial dimensions (a charged relativistic BEC does not exist in $d = 1,2$ dimensions [127, 128]), reads as

$$T_c = \frac{1}{k_B}\left(\frac{2^{d-2}\pi^{d/2}\hbar^d c^{d-2}\Gamma(\frac{d}{2})}{m\Gamma(d)\zeta(d-1)}\right)^{1/(d-1)} n^{1/(d-1)} , \tag{3.6}$$

where T_c increases with increasing total charge density n and decreasing boson mass m. Note that the above T_c depends on both, m and n, compared to the relativistic neutral boson case, where T_c depends only on n. The fraction of relativistic charged bosons in the ground state turns out to be

$$f_0 = 1 - \left(\frac{T}{T_c}\right)^{(d-1)} . \tag{3.7}$$

The reasoning behind the above f_0 is the same as for the previous two cases, but with a different power dependence of T/T_c.

To summarize, one can see that a T_c of a BEC depends on powers of m and n, determined by the above cases and the dimensionality d of a chosen Euclidean space. Similarly, a f_0 of a BEC depends on powers of T/T_c, determined by the above cases and d. Note that the

charged relativistic BEC is the most general case, which reduces to the other two cases in corresponding limits.

3.1.3 Bose-Einstein Condensation in Compact Dimensions

Compact extra dimensions are interesting from the point of view of QG, since they are an essential component in ST, where they are usually assumed to be tiny, most often, of the order of ℓ_P [11]. In the following, it is examined whether compact dimensions have an effect on the T_c and f_0 of a BEC, in which case they may be measurable. Interestingly, it turns out that there is indeed such an effect. To demonstrate this, one considers a charged relativistic BEC, described by charge density n, given in d non-compact Euclidean dimensions and N compact spherical dimensions (space topology of $\mathbb{R}^d \times S^N$) as [124]

$$n = \sum_{\ell=0}^{\infty} d_\ell \int_0^\infty \frac{\mathrm{d}^d k}{(2\pi)^d} \left[\frac{1}{e^{\beta_T \left(\sqrt{\hbar^2 k^2 c^2 + m^2 c^4 + \hbar^2 \omega_\ell^2} - \mu \right)} - 1} - \frac{1}{e^{\beta_T \left(\sqrt{\hbar^2 k^2 c^2 + m^2 c^4 + \hbar^2 \omega_\ell^2} + \mu \right)} - 1} \right] , \tag{3.8}$$

where

$$d_\ell \equiv \frac{(2\ell + N - 1)\,\Gamma(\ell + N - 1)}{\ell!\,\Gamma(N)} \quad \text{and} \quad \omega_\ell^2 \equiv \frac{c^2}{R^2}\,\ell\,(\ell + N - 1) \tag{3.9}$$

are the degeneracy factors and energy contributions from compact dimensions, respectively, $\beta_T = 1/k_B T$ is the inverse temperature and R is the radius of the compact S^N. Currently, the only available experimental realization of creating a BEC, is the non-relativistic case. Therefore, a non-relativistic BEC is considered in the following, for which $k_B T \ll m c^2$. This condition reduces Eq. (3.8) to

$$n \simeq \sum_{\ell=0}^{\infty} d_\ell \frac{1}{(2\pi\hbar^2)^{d/2}} (k_B T_c)^{d/2} \frac{1}{c^d} \left(\sqrt{\hbar^2 \omega_\ell^2 + m^2 c^4} \right)^{d/2} \times \sum_{n=1}^{\infty} \frac{1}{n^{d/2}} e^{-n\beta_{T_c}\left(\sqrt{\hbar^2\omega_\ell^2 + m^2c^4} - mc^2\right)} , \tag{3.10}$$

evaluated at T_c. Note that the second sum in the above, equals the polylogarithm function $Li_{d/2}\left(\exp\left[-\beta_{T_c}\left(\sqrt{\hbar^2\omega_\ell^2 + m^2c^4} - mc^2\right)\right]\right)$ (see Eq. (A.6) in Appendix A.1). Furthermore, it is assumed that the radius of the compact dimensions R is very small, since $R \propto \ell_P$. In this situation, the Compton wavelength of the boson is much greater than R, i.e., $(mc/h)R \ll 1$ (or equivalently $\hbar\omega_\ell \gg mc^2$). This implies that all terms in the sum over ℓ, except for $\ell = 0$, are exponentially suppressed by the Boltzmann factor from the second sum. However, they do not completely vanish for $R > 0$, no matter how small. Therefore, only the largest, first order contribution, $\ell = 1$, of the compact dimensions is kept, and higher orders, $\ell > 1$, neglected. This allows to predict measurable signatures of compact dimensions. For $\ell = 1$ and small R, the above polylogarithm function reduces to $Li_{d/2}(\exp(-\beta_{T_c}\frac{\hbar c}{R}\sqrt{N}))$, where the argument is also small. For a small argument of the polylogarithm function, one can write $Li_{d/2}(\exp(-\beta_{T_c}\frac{\hbar c}{R}\sqrt{N})) \approx \exp(-\beta_{T_c}\frac{\hbar c}{R}\sqrt{N})$ [129]. Therefore, for a small radius R of the compact dimensions, the number density of bosons from Eq. (3.10) can be written as

$$n \simeq \left(\frac{m k_B T_c}{2\pi\hbar^2}\right)^{d/2} \left[\zeta(\tfrac{d}{2}) + \frac{\hbar^{d/2}(N+1)N^{d/4}}{R^{d/2} m^{d/2} c^{d/2}} e^{-\beta_{T_c}\frac{\hbar c}{R}\sqrt{N}}\right] , \tag{3.11}$$

where the first term agrees with the standard non-relativistic BEC and the second term is a correction, induced by extra compact dimensions. The Boltzmann suppression factor makes this correction very small, since it vanishes as $R \longrightarrow 0$. One is interested in the critical temperature T_c, which is extracted from Eq. (3.11) by using a perturbative approach. To accomplish this, one needs to define $T_c = T_c^{(0)} + \Delta T(R)$, where $T_c^{(0)}$ is the standard theory

critical temperature and $\Delta T(R)$ the correction to the critical temperature, induced by extra compact dimensions. Such a critical temperature, obtained for the first time in Ref. [130], reads as

$$T_c \simeq \frac{2\pi\hbar^2}{k_B m\,\zeta(\frac{d}{2})^{2/d}}\,n^{2/d} - \frac{4\pi\hbar^{(d+4)/2}(N+1)\,N^{d/4}\,e^{-\beta_{T_c}^{(0)}\frac{\hbar c}{R}\sqrt{N}}}{k_B\,d\,R^{d/2}\,m^{(d+2)/2}\,c^{d/2}\,\zeta(\frac{d}{2})^{(2+d)/d}}\,n^{2/d}\,, \tag{3.12}$$

where $\beta_{T_c}^{(0)} = 1/k_B T_c^{(0)}$. From Eq. (3.12), one can see that the first term is identical to Eq. (3.2), and that the magnitude of the correction term increases with increasing n and decreasing m. Furthermore, the correction term has a non-trivial dependence on R. This dependence is discussed in terms of the relative magnitude of the correction, obtained from Eq. (3.12) as

$$\left|\frac{\Delta T(R)}{T_c^{(0)}}\right| = \frac{2\hbar^{d/2}(N+1)\,N^{d/4}\,e^{-\beta_{T_c}^{(0)}\frac{\hbar c}{R}\sqrt{N}}}{d\,R^{d/2}\,m^{d/2}\,c^{d/2}\,\zeta(\frac{d}{2})} \equiv 10^{-r} < 10^{-q}\,. \tag{3.13}$$

In the above, r and q take positive values, such that 10^{-q} denotes the precision at which the critical temperature of a BEC can currently be measured, and 10^{-r} denotes the required precision of such measurements to observe extra compact dimensions. The inequality in Eq. (3.13) stems from the fact that the above $\Delta T(R)$ has not been observed in experiments so far. This subsequently puts bounds on the size of extra compact dimensions, as shown below. The important point to note here is that the right-hand side of Eq. (3.13) contains the compact dimension radius R in the denominator *as well as* in the numerator, via the exponential Boltzmann factor. Therefore, interestingly, as one spans the range of R from very small to larger values, the correction term initially increases and then starts to decrease. This behaviour is shown in Fig. 3.1 for a BEC of a helium gas, where $d = 3$ and $N = 1$ are assumed. The blue line therein depicts the relative correction, given by Eq. (3.13), and the horizontal orange line signifies a hypothetical precision, expected to be attainable in the future (a line corresponding to current precision at $\sim 10^{-7}$ [131] would lie well

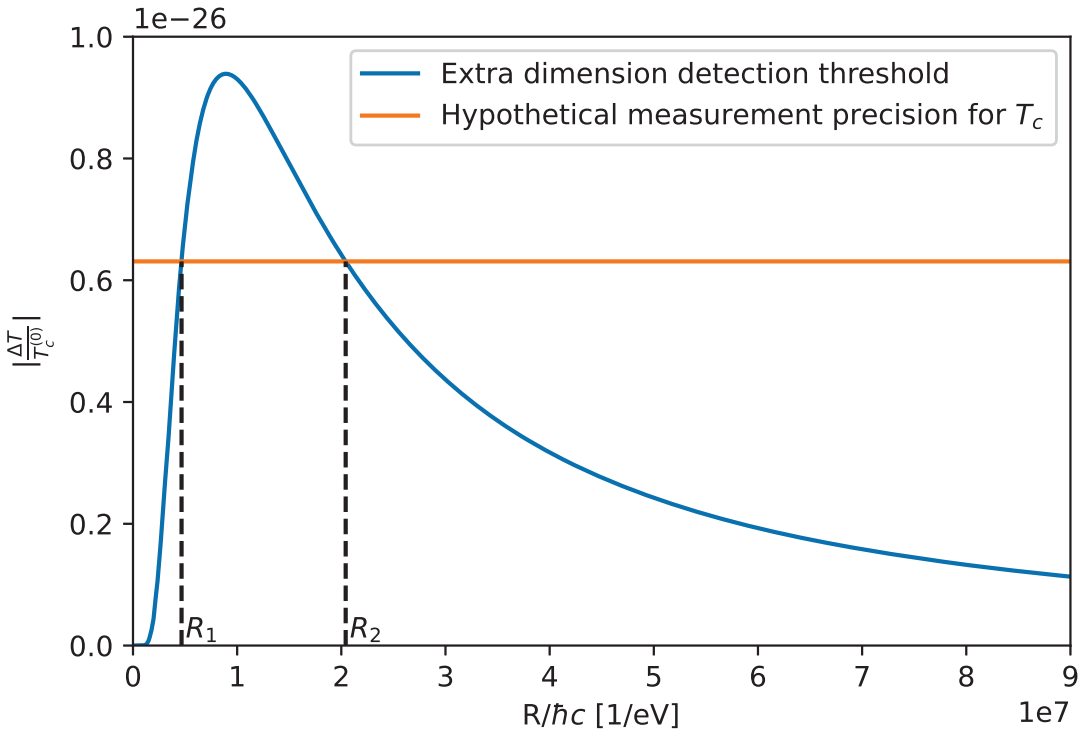

Figure 3.1: Relative correction as a function of radius $R/\hbar c$ (in energy units) of the extra compact dimension for a helium gas BEC (blue), where $m = m_{He}$, $n = 10^{23}\,\mathrm{m}^{-3}$, $d = 3$ and $N = 1$, and a hypothetical precision of an experiment (orange).

above the blue curve). Note that the curves intersect at two points, corresponding to R_1 and R_2 on the horizontal axis. Therefore, if no traces of extra compact dimensions are found in experiments, in terms of the above correction, it would mean that the correction effect can manifest for R either below R_1 or above R_2. In other words, one obtains an upper *as well as* a lower bound on the size of R. More precisely, the peak is located at $R_{\max} = 2\beta_{T_c}^{(0)}\hbar c\sqrt{N}/d$, and the two bounds always satisfy $R_1 < R_{\max}$ and $R_2 > R_{\max}$ for upper and lower bounds, respectively. Furthermore, from the example shown in Fig. 3.1, one can obtain $R_{max} = 1.77\,\mathrm{m}$. Since the actual size of extra compact dimensions cannot be of this order, otherwise they would have already been detected, it must be much smaller $R_1 \ll R_{\max}$, and the lower bound R_2 is not useful in this context. One can also notice that Eq. (3.13) is implicitly dependent on the number density n through $\beta_{T_c}^{(0)}$, since the latter

depends on n. Therefore, if n is increased, the exponential factor increases and the relative correction increases.

The order of magnitude of the correction from Eq. (3.13), signified by the quantity r, which one hopes to minimize, is given in terms of R, the number of compact dimensions N, the boson mass m and implicitly on the boson density n as

$$r = r_{d,N}(R,m) = \log\left(\frac{d\,R^{d/2}\,m^{d/2}\,c^{d/2}\,\zeta(\frac{d}{2})}{2\,\hbar^{d/2}(N+1)\,N^{d/4}}\,e^{\beta_{T_c}^{(0)}\frac{\hbar c}{R}\sqrt{N}}\right). \tag{3.14}$$

The above gives an estimate of what the precision of the temperature measurements in BECs must be, to detect such a deviation from standard theory and obtain signatures of extra compact dimensions. The second observable, the fraction of bosons in the ground state, including corrections induced by extra compact dimensions, is obtained through the standard derivation, presented in Eq. (3.3), while using the modified number density from Eq. (3.11). Such a fraction of bosons in the ground state reads as

$$f_0 = 1 - \left(\frac{T}{T_c}\right)^{d/2}\left[1 + \frac{\hbar^{d/2}(N+1)\,N^{d/4}}{R^{d/2}\,m^{d/2}\,c^{d/2}\,\zeta(\frac{d}{2})}\left(e^{-\beta_{T_c}\frac{\hbar c}{R}\sqrt{N}\left(\frac{T_c}{T}\right)} - e^{-\beta_{T_c}\frac{\hbar c}{R}\sqrt{N}}\right)\right], \tag{3.15}$$

from where one can see, that for $R \longrightarrow 0$, the above is identical to Eq. (3.3) from the standard non-relativistic BEC. Also, the correction term in square brackets in Eq. (3.15) vanishes for $T = T_c$, as expected.

In this analysis, a spherical space topology S^N was assumed for the extra compact dimensions, where there is only one R, no matter how many extra compact dimensions N are considered. If the space topology of extra compact dimensions is toroidal instead, for example $\mathcal{T}(N)$, then each of the N extra compact dimensions could have its own distinct radius. In this case, the above calculations would be similar, with the difference that the energy contributions in Eq. (3.9) would be functions of all N radii, instead of only one. However, for $N = 1$, no difference between the two topologies is expected.

3.1.4 Bose-Einstein Condensation and GUP

As shown in Sections 3.1.2 and 3.1.3, the theoretical framework for describing BECs is statistical mechanics (see also Appendix A.1). The phase space integrals in statistical mechanics are normalized by a phase space volume of a particle in a box, which is where GUP introduces QG corrections. Such corrections also modify the density of states, which is used to calculate the QG corrected number density of bosons in a BEC, and by extension, the corresponding critical temperature and fraction of bosons in the ground state. To apply GUP, given by Eq. (2.42), to a particle in a box, one considers the energy-momentum dispersion relation of a particle, confined inside a box-like potential. In QM, this is the Hamiltonian

$$H = T(p) + V(\mathbf{x}) \,, \tag{3.16}$$

where $T(p)$ is the kinetic energy of the particle, $p = |\mathbf{p}|$ the magnitude of $\mathbf{p}$, the physical momentum of the particle, and $V(\mathbf{x})$ the external box-like potential at a physical position $\mathbf{x}$, given by $V(\mathbf{x}) = 0$ inside the box and $V(\mathbf{x}) \longrightarrow \infty$ outside the box. In general, Eq. (3.16) satisfies the stationary Schrödinger equation $H\psi = E\psi$ (see Eq. (1.1)), where ψ is the particle wave function and E the corresponding energy eigenvalue.

One can notice that the standard QM operator for momentum $-i\hbar\partial_{x_i}$ cannot be used for p_i, because it does not satisfy the GUP commutation relation from Eq. (2.42). However, a set of canonical operators x_{0i} and p_{0i} can be defined, such that they satisfy the standard QM commutation relation $[x_{0i}, p_{0j}] = i\hbar\delta_{ij}$. Therefore, one can write $p_{0i} = -i\hbar\partial_{x_{0i}}$. In terms of x_{0i} and p_{0i}, one can define a transformation

$$x_i = x_{0i} \quad \text{and} \quad p_i = p_{0i}\,(1 - \alpha\, p_0 + 2\,\beta\, p_0^2) \,, \tag{3.17}$$

between physical and canonical operators, where $p_0 = \sqrt{p_{0k}\, p_{0k}}$. Note that the above transformation is one of several equivalent transformations, which satisfy the GUP commutation relation from Eq. (2.42). For convenience, transformation from Eq. (3.17) is used in what

follows, to compute QG corrections to the non-relativistic and relativistic Hamiltonians, and to examine corresponding QG signatures in a BEC.

Non-relativistic

In this case, a non-relativistic particle of mass m and kinetic energy $T(p) = p^2/2m$, is considered. The potential is defined as a three dimensional box with edges L_x, L_y and L_z, and takes values $V(\mathbf{x}) = 0$ inside the box and $V(\mathbf{x}) \longrightarrow \infty$ outside the box. This implies the wave function boundary conditions $\psi(0,y,z) = \psi(x,0,z) = \psi(x,y,0) = \psi(L_x,y,z) = \psi(x,L_y,z) = \psi(x,y,L_z) = 0$. To compute the QG corrected energy spectrum of a non-relativistic particle in a three dimensional box, one first writes the QG corrected Hamiltonian, by using Eq. (3.17) to express p in terms of p_0, as

$$H = \frac{p^2}{2m} = \frac{p_0^2}{2m} - \frac{\alpha}{m}p_0^3 + \frac{5\beta}{2m}p_0^4 \equiv H_0 + H_1 + H_2 \ , \tag{3.18}$$

where $H_0 = p_0^2/2m$, $H_1 = -\alpha\, p_0^3/m$ and $H_2 = 5\beta\, p_0^4/2m$. The corrections to the energy spectrum due to H_1 and H_2 are computed to linear order in β and quadratic order in α (note that these are of a similar order or magnitude, i.e., $O(\beta) \sim O(\alpha^2)$). It is well known, that the eigenfunctions of an unperturbed Hamiltonian H_0, for a particle in a three dimensional box, are given as [132]

$$|\psi_{\mathbf{n}}(\mathbf{x}_0)\rangle \equiv \psi_{n_x,n_y,n_z}(x_0,y_0,z_0) = \sqrt{\frac{8}{V}}\, \sin\left(\frac{\pi n_x}{L_x}x_0\right) \sin\left(\frac{\pi n_y}{L_y}y_0\right) \sin\left(\frac{\pi n_z}{L_z}z_0\right) \ , \tag{3.19}$$

where $V = L_x L_y L_z$ is the volume of the box and $n_x, n_y, n_z \in \mathbb{N}$ are quantum numbers, describing the excitation state of a particle in a three dimensional box. The above eigenfunctions span a Hilbert space $\mathcal{H} = \{|\psi_{\mathbf{n}}\rangle;\ \mathbf{n} \in \mathbb{N}^3\}$, where one can write a general state wave function as $|\Psi(\mathbf{x}_0)\rangle = \sum_{\mathbf{n}} c_{\mathbf{n}}\, |\psi_{\mathbf{n}}(\mathbf{x}_0)\rangle$, for $c_{\mathbf{n}} \in \mathbb{C}$. The standard energy spectrum of a

particle in a three dimensional box, considering an unperturbed Hamiltonian H_0, is

$$\varepsilon_{\mathbf{n}}^{(0)} = \varepsilon_{n_x,n_y,n_z}^{(0)} = \langle \psi_{\mathbf{n}}(\mathbf{x}_0)|H_0|\psi_{\mathbf{n}}(\mathbf{x}_0)\rangle = \frac{\hbar^2\pi^2}{2mL^2}\left(n_x^2+n_y^2+n_z^2\right), \tag{3.20}$$

where $L = L_x = L_y = L_z$ was assumed, without loss of generality. To obtain the QG correction to the energy spectrum from Eq. (3.20), the time independent, first order perturbation theory is used. It provides the linear (see Appendix A.2) and quadratic corrections of perturbations H_1 and H_2, respectively, as

$$\Delta\varepsilon_{\mathbf{n}}^{(1)\,Lin} = \langle \psi_{\mathbf{n}}(\mathbf{x}_0)|H_1|\psi_{\mathbf{n}}(\mathbf{x}_0)\rangle = -\frac{\alpha\hbar^3\pi^3}{mL^3}\left(n_x^2+n_y^2+n_z^2\right)^{3/2} \tag{3.21}$$

$$\Delta\varepsilon_{\mathbf{n}}^{(1)\,Quad} = \langle \psi_{\mathbf{n}}(\mathbf{x}_0)|H_2|\psi_{\mathbf{n}}(\mathbf{x}_0)\rangle = \frac{5\beta\hbar^4\pi^4}{2mL^4}\left(n_x^4+n_y^4+n_z^4 + 2n_x^2n_y^2+2n_x^2n_z^2+2n_y^2n_z^2\right). \tag{3.22}$$

The energy spectrum of a particle in a three dimensional box, up to quadratic order of the QG corrections, is then simply the sum of Eqs. (3.20), (3.21) and (3.22)

$$\begin{aligned}\varepsilon_{\mathbf{n}} &= \frac{\hbar^2\pi^2}{2mL^2}\left(n_x^2+n_y^2+n_z^2\right) - \frac{\alpha\hbar^3\pi^3}{mL^3}\left(n_x^2+n_y^2+n_z^2\right)^{3/2} \\ &\quad + \frac{5\beta\hbar^4\pi^4}{2mL^4}\left(n_x^4+n_y^4+n_z^4+2n_x^2n_y^2+2n_x^2n_z^2+2n_y^2n_z^2\right) \\ &= \frac{\hbar^2}{2m}k_{\mathbf{n}}^2 - \frac{\alpha\hbar^3}{m}k_{\mathbf{n}}^3 + \frac{5\beta\hbar^4}{2m}k_{\mathbf{n}}^4,\end{aligned} \tag{3.23}$$

where $k_{\mathbf{n}}^2 = \frac{\pi^2}{L^2}\left(n_x^2+n_y^2+n_z^2\right)$ was used in the last line. From the above, one can see that the QG corrections to the energy spectrum of a particle in a three dimensional box are dependent on quantum numbers n_x, n_y and n_z, with different powers. A procedure to obtain the exact QG corrected energy spectrum, given Eq. (2.42), of a particle in a one dimensional box, without using perturbation theory, is described in Ref. [133].

Using the QG corrected energy spectrum for a particle in a three dimensional box, given by Eq. (3.23), and taking the continuum limit ($k_{\mathbf{n}} \longrightarrow k \implies \varepsilon_{\mathbf{n}} \longrightarrow \varepsilon$; see Appendix A.3),

the QG corrected density of states, obtained for the first time in Ref. [130], reads as

$$g(\varepsilon) = \frac{V(2m)^{3/2}\varepsilon^{1/2}}{4\pi^2\hbar^3}(1 + 16\alpha\sqrt{m}\,\varepsilon^{1/2} - 25\beta m\varepsilon)\ . \tag{3.24}$$

One can see that the above reduces to the usual density of states, given by Eq. (A.2) in Appendix A.1, when $\alpha, \beta \longrightarrow 0$. The above QG corrected density of states is central in predicting QG effects in non-relativistic statistical mechanics. It is used to modify the non-relativistic BEC observables in the following. A more general procedure, described in Appendix A.4 can also be used to obtain the QG corrected density of states. However, its use is currently limited to the non-relativistic case, and for quadratic corrections only, due to the complexity of calculations.

The number of particles in the system is calculated using Eq. (A.1) from Appendix A.1 and the QG corrected density of states in Eq. (3.24). The integral is evaluated at T_c, where $\mu \longrightarrow 0$, and divided by the spatial volume V, to obtain the QG corrected number density of bosons

$$\begin{aligned} n = \frac{N_{BE}}{V} &= \frac{\sqrt{2}\,m^{3/2}}{2\pi^2\hbar^3}\left[\int_0^\infty \frac{\varepsilon^{1/2}}{e^{\beta_{T_c}\varepsilon} - 1}\,d\varepsilon + 16\alpha\sqrt{m}\int_0^\infty \frac{\varepsilon}{e^{\beta_{T_c}\varepsilon} - 1}\,d\varepsilon - 25\beta m\int_0^\infty \frac{\varepsilon^{3/2}}{e^{\beta_{T_c}\varepsilon} - 1}\,d\varepsilon\right] \\ &= \frac{\sqrt{2}\,m^{3/2}}{4\pi^{3/2}\hbar^3}\left[(k_BT_c)^{3/2}\,\zeta(\tfrac{3}{2}) + \frac{16\pi^{3/2}}{3}\alpha\sqrt{m}\,(k_BT_c)^2 - \frac{75}{2}\beta m(k_BT_c)^{5/2}\,\zeta(\tfrac{5}{2})\right]\ , \end{aligned} \tag{3.25}$$

where one can see that it reduces to the usual number density, given by Eq. (A.11) (as $\mu \longrightarrow 0$) in Appendix A.1, when $\alpha, \beta \longrightarrow 0$. Note that it is not possible to extract a closed form expression of T_c from Eq. (3.25). Therefore, a perturbative approach is used instead. One defines $T_c = T_c^{(0)} + \Delta T(\alpha) + \Delta T(\beta)$, to express the QG corrected T_c, where $\Delta T(\alpha) \propto \alpha$ and $\Delta T(\beta) \propto \beta$. The standard critical temperature $T_c^{(0)}$ is equal to that in Eq. (3.2) for $d = 3$. The QG corrected critical temperature, then reads as

$$T_c = \frac{2\pi\hbar^2}{k_B m\,\zeta(\frac{3}{2})^{2/3}}\,n^{2/3} - \alpha\frac{32\sqrt{8}\pi^3\hbar^3}{9k_B m\,\zeta(\frac{3}{2})^2}\,n + \beta\frac{100\pi^2\hbar^4\,\zeta(\frac{5}{2})}{k_B m\,\zeta(\frac{3}{2})^{7/3}}\,n^{4/3}\ , \tag{3.26}$$

where one can see that the QG corrections increase with increasing number density n and decreasing boson mass m. One can also see that higher order QG corrections ($\propto \beta$) have a stronger dependence on n. This is a direct consequence of terms of higher order in T_c from Eq. (3.25). The magnitude of the relative correction is then

$$\left|\frac{\Delta T}{T_c^{(0)}}\right| = \alpha_0 \frac{16\sqrt{8}\pi^2\hbar}{9 M_P c\, \zeta(\frac{3}{2})^{4/3}} n^{1/3} - \beta_0 \frac{50\pi\hbar^2\, \zeta(\frac{5}{2})}{(M_P c)^2\, \zeta(\frac{3}{2})^{5/3}} n^{2/3}\,, \tag{3.27}$$

where the definitions of α and β, found below Eq. (2.42), were used. The above increases with increasing n, but does not depend on the boson mass. This dependence is presented in Fig. 3.2 for a BEC of a helium gas, where the black line represents the current experimental precision, which will continue to improve with time. Eq. (3.27) differs from a similar result in Refs. [120, 121], where the relative correction decreases with increasing n as $|\Delta T/T_c^{(0)}| \propto \alpha_0/n^{1/3}$. Note that as the particle number increases in a given volume, the total energy approaches E_P, thus magnifying the QG effects [34]. This shows that the above result is perfectly reasonable.

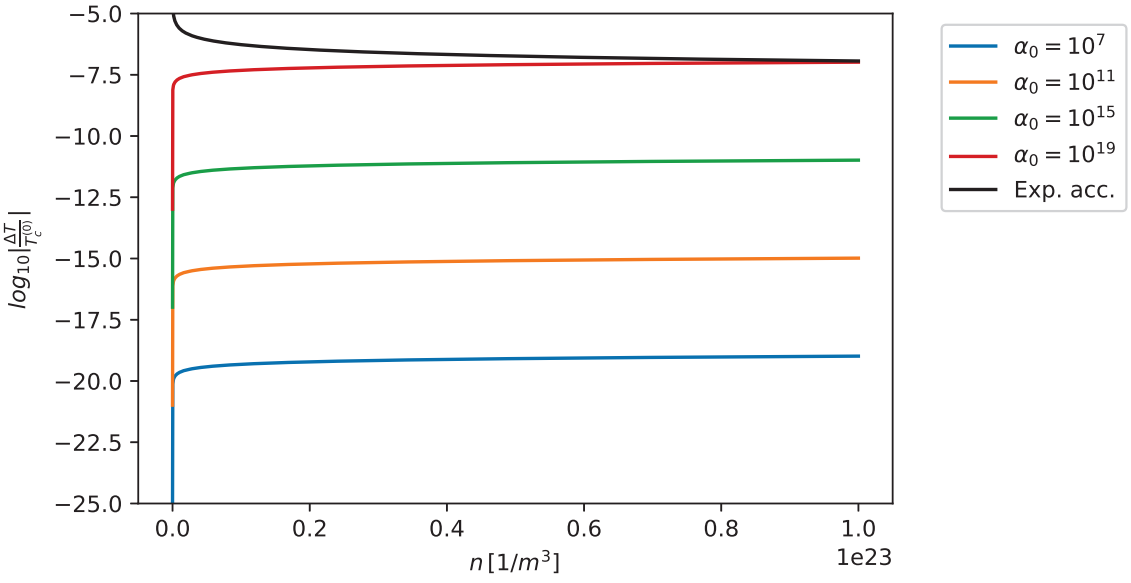

Figure 3.2: Relative temperature QG correction for a non-relativistic BEC, as a function of the number density n, at different values of parameter α_0, where $\beta_0 = \alpha_0^2$. The black line represents the experimental accuracy. The parameters of the example BEC are those of a helium gas.

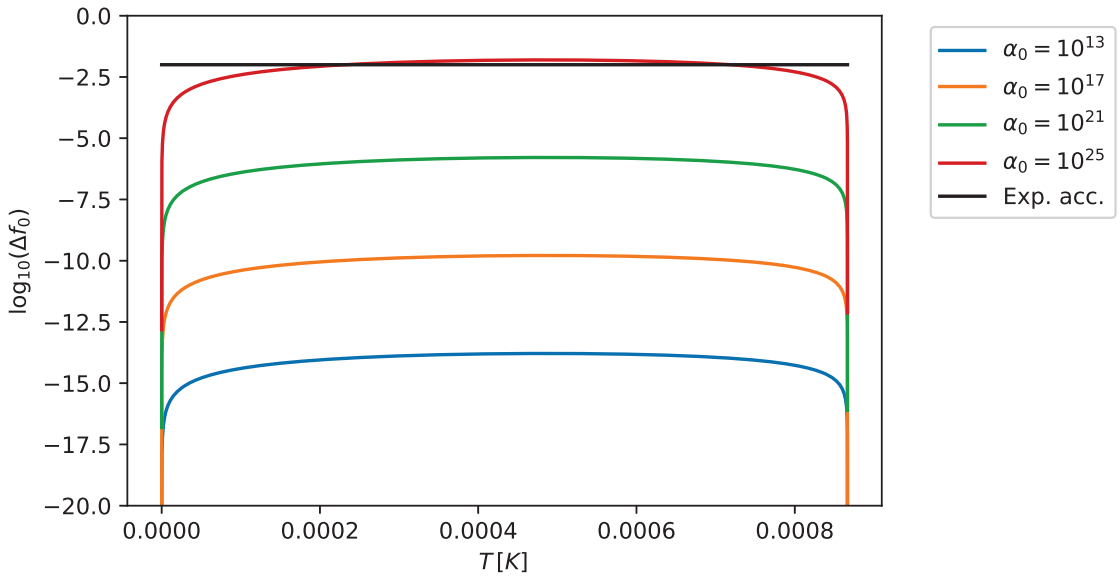

Figure 3.3: QG correction of f_0 for a non-relativistic BEC, as a function of the condensate temperature T, at different values of parameter α_0, where $\beta_0 = \alpha_0^2$. The black line represents the experimental accuracy. The parameters of the example BEC are those of a helium gas.

The second important observable is the fraction of bosons in the ground state. Following the derivation from Eq. (3.3), while using the number density from Eq. (3.25), the QG corrected fraction of bosons in the ground state for a non-relativistic BEC reads as

$$f_0 = 1 - \left(\frac{T}{T_c}\right)^{3/2} + \alpha_0 \frac{16\pi^{3/2}}{3\zeta(\frac{3}{2})} \frac{\sqrt{mk_B}}{M_P c} \left[\frac{T^{3/2}}{T_c} - \frac{T^2}{T_c^{3/2}}\right] - \beta_0 \frac{75\zeta(\frac{5}{2})}{2\zeta(\frac{3}{2})} \frac{mk_B}{(M_P c)^2} \left[\frac{T^{3/2}}{T_c^{1/2}} - \frac{T^{5/2}}{T_c^{3/2}}\right], \tag{3.28}$$

where one can see that a standard result from Eq. (3.3) is recovered for $\alpha_0, \beta_0 \longrightarrow 0$. Furthermore, one can see that at $T = T_c$, the QG corrections vanish and $f_0 = 0$, as expected, even when $\alpha_0, \beta_0 \neq 0$. This means that a deviation in fraction of bosons in the ground state, induced by QG effects, can be observed at temperatures $T < T_c$. The corrections terms from Eq. (3.28) are presented in Fig. 3.3 for a BEC of a helium gas. One can see that the correction has a maximum between absolute zero and the critical temperature T_c. It is

located at

$$T_m = \frac{9}{16}\,T_c - \frac{\beta_0}{\alpha_0}\,\frac{2025\,\zeta(\frac{5}{2})}{256\,\pi^{3/2}}\,\frac{\sqrt{m\,k_B}}{M_P\,c}\,T_c^{3/2}\ . \tag{3.29}$$

This suggests that experiments, able to measure the fraction of bosons in the ground state with high accuracy, would most likely observe QG signatures around temperature T_m.

Relativistic

For the relativistic case, the procedure outlined in Ref. [134] is followed to obtain the QG corrected energy spectrum of a relativistic boson in a three dimensional box. This is then used to obtain the relativistic density of states, the QG corrected critical temperature T_c, and fraction of bosons in the ground state f_0, for a relativistic BEC. Two distinct relativistic cases, mentioned in Section 3.1.2, are considered. In the first case, the neutral relativistic BEC is considered, and in the second case, the charged relativistic BEC is considered.

Relativistic scalar bosons (spin-0 particles) are described by the Klein-Gordon equation (see Eq. (1.6) in a flat space-time, $g^{\mu\nu} = \eta^{\mu\nu}$), which gives rise to the following effective relativistic Hamiltonian in the Feshbach-Villars formalism [134, 135, 136]

$$H_r = (\tau_3 + i\,\tau_2)\,\frac{p^2}{2\,m} + \tau_3\,m\,c^2\ , \tag{3.30}$$

where τ_i $(i = 1,2,3)$ are the Pauli matrices. Note that the Pauli matrices are not related to the spin of the particle in this context, but are used as a mathematical aid instead, to obtain the above classical-like Hamiltonian. The corresponding wave function satisfies the Schrödinger-like equation $i\,\hbar\,\partial_t \Psi = H_r \Psi$. The vector-like eigenfunctions Ψ of the effective Hamiltonian in Eq. (3.30), are given by a pair of scalar eigenfunctions φ and χ as

$$\Psi = \begin{bmatrix} \varphi \\ \chi \end{bmatrix}\ . \tag{3.31}$$

By defining the Klein-Gordon field as $\psi = \varphi + \chi$, and using the above definitions of H_r and Ψ, it is straightforward to show that ψ satisfies the Klein-Gordon equation

$$\frac{1}{c^2}\frac{\partial^2\psi}{\partial t^2} - \nabla^2\psi + \frac{m^2c^2}{\hbar^2}\psi = 0\ . \tag{3.32}$$

One can impose a three dimensional box potential $V(\mathbf{x})$, such as seen in the non-relativistic case, to H_r. This determines the boundary conditions for φ and χ, which are the same as for the non-relativistic wave function from Eq. (3.19). It turns out that the time dependent solutions for φ and χ, given H_r for a relativistic particle in a three dimensional box, are

$$\begin{aligned}
\varphi^{\pm}_{\mathbf{n}}(\mathbf{x}) &= \sqrt{\frac{8}{V}}\,\varphi^{\pm}_0(\mathbf{p})\,e^{\mp\frac{E}{\hbar}t}\sin\left(\frac{\pi n_x}{L_x}x\right)\sin\left(\frac{\pi n_y}{L_y}y\right)\sin\left(\frac{\pi n_z}{L_z}z\right)\\
\chi^{\pm}_{\mathbf{n}}(\mathbf{x}) &= \sqrt{\frac{8}{V}}\,\chi^{\pm}_0(\mathbf{p})\,e^{\mp\frac{E}{\hbar}t}\sin\left(\frac{\pi n_x}{L_x}x\right)\sin\left(\frac{\pi n_y}{L_y}y\right)\sin\left(\frac{\pi n_z}{L_z}z\right)\ ,
\end{aligned} \tag{3.33}$$

where $V = L_xL_yL_z$ is the volume of the box, $n_x, n_y, n_z \in \mathbb{N}$ the particle excitation quantum numbers and $\varphi^{\pm}_0(\mathbf{p})$, $\chi^{\pm}_0(\mathbf{p})$ relativistic momentum-dependent functions, which satisfy $(\varphi^{\pm}_0)^2 - (\chi^{\pm}_0)^2 = \pm 1$, with $\pm$ denoting particle and anti-particle solutions. Eq. (3.31) can then be rewritten in terms of Eq. (3.33) as $\Psi^{\pm}_{\mathbf{n}}(\mathbf{x})$. One can notice that the solutions in Eq. (3.33) are similar to those in the non-relativistic case from Eq. (3.19). They differ only by the relativistic momentum-dependent functions $\varphi^{\pm}_0(\mathbf{p})$ and $\chi^{\pm}_0(\mathbf{p})$.

To obtain the QG corrected energy spectrum of a relativistic particle in a box, one modifies the effective Hamiltonian H_r, using the transformation from Eq. (3.17), as

$$\begin{aligned}
H_{rQG} &= (\tau_3 + i\tau_2)\frac{p_0^2}{2m} + \tau_3 mc^2 - (\tau_3 + i\tau_2)\frac{\alpha}{m}p_0^3 + (\tau_3 + i\tau_2)\frac{5\beta}{2m}p_0^4\\
&\equiv H_{r0} + H_{r1} + H_{r2}\ ,
\end{aligned} \tag{3.34}$$

where one defines $H_{r0} = (\tau_3 + i\tau_2)\,p_0^2/2m + \tau_3 mc^2$, $H_{r1} = -(\tau_3 + i\tau_2)\,\alpha\,p_0^3/m$ and $H_{r2} = (\tau_3 + i\tau_2)\,5\beta\,p_0^4/2m$. The energy spectrum of a relativistic particle in a three dimensional

box, considering an unperturbed effective Hamiltonian H_{r0}, turns out to be

$$\varepsilon_{\mathbf{n}}^{(0)} = \pm\sqrt{\frac{c^2\hbar^2\pi^2}{L^2}\left(n_x^2+n_y^2+n_z^2\right)+m^2c^4}\,, \tag{3.35}$$

where $L = L_x = L_y = L_z$ was assumed, without loss of generality, and $\pm$ signifies the particle and anti-particle solutions. The energy spectrum in Eq. (3.35) is obtained by computing the eigenvalues of the H_{r0} operator, for the state $\Psi_{\mathbf{n}}^{\pm}$. To obtain the QG correction to the energy spectrum in Eq. (3.35), one considers the complete QG corrected, effective Hamiltonian H_{rQG} from Eq. (3.34), and uses the result from Appendix A.2. The QG corrected energy spectrum is then

$$\varepsilon_{\mathbf{n}} = \pm\sqrt{\hbar^2c^2k_{\mathbf{n}}^2 - 2\,\alpha\,\hbar^3c^2k_{\mathbf{n}}^3 + 5\,\beta\,\hbar^4c^2k_{\mathbf{n}}^4 + m^2c^4}\,, \tag{3.36}$$

which is obtained by computing the eigenvalues of the effective Hamiltonian H_{rQG}, for the state $\Psi_{\mathbf{n}}^{\pm}$. In the above, $k_{\mathbf{n}}^2 = \frac{\pi^2}{L^2}\left(n_x^2+n_y^2+n_z^2\right)$ was again used, and the $\pm$ sign plays no role in further considerations, since the square of Eq. (3.36) is used. Using the QG corrected energy spectrum for a particle in a three dimensional box, given by the relativistic relation in Eq. (3.36), and taking the continuum limit ($k_{\mathbf{n}} \longrightarrow k \implies \varepsilon_{\mathbf{n}} \longrightarrow \varepsilon$; see Appendix A.3), the QG corrected relativistic density of states reads as [130]

$$g(\varepsilon) = \frac{V\,\varepsilon\sqrt{\varepsilon^2-m^2c^4}}{2\pi^2\hbar^3c^3}\left(1+4\,\alpha\frac{1}{c}\sqrt{\varepsilon^2-m^2c^4}-\frac{25}{2}\,\beta\,\frac{1}{c^2}\left(\varepsilon^2-m^2c^4\right)\right)\,, \tag{3.37}$$

One can see that the above reduces to the usual relativistic density of states, given by Eq. (A.3) in Appendix A.1, when $\alpha, \beta \longrightarrow 0$. The above QG corrected density of states is central in predicting QG effects in relativistic statistical mechanics. It is used to modify the relativistic BEC observables in the following. It may be noted that the integrals, which take the form of Eq. (A.1) from Appendix A.1, cannot be expressed in closed form, when using the relativistic density of states from Eq. (3.37). However, they can be expressed in a

closed form in the ultra-relativistic limit, where $\varepsilon \gg mc^2$.

The number of particles in the system is obtained using Eq. (A.1) from Appendix A.1 and the QG corrected density of states from Eq. (3.37). The integral is evaluated in the ultra-relativistic limit at T_c, where $\mu \longrightarrow 0$, and divided by V to obtain the QG corrected number density for the neutral relativistic BEC as

$$\begin{aligned} n = \frac{N_{BE}^{UR-B}}{V} &= \frac{1}{2\pi^2\hbar^3c^3}\left[\int_0^\infty \frac{\varepsilon^2}{e^{\beta_{T_c}\varepsilon}-1}\,d\varepsilon + 4\frac{\alpha}{c}\int_0^\infty \frac{\varepsilon^3}{e^{\beta_{T_c}\varepsilon}-1}\,d\varepsilon - \frac{25}{2}\frac{\beta}{c^2}\int_0^\infty \frac{\varepsilon^4}{e^{\beta_{T_c}\varepsilon}-1}\,d\varepsilon\right] \\ &= \frac{1}{\pi^2\hbar^3c^3}\left[(k_BT_c)^3\,\zeta(3) + \frac{2\pi^4}{15}\frac{\alpha}{c}(k_BT_c)^4 - 150\frac{\beta}{c^2}(k_BT_c)^5\,\zeta(5)\right], \end{aligned} \tag{3.38}$$

and for the charged relativistic BEC as

$$\begin{aligned} n = \frac{N_{BE}^{UR-B\overline{B}}}{V} &= \frac{m}{2\pi^2\hbar^3c\,k_BT_c}\left[\int_0^\infty \frac{\varepsilon^2}{\cosh(\beta_{T_c}\varepsilon)-1}\,d\varepsilon + 4\frac{\alpha}{c}\int_0^\infty \frac{\varepsilon^3}{\cosh(\beta_{T_c}\varepsilon)-1}\,d\varepsilon\right. \\ &\left. - \frac{25}{2}\frac{\beta}{c^2}\int_0^\infty \frac{\varepsilon^4}{\cosh(\beta_{T_c}\varepsilon)-1}\,d\varepsilon\right] \\ &= \frac{m}{3\hbar^3c}\left[(k_BT_c)^2 + \frac{72}{\pi^2}\frac{\alpha}{c}(k_BT_c)^3\,\zeta(3) - 10\pi^2\frac{\beta}{c^2}(k_BT_c)^4\right], \end{aligned} \tag{3.39}$$

where one can see, that both cases retrieve the number densities as in the standard relativistic BECs [127], when $\alpha, \beta \longrightarrow 0$. Since it is also not possible to obtain a closed form of respective critical temperatures from Eqs. (3.38) and (3.39), a perturbative approach is used in the same way as in the non-relativistic case. The QG corrected critical temperatures then read as

$$T_c^B = \frac{\pi^{2/3}\hbar c}{k_B\,\zeta(3)^{1/3}}n^{1/3} - \alpha\frac{2}{45}\frac{\pi^{16/3}\hbar^2c}{k_B\,\zeta(3)^{5/3}}n^{2/3} + \beta\frac{50\pi^2\hbar^3c}{k_B}\frac{\zeta(5)}{\zeta(3)^2}n\,, \tag{3.40}$$

for the neutral relativistic BEC, and as

$$T_c^{B\overline{B}} = \frac{1}{k_B}\left(\frac{3\hbar^3c}{m}\right)^{1/2}n^{1/2} - \alpha\frac{108\,\hbar^3\zeta(3)}{\pi^2k_Bm}n + \beta\frac{15\pi^2}{k_B}\left(\frac{3\hbar^9}{m^3c}\right)^{1/2}n^{3/2}\,, \tag{3.41}$$

for the charged relativistic BEC, where one can see that the QG corrections increase with increasing number density n in both cases. In the charged case, the QG corrections increase with decreasing boson mass m, while the neutral case is independent of boson mass. One can also notice that higher order QG corrections have a stronger dependence on n, which is also seen in the non-relativistic case. The standard results from Eqs. (3.4) and (3.6), for $d = 3$, are recovered from Eqs. (3.40) and (3.41), when $\alpha, \beta \longrightarrow 0$. The magnitude of the relative correction of the critical temperature for the neutral case is

$$\left|\frac{\Delta T^B}{T_c^{(0)}}\right| = \alpha_0 \frac{2\pi^{14/3}\hbar}{45 M_P c \zeta(3)^{4/3}} n^{1/3} - \beta_0 \frac{50\pi^{1/2}\hbar^2 \zeta(5)}{(M_P c)^2 \zeta(3)^{5/3}} n^{2/3} , \tag{3.42}$$

while for the charged case, it is

$$\left|\frac{\Delta T^{B\bar{B}}}{T_c^{(0)}}\right| = \alpha_0 \frac{108\hbar^{3/2}\zeta(3)}{\sqrt{3}\pi^2 M_P c\sqrt{mc}} n^{1/2} - \beta_0 \frac{15\pi^2\hbar^3}{(M_P c)^2 mc} n , \tag{3.43}$$

where the definitions of α and β, found below Eq. (2.42), were used. From the above one can see that the relative correction increases only with increasing n and does not depend on m for the neutral case and increases with increasing n and decreasing m for the charged case. The relative corrections are presented in Fig. 3.4. One can see that the QG correction in the charged case requires a higher α_0 (about 5 orders of magnitude) to reach the same magnitude as the QG correction in the neutral case. In other words, the corrections are much smaller in the charged case.

One must address the second important observable, the fraction of bosons in the ground state, in context of relativistic BECs. Following the derivation from Eq. (3.3), while using the number densities from Eqs. (3.38) and (3.39), the QG corrected fraction of bosons in the ground state read as

$$f_0^B = 1 - \left(\frac{T}{T_c}\right)^3 + \alpha_0 \frac{2\pi^4}{15\zeta(3)} \frac{k_B}{M_P c^2} \left[\frac{T^3}{T_c^2} - \frac{T^4}{T_c^3}\right] - \beta_0 \frac{150\zeta(5)}{\zeta(3)} \frac{k_B^2}{M_P^2 c^4} \left[\frac{T^3}{T_c} - \frac{T^5}{T_c^3}\right] , \tag{3.44}$$

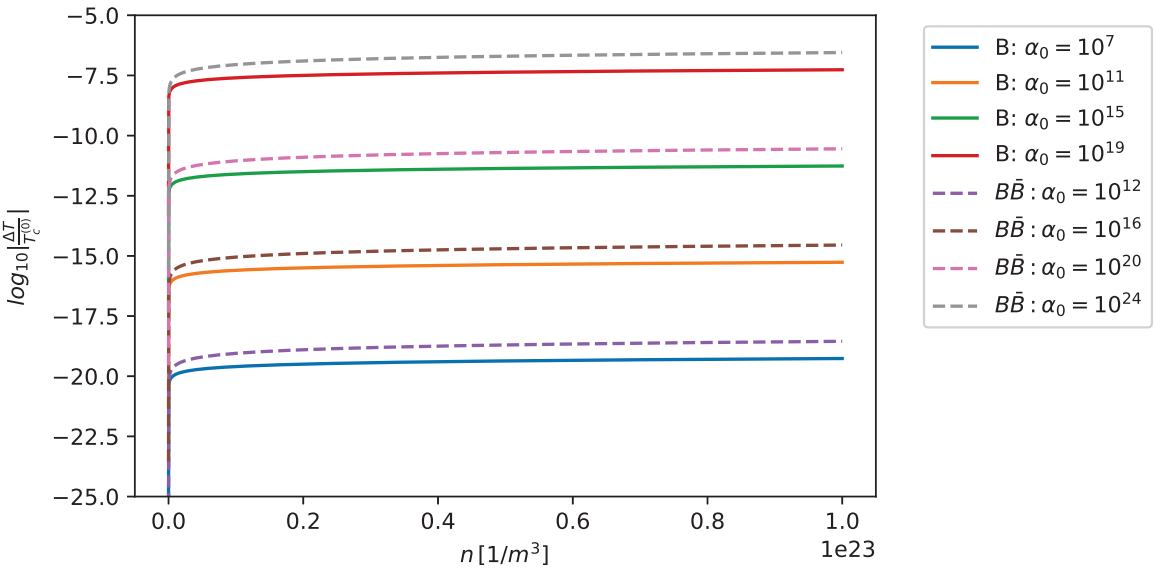

Figure 3.4: Relative temperature QG correction for a relativistic BEC, as a function of the number density n, at different values of parameter α_0, where $\beta_0 = \alpha_0^2$. The solid lines represent the neutral case and the dashed lines represent the charged case. The parameters of the example BEC are those of a helium gas.

for a neutral relativistic BEC, and as

$$f_0^{B\bar{B}} = 1 - \left(\frac{T}{T_c}\right)^2 + \alpha_0 \frac{72\,\zeta(3)}{\pi^2} \frac{k_B}{M_P c^2} \left[\frac{T^2}{T_c} - \frac{T^3}{T_c^2}\right] - \beta_0 \frac{10\pi^2 k_B^2}{M_P^2 c^4} \left[T^2 - \frac{T^4}{T_c^2}\right], \quad (3.45)$$

for a charged relativistic BEC. From the above, one can see that the standard results from Eqs. (3.5) and (3.7) are recovered, when $\alpha_0, \beta_0 \longrightarrow 0$. Note that at $T = T_c$ the QG corrections vanish and, as expected $f_0 = 0$, even when $\alpha_0, \beta_0 \neq 0$. Therefore, as in the non-relativistic case, the QG signatures in the fraction of bosons in the ground state can be observed for $T < T_c$.

The corrections terms from Eqs. (3.44) and (3.45) are presented in Fig. 3.5. Since only the charged case is dependent on the boson species, an example of a helium gas was chosen to plot it. In the same manner as in the non-relativistic case, one can see that the correction has a maximum between the absolute zero and the critical temperature T_c. It is located at

$$T_m^B = \frac{3}{4} T_c - \frac{\beta_0}{\alpha_0} \frac{3375\,\zeta(5)}{\pi^4} \frac{k_B}{M_P c^2} T_c^2 \quad (3.46)$$

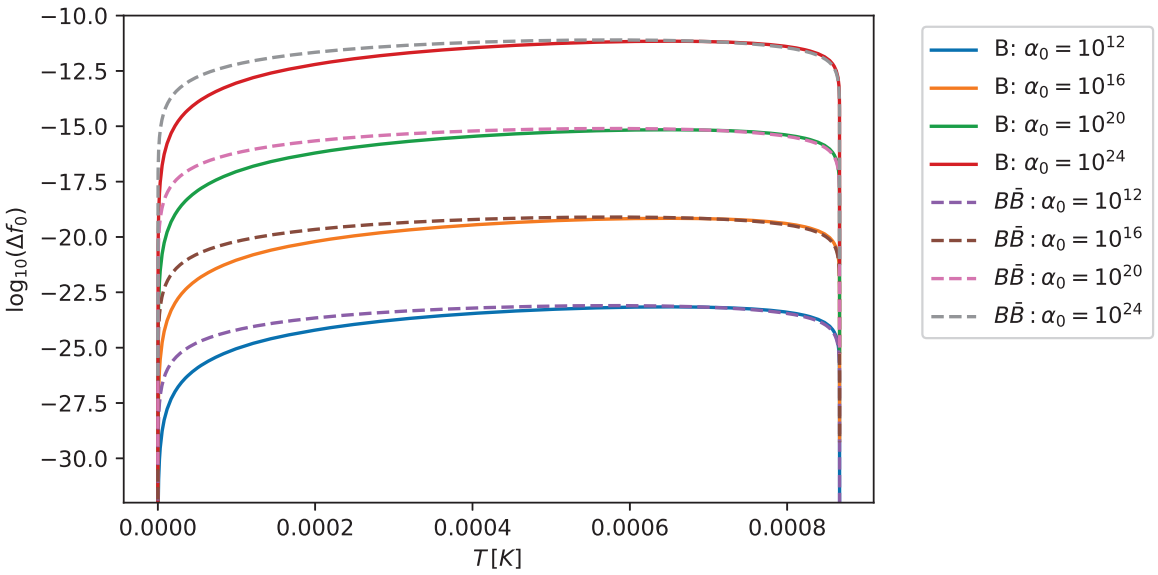

Figure 3.5: QG correction of f_0 for a relativistic BEC, as a function of the condensate temperature T, at different values of parameter α_0, where $\beta_0 = \alpha_0^2$. The solid lines represent the neutral case and the dashed lines represent the charged case. The parameters of the example BEC are those of a helium gas.

for the neutral case and

$$T_m^{B\bar{B}} = \frac{2}{3} T_c - \frac{\beta_0}{\alpha_0} \frac{5\pi^4}{54\,\zeta(3)} \frac{k_B}{M_P c^2} T_c^2 \tag{3.47}$$

for the charged case. This suggests that experiments, able to measure the fraction of bosons in the ground state for a relativistic BEC with high accuracy, would most likely observe QG signatures around temperature $T_m^{B,B\bar{B}}$.

Summary

In this section, six observables were considered, for which theoretical predictions of QG signatures are provided. These are the three critical temperatures from Eqs. (3.26), (3.40) and (3.41), and three fractions of bosons in the ground state from Eqs. (3.28), (3.44) and (3.45). Out of these possibilities, only the non-relativistic BEC can currently be realized in an experimental setup, and with ever-improving measurement precisions, one expects that such QG signatures may be observable in the future. One can also expect that relativistic

BECs will be possible to produce in experiments in the future, which will further increase the chances to measure potential QG signatures.

Currently, the detection threshold for critical temperatures is of the order $\sim 10^{-10}\,\mathrm{K}$ [131], which implies $\alpha_0 < 10^{19}$ when $\beta_0 = \alpha_0^2$ (the same holds when $\beta_0 \sim 0$), and $\beta_0 < 10^{46}$ for only quadratic QG corrections (i.e., $\alpha_0 = 0$). Since the attainable electroweak scale α_{EW} bounds the GUP parameters to $\alpha_0 < 10^{17}$ and $\beta_0 < 10^{34}$, the BEC bounds do not present an improvement and QG signatures are not expected to be observed in current BEC experiments. However, the theoretical framework provided here, should be useful to test QG, as experimental precisions improve.

The fraction of bosons in the ground state in a BEC is measured by integrating the measured velocity distribution within the ranges of velocities, where the gas is in the condensate state [137]. The precision of such a measurement is around 10^{-2}, i.e., about 1% [138, 139]. It is expected that this precision will increase with time as well, and reach a stage in the foreseeable future where the predicted effects will either be measurable, or one will be able to put strict bounds on the GUP parameters. The bounds on GUP parameters obtained by considering the precision of measuring the fraction of bosons in the ground state are $\alpha_0 < 10^{25}$ for $\beta_0 = \alpha_0^2$ (or $\beta_0 \sim 0$) and $\beta_0 < 10^{52}$ for $\alpha_0 = 0$. These bounds are not as good as the ones obtained using critical temperature. Therefore, measuring QG signatures with the fraction of bosons in the ground state is phenomenologically not yet as interesting.

3.2 Magnetometer Experiment

In this section, an approach to measure QG signatures in a magnetometer experiment is proposed. A magnetometer is a device, which can measure magnetic fields or dipole moments of atoms, depending on its purpose. A realization of the latter, where the interactions of nuclear spins with external magnetic fields are measured, is considered. It turns out that *optical magnetometers* are ideal to test fundamental physics, due to their high precision [140]. In optical magnetometer experiments, one uses light to measure the response of an-

gular momenta of atoms in an external magnetic field. In this context, the QG signatures are explored through GUP inspired modifications of the Larmor frequency of probed atoms. Specifically, QG modifications of the Larmor frequency of ^{129}Xe atoms are considered in detail. The ^{129}Xe species is chosen because it has non-zero nuclear spin, is stable and has a long relaxation time in normal conditions ($T = 20^{\circ}\,\mathrm{C}$ and $p = 1\,\mathrm{atm}$), which allows to make highly precise measurements. One of the methods to measure the Larmor frequency of such atoms is the two-photon laser spectroscopy, described in detail in Ref. [141].

The idea of the experiment is based on Refs. [140, 141, 142]. The ^{129}Xe atom in the ground state $5p^6\,{}^1S_0$ (see Ref. [143] for notation convention), with a quantum number of total angular momentum quantum number $F = 1/2$ (F is defined through the operator sum $\mathbf{F} = \mathbf{J} + \mathbf{I}$, where $\mathbf{J}$ is the total electron angular momentum and $\mathbf{I}$ the total nuclear angular momentum) and projection $m_F = -1/2$, is excited by a circularly polarized UV light with $\lambda_{UV} = 256\,\mathrm{nm}$ to the state $5p^5\,(^2P_{3/2})\,6p\,{}^2[5/2]_2$. This state then decays to one of two intermediate states $5p^5\,(^2P_{3/2})\,6p\,{}^2[3/2]_{1,2}$, which emits IR photons with wavelengths $\lambda_{IR1} = 905\,\mathrm{nm}$ and $\lambda_{IR2} = 993\,\mathrm{nm}$, respectively, before decaying back to the ground state. The ^{129}Xe atom has two ground state sublevels with $m_F = -1/2$ and $m_F = +1/2$, due to the hyperfine interaction. Probability that the above intermediate states decay to either of these sublevels is $1/2$. Since the $m_F = +1/2$ state cannot absorb the UV light, an ensemble of ^{129}Xe atoms will eventually become spin polarized, where all atoms are in the same spin state of $m_F = +1/2$. Then a uniform external magnetic field $\mathbf{B}$ is applied to induce the so-called *Larmor precession* of ^{129}Xe atoms. They start to oscillate between the $m_F = +1/2$ and $m_F = -1/2$ states with the corresponding Larmor frequency. As the UV light reinitiates the above excitation-decay process of atoms, which pass through the state $m_F = -1/2$, the IR emission starts to oscillate with the exact Larmor frequency of the ^{129}Xe atoms, which can be precisely measured. A similar experiment, considering two-photon laser spectroscopy of an ensemble of ^{129}Xe atoms, has been conducted by the authors in Ref. [144], where they use an atomic transition, different than the one described above.

To apply QG modifications to the Larmor frequency of an atom, one needs to consider contributions of electrons and the nucleus, which comprise the atom in question. From the ground state structure $5p^6\,{}^1S_0$ of the ^{129}Xe atom, one can see that the total electron angular momentum $\mathbf{J} = 0$, and the total angular momentum $\mathbf{F} = \mathbf{I}$. Therefore, the electrons do not provide a magnetic dipole moment and consequently do not contribute to the Larmor precession. Furthermore, the only cause of the magnetic dipole moment and the Larmor precession is the nucleus. To describe the interaction between the magnetic dipole moment of the nucleus and the external magnetic field $\mathbf{B}$, a suitably adapted Hamiltonian is considered [145, 146]

$$\begin{aligned} H_N &= H_{0N} - \mathbf{m}_N \cdot \mathbf{B} + \frac{e^2}{8\,m_p\,c^2} \sum_i (\mathbf{B} \times \mathbf{r_i})^2 \\ &\equiv H_{0N} + H_{BN} + H_{1N}\ , \end{aligned} \tag{3.48}$$

where H_{0N} is the Hamiltonian of the nucleus in the absence an external magnetic field, $\mathbf{m}_N$ the nuclear magnetic dipole moment operator, $e = +e_0$ the proton charge, m_p the proton mass and $\mathbf{r}_i$ the radius of proton i in the nucleus. The sum in the last term from Eq. (3.48) goes over all protons i in the nucleus. The notation of H_{BN} and H_{1N} in Eq. (3.48) is defined for convenience. It is useful to estimate the magnitudes of terms from Eq. (3.48), to have an idea which effects are expected to contribute most in the following considerations. The expectation value of the leading order term $\langle H_{0N} \rangle$ is clearly the largest of the three [145], and needs no further discussion in this context. However, the other two terms from Eq. (3.48) need to be examined carefully.

The magnitude of the H_{BN} term can be estimated by taking an experimentally plausible external magnetic field $\mathbf{B} = 1\,\mathrm{T}\,\hat{z}$ [142], assumed parallel to the nuclear spin orientation, and by evaluating the expectation value of the nuclear magnetic dipole operator $\mathbf{m}_N$ in the ground state of ^{129}Xe. This expectation value turns out as $\langle \mathbf{m}_N \rangle_{Xe} = g_{Xe}\,\mu_N\,I\,\hat{z}$, where g_{Xe} is the nuclear gyromagnetic factor for ^{129}Xe and $\mu_N = e\,\hbar/2\,m_p$ the nuclear magneton [145].

The magnitude of H_{BN} can then be estimated as

$$|\langle H_{BN}\rangle| = |g_{Xe}\mu_N I B| = 3.93\times10^{-27}\,\mathrm{J}\,, \tag{3.49}$$

where $g_{Xe} = -1.556$ [147], $I = F = 1/2$ and $\mu_N = 5.05\times10^{-27}\,\mathrm{J/T}$ were used. One can find the nuclear magnetic dipole moment of the ^{129}Xe atom as $\mu_{Xe} = g_{Xe}\mu_N I = -0.778\,\mu_N = -3.39\times10^{-27}\,\mathrm{J/T}$. The magnitude of the H_{1N} term can be estimated by the external magnetic field $\mathbf{B}$, assumed above, and a distribution of protons in the nucleus, which maximizes the contribution of this term. This provides a theoretical upper bound of the magnitude, which the H_{1N} term can contribute. Such a distribution of protons, which maximizes the H_{1N} term, is realized by assuming all protons are located in a circle on the surface of the nucleus ($|\mathbf{r}_i| \sim R_{Xe}$ for all i, where R_{Xe} is the radius of a ^{129}Xe nucleus), where this circle is perpendicular to the external magnetic field, i.e., $\mathbf{r}_i \perp \mathbf{B}$ for all i, which maximizes the cross products from H_{1N} in the ground state of ^{129}Xe. The radius of a stable ^{129}Xe nucleus is approximated by $R_{Xe} = R_0 A_{Xe}^{1/3} = 6.06\times10^{-15}\,\mathrm{m}$, where $R_0 = 1.2\times10^{-15}\,\mathrm{m}$ is an experimentally determined nuclear scale, and $A_{Xe} = 129$ the atomic mass number of ^{129}Xe [145]. Since the sum in H_{1N} goes only over the protons in the nucleus, there will be as much terms in the sum, as there is protons in the ^{129}Xe nucleus, which is $Z_{Xe} = 54$. The magnitude of H_{1N} can then be estimated as

$$|\langle H_{1N}\rangle| \lesssim \frac{e^2}{8\,m_p\,c^2}\,54\,B^2R_{Xe}^2 = \frac{27\,e_0^2}{4\,m_p\,c^2}\,B^2R_{Xe}^2 = 4.2\times10^{-56}\,\mathrm{J}\,, \tag{3.50}$$

where the accepted values for m_p, e_0 and c were used. One can then compare the contributions of the H_{BN} and H_{1N} terms, given by Eqs. (3.49) and (3.50), respectively, as

$$\frac{|\langle H_{1N}\rangle|}{|\langle H_{BN}\rangle|} \lesssim 10^{-29}\,, \tag{3.51}$$

from where it can be seen that the contribution of the H_{1N} term is more than 29 orders of

magnitude smaller than the contribution of the H_{BN} term. This implies the H_{1N} term can be safely neglected in further considerations. Given the estimation of the GUP parameters obtained in the following, the H_{1N} term is also negligible compared to the GUP correction terms.

3.2.1 Larmor Frequency and GUP

The QG corrections, motivated by GUP from Eq. (2.42), to the Larmor frequency of atoms, has been explored in detail in Ref. [48], where the analysis considers the Larmor precession of atoms, caused by the the total electron spin $\mathbf{J}$. However, for the purposes of the proposed ^{129}Xe experiment, one needs to generalize this analysis to include nuclear spin, since $\mathbf{J} = 0$ and $\mathbf{F} = \mathbf{I}$. It turns out that such a generalization is straightforward, following Ref. [48], where an arbitrary nucleus with a nuclear gyromagnetic factor g_{nuc} and a nuclear magnetic dipole moment $\mu_{nuc} = g_{nuc}\mu_N I$ is considered. To achieve this, one considers the nuclear Hamiltonian from Eq. (3.48), suitably modified by GUP through Eq. (3.17) and denoted by H_N^{QG}, while neglecting the H_{1N} term. The GUP corrected electron magnetic moment operator is replaced by a GUP corrected nuclear magnetic moment operator

$$\mathbf{m}_N = \mathbf{m}_{N0}\left(1 - \alpha\, p_0 + \beta\, p_0^2\right) , \tag{3.52}$$

where $\mathbf{m}_{N0} = -\dfrac{g_{nuc}\mu_N}{\hbar}\mathbf{I}$ and p_0 operators act on the nuclear wave function

$$\Psi_N(\mathbf{r},t) = \psi_N(\mathbf{r},t)\left[a(t)\,|+\rangle_N + b(t)\,|-\rangle_N\right] . \tag{3.53}$$

In the above $\psi_N(\mathbf{r},t)$ is the spatial part and the linear combination $a(t)\,|+\rangle_N + b(t)\,|-\rangle_N$ is the spin part, with $a(t)$ and $b(t)$ time dependent functions, which satisfy $|a(t)|^2 + |b(t)^2| = 1$. For a quantization axis $\hat{z}$, parallel to $\mathbf{B}$, it turns out that $m_{Nz}|+\rangle_N = \mu_{nuc}|+\rangle_N$ and $m_{Nz}|-\rangle_N = -\mu_{nuc}|-\rangle_N$. Considering the above generalizations, one solves the Schrödinger

equation $i\hbar\partial_t\Psi_N(\mathbf{r},t) = H_N^{QG}\Psi_N(\mathbf{r},t)$ (see also Eq. (1.1)), which splits in two equations

$$i\hbar\frac{\partial}{\partial t}\psi_N(\mathbf{r},t) = H_{0N}^{QG}\psi_N(\mathbf{r},t)\ , \tag{3.54}$$

and

$$\begin{aligned} i\hbar\frac{\mathrm{d}}{\mathrm{d}t}\left[a(t)\left|+\right\rangle_N + b(t)\left|-\right\rangle_N\right] = \\ -\mathbf{m}_{N0}\cdot\mathbf{B}\left(1-\alpha\, p_0+\beta\, p_0^2\right)\left[a(t)\left|+\right\rangle_N + b(t)\left|-\right\rangle_N\right]\ . \end{aligned} \tag{3.55}$$

It turns out that Eq. (3.54) is not relevant in describing the Larmor precession, and is therefore ignored in the following considerations. However, it can provide QG corrections to the nuclear shell model, which can be a topic for a future project. On the other hand, the solutions of $a(t)$ and $b(t)$ of Eq. (3.55) return harmonic solutions of the Larmor precession, which oscillate with a QG corrected Larmor frequency

$$\omega_L = -\frac{2\mu_{nuc}B}{\hbar}(1-\alpha\langle p\rangle+\beta\langle p^2\rangle)\ , \tag{3.56}$$

where the expectation values of powers of momentum p, are related to the nuclear spin $\mathbf{I}$ of the atom. In principle, one could additionally consider corrections arising from the internal structure of the nucleus, which would manifest as corrections to μ_{nuc}. Note that the above Larmor frequency takes the same shape as in Ref. [48], with the difference that μ_{nuc} refers to the magnetic dipole moment of the nucleus, and p is now related to the spin of the nucleus. Since p represents a measure of momentum, related to $\mathbf{I}$, it can be interpreted as the momentum of the nucleus up to leading order (see Ref. [148] for higher order corrections). Such a generalization can be done for any atom, where both, $\mathbf{J}\neq 0$ and $\mathbf{I}\neq 0$, cause the Larmor precession through the total spin $\mathbf{F}=\mathbf{J}+\mathbf{I}$. Eq. (3.56) remains the same, where the total magnetic dipole moment is just the sum of the electron and nuclear magnetic dipole moments $\mu_0 = \mu_{nuc}+\mu_e$, and p can be interpreted in the same way.

The velocities of atoms in the proposed experiment are expected to be non-relativistic [142] (see Section 3.2.2). Therefore, the expectation value of momentum and its square can be written in terms of the classical momentum as $\langle p\rangle = m\langle v\rangle$ and $\langle p^2\rangle = m^2\langle v^2\rangle$, respectively, where m is the mass of an atom, $\langle v\rangle$ the expectation value of its velocity and $\langle v^2\rangle$ the expectation value of the square of its velocity. Therefore, one can rewrite Eq. (3.56) as

$$\omega_L = \frac{2|\mu_0|B}{\hbar}(1-\alpha m\langle v\rangle + \beta m^2\langle v^2\rangle)\ , \tag{3.57}$$

where the absolute value $|\mu_0|$ is taken, without loss of generality, since only the magnitude of ω_L can be measured. For convenience, one can define the expectation value of the QG correction as $\langle C\rangle = \alpha m\langle v\rangle - \beta m^2\langle v^2\rangle$. The above Larmor frequency can then be simplified as

$$\omega_L = \frac{2|\mu_0|B}{\hbar}(1-\langle C\rangle)\ . \tag{3.58}$$

To discuss experimental implications of the above QG corrected Larmor frequency, one needs to quantify the magnitude of the QG correction $\langle C\rangle$ and compare it to the precision of the proposed experiment, quantified in the same manner. The magnitude of the relative QG correction is quantified by r as

$$\left|\frac{\delta\omega_L}{\omega_{L0}}\right|_{QG} = \langle C\rangle \equiv 10^{-r}\ , \tag{3.59}$$

where $r \in \mathbb{N}$ and $\omega_{L0} = 2|\mu_0|B/\hbar$. The above allows one to compare the QG corrections with the precision of the proposed experiment [142]

$$\left|\frac{\delta\omega_L}{\omega_{L0}}\right|_{exp} \simeq 10^{-15} \equiv 10^{-q}\ , \tag{3.60}$$

where $q = 15$ quantifies the experimental precision. The main idea of this discussion is to optimize the parameters α_0, β_0, m and v, in order to bring r as close to q as possible. The

same method for comparison with experimental precision in terms of r and q was used in Section 3.1.3. Such optimization provides an estimate of conditions, at which QG effects are most likely to be detected. Since Eq. (3.58) is valid for any atom, different species of atoms with different m and μ_0 are explored, while providing detailed estimates for the ^{129}Xe atom.

3.2.2 Thermal Distribution of Atom Velocities

In this section, QG signatures in measurements of the Larmor frequency, using ensembles of atoms, are explored. Since the considered magnetometer experiment is proposed to be conducted in normal conditions [142], the thermal velocity distribution of an ensemble of chosen atoms with masses m, is assumed to be the three dimensional Maxwell-Boltzmann (MB) distribution [123, 146]

$$f_v(v) = \left(\frac{m}{2\pi k_B T}\right)^{3/2} \exp\left(-\frac{m v^2}{2 k_B T}\right) 4\pi v^2 \,, \tag{3.61}$$

where $v \in [0,\infty)$. In the following, QG signatures are discussed in terms of average thermal velocities of atoms, suggested by $\langle C\rangle$, and in terms of individual velocities of atoms, described by $\langle C\rangle \longrightarrow C$. Note that $\langle C\rangle$ corresponds to a single particle. Therefore, for a distribution, C can take a range of values, as explained in detail later in this section.

Average Thermal Velocities

The provided version of QG corrections $\langle C\rangle = \alpha m \langle v\rangle - \beta m^2 \langle v^2\rangle$ suggests that it is natural to take the average thermal velocity $\langle v\rangle$ and the mean square of the velocity $\langle v^2\rangle$ of an atom in a thermalized ensemble, obtained from the MB distribution, to estimate the magnitude of $\langle C\rangle$. For convenience, one can approximately parameterize the atom mass with the atomic mass number A, as $m = A\, m_p$ [145]. Using this parameterization, one can write the average thermal velocity of species A at temperature T as

$$\begin{aligned}\langle v\rangle = \int_0^\infty v\, f_v(v)\,\mathrm{d}v &= \sqrt{\frac{8\,k_B T}{\pi m}} \\ &= \frac{1}{\sqrt{A}}\sqrt{\frac{8\,k_B T_{RT}}{\pi m_p}}\sqrt{\frac{T}{T_{RT}}} \\ &= \frac{1}{\sqrt{A}}\,\langle v_H\rangle_{RT}\sqrt{\frac{T}{T_{RT}}}\,,\end{aligned} \tag{3.62}$$

and the mean square of the velocity as

$$\begin{aligned}\langle v^2\rangle = \int_0^\infty v^2 f_v(v)\,\mathrm{d}v &= \frac{3\,k_B T}{m} \\ &= \frac{1}{A}\,\frac{3\,k_B T_{RT}}{m_p}\,\frac{T}{T_{RT}} \\ &= \frac{1}{A}\,\langle v_H^2\rangle_{RT}\,\frac{T}{T_{RT}}\,,\end{aligned} \tag{3.63}$$

which are given in terms of the average velocity and the mean square of the velocity of an ensemble of Hydrogen atoms at room temperature $T_{RT} = 20^\circ\,\mathrm{C}$ as $\langle v_H\rangle_{RT} \approx 2480\,\mathrm{m/s}$ and $\langle v_H^2\rangle_{RT} \approx 7.256\times 10^6\,\mathrm{m^2/s^2}$, respectively. Plugging Eqs. (3.62) and (3.63) in the definition of $\langle C\rangle$, and considering the parameterization of m, one obtains [149]

$$\langle C\rangle(\alpha_0,\beta_0;A,T) = \alpha_0\,\frac{\sqrt{A}\,m_p\,\langle v_H\rangle_{RT}}{M_P\,c}\sqrt{\frac{T}{T_{RT}}} - \beta_0\,\frac{A\,m_p^2\langle v_H^2\rangle_{RT}}{(M_P\,c)^2}\,\frac{T}{T_{RT}}\,, \tag{3.64}$$

where the definitions of α and β, found below Eq. (2.42), have been used. For clarity, the logarithm of Eq. (3.64) is shown in Fig. 3.6, as a monotonically increasing function of both, A and T, where $\beta_0 = \alpha_0^2$ is assumed. The dependence is shown for several different values of α_0. The black flat surface corresponds to the experimental precision. One can see that QG signatures can be detected if $\alpha_0 \approx 10^8$. In this case, the detection of QG signatures, using ^{129}Xe atoms with $A = A_{Xe} = 129$, would take place at $T \approx 560\,\mathrm{K}$, given Eq. (3.64).

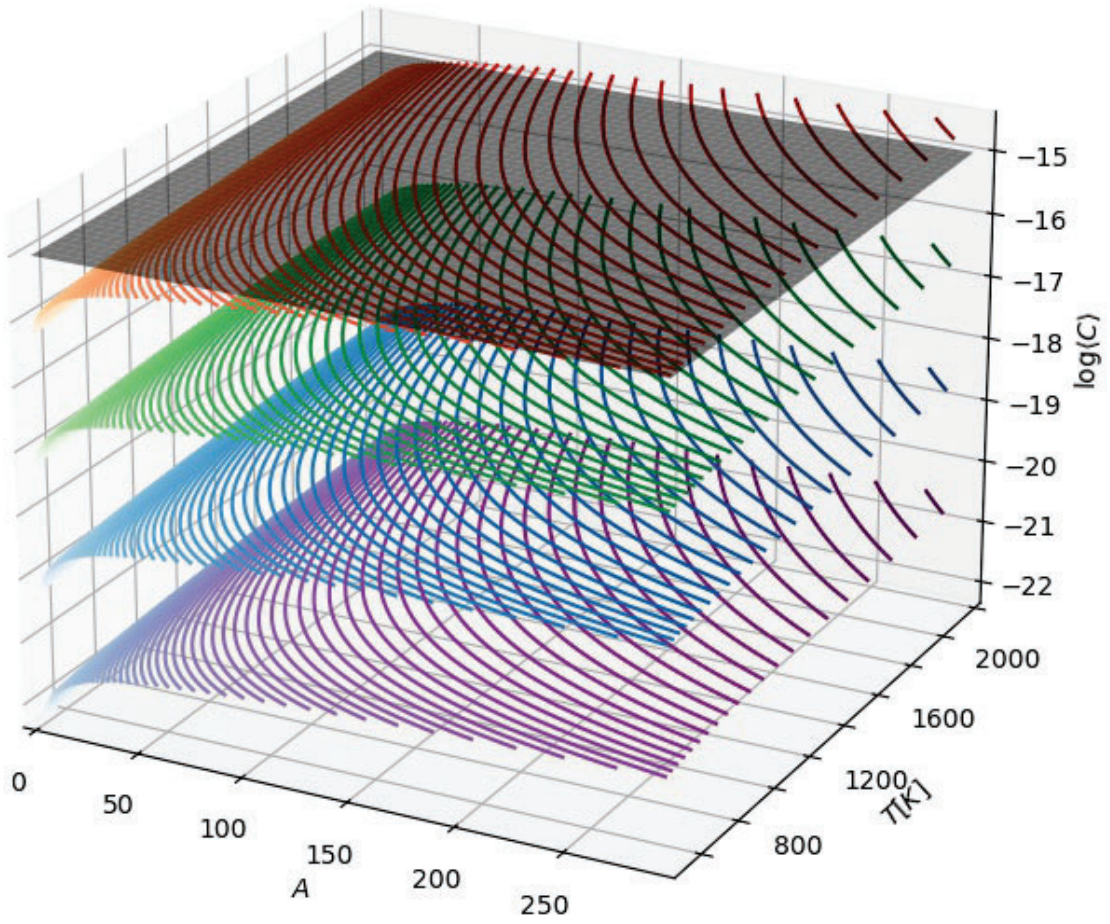

Figure 3.6: Logarithmic dependence of $\langle C \rangle$ on mass number A and temperature T for four different values of α_0; purple: $\alpha_0 = 10^2$, blue: $\alpha_0 = 10^4$, green: $\alpha_0 = 10^6$ and red: $\alpha_0 = 10^8$. The black flat surface is the experimental precision limit.

Distribution of Thermal Velocities

In the above, it was assumed that the expectation values in $\langle C \rangle$ refer to the averages of the whole distribution of atoms. However, Eq. (3.58) is derived for a single atom, which suggests that the expectation values $\langle p \rangle$ and $\langle p^2 \rangle$ correspond to the single particle momentum p and its square p^2 for that atom, and not to the averages of the whole ensemble. This single atom correspondence then implies $\langle C \rangle \longrightarrow C$, $\langle v \rangle \longrightarrow v$ and $\langle v^2 \rangle \longrightarrow v^2$. Therefore, it turns out that atoms are distributed over ranges of ω_L and C as well, since they are MB distributed over all velocities $v \in [0, \infty)$, following Eq. (3.61), resulting in a QG induced broadening of the Larmor frequency. To see this, one rewrites Eq. (3.57), considering the

single atom correspondence and atomic mass number parameterization, as

$$\omega_L = \omega_{L0}\left(1 - \alpha A\, m_p\, v + \beta A^2 m_p^2 v^2\right) . \tag{3.65}$$

For convenience, one can also rewrite the MB distribution from Eq. (3.61) in terms of the atomic mass number A as

$$f_v(v) = \left(\frac{m_p}{2\pi k_B T}\right)^{3/2} A^{3/2} \exp\left(-\frac{A\, m_p\, v^2}{2 k_B T}\right) 4\pi v^2 . \tag{3.66}$$

To obtain a QG corrected distribution of atoms over Larmor frequencies $f_\omega(\omega_L)$, given Eqs. (3.65) and (3.66), one makes the following change of variables

$$f_v(v)\,\mathrm{d}v = f_\omega(\omega_L)\,\mathrm{d}\omega_L \quad \Longrightarrow \quad f_\omega(\omega_L) = f_v(v)\left|\frac{\mathrm{d}v}{\mathrm{d}\omega_L}\right| . \tag{3.67}$$

The derivative $|\mathrm{d}v/\mathrm{d}\omega_L|$ on the right-hand side of Eq. (3.67) is obtained by solving Eq. (3.65) for

$$v = \frac{\alpha}{2\beta A\, m_p}\left(1 - \sqrt{1 + 4\,\frac{\beta}{\alpha^2}\left(\frac{\omega_L}{\omega_{L0}} - 1\right)}\right) , \tag{3.68}$$

where only the $-$ solution was considered, since the $+$ solution does not recover the standard result $\omega_L = \omega_{L0}$ for $v = 0$, and deriving v over ω_L, which then reads as

$$\left|\frac{\mathrm{d}v}{\mathrm{d}\omega_L}\right| = \frac{1}{\alpha A\, m_p\, \omega_{L0}} \frac{1}{\sqrt{1 + 4\,\frac{\beta}{\alpha^2}\left(\frac{\omega_L}{\omega_{L0}} - 1\right)}} . \tag{3.69}$$

By using Eqs. (3.68) and (3.69) in the change of variables from Eq. (3.67), the distribution of atoms over ω_L, is obtained for the first time, as [149]

$$f_\omega(\omega_L) = \left(\frac{1}{2\pi A m_p k_B T}\right)^{3/2} \exp\left(-\frac{\alpha_0^2 (M_P c)^2}{\beta_0^2} \frac{\left(1-\sqrt{1+4\frac{\beta_0}{\alpha_0^2}\left(\frac{\omega_L}{\omega_{L0}}-1\right)}\right)^2}{8 A m_p k_B T}\right)$$
$$\times \pi \frac{\alpha_0 (M_P c)^3}{\beta_0^2 \omega_{L0}} \frac{\left(1-\sqrt{1+4\frac{\beta_0}{\alpha_0^2}\left(\frac{\omega_L}{\omega_{L0}}-1\right)}\right)^2}{\sqrt{1+4\frac{\beta_0}{\alpha_0^2}\left(\frac{\omega_L}{\omega_{L0}}-1\right)}}\,, \tag{3.70}$$

where the definitions of α and β, found below Eq. (2.42), have been used. From the above distribution, one can obtain, for the first time, the standard phenomenological quantities, similarly as with the MB distribution, such as the most probable Larmor frequency (at the peak of the distribution; $\mathrm{d}f_\omega/\mathrm{d}\omega_L = 0$)

$$\omega_{L,\mathrm{peak}} = \omega_{L0}\left(1-\alpha_0\frac{\sqrt{2 A m_p k_B T}}{M_P c}+\beta_0\frac{2 A m_p k_B T}{(M_P c)^2}\right)\,, \tag{3.71}$$

the average Larmor frequency

$$\langle\omega_L\rangle = \int_{\omega_{L0}}^{\infty}\omega_L\, f_\omega(\omega_L)\,\mathrm{d}\omega_L = \omega_{L0}\left(1-\alpha_0\frac{\sqrt{8 A m_p k_B T}}{\sqrt{\pi} M_P c}+\beta_0\frac{3 A m_p k_B T}{(M_P c)^2}\right)\,, \tag{3.72}$$

and the mean square of the Larmor frequency

$$\begin{aligned}\langle\omega_L^2\rangle &= \int_{\omega_{L0}}^{\infty}\omega_L^2\, f_\omega(\omega_L)\,\mathrm{d}\omega_L \\ &= \omega_{L0}^2\left(1-\alpha_0\frac{2}{M_P c}\sqrt{\frac{8 A m_p k_B T}{\pi}}+(\alpha_0^2+2\beta_0)\frac{3 A m_p k_B T}{(M_P c)^2}\right. \\ &\qquad \left.-\alpha_0\beta_0\sqrt{\frac{8}{\pi}}\frac{8\,(A m_p k_B T)^{3/2}}{(M_P c)^3}+\beta_0^2\frac{15 A^2 m_p^2 k_B^2 T^2}{(M_P c)^4}\right)\,.\end{aligned} \tag{3.73}$$

One can see that the correction terms in Eq. (3.72) correspond exactly to Eq. (3.64), if expressed in terms of $\langle v_H\rangle_{RT}$ and $\langle v_H^2\rangle_{RT}$. However, this consideration provides more

information, since now one has the distribution $f_\omega(\omega_L)$.

For detailed phenomenological research, where different GUP models are considered, one can straightforwardly reduce Eq. (3.70) to obtain $f_\omega(\omega_L)$ for such models. For the linear GUP model ($\beta_0 \longrightarrow 0$), the above distribution turns out as [149]

$$f_\omega^{\text{Lin}}(\omega_L) = \left(\frac{1}{2\pi A m_p k_B T}\right)^{3/2} \exp\left(-\frac{(M_P c)^2}{\alpha_0^2}\frac{\left(\frac{\omega_L}{\omega_{L0}}-1\right)^2}{2A m_p k_B T}\right) \times 4\pi\frac{(M_P c)^3}{\alpha_0^3\,\omega_{L0}}\left(\frac{\omega_L}{\omega_{L0}}-1\right)^2, \tag{3.74}$$

for which $\omega_{L,\text{peak}}^{\text{Lin}}$ and $\langle\omega_L\rangle^{\text{Lin}}$ are those from Eqs. (3.71) and (3.72), respectively, when $\beta_0 \longrightarrow 0$. Next, for the quadratic GUP model ($\alpha_0 \longrightarrow 0$), the distribution from Eq. (3.70) turns out as [149]

$$f_\omega^{\text{Quad}}(\omega_L) = \left(\frac{1}{2\pi A m_p k_B T}\right)^{3/2} \exp\left(-\frac{(M_P c)^2}{\beta_0}\frac{\left(\frac{\omega_L}{\omega_{L0}}-1\right)}{2A m_p k_B T}\right) \times 2\pi\frac{(M_P c)^3}{\beta_0^{3/2}\,\omega_{L0}}\sqrt{\frac{\omega_L}{\omega_{L0}}-1}\,, \tag{3.75}$$

for which $\omega_{L,\text{peak}}^{\text{Quad}}$ and $\langle\omega_L\rangle^{\text{Quad}}$ are those from Eqs. (3.71) and (3.72), respectively, when $\alpha_0 \longrightarrow 0$.

From Eqs. (3.71) and (3.72) one can see that the peak and mean of the Larmor frequencies are shifted with respect to the standard theory Larmor frequency ω_{L0}, as long as $T > 0$. Furthermore, Eq. (3.70) implies a broadening of the measured Larmor frequency, due to thermal motion of atoms. With increasing α_0 and β_0, the deviation of ω_L from ω_{L0} gets larger and the width of the distribution gets broader, and vice-versa. Increasing the temperature T and the atomic mass number A, provide the same effect on the distribution. Since the distribution of QG corrections, described by Eq. (3.70), is so close to ω_{L0}, the sampling of such small steps of ω_L is not possible with current computing power. Therefore,

it is more convenient to visualize the distribution of atoms over QG corrections C instead, where

$$C = \alpha_0 \frac{A m_p v}{M_P c} - \beta_0 \frac{A^2 m_p^2 v^2}{(M_P c)^2} = \left| \frac{\delta\omega_L}{\omega_L} \right| \equiv \left| \frac{\delta\omega}{\omega} \right| \tag{3.76}$$

is the new distribution variable. To achieve this, the same procedure used to derive Eq. (3.70) is followed. The corresponding change of variables is

$$f_C(C) = f_v(v) \left| \frac{\mathrm{d}v}{\mathrm{d}C} \right| , \tag{3.77}$$

which implies the replacement

$$\frac{\omega_L}{\omega_{L0}} - 1 \implies \frac{\delta\omega}{\omega} \tag{3.78}$$

of all such factors in distributions from Eqs. (3.70), (3.74) and (3.75), and does not include the ω_{L0} factor in the denominator. These distributions then respectively read as [149]

$$f_C\left(\frac{\delta\omega}{\omega}\right) = \left(\frac{1}{2\pi A m_p k_B T}\right)^{3/2} \exp\left(-\frac{\alpha_0^2 (M_P c)^2}{\beta_0^2} \frac{\left(1 - \sqrt{1 + 4\frac{\beta_0}{\alpha_0^2}\left(\frac{\delta\omega}{\omega}\right)}\right)^2}{8 A m_p k_B T} \right)$$
$$\times \pi \frac{\alpha_0 (M_P c)^3}{\beta_0^2} \frac{\left(1 - \sqrt{1 + 4\frac{\beta_0}{\alpha_0^2}\left(\frac{\delta\omega}{\omega}\right)}\right)^2}{\sqrt{1 + 4\frac{\beta_0}{\alpha_0^2}\left(\frac{\delta\omega}{\omega}\right)}} , \tag{3.79}$$

for $\alpha_0, \beta_0 \neq 0$,

$$f_C^{\mathrm{Lin}}\left(\frac{\delta\omega}{\omega}\right) = \left(\frac{1}{2\pi A m_p k_B T}\right)^{3/2} \exp\left(-\frac{(M_P c)^2}{\alpha_0^2} \frac{\left(\frac{\delta\omega}{\omega}\right)^2}{2 A m_p k_B T} \right)$$
$$\times 4\pi \frac{(M_P c)^3}{\alpha_0^3} \left(\frac{\delta\omega}{\omega}\right)^2 , \tag{3.80}$$

for $\alpha \neq 0$ and $\beta_0 = 0$, and

$$f_C^{\text{Quad}}\left(\frac{\delta\omega}{\omega}\right) = \left(\frac{1}{2\pi A m_p k_B T}\right)^{3/2} \exp\left(-\frac{(M_P c)^2}{\beta_0}\frac{\frac{\delta\omega}{\omega}}{2A m_p k_B T}\right) \times 2\pi \frac{(M_P c)^3}{\beta_0^{3/2}}\sqrt{\frac{\delta\omega}{\omega}}\,, \tag{3.81}$$

for $\alpha_0 = 0$ and $\beta_0 \neq 0$. The QG induced broadening, implied by Eq. (3.79), for an ensemble of ^{129}Xe atoms, $A = 129$, is shown in Fig. 3.7, for different values of α_0 and temperatures $T = 400\,\text{K}$ (top) and $T = 1200\,\text{K}$ (bottom), where $\beta_0 = \alpha_0^2$ was assumed. For various choices of the parameter α_0, the heights of the peaks of the distributions differ by several orders of magnitude. Therefore, to present and compare them in the same figure, they are normalized, such that each peak assumes a maximum value of unity. Notice that for $\alpha_0 \gtrsim 10^8$, the peak is close to, or even crosses the projected sensitivity of the magnetometer. Fig. 3.7 can be interpreted in the following way. The horizontal axis represents the magnitude of QG corrections, while the vertical axis represents the fraction of atoms. Given a thermal distribution of atoms and α_0, the average magnitude of the QG signature will be localized around the peak of the distribution, since most of the atoms display this deviation, due to their movement with speeds near the average speed $\langle v\rangle$. Furthermore, since the horizontal axis is in a logarithmic scale, the broadening of the distribution is much higher for larger values of α_0 and T.

For a better visualization of the broadening, the measures of the second moment (standard deviation) and the Full Width Half Maximum (FWHM) of the distribution are considered. The second moment of the distribution from Eq. (3.70) is [149]

$$\begin{aligned}\sigma_\omega^2 &= \int_{\omega_{L0}}^{\infty} (\omega_L - \langle\omega_L\rangle)^2 f_\omega(\omega_L)\,\mathrm{d}\omega_L \\ &= \alpha_0^2\left(3 - \frac{8}{\pi}\right)\frac{\omega_{L0}^2 A m_p k_B T}{(M_P c)^2} - \alpha_0\beta_0\sqrt{\frac{8}{\pi}}\frac{2\omega_{L0}^2 (A m_p k_B T)^{3/2}}{(M_P c)^3} \\ &\quad + \beta_0^2 \frac{6\omega_{L0}^2 A^2 m_p^2 k_B^2 T^2}{(M_P c)^4}\,.\end{aligned} \tag{3.82}$$

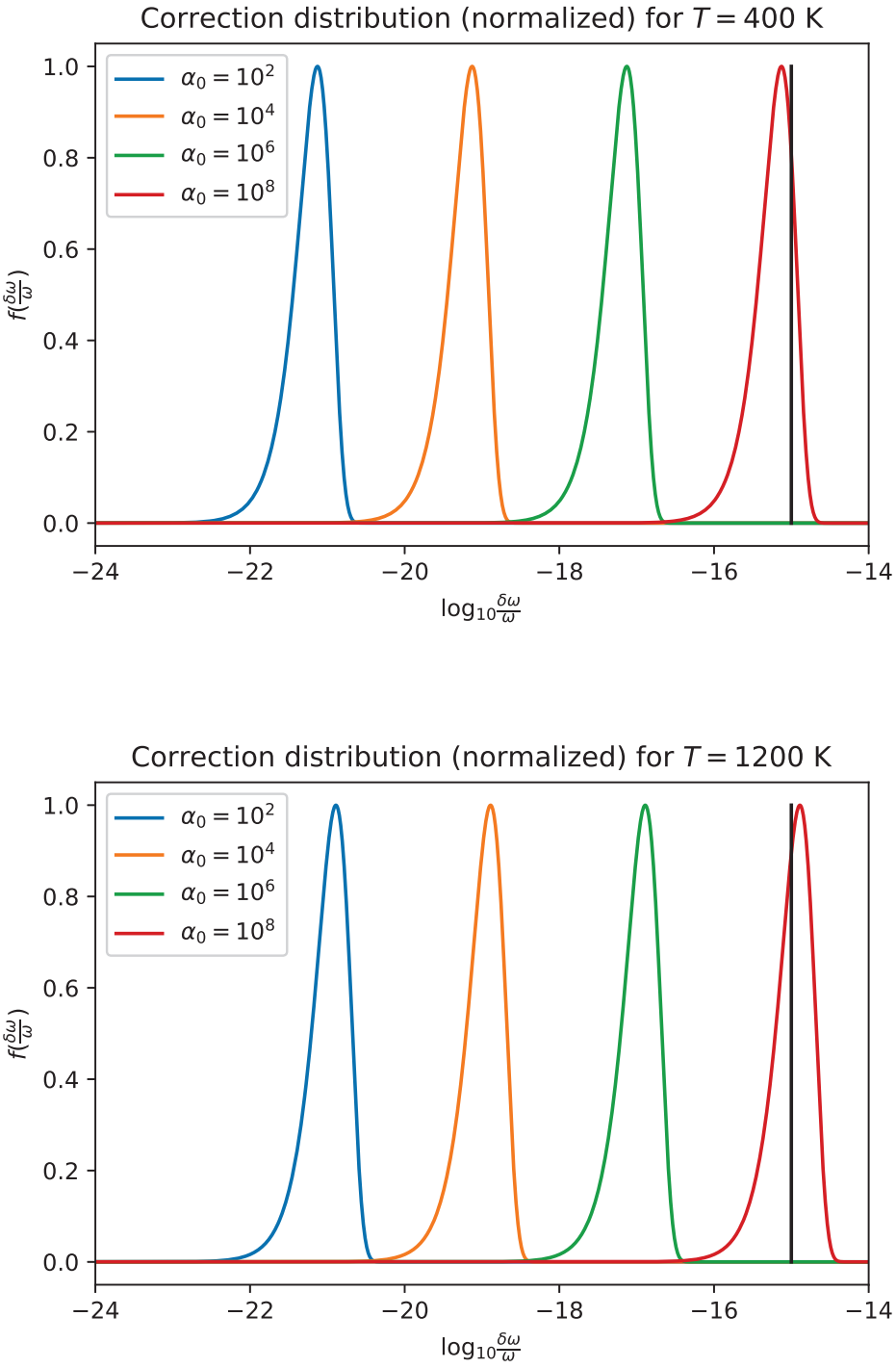

Figure 3.7: Distributions of ^{129}Xe atoms over $\delta\omega/\omega$ for different values of α_0, at temperatures $T = 400\,\mathrm{K}$ (top) and $T = 1200\,\mathrm{K}$ (bottom). The black vertical line is the experimental precision limit.

From the above one can see that such broadening is caused entirely by QG effects, since as $\alpha_0, \beta_0 \longrightarrow 0$, the σ_ω^2 vanishes. On the other hand, the FWHM of the distribution is obtained as

$$\mathrm{FWHM}_\omega = \omega_{L_2}^{\mathrm{FWHM}} - \omega_{L_1}^{\mathrm{FWHM}} \,, \tag{3.83}$$

where $\omega_{L_1}^{\mathrm{FWHM}}$ and $\omega_{L_2}^{\mathrm{FWHM}}$ are values, corresponding to both sides of the distribution at the half of its maximum. These values are obtained from Eq. (3.70), by solving the following equation

$$f_\omega\left(\omega_{L_{1,2}}^{\mathrm{FWHM}}\right) = \frac{f_\omega\left(\omega_{L,\mathrm{peak}}\right)}{2} \,. \tag{3.84}$$

The above has no closed form solution for $\omega_{L_1}^{\mathrm{FWHM}}$ and $\omega_{L_2}^{\mathrm{FWHM}}$. However, it is still possible to obtain these values numerically, by the following procedure. A short manipulation of Eq. (3.84) provides a transcendental equation [149]

$$\begin{aligned} &\frac{\alpha_0^2\,(M_P\,c)^2}{\beta_0^2}\,\frac{\mathcal{G}_{1,2}^2}{8A\,m_p\,k_B T} + \ln\left(4\,\frac{\beta_0^2}{\alpha_0^2\,(M_P\,c)^2}\,\frac{A\,m_p\,k_B T}{1-2\,\frac{\beta_0}{\alpha_0\,(M_P\,c)}\sqrt{2A\,m_p\,k_B T}}\right) - 1 \\ &= \ln\left(\frac{\mathcal{G}_{1,2}^2}{1-\mathcal{G}_{1,2}}\right) \,, \end{aligned} \tag{3.85}$$

where

$$\mathcal{G}_{1,2} = 1 - \sqrt{1 + 4\,\frac{\beta_0}{\alpha_0^2}\left(\frac{\omega_{L_{1,2}}^{\mathrm{FWHM}}}{\omega_{L0}} - 1\right)} \,. \tag{3.86}$$

The above transcendental equation can be numerically solved for $\mathcal{G}_{1,2}$. Note that one would have also arrived at Eq. (3.85), by using distribution Eq. (3.79). To solve Eq. (3.85), one

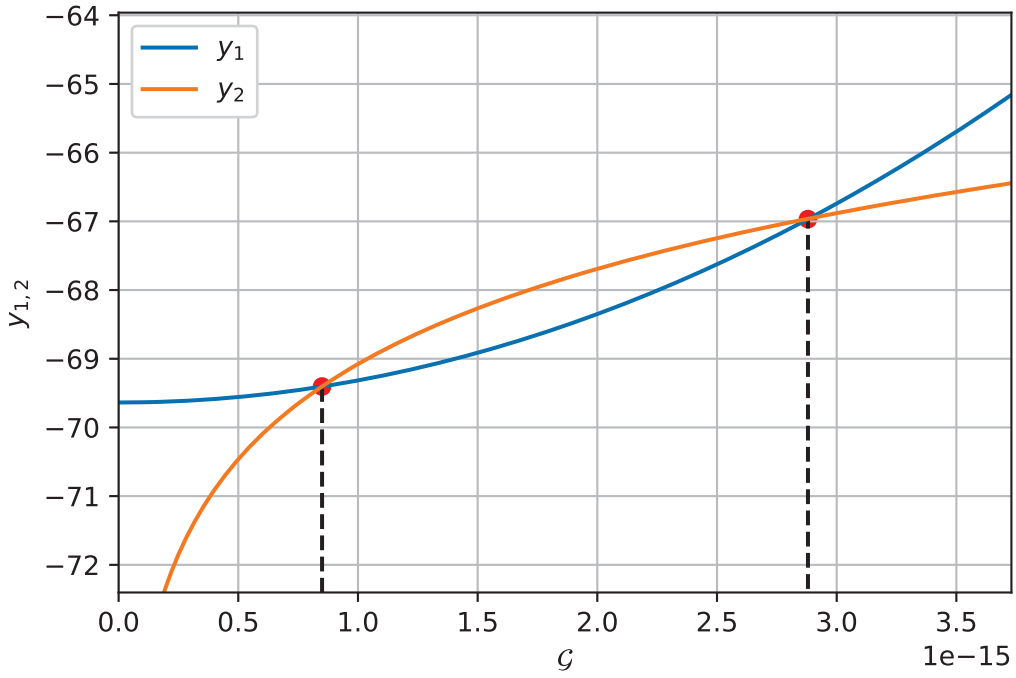

Figure 3.8: Intersection points of y_1 and y_2, for an example of an ensemble of ^{129}Xe atoms. $A = 129$, at $T = 560\,\mathrm{K}$ for $\alpha_0 = 10^8$.

needs to split it in two functions

$$y_1 = \frac{\alpha_0^2 (M_P c)^2}{\beta_0^2} \frac{\mathcal{G}_{1,2}^2}{8 A m_p k_B T} + \ln\left(4 \frac{\beta_0^2}{\alpha_0^2 (M_P c)^2} \frac{A m_p k_B T}{1 - 2 \frac{\beta_0}{\alpha_0 (M_P c)} \sqrt{2 A m_p k_B T}} \right) - 1 \quad (3.87)$$

$$y_2 = \ln\left(\frac{\mathcal{G}_{1,2}^2}{1 - \mathcal{G}_{1,2}} \right), \quad (3.88)$$

and plot them in the same graph. They are expected to intersect at two points, where $y_1 = y_2$, which are the solutions for $\mathcal{G}_{1,2}$. An example of this is shown in Fig. 3.8 for the relevant case of an ensemble of ^{129}Xe atoms at $T = 560\,\mathrm{K}$ and for $\alpha_0 = 10^8$, where $\beta_0 = \alpha_0^2$ was assumed. It is then straightforward to obtain $\omega_{L_1}^{\mathrm{FWHM}}$ and $\omega_{L_2}^{\mathrm{FWHM}}$ from the obtained values of $\mathcal{G}_{1,2}$, using Eq. (3.86). The FWHM for the above ^{129}Xe case turns out as $\mathrm{FWHM}_\omega \simeq 1.5 \times 10^{-7}\,\mathrm{Hz}$. Note that the FWHM values for distributions from Eqs. (3.70) and (3.79) are related by $\mathrm{FWHM}_\omega = \omega_{L0}\,\mathrm{FWHM}_C$. Therefore, one can also evaluate $\mathrm{FWHM}_C \simeq 2 \times 10^{-15}$, which does not rely on the actual value of ω_{L0}.

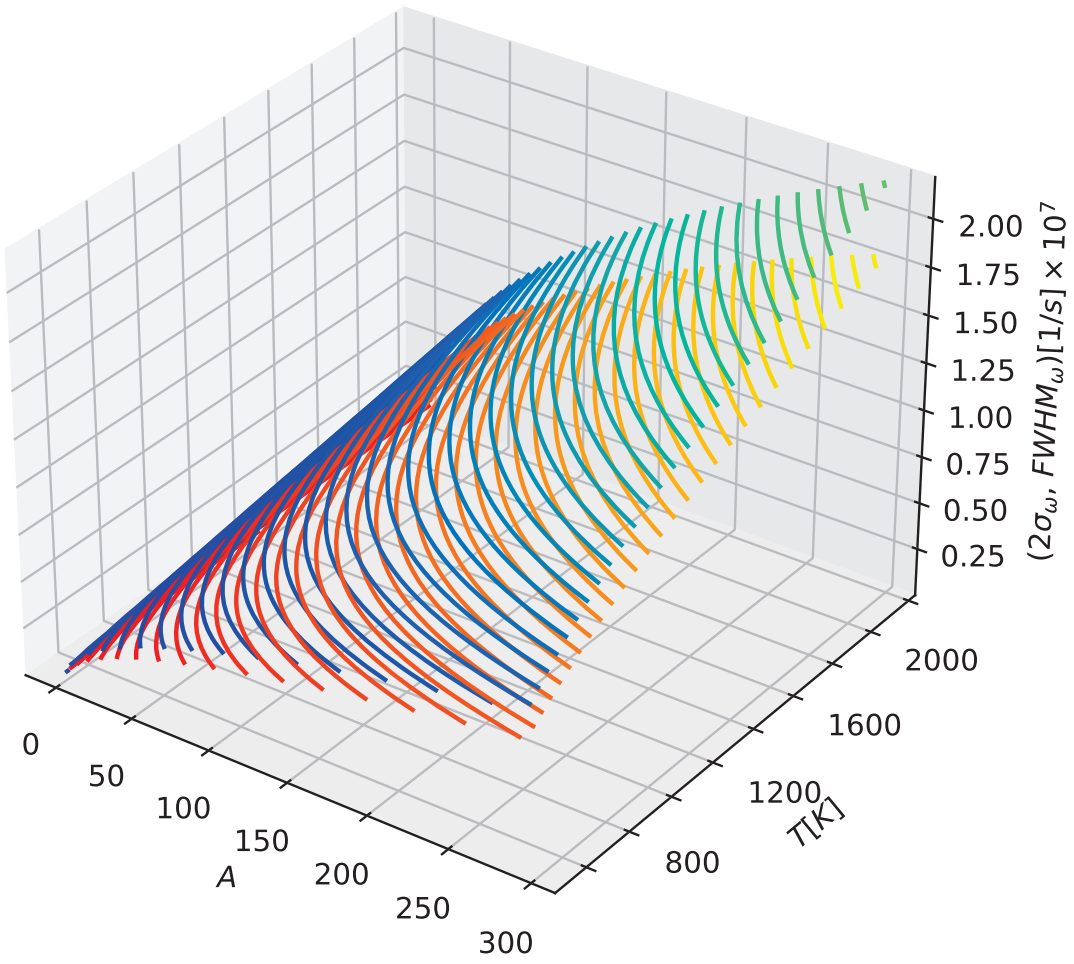

Figure 3.9: Full width half maximum FWHM_ω (blue-cyan) and standard deviation σ_ω (red-yellow) of the Larmor frequency distribution, as a function of atomic mass number A and temperature T, at $\alpha_0 = 10^8$.

The FWHM_ω is obtained, as described above, for a range of atomic mass numbers A and temperatures T, at the relevant $\alpha_0 = 10^8$, and shown in Fig. 3.9, alongside $2\sigma_\omega$ (see Eq. (3.82)). Note the factor 2 in front of σ_ω. It is there to provide a measure of width, since σ_ω alone is a measure of deviation from the average. One can see that both, $2\sigma_\omega$ and FWHM_ω scale approximately as a square root in both, A and T, and that they are of the same order of magnitude at a given parameter α_0, where the FWHM_ω is slightly greater. This is expected, since FWHM_ω is the width of the distribution at half of its maximum value, and $2\sigma_\omega$ is the width of the distribution at a slightly higher value than that of half maximum, which makes

it slightly narrower. For the projected experimental precision $q = 15$, the line broadening for $\alpha_0 = 10^8$ is within reach of detection.

3.2.3 Non-Thermal Distribution of Atom Velocities

In the previous sections, QG signatures induced by thermal distributions of ensembles of atoms were considered. While such considerations provide promising results, they are limited by the temperature dependence of QG signatures, which are expected to increase with temperature. This is because high temperatures induce thermal noise and can therefore decrease the precision of the experiment. Since QG signatures in Larmor frequencies depend on the velocities of atoms, one can introduce methods, other than thermal motion, to control the velocities. For a non-thermal distribution of velocities, one can write the QG correction as

$$\langle C \rangle (\alpha_0, \beta_0; A, v) = \alpha_0 \frac{A\, m_p\, v}{M_P\, c} - \beta_0 \frac{A^2 m_p^2 v^2}{(M_P\, c)^2} \,. \tag{3.89}$$

For clarity, the logarithm of Eq. (3.89) is shown in Fig. 3.10, as a monotonically increasing function of both, A and v, where $\beta_0 = \alpha_0^2$ is assumed. The dependence is shown for several different values of α_0. The black flat surface corresponds to the experimental precision. One can again see that QG signatures can be detected if $\alpha_0 \approx 10^8$. In this case, the detection of QG signatures, using ^{129}Xe atoms with $A = A_{Xe} = 129$, would take place at $v \approx 300\,\mathrm{m/s}$, given Eq. (3.89). Note that Fig. 3.10 is similar to Fig. 3.6. This is expected, since the same form of $\langle C \rangle$ is used, with the difference that in Fig 3.6 the velocity is taken to be thermal.

One of the methods to induce non-thermal motion of atoms is convection, where a current of atoms is passed through a duct. Once the flow is stationary, one can use the two-photon laser spectroscopy method, to measure the Larmor frequency of atoms. For the purposes of the proposed experiment, a velocity distribution of an incompressible, viscous

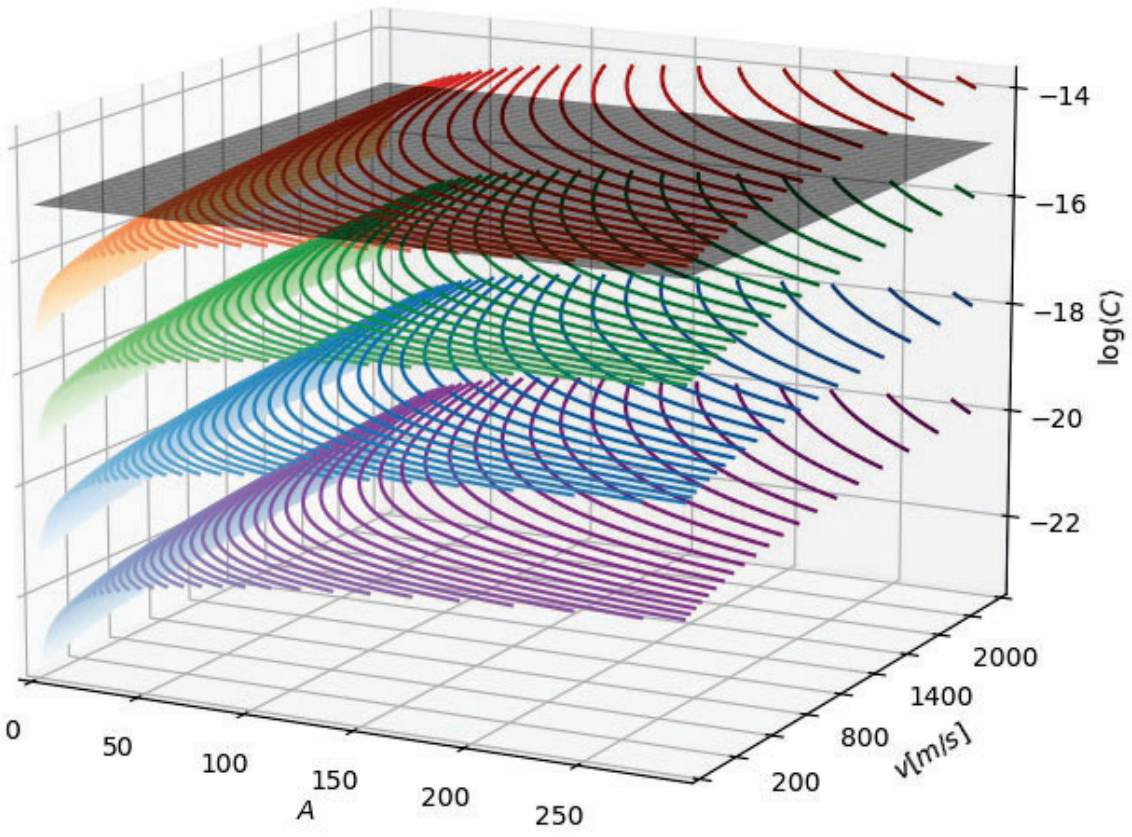

Figure 3.10: Logarithmic dependence of $\langle C \rangle$ on mass number A and atom velocity v for four different values of α_0; purple: $\alpha_0 = 10^2$, blue: $\alpha_0 = 10^4$, green: $\alpha_0 = 10^6$ and red: $\alpha_0 = 10^8$. The black flat surface is the experimental precision limit.

fluid in a square duct is assumed [150]

$$v = v_{max}\left[1-\left(\frac{x}{a/2}\right)^2\right]\left[1-\left(\frac{y}{a/2}\right)^2\right], \tag{3.90}$$

where v_{max} is the maximum velocity in the centre of the duct and a is the length of the inner side of the duct. Eq. (3.90) is then inserted in Eq. (3.57) to obtain the QG corrected Larmor frequency, as a function of v_{max}, and the position x and y inside the duct as [149]

$$\omega_L(x,y) = \omega_{L0}\left(1-\alpha_0\frac{A m_p v_{max}}{M_P c}\left[1-\left(\frac{x}{a/2}\right)^2\right]\left[1-\left(\frac{y}{a/2}\right)^2\right] + \beta_0\frac{A^2 m_p^2 v_{max}^2}{(M_P c)^2}\left[1-\left(\frac{x}{a/2}\right)^2\right]^2\left[1-\left(\frac{y}{a/2}\right)^2\right]^2\right). \tag{3.91}$$

A maximum QG induced deviation of the Larmor frequency is located at the centre of the duct, where $x = y = 0$. In this case, $\langle C \rangle$ follows Eq. (3.89) for $v = v_{max}$ (see Fig. 3.10). The same holds for any location (x,y) in the duct, where v from Eq. (3.90) is considered. However, such point measurements are not possible in actual experimental applications. Therefore, two possible scenarios are considered in the following, namely an average measurement in a line perpendicular to the duct and an average measurement in the total cross section of the duct.

In the case where the Larmor frequency is measured in a line which runs perpendicularly through the duct, one needs to average Eq. (3.91) over either of the (x,y) dimensions as

$$\begin{aligned}\omega_L(x) &= \frac{1}{a}\int_{-a/2}^{a/2} \omega_L(x,y)\,\mathrm{d}y \\ &= \omega_{L0}\left(1 - \alpha_0 \frac{2A\,m_p\,v_{max}}{3M_P\,c}\left[1-\left(\frac{x}{a/2}\right)^2\right]\right. \\ &\qquad \left. + \beta_0 \frac{8A^2 m_p^2\,v_{max}^2}{15\,(M_P\,c)^2}\left[1-\left(\frac{x}{a/2}\right)^2\right]^2\right)\,, \end{aligned} \tag{3.92}$$

from where one can see that the maximum deviation is obtained for $x = 0$. In the case where the Larmor frequency is measured over the whole cross section area of the duct, then one needs to average Eq. (3.91) over both, x and y, as

$$\begin{aligned}\overline{\omega}_L &= \frac{1}{a^2}\int_{-a/2}^{a/2}\int_{-a/2}^{a/2} \omega_L(x,y)\,\mathrm{d}x\,\mathrm{d}y \\ &= \omega_{L0}\left(1 - \alpha_0 \frac{4A\,m_p\,v_{max}}{9M_P\,c} + \beta_0 \frac{64A^2 m_p^2\,v_{max}^2}{225\,(M_P\,c)^2}\right)\,. \end{aligned} \tag{3.93}$$

One can see from Eqs. (3.92) and (3.93) that in either choice of measurements, QG signatures will approximately be described by Eq. (3.89). The only difference is in the value of the particle velocity, which is of order $v \approx v_{max}$. It is not trivial to determine which of the above two applications would work best in an actual experimental setup, due the non-linear dependence of the atomic transition rate on intensity, and the dependence on the number of

atoms in the illuminated volume [142].

3.2.4 Summary

The predicted QG signatures by either thermal or non-thermal velocities are promising. It turns out that the Larmor frequency of an atom obtains QG corrections at non-vanishing velocities. In this section, detailed considerations were provided in the case of thermal movement of atoms, described by the MB distribution, and in the case of convection currents. Given the projected experimental precision of the magnetometer, using ^{129}Xe atoms, one can observe QG signatures for $\alpha_0 = 10^8$ in both cases. However, if QG signatures are not observed, this experiment will set an unprecedented bound $\alpha_0 < 10^8$. It will improve the electroweak bound, set by $\alpha_{EW} = 10^{17}$, by nine orders of magnitude.

Chapter 4

Cosmology

"We are like butterflies who flutter for a day and think it is forever."

Carl Sagan

Cosmology is a field of study, which concerns with the origin, evolution, structure and the fate of the Universe. While a significant amount of QGP research is related to Earth-based experiments (see Chapter 3) and Astrophysics [50, 54, 58, 61, 64, 70, 71, 74, 76, 77, 78, 151, 152, 153, 154], it is not as widely studied in cosmology. However, due to the unique observations which cannot be recreated in Earth-based experiments, cosmology is emerging as an important field in QGP [75, 76, 81, 84, 155, 156, 157, 158, 159, 160, 161, 162].

Contrary to Earth-based experiments, one cannot control the conditions and parameters of cosmological events and needs to solely rely on observations of such events, as they naturally occur. However, this does not present a significant drawback, as one may expect. Cosmological observations provide a range of measurements of phenomena, which cannot be explained, using standard theories of QT and GR. Since QG is believed to have played a key role in the early stages of the Universe, it is reasonable to expect that the observed anomalous phenomena are remnants of such QG effects. Therefore, it can provide a rich ground for testing QG theories.

In this chapter, new QGP results from cosmology are presented. Specifically, viable explanations of the observed EDGES anomaly (see Section 4.1) and the observed Baryon Asymmetry in the Universe (see Section 4.2), are provided. The EDGES anomaly is ex-

plored in terms of modified dispersion relations, and the Baryon Asymmetry is explored in terms of GUP.

4.1 The EDGES Anomaly

The *Experiment to Detect the Global Epoch-of-reionisation Signature* (EDGES) is a radio observatory, located in western Australia, which aims to detect signatures of neutral hydrogen in the early stages of the Universe. It is designed to probe the so-called reionisation epoch, when the first stars were formed, through the absorption of radiation due to the 21-cm hyperfine hydrogen transition. Specifically, as the UV light, emitted from the first stars in the Universe, interacted with the primordial gas, it changed the ground state excitation of hydrogen atoms. This happened due to the hyperfine splitting of energy levels, induced by coupling between electronic and nuclear spins. The energy difference between the hyperfine levels of the ground state, corresponds to the energy of a photon with wavelength $\lambda = 21\,\text{cm}$ (see Appendix B.1 for more details). A population of hydrogen atoms in the primordial gas is expected to absorb the Cosmic Microwave Background (CMB) photons with this wavelength and produce an absorption line in the CMB spectrum [163].

Recently, the EDGES collaboration has reported an unexpected result [164]. In the redshift range $z \in (15, 20)$, they found an anomalous absorption profile in the radio spectrum of the CMB, with a brightness temperature minimum at redshift $z = z_E \simeq 17.2$, which has a magnitude of about a factor of two greater than predicted by the Lambda Cold Dark Matter (ΛCDM) model. In this section, an explanation of this anomaly is proposed, using Modified Dispersion Relations (MDRs). More precisely, MDRs are used to modify the thermal spectrum of photons, which is applied to CMB, where the anomaly was observed. This modification can be used to predict other effects in the CMB, such as the deviation of the measured CMB temperature from the predicted value. Supporting material for this section is found in Appendices A.1 and B.

The general form of the MDRs reads as [35, 118, 165]

$$E^2 f(E/E_P)^2 - p^2 c^2 g(E/E_P)^2 = m^2 c^4 \,, \tag{4.1}$$

where $f(E/E_P)$ and $g(E/E_P)$ are the modification (rainbow) functions (see Section 2.1.4, and Refs. [166, 167, 168, 169, 170, 171, 172, 173] for more details). As shown in the following, whenever $f, g \neq 1$, i.e., one deviates from the standard relativistic dispersion relation, the Planck radiation spectrum changes as well. It turns out that the standard MDRs do not adequately explain the EDGES anomaly. However, by imposing redshift dependent MDR parameters, or by imposing a non-trivial power dependence for the MDRs (see Ref. [174]), one can provide a viable explanation.

4.1.1 Modification of Thermal Spectrum

As shown in Section 2.1.4, MDRs are related to the modified Heisenberg commutator, which is predicted by various theories of QG (see Chapter 2), and have the general form of Eq. (4.1). The modification functions can in general be expressed in a power series expansion (MacLaurin series) as $f(E/E_P) = \sum_{n=0}^{\infty} \frac{f^{(n)}(0)}{n!} (E/E_P)^n$ and $g(E/E_P) = \sum_{n=0}^{\infty} \frac{g^{(n)}(0)}{n!} (E/E_P)^n$, where constraints $f(0) = 1$ and $g(0) = 1$ must be imposed to obtain the standard relativistic dispersion relation at low energies. Several interesting special cases are considered in the following.

- Case 1: $f(E/E_P) = 1$ and $g(E/E_P) = \sqrt{1 - \eta (E/E_P)^{\omega}}$, which is one of the most studied in literature. In the above, η is a parameter which signifies the effective scale of the modification, and ω is the order of the modification. In general, the modifications for different values of η and ω can be studied. In particular, three special cases are considered. The first case is compatible with LQG and non-commutative space-time [7, 175], while the next two are compatible with the linear and quadratic GUP, respectively [176, 177]:

i) $\omega = 1$ and $\eta > 0 \Longrightarrow f(E/E_P) = 1$ and $g(E/E_P) = \sqrt{1-\eta(E/E_P)}$,

ii) $\omega = 1$ and $\eta = \mp 2\alpha_0 \Longrightarrow f(E/E_P) = 1$ and $g(E/E_P) = \sqrt{1 \pm 2\alpha_0(E/E_P)}$,

iii) $\omega = 2$ and $\eta = 2\beta_0 \Longrightarrow f(E/E_P) = 1$ and $g(E/E_P) = \sqrt{1-2\beta_0(E/E_P)^2}$,

where restrictions on α_0 from Ref. [176] have been relaxed to include both positive and negative values. In general, $f(E/E_P) \neq 1$ and, specifically, in the presence of a strong gravitational field $f(E/E_P) = 1/\sqrt{-g_{00}}$, where g_{00} is the 00 component of the metric [176, 177]. However, in the reionization epoch, most of the hydrogen gas was practically in a vanishing gravitational field, since the first gravitational objects just started to form. Therefore, one can safely assume $f(E/E_P) = 1$, as far as space-time curvature corrections to the MDR are concerned.

- Case 2: $f(E/E_P) = \frac{\exp(\alpha(E/E_P))-1}{\alpha(E/E_P)}$ and $g(E/E_P) = 1$, proposed for explaining the spectra from Gamma Ray Bursts at cosmological distances [101]. Note that α here is different than the linear GUP parameter.

- Case 3: $f(E/E_P) = 1$ and $g(E/E_P) = [1+(\lambda E)^\gamma]^\delta = [1+\lambda'(E/E_P)^\gamma]^\delta$, with $\lambda' = (\lambda E_P)^\gamma$. For $\delta = 1/2$ and $\lambda = -\eta$, one recovers Case 1. The special case $\delta = 1$ has been proposed for models in which a varying speed of light occurs [93], while the special case $\gamma = \delta = 1$ has been proposed in Refs. [41, 178]. It turns out that GUP, including linear and quadratic terms, with $\beta_0 = \alpha_0^2$, is a general case for the latter [177]:

  i) $\delta = 1, \gamma = 1$ and $\lambda' = \pm\alpha_0 \Longrightarrow f(E/E_P) = 1$ and $g(E/E_P) = 1 \pm \alpha_0(E/E_P)$.

In the above, η, α_0, β_0, α and λ' are dimensionless parameters, where α_0 and β_0 are the linear and quadratic GUP parameters, respectively, defined after Eq. (2.42). It is often assumed that η, α_0, β_0, α, $\lambda' \sim O(1)$, by candidate QG theories (see Chapter 1). However, in the same way as discussed in Chapter 2 for α_0 and β_0, such a restriction on η, α and λ',

may be relaxed as well. Therefore, one can set a common upper bound $\eta \sim \alpha_0 \sim \sqrt{\beta_0} \sim \alpha \sim \lambda' < \alpha_{EW} = 10^{17}$ (see Section 2.2).

To demonstrate how the thermal spectrum of photons is affected by the above modifications, one writes the MDR, given by Eq. (4.1) in the case where $m = 0$, as

$$E^2 - p^2 c^2 F^2 = 0 \,, \quad \text{where } F = \frac{g}{f} \,. \tag{4.2}$$

Using the above, one may derive the modified thermal spectrum of photons ρ_{MDR}, following Refs. [93, 178]. The density of states per volume for photons (which have 2 polarization states, i.e., degrees of freedom) is obtained as

$$\Omega(p) = 2\,\frac{g_{ds}(p, m=0)}{V} = \frac{p^2}{\pi^2 \hbar^3} \,, \tag{4.3}$$

where $g_{ds}(p, m=0)$ is the relativistic density of states for massless particles (see Eq. (A.3) in Appendix A.1). By making a change of variables $\Omega(E)\,\mathrm{d}E = \Omega(p)\,\mathrm{d}p$, considering the MDR in Eq. (4.2), one obtains

$$\Omega(E) = \frac{E^2}{\pi^2 \hbar^3 \hat{c}^2 \tilde{c}} \,, \tag{4.4}$$

where the above two "speeds" turn out as

$$\hat{c} = \frac{E}{p} = cF \quad \text{and} \quad \tilde{c} = \frac{\mathrm{d}E}{\mathrm{d}p} = \frac{cF}{1 - \frac{F'E}{F}} \,, \tag{4.5}$$

and $F' = \frac{\mathrm{d}F}{\mathrm{d}E}$. Therefore, one can write the modified density of states per volume as

$$\Omega(E) = \frac{E^2}{\pi^2 \hbar^3 c^3} \frac{1}{F^3} \left| 1 - \frac{F'E}{F} \right| \,. \tag{4.6}$$

Note that the above is analogous to Eq. (3.37) from the BEC considerations in Chapter 3.

Since photons are bosons, their modified thermal spectrum is obtained using[3] $\rho_{MDR}(T,E) = 2\pi\hbar E\, f_{BE}(E)\,\Omega(E)$, where $f_{BE}(E)$ is the BE distribution (see Eq. (A.4) in Appendix A.1). It reads as

$$\rho_{MDR}(E,T) = \rho(E,T)\frac{1}{F^3}\left|1 - \frac{F'E}{F}\right| \equiv \rho(E,T)\,R\,, \tag{4.7}$$

where

$$\rho(E,T) = \frac{2}{\pi\hbar^2 c^3}\frac{E^3}{e^{\beta_T E} - 1} \tag{4.8}$$

is the standard thermal distribution of photons and R is the correction factor, formally defined in the following section. Note that the standard result from Eq. (4.8) is obtained from Eq. (4.7) when the MDR parameters vanish, i.e., η, α_0, β_0, α, $\lambda' \longrightarrow 0$.

4.1.2 Experimental Bounds

The 21-cm cosmology is related to the history of the Universe, and represents a novel framework for probing fundamental physics [181] (see also Refs. [182, 183, 184, 163, 185, 186, 187, 188, 189, 190]). In this section, the effects of the modified thermal spectrum of photons, given by Eq. (4.7), on the 21-cm cosmology (see Appendix B.1) are explored. In particular, the anomaly, recently discovered by the EDGES collaboration [164] (see also Ref. [191]), is considered.

EDGES High and Low band antennas probe the frequency ranges $90 - 200\,\mathrm{MHz}$ and $50 - 100\,\mathrm{MHz}$, respectively, overall measuring the 21-cm signal within the redshift range $z \in (6, 27)$, corresponding to a Universe age range $100\,\mathrm{Myr} - 1\,\mathrm{Gyr}$, i.e., the *dark ages*. This includes the epochs of reionization and cosmic dawn, in which the first astrophysical sources form. At $z = z_E$, the observed magnitude of the absorption line is about a factor of two greater than the one predicted by the ΛCDM model. The frequency of CMB radiation for this redshift is $\nu_{21}(z_{\mathrm{E}}) \simeq 78\,\mathrm{MHz}$, where the measured 21-cm brightness temperature is $T_{21}(z_{\mathrm{E}}) = -0.5^{+0.2}_{-0.5}\,\mathrm{K}$ (99% C.L., including estimates of systematic uncertainties). Since

[3] This definition is used to obtain the standard thermal spectrum of photons, as can be found in [179, 180]. This differs from the definition used in [178], by an unimportant factor of $2\pi\hbar$, which has no effect on further calculations or results.

at $z = z_E$ one has $(1+\delta_B)\,x_{H_I}(z_E) \simeq 1$, where δ_B is the baryon overdensity and x_{H_I} the fraction of neutral hydrogen, Eq. (B.5) from Appendix B.1 implies $T_\gamma(z_E)/T_S(z_E) = 15^{+15}_{-5.5}$ [181, 191], where T_γ is the effective temperature of the photon background and T_S the spin temperature (see Eq. (B.6) in Appendix B.1 for details). On the other hand, in the context of the ΛCDM model, one also gets

$$T_\gamma(z_E) = T_{CMB}(z_E) = T_{CMB,0}\,(1+z_E) \simeq 50\,\mathrm{K}\,, \tag{4.9}$$

where $T_{CMB,0} \simeq 2.73\,\mathrm{K}$ is the CMB temperature in the current epoch, and

$$T_{gas}(z_E) \simeq T_{CMB}(z^{gas}_{dec}) \left(\frac{1+z_E}{1+z^{gas}_{dec}}\right)^2 \simeq 6\,\mathrm{K}\,, \tag{4.10}$$

where $z^{gas}_{dec} \simeq 150$ and $T^{gas}_{dec} \simeq 410\,\mathrm{K}$ are the redshift and the temperature, respectively, at which the gas and radiation decouple. Using Eq. (B.5) from Appendix B.1, one infers $T_{21}(z_E) \gtrsim -0.2\,\mathrm{K}$. Notice that the minimum is saturated for $T_S(z_E) = T_{gas}(z_E)$, which corresponds to $T_\gamma(z_E)/T_{gas}(z_E) \simeq 8$. As a consequence of these results, one finds that the best fit value for $T_{21}(z_E)$ is about 2.5 times lower than expected within the ΛCDM model.

The energy density of photons from Eq. (4.8) can be used to describe the CMB spectrum as a function of redshift z, by considering $T = T_{CMB}(z)$, and reads as

$$\rho_{CMB}(E,z) = \frac{2}{\pi\hbar^2 c^3}\,\frac{E^3}{e^{\beta_{T_{CMB}(z)}\,E} - 1}\,, \tag{4.11}$$

where $\beta_{T_{CMB}}(z) = 1/k_B T_{CMB}(z)$. To explain the EDGES anomaly, one rewrites ρ_{MDR} from Eq. (4.7), in terms of ρ_{CMB} from Eq. (4.11), and defines the parameter R as

$$R \equiv \frac{\rho_{MDR}(E_{21},z_E)}{\rho_{CMB}(E_{21},z_E)} = \frac{1}{F^3}\left|1 - \frac{F' E_{21}}{F}\right|\,, \tag{4.12}$$

with ρ_{MDR} and ρ_{CMB} evaluated at $E = E_{21}$ and $z = z_E$. This is because neutral hydrogen can absorb only photons with energy E_{21} from the CMB spectrum at $T = T_{CMB}(z_E)$. It may

appear that such a modification may affect the optical depth τ_{ν} (introduced in Appendix B.1) and therefore, the intensity and shape of the 21-cm line profile. However, as shown in Appendix B.2, such a modification does not affect τ_{ν} in any way. The experimental values from the EDGES experiment can then be explained by imposing (see Ref. [191] for details)

$$R = 2.15^{+2.15}_{-0.8} \,. \tag{4.13}$$

Parameter R, defined in Eq. (4.12), is then only a function of F, F' and E, since everything else except the relevant correction cancels out. Since the modification functions f and g can be written as a power series in E/E_P, one can also write the function $F = g/f$ as a power series expansion

$$F\left(E/E_P\right) = \frac{g\left(E/E_P\right)}{f\left(E/E_P\right)} = \sum_{n=0}^{\infty} \frac{F^{(n)}(0)}{n!} \left(E/E_P\right)^n \,. \tag{4.14}$$

Note that $F(0) = 1$ corresponds to the standard ΛCDM result. The parameter R from Eq. (4.12) for such $F\left(E/E_P\right)$ reads

$$R = \frac{\left|1 - \sum_{n=1}^{\infty} \frac{F^{(n)}(n-1)}{n!} \left(E/E_P\right)^n\right|}{\left[\sum_{m=0}^{\infty} \frac{F^{(m)}}{m!} \left(E/E_P\right)^m\right]^4} \,. \tag{4.15}$$

Either, Eq. (4.12) or Eq. (4.15), can be used to estimate R for the cases studied here, and compare it with experimentally measured values and, for the first time, obtain estimates on the various parameters from the EDGES anomaly [156]:

Case 1: $f(E/E_P) = 1$ and $g(E/E_P) = \sqrt{1-\eta\,(E/E_P)^{\omega}}$. R reads as

$$R = \frac{|1-\left(1-\frac{\omega}{2}\right)\eta\,(E/E_P)^{\omega}|}{(1-\eta\,(E/E_P)^{\omega})^{5/2}} \tag{4.16}$$

for arbitrary parameters η and ω. For the special cases, one obtains:

i) $\omega = 1$ and $\eta > 0$:

$$R = \frac{|1-\eta\,E/2E_P|}{(1-\eta\,E/E_P)^{5/2}}\,. \tag{4.17}$$

R is plotted as a function of η in Fig. 4.1. To fit the EDGES experimental bounds, the parameter is fixed at $\eta = 6.5^{+4.0}_{-3.6} \times 10^{32}$.

ii) $\omega = 1$ and $\eta = \mp 2\,\alpha_0$:

$$R = \frac{|1 \pm \alpha_0\,(E/E_P)|}{[1 \pm 2\,\alpha_0\,(E/E_P)]^{5/2}}\,. \tag{4.18}$$

R is plotted as a function of α_0 for both branches in Fig. 4.2. However, only the branch with $\eta = +2\,\alpha_0$ can fix α_0. To fit the EDGES experimental bounds, the parameter is fixed at $\alpha_0 = 3.2^{+2.0}_{-1.8} \times 10^{32}$.

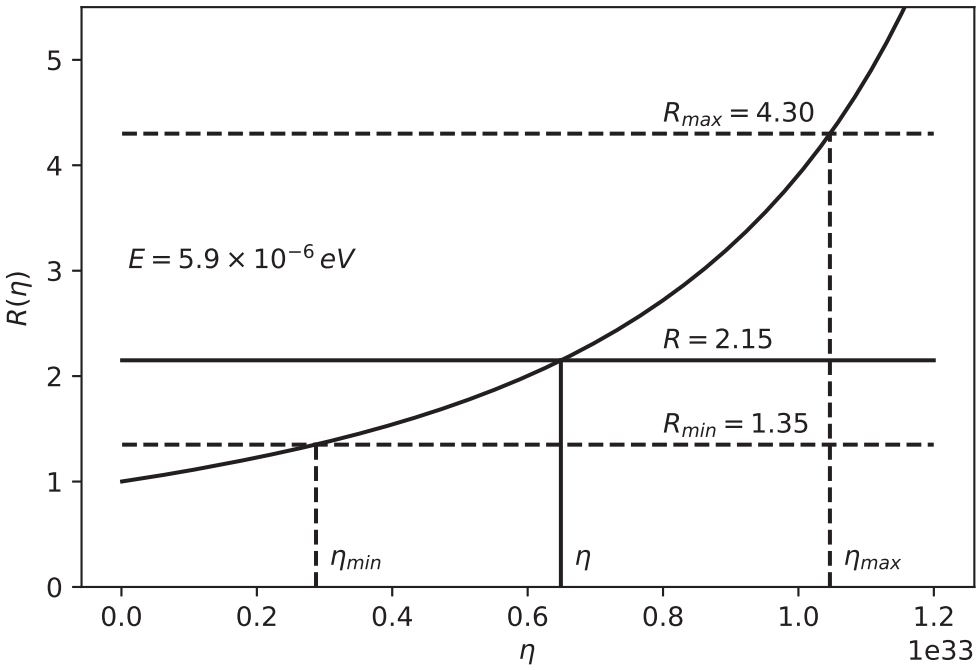

Figure 4.1: R vs η for fixed energy $E = E_{12} \simeq 5.9 \times 10^{-6}$eV.

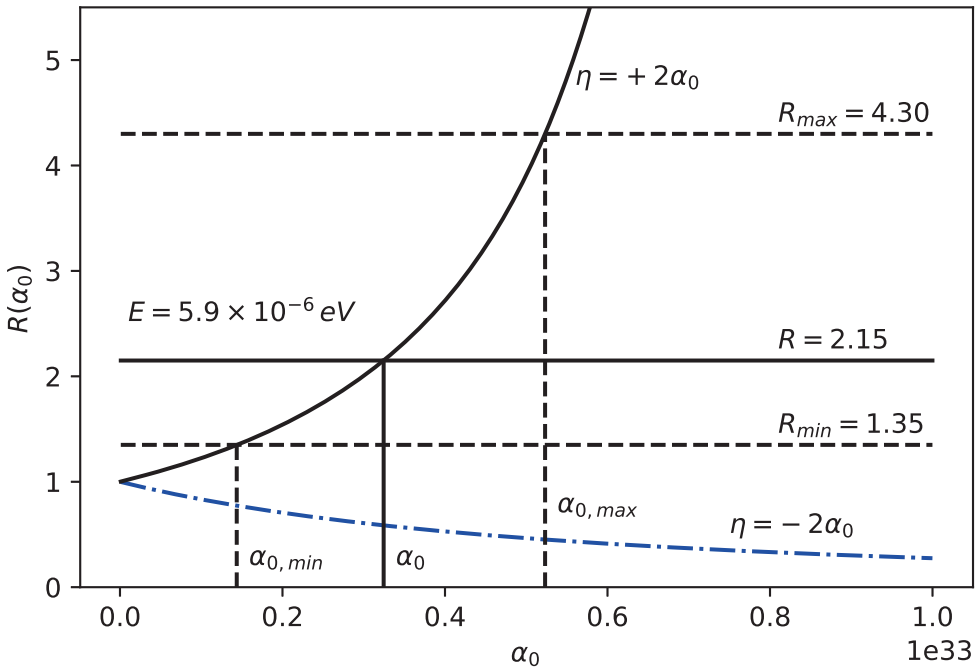

Figure 4.2: R vs α_0 for fixed energy $E = E_{12} \simeq 5.9 \times 10^{-6}$eV. The $\eta = -2\alpha_0$ branch is presented in dash-dot blue and the $\eta = +2\alpha_0$ branch is presented in solid black.

iii) $\omega = 2$ and $\eta = 2\beta_0$:

$$R = \frac{1}{(1-2\beta_0 (E/E_P)^2)^{5/2}} \ . \tag{4.19}$$

R is plotted as a function of β_0 in Fig. 4.3. To fit the EDGES experimental bounds, the parameter is fixed at $\beta_0 = 5.7^{+3.9}_{-3.3} \times 10^{65}$.

Case 2: $f(E/E_P) = \frac{\exp(\alpha(E/Ep))-1}{\alpha(E/E_P)}$ and $g(E/E_P) = 1$. R reads as

$$R = \frac{\exp\alpha(E/E_P)(\exp\alpha(E/E_P)-1)^2}{(\alpha(E/E_P))^2} \ . \tag{4.20}$$

R is plotted as a function of α in Fig. 4.4. To fit the EDGES experimental bounds, the parameter is fixed at $\alpha = 7.8^{+6.9}_{-4.7} \times 10^{32}$.

Case 3: $f = 1$ and $g = [1+\lambda'(E/E_P)^\gamma]^\delta$. R reads as

$$R = \frac{|1+(1-\delta\gamma)\lambda'(E/E_P)^\gamma|}{[1+\lambda'(E/E_P)^\gamma]^{3\delta+1}} \ , \tag{4.21}$$

for arbitrary parameters λ', γ and δ. For the special case, one obtains:

i) $\delta = 1$, $\gamma = 1$ and $\lambda' = \pm\alpha_0$:

$$R = \frac{1}{(1\pm\alpha_0(E/E_P))^4} \ . \tag{4.22}$$

R is plotted as a function of α_0 for both branches in Fig. 4.5. However, only the branch with $\lambda' = -\alpha_0$ can fix α_0. To fit the EDGES experimental bounds, the parameter is fixed at $\alpha_0 = 3.6^{+2.7}_{-2.1} \times 10^{32}$.

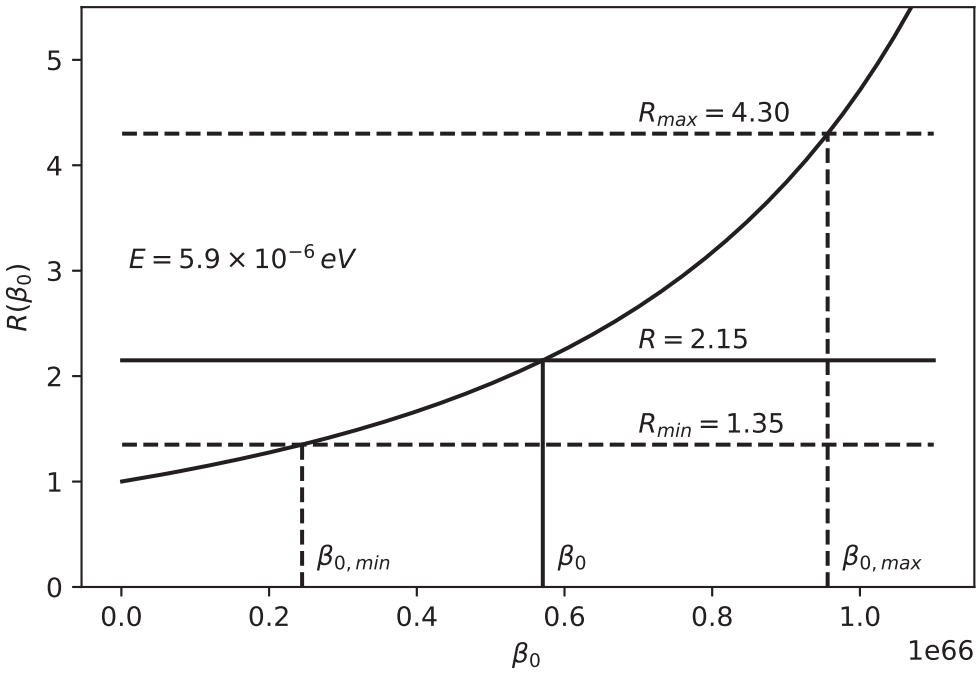

Figure 4.3: R vs β_0 for fixed energy $E = E_{12} \simeq 5.9 \times 10^{-6}$ eV.

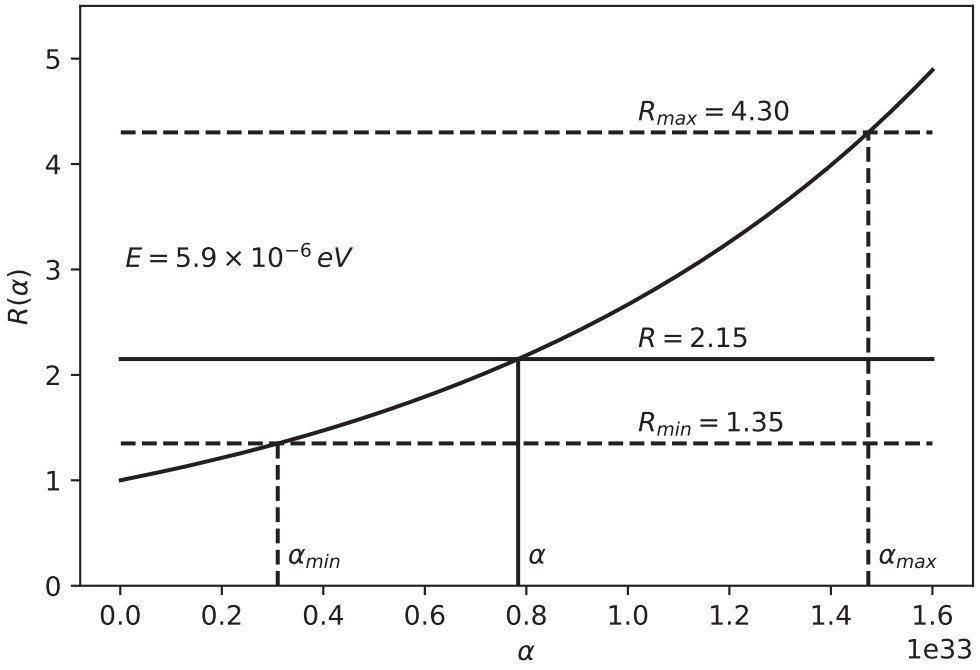

Figure 4.4: R vs α for fixed energy $E = E_{12} \simeq 5.9 \times 10^{-6}$ eV.

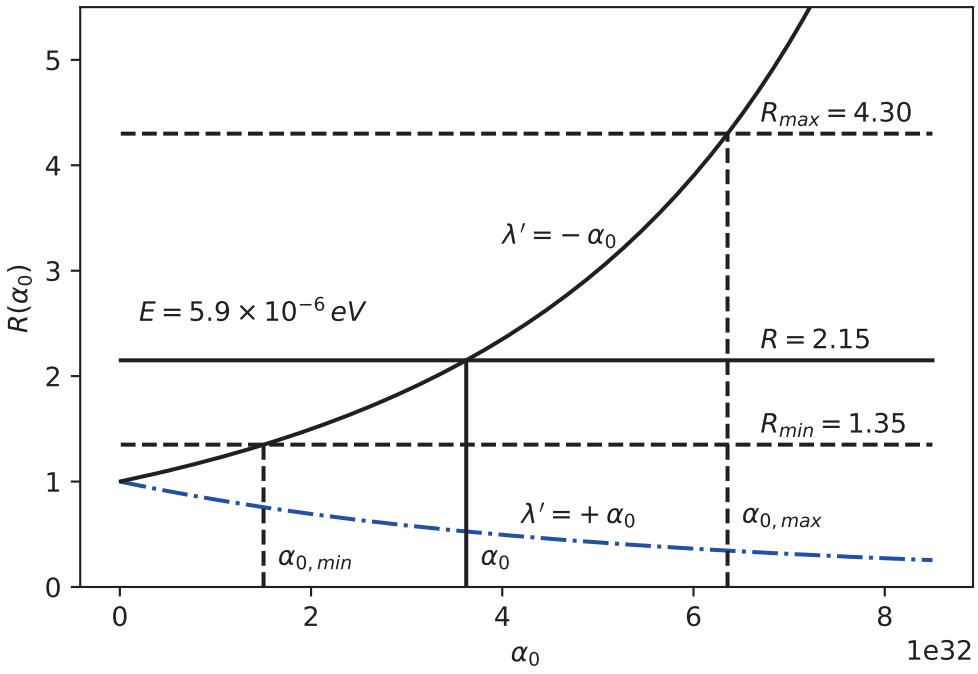

Figure 4.5: R vs α_0 for fixed energy $E = E_{12} \simeq 5.9 \times 10^{-6}\,\text{eV}$. The $\lambda' = +\alpha_0$ branch is presented in dash-dot blue and the $\lambda' = -\alpha_0$ branch is presented in solid black.

At this point it should be stressed that the above plots indicate that the MDRs provided by cases 1, 2 and 3, give $(\eta, \alpha_0, \sqrt{\beta_0}, \alpha, \lambda')\big|_{z=z_E} \approx 10^{32}$ at redshift $z = z_E$. These values are much larger than the bound set by the electroweak scale $\alpha_{EW} = 10^{17}$. To verify the compatibility with known observations, and obtain the bounds on the above parameters in the current epoch ($z = 0$), the experimental precision of the CMB temperature $\left(\frac{\delta T}{T}\right)_{exp} = 2 \times 10^{-4}$ [192] (see also Refs. [193, 194]) of a perfect black body, is compared to the theoretical deviation due to MDRs in the current epoch [156]

$$\frac{\delta T}{T}(z=0) = (R(E)-1)\,\frac{\cosh\left(\beta_{T_{CMB}}(0)\,E\right)-1}{e^{\beta_{T_{CMB}}(0)\,E}-1}\,\frac{2}{\beta_{T_{CMB}}(0)\,E}\,. \tag{4.23}$$

In the above, $R(E)$ is given by Eq. (4.12) and $\beta_{T_{CMB}}(0)$ is given in terms of the CMB temperature in the current epoch. Eq. (4.23) is obtained by expressing $\delta T/T$ from $\rho_{MDR}(E,T) = \rho(E,T)\,R \approx \rho(E,T) + \frac{d\rho}{dT}(E,T)\,\delta T$. Given Eq. (4.23), the parameters in the current epoch must satisfy an upper bound of $(\eta, \alpha_0, \sqrt{\beta_0}, \alpha, \lambda')\big|_{z=0} < 10^{28}$ to be consistent with the

observed CMB spectrum in the current epoch. This bound is weaker than the bound set by the electroweak scale α_{EW}. Therefore, α_{EW} should be considered as the relevant MDR parameter bound in the current epoch. The MDR parameters, obtained from the EDGES anomaly at $z = z_E$, combined with the electroweak bound α_{EW} at $z = 0$, suggest that MDR parameters are increasing functions of redshift z. Therefore, R is also expected to increase with z for a given energy E and have a value of $R \approx 1$ at $z = 0$.

The compatibility of such MDRs with epochs earlier than z_E should be taken into consideration as well. For example, in the epoch of the Big Bang Nucleosynthesis (BBN), at $z \approx 3 \times 10^8$ [195], a bound of $\beta_0 \lesssim 10^{87}$ was obtained in Ref. [159] for the quadratic GUP parameter β_0, which corresponds to an upper bound $\lesssim 10^{44}$ for the MDR parameters. Therefore, the values of the MDR parameters, measured by the EDGES anomaly are consistent with the BBN measurements, even if they increase to $\sim 10^{44}$ at $z \approx 3 \times 10^8$. This supports the increasing trend of the redshift dependence of the MDR parameters and may in fact provide a clue in determining the exact form of this dependence. Estimations of the MDR parameters from the modified CMB spectrum would not be relevant in the BBN epoch, since it has not been created until the epoch of recombination at $z = 1090$ [195].

The standard MDRs used in this work can be found in Refs. [7, 41, 175, 176, 177, 178] as mentioned in Section 4.1.1, but they consider the MDR parameters as constants. The assumption that the MDR parameters are functions of another parameter, such as redshift, is fairly new. However, such an assumption is indirectly supported by Ref. [152], where the author finds a mass/radius dependent GUP parameter. This is also supported by the difference between estimations of the quadratic GUP parameter in Earth-based experiments, where $\beta_0 > 0$ [69, 71, 72, 130, 196], and astrophysical/cosmological observations, where $\beta_0 < 0$ [54, 81, 152, 153, 154, 157]. This shows that the MDR parameters can in fact be dependent on scale or redshift.

Since the usual models of modified dispersion relations cannot explain the EDGES anomaly without additional assumptions, it is also legitimate to investigate if it can be

explained by considering the cases in which $\eta, \alpha_0, \lambda' = \alpha_{EW}$, i.e., they are fixed to the electroweak scale, while ω and δ are treated as free parameters [156]. Only cases 1 and 3 are considered, since case 2 has no other parameters to tweak. Also, the special case 1, iii) is not separately considered, because it is automatically implied as $\omega \longrightarrow 2$.

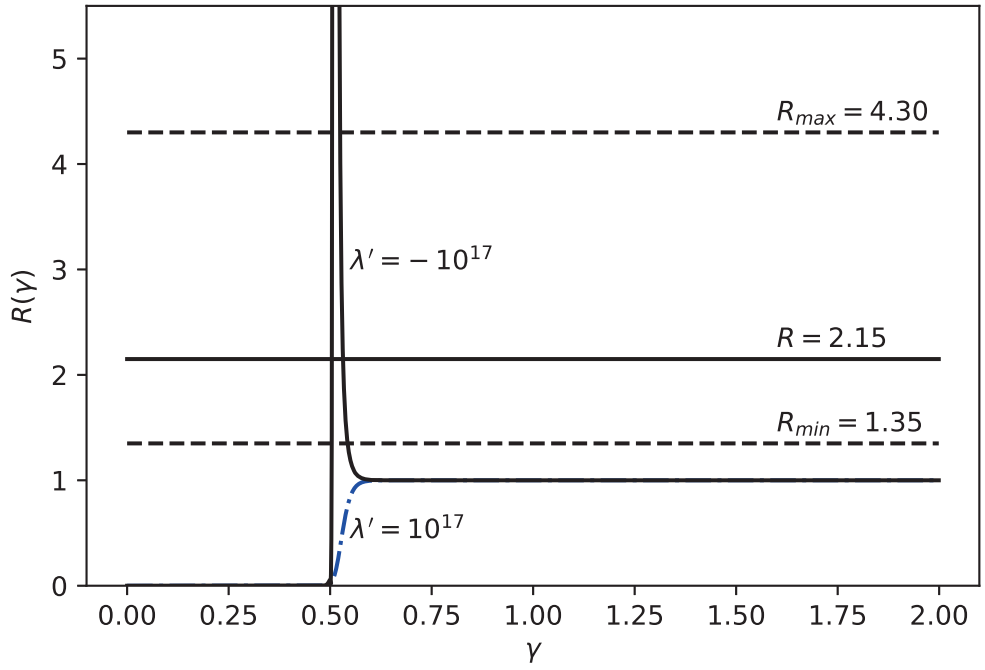

Figure 4.6: R vs γ at $\delta = 1$ for fixed energy $E = E_{12} \simeq 5.9 \times 10^{-6}$eV. The $\lambda' = +10^{17}$ branch is presented in dash-dot blue and the $\lambda' = -10^{17}$ branch is presented in solid black.

In Fig. 4.6, R from Eq. (4.21) is plotted as a function of γ for fixed $\lambda' = \pm 10^{17}$ and for fixed $\delta = 1$. The values of R for $\lambda' = 10^{17}$ fall outside the EDGES bounds and cannot provide an explanation for the EDGES anomaly. However, the values of R for $\lambda' = -10^{17}$ fall inside the EDGES bounds twice in a narrow range around $\gamma \approx 0.5$, and can therefore provide an explanation for the EDGES anomaly. Changing the δ parameter only moves the peak to a different location.

The power dependencies on ω and δ of their respective cases are shown in Figs. 4.7 and 4.8, respectively. One can see that the EDGES anomaly can be explained by powers $\omega_{max} < 0.544$ and $\delta_{max} < -0.05$. Note that only an upper bound to the powers ω and δ can be obtained, since α_{EW} is still an upper bound for the new length scale.

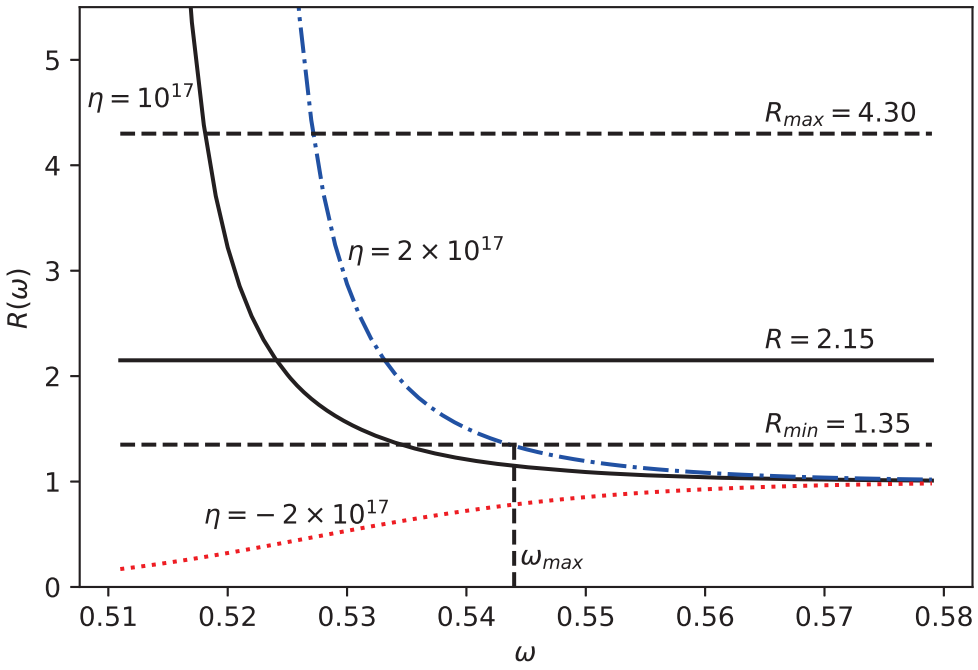

Figure 4.7: R vs ω for fixed $\eta, \alpha_0 = 10^{17}$ and energy $E = E_{12} \simeq 5.9 \times 10^{-6}$ eV. The solid black, the dash-dot blue and dotted red lines represent cases 1) i) and ii) (positive and negative branch), respectively.

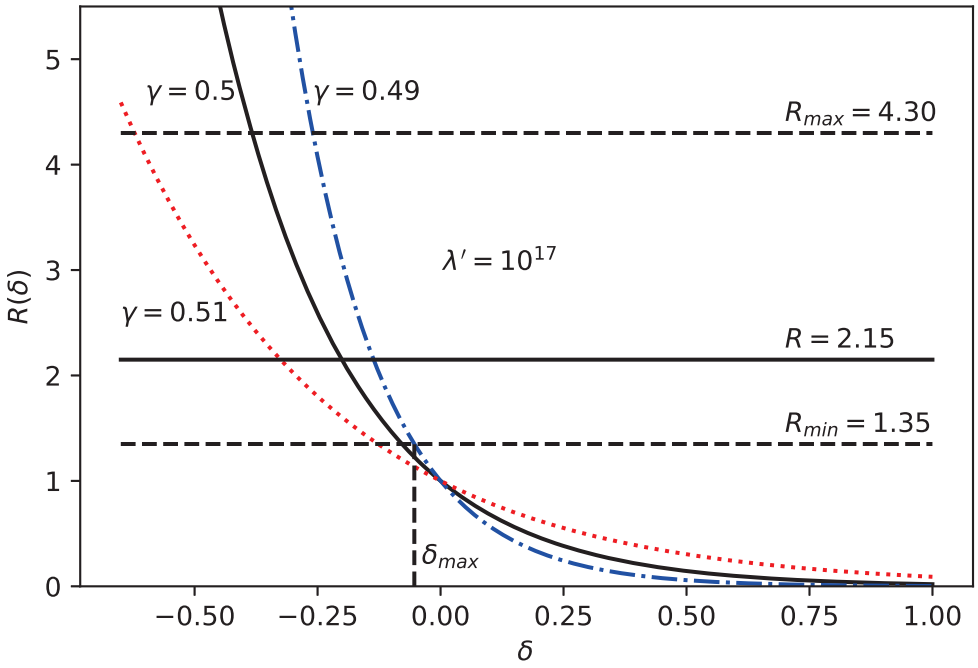

Figure 4.8: R vs δ for fixed $\lambda' = 10^{17}$ and energy $E = E_{12} \simeq 5.9 \times 10^{-6}$ eV. The dash-dot blue, solid black and dotted red lines represent $\gamma = 0.49, 0.50, 0.51$, respectively.

4.1.3 Summary

In this section, a framework in which MDRs can account for the EDGES anomaly, was proposed. The estimation of the MDR parameters from the EDGES anomaly at $z = z_E$ and the bound α_{EW} at $z = 0$, suggest that the MDR parameters are functions of redshift z, and as such could explain the EDGES anomaly. One can assume that the evolution of MDR parameters with time in the current epoch is slow or nearly constant, since the same physics is observed in all observable astrophysical objects, such as distant galaxies. However, the time evolution of MDR parameters could have been faster in the early stages of the Universe as the EDGES anomaly suggests.

On the other hand, one can set η, α_0, $\sqrt{\beta_0}$, α, $\lambda' = \alpha_{EW}$, and treat the powers ω, γ and δ of the MDRs as free parameters. The bounds on their values are obtained by fitting the corresponding modified thermal spectra of photons to the EDGES anomaly, as seen in Figs. 4.6, 4.7 and 4.8. One can see that a narrow range around $\gamma \approx 0.5$ provides a good fit for the EDGES anomaly, while ω and δ obtain an upper bound. The stringent values of ω and δ, with their respective uncertainties will be obtained in the future, once the true QG scale is measured. It may be noted that the case of positive δ and negative λ' (see Figs. 4.5 and 4.6), is equivalent to the case of negative δ and positive λ' (see Fig. 4.8) to leading order. This creates an ambiguity in their estimation, which can be resolved by probing signatures of higher order corrections. However, due to experimental limitations, this is currently not possible.

4.2 Baryon Asymmetry in the Universe

The origin of the observed baryon asymmetry in the Universe is an unsolved problem up to this day. Observational evidence shows that the Universe is mostly made up of matter, rather than equal amounts of matter and anti-matter, as expected from QT and GR [197]. For such asymmetry to occur, three necessary conditions, called Sakharov conditions, must be met [198]: 1) Baryon number violation, 2) C and CP violation, 3) Deviation from thermal

equilibrium. It should be pointed out that the CMB temperature anisotropies provide a strong probe of the baryon asymmetry, since the acoustic peaks in the CMB power spectrum allow measurements of large scale structures, and provide an indirect measurement of the baryon asymmetry parameter $\eta_{BA}^{(CMB)} = (6.225 \pm 0.170) \times 10^{-10}$ [199]. η_{BA} is defined as the difference of baryon and anti-baryon densities per unit entropy density (see Eq. (4.45) for details). On the other hand, measurement of η_{BA} can also be carried out in the context of the BBN. In this case, $\eta_{BA}^{(BBN)} \in (3.4, 6.9) \times 10^{-10}$ [200], which agrees with $\eta_{BA}^{(CMB)}$, although the two measurements are obtained from considerations in two different epochs in the evolution of the Universe.

Although several explanations for the observed baryon asymmetry have been offered so far [197, 201, 202], none of them has been confirmed yet. In this section, a proposal that the baryon asymmetry manifests due to coupling of matter and space-time, and the existence of a minimum measurable length, implied by GUP, is explored. In Refs. [155, 160, 161, 162], it has been shown that GUP can modify the Friedmann equations, through modifying the Bekenstein-Hawking entropy and using the holographic principle. In the following, this approach is used to derive the exact modified Friedmann equations using GUP. This in turn provides a general framework, which allows one to explore QG effects at cosmological scales.

An interaction term, motivated by Supergravity proposals, which couples space-time and baryon current is used to satisfy the first two Sakharov conditions, while the QG modified Friedmann equations break thermal equilibrium to satisfy the third Sakharov condition. In contrast to Earth-based QGP, this prediction has an observational counterpart (such as the EDGES anomaly; see Section 4.1), and thus offers an explanation for a measured and established feature of Nature, i.e., the baryon asymmetry in the Universe. In addition, this proposal predicts the values of the dimensionless GUP parameters, $\alpha_0 \approx 10^5$ and $|\beta_0| \approx 10^9$, and thus determines a possible minimum measurable length scale of $\ell_{min} \approx 10^{-30}\,\mathrm{m}$. Supporting material for this section is found in Appendix C.

4.2.1 Modification of the Bekenstein-Hawking Entropy

To explain the origin of the baryon asymmetry in the Universe, one must first modify the Friedmann equations, since such modifications lead to energy density and pressure variations. These variations break thermal equilibrium and allow the asymmetry to manifest. In order to modify the Friedmann equations, one uses the holographic principle. The holographic principle states that a description of a theory inside a d-dimensional volume in space can be encoded in its $(d-1)$-dimensional boundary, such as an event horizon of a black hole, or the cosmic horizon [203, 204]. The holographic principle provides a mechanism to introduce quantum corrections to large scale systems.

A QG modification of the Friedmann equations was derived in Ref. [155] (see also Ref. [205]), using the quadratic GUP (KMM model; see Eq. (2.36)). To examine the conclusions of a more general model, GUP given by Eq. (2.42) is considered. The corresponding minimal modified uncertainty relation is Eq. (2.45), which is written again for convenience

$$\Delta x \Delta p \geq \frac{\hbar}{2}\left[1-\alpha\Delta p+4\beta\Delta p^2\right] . \tag{4.24}$$

As a particle gets absorbed by an apparent horizon, it will increase the total energy inside the horizon and consequently change the area of that horizon [61, 206, 207]. A particle, whose uncertainty is governed by GUP, as given by Eq. (4.24), will produce a QG corrected change to the apparent horizon area, as shown in the following. Energy of such a particle is taken to be $E=\Delta p c$ [61, 207]. Therefore, one solves Eq. (4.24) for Δp as

$$\Delta p \geq \frac{2\Delta x+\alpha\hbar}{8\hbar\beta}\left(1-\sqrt{1-\frac{16\hbar^2\beta}{4\Delta x^2+4\alpha\hbar\Delta x+\hbar^2\alpha^2}}\right) , \tag{4.25}$$

where the negative solution has been chosen, because it is the only one which reduces to the standard Heisenberg uncertainty relation for $\alpha,\beta \longrightarrow 0$. The area of an apparent horizon with radius R, which absorbs a particle with energy E, changes by $\Delta A \geq 16\pi\ell_P^2 E R/\hbar c$

[208, 209, 210]. As the particle gets re-emitted from the horizon, its position uncertainty is the radius of the apparent horizon $\Delta x = R$ (see Section 2.1.1), which determines the minimal change of the area of the apparent horizon as

$$\Delta A_{min} \geq 16\pi\ell_P^2 \frac{E\,\Delta x}{\hbar c} \,. \tag{4.26}$$

Considering $\Delta x = R_S$ (the Schwarzschild radius of the apparent horizon; see Eq. (2.2)), given in terms of the area of the apparent horizon A as $\Delta x^2 = A/4\pi$ and $E = \Delta p\, c$ (Δp from Eq. (4.49)), one can rewrite Eq. (4.26) as

$$\Delta A_{min} \simeq \lambda_{BH} \frac{\ell_P^2 \left(A + \alpha\hbar\sqrt{\pi}A^{1/2}\right)}{\hbar^2\beta} \left(1 - \sqrt{1 - \frac{16\pi\hbar^2\beta}{A + 2\alpha\hbar\sqrt{\pi}A^{1/2} + \alpha^2\hbar^2\pi}}\right) \,, \tag{4.27}$$

where λ_{BH} is a normalization parameter, calibrated by the Bekenstein-Hawking entropy formula as $\lambda_{BH} = b/2\pi$ [206], with b defined by the minimal change in entropy $\Delta S_{min} = k_B\, b = k_B \ln 2$, corresponding to one bit of information [211]. Therefore, the minimal change of entropy for a minimal change in the apparent horizon area reads

$$\frac{\mathrm{d}S}{\mathrm{d}A} = \frac{\Delta S_{min}}{\Delta A_{min}} = \frac{k_B\,\beta^*}{8\,\ell_P^2 \left(A + \alpha^* A^{1/2} - \sqrt{A^2 + 2\,\alpha^* A^{3/2} + (\alpha^{*2} - \beta^*)A}\right)} \,, \tag{4.28}$$

where $\alpha^* = \sqrt{\pi}\hbar\alpha$ and $\beta^* = 16\pi\hbar^2\beta$ are defined for convenience. The standard result for the entropy of a black hole reads as [212, 213]

$$S = \frac{k_B\, c^3 A}{4\,\hbar G} = \frac{k_B A}{4\,\ell_P^2} \,. \tag{4.29}$$

Note that the holographic principle implies that the above entropy applies to any region of space with a horizon. In general, if one wants to modify the entropy from Eq. (4.29), S and A will no longer be linearly related, i.e., one defines $f(A)$ [160]. Such modified entropy can then be written as $S = k_B\, f(A)/4\,\ell_P^2$. By taking the derivative of this entropy over area A,

one obtains

$$\frac{\mathrm{d}S}{\mathrm{d}A} = \frac{k_B\, f'(A)}{4\,\ell_P^2}\ . \tag{4.30}$$

In the relevant case of GUP motivated QG modifications, $f'(A)$ can be identified by comparing the above derivative with the one in Eq. (4.28), and thus

$$f'(A) = \frac{1}{2}\,\frac{\beta^*}{\left(A + \alpha^* A^{1/2} - \sqrt{A^2 + 2\,\alpha^* A^{3/2} + (\alpha^{*2} - \beta^*)\,A}\right)}\ . \tag{4.31}$$

It should be pointed out that one obtains the standard result $f'(A) = 1$ for $\alpha^*,\, \beta^* \longrightarrow 0$. The QG modified Bekenstein-Hawking entropy, using Eq. (4.31), is obtained for the first time by integrating Eq. (4.28) over A, which reads as [157]

$$\begin{aligned} S = \frac{k_B}{8\,\ell_P^2}\Bigg[& A\left(1 + \sqrt{1 + 2\,\alpha^*\frac{1}{A^{1/2}} + (\alpha^{*2} - \beta^*)\,\frac{1}{A}}\right) \\ & + \alpha^* A^{1/2}\left(2 + \sqrt{1 + 2\,\alpha^*\frac{1}{A^{1/2}} + (\alpha^{*2} - \beta^*)\,\frac{1}{A}}\right) \\ & - \beta^* \ln\left(1 + \frac{A^{1/2}}{\alpha^*}\left(1 + \sqrt{1 + 2\,\alpha^*\frac{1}{A^{1/2}} + (\alpha^{*2} - \beta^*)\,\frac{1}{A}}\right)\right)\Bigg]\ , \end{aligned} \tag{4.32}$$

where the standard result from Eq. (4.29) is obtained for $\alpha^*,\, \beta^* \longrightarrow 0$. The above equation includes both, linear and quadratic QG corrections to the Bekenstein-Hawking entropy, in contrast to the one obtained in Ref. [155], which contains only quadratic corrections.

4.2.2 Modification of the Friedmann Equations

The QG modification of the Bekenstein-Hawking entropy obtained in Section 4.2.1 is necessary to modify the Friedmann equations through the holographic principle. The modification of the Friedmann equations to second order in α^* and first order in β^* were considered separately (and perturbatively) in Ref. [162]. In the following, exact QG modifications of the Friedmann equations, in terms of both, α^* and β^*, are obtained. One starts with the

standard Friedmann-Lemaître-Robertson-Walker (FLRW) metric in spherical coordinates, incorporating homogeneity and isotropy, in a $(n+1)-$dimensional space-time, which reads as

$$\mathrm{d}s^2 = h_{cd}\,\mathrm{d}x^c\mathrm{d}x^d + \tilde{r}^2\,\mathrm{d}\Omega_{n-1}^2\ , \tag{4.33}$$

where $h_{cd} = \mathrm{diag}(-1,\, a^2/(1-k\,r^2))$, $x^c = (c\,t, r)$, $\tilde{r} = a(t)\,r$, $\mathrm{d}\Omega_{n-1}$ is the angular part of the $(n-1)$-dimensional sphere (see Appendix C.1 for details), $a = a(t)$ the scale factor, r the comoving radius and k the spatial curvature constant. Indices c and d can only take values 0 and 1. The Friedmann equations, which govern the dynamics of the scale factor $a(t)$, and hence the evolution of the Universe, undergo modifications depending on the precise form of the function $f(A)$, introduced in Section 4.2.1. The derivation of modified Friedmann equations for an arbitrary $f(A)$ follows from the the first law of thermodynamics and the holographic principle, which ensures that Eq. (4.32) is valid for the cosmic horizon. A detailed derivation is shown in Appendix C.1. In a space-time with a metric from Eq. (4.33), the modified Friedmann equations read

$$-\frac{8\,\pi\,G}{n-1}\left(\rho + \frac{p}{c^2}\right) = \left(\dot{H} - \frac{k\,c^2}{a^2}\right) f'(A) \tag{4.34}$$

and

$$-\frac{8\,\pi\,G}{n\,(n-1)}\,\rho = \frac{c^2\,(n\,\Omega_n)^{\frac{n+1}{n-1}}}{n\,(n-1)\,\Omega_n}\int f'(A)\frac{\mathrm{d}A}{A^{\frac{n+1}{n-1}}}\ , \tag{4.35}$$

where ρ is the matter density, p pressure and $H = \dot{a}/a$ the Hubble parameter. The above two Friedmann equations are written in the most general form, given an arbitrary function $f(A)$. When $f(A) = A$, one obtains the standard Friedmann equations, while $f(A) \neq A$ gives rise to modified Friedmann equations. Modifications, implied by $f(A)$, are quantum in nature, since they come from the Bekenstein-Hawking entropy, which is of quantum

origin. To obtain the QG modified Friedmann equations, one needs to plug Eq. (4.31) in Eqs. (4.34) and (4.35). This yields a general and exact form, for a specific GUP given by Eq. (2.42), of the QG modified Friedmann equations for $n = 3$, expressed in terms of the standard cosmological parameters H, a, and k as [157]

$$-4\pi G\left(\rho+\frac{p}{c^2}\right)=\left(\dot{H}-\frac{kc^2}{a^2}\right)\frac{\beta^*}{8\pi c^2} \times\frac{\left(H^2+\frac{kc^2}{a^2}\right)}{1+\frac{\alpha^*}{(4\pi)^{1/2}c}\left(H^2+\frac{kc^2}{a^2}\right)^{1/2}-\sqrt{1+\frac{2\alpha^*}{(4\pi)^{1/2}c}\left(H^2+\frac{kc^2}{a^2}\right)^{1/2}+\frac{(\alpha^{*2}-\beta^*)}{4\pi c^2}\left(H^2+\frac{kc^2}{a^2}\right)}} \tag{4.36}$$

and

$$\begin{aligned}\frac{8\pi G}{3}(\rho-\Lambda)&=\frac{1}{2}\left(H^2+\frac{kc^2}{a^2}\right)+\frac{\alpha^*}{3(4\pi)^{1/2}c}\left(H^2+\frac{kc^2}{a^2}\right)^{3/2}+\frac{2\pi c^2(\alpha^{*2}+2\beta^*)}{3(\alpha^{*2}-\beta^*)^2}\\&+\left[\frac{1}{3}\left(H^2+\frac{kc^2}{a^2}\right)+\frac{(4\pi)^{1/2}c\,\alpha^*}{6(\alpha^{*2}-\beta^*)}\left(H^2+\frac{kc^2}{a^2}\right)^{1/2}-\frac{2\pi c^2(\alpha^{*2}+2\beta^*)}{3(\alpha^{*2}-\beta^*)^2}\right]\\&\quad\times\sqrt{1+\frac{2\alpha^*}{(4\pi)^{1/2}c}\left(H^2+\frac{kc^2}{a^2}\right)^{1/2}+\frac{(\alpha^{*2}-\beta^*)}{4\pi c^2}\left(H^2+\frac{kc^2}{a^2}\right)}\\&+\frac{2\pi c^2\alpha^*\beta^*}{(\alpha^{*2}-\beta^*)^{5/2}}\ln\left[1+\frac{(\alpha^{*2}-\beta^*)}{(4\pi)^{1/2}c\,(\alpha^*+\sqrt{\alpha^{*2}-\beta^*})}\left(H^2+\frac{kc^2}{a^2}\right)^{1/2}\right.\\&\quad\left.+\frac{\sqrt{\alpha^{*2}-\beta^*}}{\alpha^*+\sqrt{\alpha^{*2}-\beta^*}}\left(\sqrt{1+\frac{2\alpha^*}{(4\pi)^{1/2}c}\left(H^2+\frac{kc^2}{a^2}\right)^{1/2}+\frac{(\alpha^{*2}-\beta^*)}{4\pi c^2}\left(H^2+\frac{kc^2}{a^2}\right)}-1\right)\right],\end{aligned} \tag{4.37}$$

where

$$A=4\pi\tilde{r}_A^2=\frac{4\pi c^2}{H^2+\frac{kc^2}{a^2}} \tag{4.38}$$

was used. In the above $\tilde{r}_A$ is the radius of the apparent horizon, and is defined in Eq. (C.2) in Appendix C.1. For vanishing GUP parameters $\alpha^*, \beta^* \longrightarrow 0$ in Eqs. (4.36) and (4.37), one obtains the standard Friedmann equations. Details of this limit are given in Appendix C.2.

It is evident that if one wants to study the radiation-dominated era, the tiny observed

cosmological constant Λ will be ignored, and the spatial curvature constant has to be set $k = 0$, consistent with the observed spatially flat Universe. As a result, the QG modified Friedmann equations from Eqs. (4.36) and (4.37) are further simplified, respectively, to

$$-4\pi G\left(\rho+\frac{p}{c^2}\right)=\frac{\dot{H}\beta^*}{8\pi c^2}\frac{H^2}{1+\frac{\alpha^*}{(4\pi)^{1/2}c}H-\sqrt{1+\frac{2\alpha^*}{(4\pi)^{1/2}c}H+\frac{(\alpha^{*2}-\beta^*)}{4\pi c^2}H^2}} \tag{4.39}$$

and

$$\begin{aligned}\frac{8\pi G}{3}\rho=&\frac{1}{2}H^2+\frac{\alpha^*}{3(4\pi)^{1/2}c}H^3+\frac{2\pi c^2(\alpha^{*2}+2\beta^*)}{3(\alpha^{*2}-\beta^*)^2}\\&+\left[\frac{1}{3}H^2+\frac{(4\pi)^{1/2}c\,\alpha^*}{6(\alpha^{*2}-\beta^*)}H-\frac{2\pi c^2(\alpha^{*2}+2\beta^*)}{3(\alpha^{*2}-\beta^*)^2}\right]\\&\quad\times\sqrt{1+\frac{2\alpha^*}{(4\pi)^{1/2}c}H+\frac{(\alpha^{*2}-\beta^*)}{4\pi c^2}H^2}\\&+\frac{2\pi c^2\alpha^*\beta^*}{(\alpha^{*2}-\beta^*)^{5/2}}\ln\left[1+\frac{(\alpha^{*2}-\beta^*)}{(4\pi)^{1/2}c\,(\alpha^*+\sqrt{\alpha^{*2}-\beta^*})}H\right.\\&\quad\left.+\frac{\sqrt{\alpha^{*2}-\beta^*}}{\alpha^*+\sqrt{\alpha^{*2}-\beta^*}}\left(\sqrt{1+\frac{2\alpha^*}{(4\pi)^{1/2}c}H+\frac{(\alpha^{*2}-\beta^*)}{4\pi c^2}H^2}-1\right)\right].\end{aligned} \tag{4.40}$$

The above QG modified Friedmann equations provide a framework on which density and pressure variations in the early Universe are studied. In the following, they will also be used to break thermodynamic equilibrium, and explain the baryon asymmetry, formed in the early Universe.

4.2.3 Gravitational Baryon Asymmetry

All three Sakharov conditions, listed at the beginning of Section 4.2, must be met to explain the observed baryon asymmetry. As seen from the following considerations, the first two Sakharov conditions are satisfied by introducing a coupling term, which couples space-time to the baryon current, and the final Sakharov condition is satisfied by breaking thermal equilibrium through the QG modified Friedmann equations, derived in Section 4.2.2.

Within supergravity theories, a mechanism for generating baryon asymmetry during the expansion of the universe, by means of dynamical breaking of CPT (and CP) symmetry, is proposed [214, 215]. However, this mechanism does not break the thermal equilibrium, thus not all Sakharov conditions are satisfied. The interaction, responsible for the CPT violation, is described by a coupling between the derivative of the Ricci scalar curvature R and the baryon current J^μ [216]

$$\frac{\hbar^3}{M_*^2\,c^2}\int \mathrm{d}^4x\,\sqrt{-g}\,J^\mu\,\partial_\mu R\;, \tag{4.41}$$

where M_* is the cutoff scale characterizing the effective theory (see Refs. [217, 218, 219, 220, 221, 222, 223, 224, 225, 226] for further applications). The above term satisfies the second Sakharov condition. If there exist interactions that violate the conservation of the baryon number B in thermal equilibrium, such as those allowed in Grand Unified Theories (GUT), to satisfy the first Sakharov condition, then a net baryon asymmetry can be generated and gets frozen-in below the decoupling temperature[4] T_D. By taking the integrand from Eq. (4.41), i.e., the Lagrangian density, and noting that the spatial part of $\partial_\mu R$ vanishes for the FLRW metric, one gets

$$\frac{\hbar^3}{M_*^2\,c^2}\,J^\mu\,\partial_\mu R=\frac{\hbar^3}{M_*^2\,c^2}\,(n_B-n_{\overline{B}})\,\dot{R}\;. \tag{4.42}$$

The effective chemical potential for baryons, i.e., μ_B, and for anti-baryons, i.e., $\mu_{\overline{B}}$, can be read from the equation above as

$$\mu_B=-\mu_{\overline{B}}=-\frac{\hbar^3\,\dot{R}}{M_*^2\,c^2}\;, \tag{4.43}$$

[4]During the evolution of the Universe, the CPT symmetry violation generates the baryon asymmetry. This occurs when baryon (or lepton) violating interactions are still in thermal equilibrium. The asymmetry is frozen-in at the decoupling temperature T_D, when the baryon (or lepton) number violation goes out of thermal equilibrium. The temperature T_D is derived from the relation $\Gamma(T_D)\simeq H(T_D)$, where Γ is the interaction rate of processes and H the expansion rate of the Universe. More specifically, in the regime $\Gamma\gg H$, or $T>T_D$, the B-violating processes are in thermal equilibrium, and at $T=T_D$, i.e., $\Gamma\simeq H$, the decoupling occurs, while when $\Gamma<H$, or $T<T_D$ the baryon asymmetry gets frozen-in.

since Eq. (4.42) corresponds to the energy density term of a grand canonical ensemble. For relativistic particles, the net baryon number density of matter in the early Universe is given by [227]

$$n_B - n_{\overline{B}} = \frac{g_B}{6\hbar^3 c^3}\mu_B k_B^2 T^2 \,, \tag{4.44}$$

where $g_B \sim O(1)$ is the number of intrinsic degrees of freedom of baryons. The baryon asymmetry is defined in the standard notation as [227]

$$\eta_{BA} \equiv \frac{n_B - n_{\overline{B}}}{n_\gamma} \simeq 7\, k_B \frac{n_B - n_{\overline{B}}}{s} = -\frac{105\, g_B \hbar^3}{4\pi^2 g_* k_B c^2} \frac{\dot{R}}{M_*^2 T}\bigg|_{T_D} \,, \tag{4.45}$$

where $n_\gamma \simeq s/7\,k_B$ is the number density of photons,

$$s = \frac{2\pi^2 g_{*s} k_B^4}{45\hbar^3 c^3} T^3 \tag{4.46}$$

the entropy per unit volume, i.e., entropy density, in the radiation-dominated era, and g_{*s} is the number of degrees of freedom for particles which contribute to the entropy of the Universe. It may be noted that g_{*s} takes values very close to the total number of degrees of freedom of relativistic Standard Model particles g_*, i.e., $g_{*s} \approx g_* \sim 106$, as discussed in Ref. [227]. The parameter η_{BA} is different from zero, provided that the time derivative of the Ricci scalar $\dot{R}$ is non-vanishing. In the ΛCDM model, the baryon asymmetry vanishes, because $\dot{R} = 0$ in the radiation-dominated era, due to thermal equilibrium still being satisfied, as is evident from the following consideration.

The deviation from thermal equilibrium is described in terms of variations in density and pressure. The density and pressure, including these variations, can be written as

$$\rho = \rho_0 + \delta\rho \qquad \text{and} \qquad p = p_0 + \delta p \,, \tag{4.47}$$

where ρ_0 and p_0 are the equilibrium density and pressure, respectively. The above density

and pressure expressions are then plugged in the QG modified Friedmann equations, namely Eqs. (4.39) and (4.40), to obtain the QG induced variations as

$$\delta\rho = \frac{\alpha^*}{3c}\sqrt{\frac{8G}{3}}\,\rho_0^{3/2} - \frac{\beta^*}{12c^2}\,G\rho_0^2 \tag{4.48}$$

and

$$\delta p = \frac{\alpha^* c}{6}\sqrt{\frac{8G}{3}}\,(1+3w)\,\rho_0^{3/2} - \frac{\beta^*}{12}\,G\,(1+2w)\,\rho_0^2\,, \tag{4.49}$$

where w is defined through the equation of state $p_0 = w\rho_0 c^2$, and can take a range of values $w \in [-1, 1/3]$ for different epochs in the evolution of the Universe. To obtain the variations in Eqs. (4.48) and (4.49), the QG modified Friedmann Eqs. (4.39) and (4.40) were expanded in a Taylor series up to the fourth order in α^* and second order in β^*, to obtain all terms up to quadratic order in the GUP parameters.

In considerations of generating the baryon asymmetry, w is taken to be constant, since all the relevant physics happens in the radiation-dominated era with $w = 1/3$. As seen from the following, QG effects break thermal equilibrium and modify $\dot{R}$, making it non-vanishing. To obtain the QG corrected derivative of the Ricci scalar $\dot{R}$, one takes the trace of the Einstein equations

$$R = -\frac{8\pi G}{c^4}\,T_g = -\frac{8\pi G}{c^4}(\rho c^2 - 3p)\,, \tag{4.50}$$

where $T_g = \rho c^2 - 3p$ is the trace of the energy-momentum tensor. The QG corrected Ricci scalar is obtained by plugging the density and pressure from Eq. (4.47), with their respective variations from Eqs. (4.48) and (4.49) in Eq. (4.50), and reads as

$$R = -\frac{8\pi G}{c^2}\,(1-3w)\,\rho_0 + \alpha^*\,\frac{8\sqrt{2}\pi}{3\sqrt{3}c^3}G^{3/2}(1+9w)\,\rho_0^{3/2} - \beta^*\,\frac{4\pi}{3c^4}\,G^2(1+3w)\,\rho_0^2\,. \tag{4.51}$$

Next, to compute the time derivative of the Ricci scalar from Eq. (4.51), one considers the

continuity equation from Eq. (C.4) from Appendix C.1 for $n = 3$, which reads as

$$\dot{\rho}_0 + 3H(1+w)\rho_0 = 0 \tag{4.52}$$

and the equilibrium form of the second Friedmann equation $H^2 = 8\pi G\rho_0/3$ (as corrections to the latter would only contribute to orders higher than those considered in this paper). Also, even if the constant vacuum energy density Λ is not negligible, its time derivative would vanish and the following results would remain unchanged. Therefore, the QG corrected time derivative of the Ricci scalar turns out as

$$\begin{aligned}\dot{R} = \sqrt{3}(8\pi)^{3/2}\frac{G^{3/2}}{c^2}(1-2w-3w^2)\rho_0^{3/2} - \alpha^* 16\pi^{3/2}\frac{G^2}{c^3}(1+w)(1+9w)\rho_0^2 \\ + \beta^*\frac{(8\pi)^{3/2}}{\sqrt{3}}\frac{G^{5/2}}{c^4}(1+3w)(1+w)\rho_0^{5/2}\,.\end{aligned} \tag{4.53}$$

The above derivative of the Ricci scalar is then evaluated at the radiation-dominated era, when $w = 1/3$, and reads as

$$\dot{R} = -\alpha^*\frac{256}{3}\pi^{3/2}\frac{G^2}{c^3}\rho_0^2 + \beta^* 8\left(\frac{8\pi}{3}\right)^{3/2}\frac{G^{5/2}}{c^4}\rho_0^{5/2}\,. \tag{4.54}$$

From the above one can see, that QG effects provide an essential mechanism to break the thermal equilibrium, thus satisfying the third and final Sakharov condition. One then substitutes Eq. (4.54) in the baryon asymmetry formula from Eq. (4.45) to obtain [157]

$$\begin{aligned}\eta_{BA} = \alpha_0\frac{112\pi^2 g_* g_B}{45}\left(\frac{k_B T_D}{M_P c^2}\right)^7\left(\frac{M_P}{M_*}\right)^2 \\ -\beta_0\frac{896\sqrt{5}\,\pi^3 g_*^{3/2} g_B}{675}\left(\frac{k_B T_D}{M_P c^2}\right)^9\left(\frac{M_P}{M_*}\right)^2\,,\end{aligned} \tag{4.55}$$

where the gravitational constant is expressed in terms of the Planck mass, i.e., $G = \hbar c/M_P^2$,

and the equilibrium density ρ_0, in the radiation-dominated era, is replaced by [227]

$$\rho_0 = \frac{\pi g_*}{30\hbar^3 c^5} (k_B T)^4 \ . \tag{4.56}$$

In order to obtain an estimate of the GUP parameters, the expression in Eq. (4.55) is evaluated at the relevant epoch in the evolution of the Universe. That is, at the decoupling temperature T_D, given by $k_B T_D = M_I c^2$, where $M_I \sim 2\times 10^{16}\,\mathrm{GeV}/c^2$ is the upper bound on the tensor mode fluctuation constraints in the inflationary scale [228], and the cutoff scale M_* is taken to be the reduced Planck mass, namely $M_* = M_P/\sqrt{8\pi}$. The baryon asymmetry then reads as

$$\eta_{BA} = \alpha_0\, 2.08\times 10^{-15} - \beta_0\, 2.16\times 10^{-19} \ . \tag{4.57}$$

Given the measured baryon asymmetry $5.7\times 10^{-10} \lesssim \eta_{BA} \lesssim 9.9\times 10^{-10}$ [229, 230, 231, 232, 233, 234], the dimensionless GUP parameters can be estimated for four distinct cases [157]:

- Only linear GUP ($\beta_0 = 0$): $2.74\times 10^5 \lesssim \alpha_0 \lesssim 4.76\times 10^5$
- Only quadratic GUP ($\alpha_0 = 0$): $-4.58\times 10^9 \lesssim \beta_0 \lesssim -2.64\times 10^9$
- Linear and Quadratic GUP ($\beta_0 = -\alpha_0^2$): $6.37\times 10^4 \lesssim \alpha_0 \lesssim 8.66\times 10^4$ and $-7.50\times 10^9 \lesssim \beta_0 \lesssim -4.05\times 10^9$
- Linear and Quadratic GUP: $\alpha_0 \gtrsim 10^4$ and $\beta_0 \lesssim -2.59\times 10^9$

Based on the available measurements of the baryon asymmetry, the dimensionless GUP parameters are estimated by the above ranges, depending on the choice of model. Overall, the parameters α_0 and $\sqrt{-\beta_0}$ are expected to lie between 5.14×10^4 and 4.76×10^5, except for the last case, where the lower bounds $\alpha_0 \gtrsim 10^4$ and $\sqrt{-\beta_0} \gtrsim 5.09\times 10^4$ are obtained. To estimate these bounds $\beta_0 = \alpha_0^2 + \beta_0'$ was used in Eq. (4.57), since $O(\beta_0) \sim O(\alpha_0^2)$. Here

β_0' is a deviation of β_0 from α_0^2. The first three cases set the minimum measurable length scale to be $8.33 \times 10^{-31}\,\mathrm{m} \lesssim \ell_{min} \lesssim 7.71 \times 10^{-30}\,\mathrm{m}$, depending on the model. Note that the dimensionless quadratic GUP parameter β_0 has a negative value.

4.2.4 Summary

The baryon asymmetry produced in the radiation-dominated era of the Universe can be explained, if there is a mechanism satisfying the three Sakharov conditions. In the above, it has been shown that this mechanism can indeed be achieved within the context of QG effects. The CP symmetry is broken by the coupling between the derivative of the Ricci scalar and the baryon current, described by Eq. (4.41) and interactions which break the baryon number B (GUT interactions, for example see Ref. [227]) are considered. Finally, the thermal equilibrium is broken by QG effects, implied by GUP. Therefore, through this mechanism, all three Sakharov conditions are satisfied.

The obtained values of GUP parameters, α_0 and $\sqrt{-\beta_0}$ between 5.14×10^4 and 4.76×10^5, are one of the most stringent that have been obtained so far, and can be interpreted as their measurements. Note that a negative value of the quadratic GUP parameter, i.e., $\beta < 0$, is a common result in cosmological QGP considerations [54, 81, 152, 154, 157].

Chapter 5

The Quantum Equivalence Principle

> "Nobody ever figures out what life is all about, and it doesn't matter. Explore the world. Nearly everything is really interesting if you go into it deeply enough."
>
> *Richard P. Feynman*

Since the Equivalence Principle provided a basis for the formulation of GR, it is natural that a precise formulation of the Quantum Equivalence Principle (QEP) would be an important step towards a successful theory of QG [235]. The classical Equivalence Principle states that one can choose a locally inertial coordinate system at every point in an arbitrary space-time background (i.e. in an arbitrary gravitational field), so that in a very small region around that point, the laws of Nature take the same form as in an unaccelerated coordinate system in flat space-time (i.e., in a zero gravitational field) [236]. This statement of the equivalence principle can be divided into three short postulates. First is the weak equivalence principle (WEP), which states the equality between inertial and gravitational masses of the test particle. Second, laws of physics, excluding gravitation, in a freely falling reference frame are independent of the velocity of such a reference frame, which is also known as local Lorentz invariance (LLI). Third, all laws of physics are independent of the position and time, which is also known as local position invariance (LPI) [3]. Note that the statements of WEP, LLI and LPI taken together, are known as the Einstein Equiv-

alence Principle, and when extended to include gravitation, they are known as the Strong Equivalence Principle [237].

A quantum formulation of the Equivalence Principle, encompassing all of the above, was introduced in Ref. [238], where different inertial, gravitational and rest masses are introduced and promoted to quantum operators. The equality of these mass operators constitutes the QEP (see Eq. (5.7)). However, the application of QEP, in the above, is limited to particles at non-relativistic speeds, weak gravitational fields and does not take the spin of particles into account. Therefore, a generalized application of QEP, for particles at relativistic speeds, arbitrary curved space-times and which is valid for bosons as well as fermions, is important and proposed in this chapter. To the best of one's knowledge, there are no previous works on QEP, considering a formulation which is applicable to both, bosons and fermions, and in an arbitrary curved space-time. If QEP is violated in Nature, the above generalization implies that the Lorentz transformation and the space-time geometry obtain modifications, which make them dependent on the massive test particle under consideration. This in turn predicts deviations from standard results, obtained from QT and GR, and provides a novel framework to conduct experimental tests of QEP. Such tests are important to establish concepts which will lead towards a consistent theory of QG, and present a novel approach in the field of QGP. In the following, the metric signature $(+,-,-,-)$ is used. Supporting material for this chapter is found in Appendix D.

5.1 Particle Statistics

To formulate a framework for QEP, valid for particles with arbitrary speeds and in curved space-times, one must first consider the statistics of particles, i.e., the spin of particles. Special relativistic generalization of QM (relativistic QFTs) naturally introduces the spin of particles, which is reflected in their equations of motion [239]. The relativistic equations of motion, for spin-0 particles (bosons) and spin-$1/2$ particles (fermions), are the Klein-Gordon equation and the Dirac equation, respectively, which can be generalized in an

arbitrary curved space-time [4, 5] (see Eqs. (1.6) and (1.7)). In order to conveniently verify that the following generalization agrees with the results obtained in Ref. [238], in the non-relativistic and weak gravitational field limits, one adopts the Hamiltonian formalism. This is achieved by using the Feshbach-Villars formalism [136] (see also Refs. [134, 135] and the relativistic BEC considerations in Section 3.1.4), suitably adapted to obtain an effective Hamiltonian in curved space-time for bosons, and by using the standard Dirac Hamiltonian in curved space-time for fermions.

For a relativistic boson with mass m, one takes the effective Hamiltonian in the Feshbach-Villars formalism, generalized in an arbitrary curved space-time, which reads as

$$H = \tau_3 \frac{1}{\sqrt{g^{00}}} mc^2 - (\tau_3 + i\tau_2) \frac{g^{ij}}{\sqrt{g^{00}}} \frac{p_i p_j}{2m} + (\tau_3 + i\tau_2) \frac{g^{0i}}{\sqrt{g^{00}}} \frac{p_0 p_i}{m} , \tag{5.1}$$

where τ_k ($k = 1,2,3$) are the Pauli matrices, $g^{\mu\nu}$ the curved space-time metric, $p_0 = i\frac{\hbar}{c}\nabla_0$ the energy operator and $p_i = -i\hbar\nabla_i$ the momentum operators. The Pauli matrices in this formalism are used simply for convenience, and in no way reflects the actual spin of the particle. They are also not affected by the curvature of space-time. Note that the Feshbach-Villars formalism in curved space-time has been studied previously in other representations (see Refs. [240, 241]). However, the formulation in the representation, given by Eq. (5.1), is introduced for the first time here, to the best of one's knowledge. For details on obtaining the Klein-Gordon equation in curved space-time from the above Feshbach-Villars Hamiltonian in curved space-time, see Appendix D.1.

For a relativistic fermion with mass m, one takes the Dirac Hamiltonian in curved space-time, suitably adapted to the metric signature used here, which reads as [5]

$$H = \frac{1}{g^{00}} \underline{\gamma}^0 \underline{\gamma}^i p_i c + i\hbar\Gamma_0 + \frac{1}{g^{00}} \underline{\gamma}^0 mc^2 , \tag{5.2}$$

where $\underline{\gamma}^\mu = e^\mu_a \gamma^a$ are the curved space-time Dirac gamma matrices, with e^μ_a the tangent space basis vectors, called vierbeins (or tetrads) and γ^a the flat space-time Dirac gamma

matrices in the tangent space. The vierbeins are defined by $g^{\mu\nu} = e^{\mu}_{a} e^{\nu}_{b} \eta^{ab}$, where η^{ab} is the Minkowski metric of the tangent space. The momentum operator $p_i = -i\hbar D_i$ is defined in terms of the covariant derivative for fermions, which takes the form $D_\mu = \partial_\mu - \Gamma_\mu$, where

$$\Gamma_\mu = -\frac{1}{4} \gamma_a \gamma_b e^{a}_{\nu} g^{\nu\lambda} e^{b}_{\lambda;\mu} \tag{5.3}$$

is the spinor affine connection for a free fermion. In the above $e^{b}_{\lambda;\mu} = \partial_\mu e^{b}_{\lambda} - \Gamma^{\rho}_{\mu\lambda} e^{b}_{\rho}$, where $\Gamma^{\rho}_{\mu\lambda}$ are the standard Christoffel symbols. The curved space-time Dirac gamma matrices $\underline{\gamma}^{\mu}$ satisfy the algebra

$$\underline{\gamma}^{\mu} \underline{\gamma}^{\nu} + \underline{\gamma}^{\nu} \underline{\gamma}^{\mu} = 2 g^{\mu\nu} \ . \tag{5.4}$$

For details on obtaining the Dirac equation in curved space-time from the above Dirac Hamiltonian in curved space-time, see Appendix D.1.

Hamiltonians in Eqs. (5.1) and (5.2) are the starting point for the generalization of the formalism from Ref. [238]. In the non-relativistic and weak gravitational field limits, they both reduce to

$$H = mc^2 + \frac{p^2}{2m} + m\phi \ , \tag{5.5}$$

where ϕ is the Newtonian gravitational potential. Note that a spin of a particle is no longer relevant in these limits, which why Eqs. (5.1) and (5.2) reduce to the same expression. The above Hamiltonian is used as a starting point in Ref. [238]. The first term corresponds to the rest energy, the second term to the kinetic energy and the third term to the gravitational energy of a classical particle.

5.2 Generalized Formalism

To formulate QEP, one must discriminate between the inertial, gravitational and rest masses m_I, m_G and m_R, respectively, of a test particle. Measurements show that their values agree with each other up to a relative difference $\sim 10^{-15}$ for m_I and m_G (WEP) [242], $\sim 10^{-19}$ for m_I and m_R (LLI) [243], and $\sim 10^{-7}$ for m_G and m_R (LPI) [244], within the current precision of experiments (see also Refs. [3, 245]). However, at some scale they may be different from each other, since there is no known fundamental reason, why they should be identical. In this case, the mass of a composite test particle can be affected by internal quantum effects. To describe such effects, masses m_α, where $\alpha = I, G, R$, are promoted to quantum operators $m_\alpha \longrightarrow \mathcal{M}_\alpha$ as [238]

$$\mathcal{M}_\alpha = m_\alpha + \frac{H_{int,\alpha}}{c^2} \ , \tag{5.6}$$

where $H_{int,\alpha}$ effectively describe internal quantum effects of the composite particle, related to its internal degrees of freedom, and drives the non-trivial internal evolution (see Ref. [238] for details on $H_{int,\alpha}$). Note that operators $\mathcal{M}_\alpha$ describe the total mass-energy of a composite quantum particle, where m_α is the ground state. Furthermore, the definition of mass operators $\mathcal{M}_\alpha$ in this generalization does not change from that in Ref. [238], since they are defined in an unaccelerating frame of the particle. However, at relativistic speeds and strong gravitational fields, their eigenvalues are expected to differ from the non-relativistic ones. As in Ref. [238], QEP is postulated as

$$\mathcal{M}_I = \mathcal{M}_G = \mathcal{M}_R \ . \tag{5.7}$$

The above equalities are quantum generalizations of the three short postulates of the classical Equivalence Principle. $\mathcal{M}_I = \mathcal{M}_G$ corresponds to the WEP, $H_{int,R} = H_{int,I}$ corresponds to the LLI and $H_{int,R} = H_{int,G}$ corresponds to the LPI.

To apply the above QEP to particles at relativistic speeds and arbitrary curved space-

times, one must first identify masses m_α in the Hamiltonian under consideration, before promoting them to quantum operators. Such identification of masses is obvious for the Hamiltonian in Eq. (5.5). The mass in the rest energy term corresponds to m_R, the mass in the kinetic energy term to m_I and the mass in the gravitational energy term to m_G. For Hamiltonians in Eqs. (5.1) and (5.2), such identification of masses m_α is more involved. One starts with classical SR in flat space-time, continues with classical GR, and finally, applies these results to Hamiltonians in Eqs. (5.1) and (5.2), where m_α are promoted to quantum operators.

5.2.1 Special Relativity

Since SR is formulated in flat space time, i.e., no gravitational field, one cannot define m_G for a massive relativistic particle in this context. On the other hand, such a particle at rest has rest energy defined by mass m_R, and can have kinetic energy when accelerated, which implies it has inertial mass m_I as well. The standard relativistic energy-momentum dispersion relation $E^2 = p^2c^2 + m^2c^4$ suggests there is only one mass m. However, by a careful comparison with the above non-relativistic case (see Appendix D.2), one obtains a modified energy-momentum dispersion relation as [246]

$$E^2 = \frac{m_R}{m_I}\, p^2c^2 + m_R^2 c^4 \ . \tag{5.8}$$

Using the above, one can show that the Lorentz factor γ obtains corresponding modifications (see Appendix D.2) as

$$\gamma = \frac{1}{\sqrt{1 - \frac{m_I}{m_R}\frac{v^2}{c^2}}} \ . \tag{5.9}$$

To see how this affects the Lorentz transformation, one considers a particle at rest, $\mathbf{p} = 0$, with energy $E = m_R c^2$, and applies a Lorentz boost transformation to an inertial frame with velocity $\mathbf{v} = (v_x, v_y, v_z)$. The particle is now in motion, $\mathbf{p} = m_I \mathbf{v}\gamma$, and has energy given by

Eq. (5.8). Such a Lorentz boost transformation, obtained for the first time, reads as [246]

$$\Lambda^{\mu}_{\nu}(\mathbf{v}, m_{\alpha}) = \begin{bmatrix} \gamma & -\gamma\sqrt{\frac{m_I}{m_R}}\frac{v_x}{c} & -\gamma\sqrt{\frac{m_I}{m_R}}\frac{v_y}{c} & -\gamma\sqrt{\frac{m_I}{m_R}}\frac{v_z}{c} \\ -\gamma\sqrt{\frac{m_I}{m_R}}\frac{v_x}{c} & 1+(\gamma-1)\frac{v_x^2}{v^2} & (\gamma-1)\frac{v_x v_y}{v^2} & (\gamma-1)\frac{v_x v_z}{v^2} \\ -\gamma\sqrt{\frac{m_I}{m_R}}\frac{v_y}{c} & (\gamma-1)\frac{v_y v_x}{v^2} & 1+(\gamma-1)\frac{v_y^2}{v^2} & (\gamma-1)\frac{v_y v_z}{v^2} \\ -\gamma\sqrt{\frac{m_I}{m_R}}\frac{v_z}{c} & (\gamma-1)\frac{v_z v_x}{v^2} & (\gamma-1)\frac{v_z v_y}{v^2} & 1+(\gamma-1)\frac{v_z^2}{v^2} \end{bmatrix} . \quad (5.10)$$

Such a modification can also be considered for a general Lorentz transformation, which includes rotations. However, one would learn nothing new, since the rotational part remains unmodified. The Lorentz transformation, given by Eq. (5.10), ensures that for an arbitrary 4-vector V^{μ}, the norm $|V|^2 = V_{\mu}V^{\mu}$ is preserved in any reference frame. Note that vectors with modifications to the spatial components, such as seen in Eq. (D.14) from Appendix D.2, also have their norm preserved. By considering a system with two non-interacting particles, it turns out that the modified Lorentz transformation from Eq. (5.10) implies a violation

$$\Lambda^{\mu}_{\nu}(\mathbf{v}, m_{1,\alpha})\, p_1^{\nu} + \Lambda^{\mu}_{\nu}(\mathbf{v}, m_{2,\alpha})\, p_2^{\nu} \neq \Lambda^{\mu}_{\nu}(\mathbf{v}, m_{1,\alpha} + m_{2,\alpha})\, (p_1^{\nu} + p_2^{\nu}) \,, \quad (5.11)$$

from where one can see that the particle masses do not just simply add up under the new Lorentz transformation. This is known as the *soccer-ball problem* [42], and is a common feature in most candidate theories of QG. The above result implies that if Nature does not exhibit this problem on any scale, the LLI must necessarily be satisfied. Note however, that regardless of whether LLI holds, or is broken, the modified Lorentz transformation from Eq. (5.10) still forms a group and the generators of this group are still the standard Lorentz generators, since modifications affect only the boost parameters. The above modifications can be effectively interpreted as modifications to the speed of light $c' = c\sqrt{m_R/m_I}$, which is different for particles with different masses. See Appendix D.2 for further details on modifications of SR.

5.2.2 General Relativity

Near gravitating objects, a massive test particle interacts with their gravitational fields, where one can naturally define m_G, and include it in the above considerations. In GR gravitational fields are treated as curvature of space-time, described by a metric $g^{\mu\nu}$. Note that a contravariant metric is considered, in order for the following results to be directly applicable in Eqs. (5.1) and (5.2), given their definitions. In principle, one could start with a covariant metric $g_{\mu\nu}$, but would then need to obtain its inverse to apply it in Eqs. (5.1) and (5.2). To modify GR in this formalism, one must solve the Einstein equations (see Eq. (1.3)) for a given curved space-time, and carefully evaluate the integration constants, which turn out to be affected by m_α. The integration constants are evaluated in the asymptotic limit, where the gravitational potential is classical, i.e., described by ϕ, and modified through Newton's second law

$$m_I \mathbf{a} = -m_G \nabla\phi \,, \tag{5.12}$$

which defines the WEP. Since GR is a relativistic theory, m_R appears by means of SR modifications. Therefore, the resulting $g^{\mu\nu}$ obtains modification factors in the form of mass ratios $m_\alpha/m_{\alpha'}$, where $\alpha, \alpha' = I, G, R$. Note that similar proposals, where properties of curved space-times depend on test particle properties, have been studied elsewhere (for example, see Refs. [40, 165, 247, 248, 249, 250]). In this section, three special cases of curved space-times are considered, namely a curved space-time corresponding to a spherically symmetric weak gravitational field, its generalization to the Schwarzschild space-time and the Kerr space-time. The above mass ratios change the differential equations of GR (Einstein equations) only in the constant κ (see Appendix D.4). They effectively modify the universal gravitational constant G (see following sections) and the speed of light c (see Section 5.2.1). This implies that such modifications are universal for a given test particle, which also applies in the case of time dependent curved space-times, such as gravitational

wave considerations [236] and particle emitting (or absorbing) objects, for example, described by the Vaidya metric [251].

Weak Gravitational Field

The most relevant case for Earth-based experiments is that of a weak gravitational field, i.e., $|\phi/c^2| \ll 1$. This approximation is also valid for gravitational fields of planets and far from other gravitating objects. The standard metric of a weak gravitational field in Cartesian coordinates is given by [252]

$$g^{\mu\nu} = \begin{bmatrix} 1-2\frac{\phi}{c^2} & O(c^{-5}) \\ O(c^{-5}) & -\mathbb{1}_{3x3}\left(1+2\frac{\phi}{c^2}\right) \end{bmatrix}, \tag{5.13}$$

where the off-diagonal elements are of order $O(c^{-5})$ and can be ignored. In the standard derivation of the above metric, there is one integration constant $K = -2GM/c^2 = 2\phi r/c^2$, where M is the mass of the central object (in context of the different masses, M is the rest mass of the central object). However, in the case where one identifies masses m_α of a test particle, it turns out that K obtains a factor m_G/m_R (see Appendix D.3), which affects the metric as [246]

$$g^{\mu\nu}(m_\alpha) = \begin{bmatrix} 1-2\frac{m_G}{m_R}\frac{\phi}{c^2} & O(c^{-5}) \\ O(c^{-5}) & -\mathbb{1}_{3x3}\left(1+2\frac{m_G}{m_R}\frac{\phi}{c^2}\right) \end{bmatrix}, \tag{5.14}$$

from where one can see that the mass ratio m_G/m_R modifies the metric in the temporal and all spatial components, while the inertial mass m_I does not affect it. Note that the above metric is given in a Cartesian coordinate system for convenience of use in Earth-based experiments. Because of the weakness of the gravitational field, it is straightforward to expand the g^{00} component in Hamiltonians from Eqs. (5.19) and (5.24) as a power series.

Schwarzschild Space-time

One of the most studied space-times in GR is the Schwarzschild space-time. Its metric is obtained by solving the vacuum Einstein equations under the assumptions of staticity, spherical symmetry and asymptotic flatness. The standard Schwarzchild metric in spherical coordinates is given by [253]

$$g^{\mu\nu} = \begin{bmatrix} \left(1-\frac{2GM}{c^2 r}\right)^{-1} & 0 & 0 & 0 \\ 0 & -\left(1-\frac{2GM}{c^2 r}\right) & 0 & 0 \\ 0 & 0 & -\frac{1}{r^2} & 0 \\ 0 & 0 & 0 & -\frac{1}{r^2\sin^2\theta} \end{bmatrix}. \tag{5.15}$$

In the standard derivation, there is also one integration constant $K = -2GM/c^2$. However, in the case where one identifies masses m_α of a test particle, it turns out that K obtains a factor m_G/m_R (see Appendix D.3), which affects the metric as [246]

$$g^{\mu\nu}(m_\alpha) = \begin{bmatrix} \left(1-\frac{m_G}{m_R}\frac{2GM}{c^2 r}\right)^{-1} & 0 & 0 & 0 \\ 0 & -\left(1-\frac{m_G}{m_R}\frac{2GM}{c^2 r}\right) & 0 & 0 \\ 0 & 0 & -\frac{1}{r^2} & 0 \\ 0 & 0 & 0 & -\frac{1}{r^2\sin^2\theta} \end{bmatrix}, \tag{5.16}$$

from where one can again see that the mass ratio m_G/m_R modifies the metric only in the temporal and radial components, while the inertial mass m_I does not affect it. Note that the Schwarzschild metric in Eq. (5.16) and the weak field metric in Eq. (5.14) obtain modifications in the same way. This is because the latter is a weak field limit of the former.

Kerr Space-time

One of the most interesting space-times in GR is the Kerr space-time, since it incorporates rotation of the central object. Most objects in the Universe, including astrophysical

black holes, rotate at one rate or another and can in general be described by the Kerr space-time. The Kerr metric is obtained by solving the Einstein equations under the assumptions of stationarity, axisymmety and asymptotic flatness. The standard Kerr metric in spherical coordinates is given by [253]

$$g^{\mu\nu} = \begin{bmatrix} \frac{\Sigma^2}{\rho^2\Delta} & 0 & 0 & 2\frac{GMar}{c^2\rho^2\Delta} \\ 0 & -\frac{\Delta}{\rho^2} & 0 & 0 \\ 0 & 0 & -\frac{1}{\rho^2} & 0 \\ 2\frac{GMar}{c^2\rho^2\Delta} & 0 & 0 & -\frac{\Delta - a^2\sin^2\theta}{\rho^2\Delta\sin^2\theta} \end{bmatrix}, \tag{5.17}$$

where $\Sigma^2 = \left(r^2+a^2\right)^2 - a^2\Delta\sin^2\theta$, $\Delta = r^2 - (2GM/c^2)\,r + a^2$, $\rho^2 = r^2 + a^2\cos^2\theta$ and a is the reduced angular momentum of the central object. In the standard derivation, there are two integration constants $K = -2GM/c^2$ and $L = J/Mc \equiv a$, where J is the angular momentum of the central object. K is obtained in the same way as in the Schwarzschild case and L is obtained from the relativistic angular momentum, given by the energy-momentum tensor of a rotating body [254]. However, in the case where one identifies test masses m_α of a test particle, it turns out K obtains a factor m_G/m_R and L obtains a factor $\sqrt{m_I/m_R}$ (see Appendix D.4), which affect the metric as [246]

$$g^{\mu\nu}(m_\alpha) = \begin{bmatrix} \frac{\Sigma^2(m_\alpha)}{\rho^2(m_\alpha)\,\Delta(m_\alpha)} & 0 & 0 & 2\frac{m_G m_I^{1/2}}{m_R^{3/2}}\frac{GMar}{c^2\rho^2(m_\alpha)\,\Delta(m_\alpha)} \\ 0 & -\frac{\Delta(m_\alpha)}{\rho^2(m_\alpha)} & 0 & 0 \\ 0 & 0 & -\frac{1}{\rho^2(m_\alpha)} & 0 \\ 2\frac{m_G m_I^{1/2}}{m_R^{3/2}}\frac{GMar}{c^2\rho^2(m_\alpha)\,\Delta(m_\alpha)} & 0 & 0 & -\frac{\Delta(m_\alpha) - \frac{m_I}{m_R}a^2\sin^2\theta}{\rho^2(m_\alpha)\,\Delta(m_\alpha)\sin^2\theta} \end{bmatrix}, \tag{5.18}$$

where $\Sigma^2(m_\alpha) = \left(r^2 + \frac{m_I}{m_R}a^2\right)^2 - \frac{m_I}{m_R}a^2\Delta(m_\alpha)\sin^2\theta$, $\Delta(m_\alpha) = r^2 - \frac{m_G}{m_R}(2GM/c^2)\,r + \frac{m_I}{m_R}a^2$ and $\rho^2(m_\alpha) = r^2 + \frac{m_I}{m_R}a^2\cos^2\theta$. From the above modified Kerr metric, one can see that all three masses m_α modify the metric in all its non-vanishing components, unlike the

Schwarzschild case in which only m_G/m_R are involved. If the rotation of such an object vanishes, i.e., $a \longrightarrow 0$, then the modified Schwarzschild solution from Eq. (5.16) is recovered. The fact that the inertial mass m_I affects the metric only for the rotating (non-static) case, can be interpreted as a consequence of inertial frame dragging induced by the rotation of the central object.

The modifications from the above cases, can be effectively interpreted as modifications to the universal gravitational constant $G' = G m_G/m_I$. The modification of constant L (see definition above), stems from the modification of c, shown in Section 5.2.1. To avoid the above procedure for arbitrary space-times, one can assume $G \longrightarrow G'$ and $c \longrightarrow c'$ for a given particle species, and solve the Einstein equations using standard methods.

5.2.3 Bosons

In the case of relativistic bosons in curved space-time, the Hamiltonian from Eq. (5.1) contains three terms with mass. Since it has a form, similar to the classical Hamiltonian in Eq. (5.5), one can identify m_R and m_I in the first two terms. The mass in the third term turns out to be a combination of m_R and m_I, which is consistent with the modified Klein-Gordon equation in curved space-time (see Appendix D.1). The gravitational mass m_G plays a role in the Hamiltonian through $g^{\mu\nu}(m_\alpha)$. The effective Hamiltonian for relativistic bosons from Eq. (5.1) can then be written as

$$\begin{aligned} H = \tau_3 \frac{1}{\sqrt{g^{00}(m_\alpha)}} m_R c^2 - (\tau_3 + i\tau_2) \frac{g^{ij}(m_\alpha)}{\sqrt{g^{00}(m_\alpha)}} \frac{p_i p_j}{2 m_I} \\ + (\tau_3 + i\tau_2) \frac{g^{0i}(m_\alpha)}{\sqrt{g^{00}(m_\alpha)}} \frac{p_0 p_i}{\sqrt{m_R m_I}} \, . \end{aligned} \tag{5.19}$$

From the above, one can obtain the modified Klein-Gordon equation in curved space-time (see Appendix D.1), which is used to determine the corresponding modified scalar field

Lagrangian in curved space-time [246]

$$\mathcal{L} = \frac{1}{2}\, g^{\mu\nu}(m_\alpha)\, \tilde{\partial}_\mu \Phi\, \tilde{\partial}_\nu \Phi - \frac{1}{2}\, \frac{m_R^2 c^2}{\hbar^2}\, \Phi^2 \,, \tag{5.20}$$

where $\tilde{\partial}_\mu = \left(\frac{1}{c}\partial_0, \sqrt{\frac{m_R}{m_I}}\boldsymbol{\partial} \right)$ (see Appendix D.2). The above Lagrangian can be used to test QEP with bosons in the framework of QFT in curved space-time.

By promoting m_α to quantum operators, $m_\alpha \longrightarrow \mathcal{M}_\alpha$ as seen in Eq. (5.6), one notices that the metric gets promoted to a quantum operator as well, $g^{\mu\nu}(m_\alpha) \longrightarrow \mathfrak{g}^{\mu\nu}(\mathcal{M}_\alpha)$. Considering $m_\alpha \gg \langle H_{int,\alpha} \rangle / c^2$ and using Eq. (5.6), the Hamiltonian from Eq. (5.19) can be written as [246]

$$\begin{aligned}
H = {} & \tau_3 \frac{1}{\sqrt{\mathfrak{g}^{00}(\mathcal{M}_\alpha)}}\, m_R c^2 - (\tau_3 + i\tau_2)\, \frac{\mathfrak{g}^{ij}(\mathcal{M}_\alpha)}{\sqrt{\mathfrak{g}^{00}(\mathcal{M}_\alpha)}}\, \frac{p_i\, p_j}{2\, m_I} + (\tau_3 + i\tau_2)\, \frac{\mathfrak{g}^{0i}(\mathcal{M}_\alpha)}{\sqrt{\mathfrak{g}^{00}(\mathcal{M}_\alpha)}}\, \frac{p_0\, p_i}{\sqrt{m_R\, m_I}} \\
& + \tau_3 \frac{1}{\sqrt{\mathfrak{g}^{00}(\mathcal{M}_\alpha)}}\, H_{int,R} + (\tau_3 + i\tau_2)\, \frac{\mathfrak{g}^{ij}(\mathcal{M}_\alpha)}{\sqrt{\mathfrak{g}^{00}(\mathcal{M}_\alpha)}}\, H_{int,I}\, \frac{p_i\, p_j}{2\, m_I^2 c^2} \\
& - (\tau_3 + i\tau_2)\, \frac{\mathfrak{g}^{0i}(\mathcal{M}_\alpha)}{\sqrt{\mathfrak{g}^{00}(\mathcal{M}_\alpha)}}\, H_{int,R}\, \frac{p_0\, p_i}{2\, m_R^{3/2}\, m_I^{1/2}\, c^2} \\
& - (\tau_3 + i\tau_2)\, \frac{\mathfrak{g}^{0i}(\mathcal{M}_\alpha)}{\sqrt{\mathfrak{g}^{00}(\mathcal{M}_\alpha)}}\, H_{int,I}\, \frac{p_0\, p_i}{2\, m_R^{1/2}\, m_I^{3/2}\, c^2} \,,
\end{aligned} \tag{5.21}$$

where the additional terms with $H_{int,\alpha}$ represent first order corrections due to internal quantum effects of a composite boson. They allow to make predictions to test such effects and probe QEP. Note that terms with $H_{int,G}$ are implicit in $\mathfrak{g}^{\mu\nu}(m_\alpha)$ and depend on the given space-time. Note that also inverses of quantum operators are part of Eq. (5.21). Applying this formalism to concrete physical problems may present a difficult computational challenge, which needs to be dealt with appropriately.

Considering the weak gravitational field space-time, given by the metric in Eq. (5.14), one can see that the $\mathfrak{g}^{0i}(\mathcal{M}_\alpha)$ terms in the effective Hamiltonian in Eq. (5.21) vanish, because the off-diagonal components of the metric vanish. Since $\phi/c^2 \ll 1$, one can expand $\mathfrak{g}^{00}(\mathcal{M}_\alpha)$ as a power series to first order in ϕ/c^2. Eq. (5.21) in a weak gravitational field

then reads as

$$
\begin{aligned}
H = {} & \tau_3 m_R c^2 + \tau_3 m_G \phi + (\tau_3 + i\tau_2)\frac{p^2}{2m_I} + \tau_3 H_{int,R} + \tau_3 H_{int,G}\frac{\phi}{c^2} \\
& + (\tau_3 + i\tau_2)\frac{\phi}{c^2}\frac{3m_G p^2}{2m_I m_R} - (\tau_3 + i\tau_2) H_{int,R}\frac{\phi}{c^2}\frac{3m_G p^2}{2m_I m_R^2 c^2} \\
& + (\tau_3 + i\tau_2) H_{int,G}\frac{\phi}{c^2}\frac{3p^2}{2m_I m_R c^2} - (\tau_3 + i\tau_2) H_{int,I}\frac{\phi}{c^2}\frac{3m_G p^2}{2m_I^2 m_R c^2} \\
& - (\tau_3 + i\tau_2) H_{int,I}\frac{p^2}{2m_I^2 c^2} \, ,
\end{aligned} \tag{5.22}
$$

which corresponds to a relativistic boson in a weak gravitational field. To obtain a Hamiltonian for a non-relativistic boson, one must diagonalize the above effective Hamiltonian, represented by a 2×2 matrix, and expand the obtained square root in a Taylor series, up to terms of $O(1/c^2)$, since $\langle p^2 \rangle \ll m_I^2 c^2$ in the non-relativistic limit. The two diagonal elements correspond to a particle and an anti-particle. The obtained Hamiltonian then reads as

$$
H = m_R c^2 + m_G \phi + \frac{p^2}{2m_I} + H_{int,R} - H_{int,I}\frac{p^2}{2m_I^2 c^2} + H_{int,G}\frac{\phi}{c^2} \, , \tag{5.23}
$$

which is exactly the non-relativistic, weak gravitational field result, obtained in Ref. [238]. One can use Eqs. (5.22) and (5.23) to test QEP in their respective regimes.

5.2.4 Fermions

In the case of relativistic fermions in curved space-time, the Hamiltonian from Eq. (5.2) contains one term with mass, which can be identified as m_R. By a similar reasoning as was used to obtain Eq. (5.8) (see also Appendix D.3), one finds that the rest and inertial masses also affect the first term in Eq. (5.2). The second term acquires no such modifications. The gravitational mass m_G plays a role in the Hamiltonian through $g^{\mu\nu}(m_\alpha)$, and implicitly also through $\underline{\gamma}^\mu$ and Γ_μ. The Dirac Hamiltonian for relativistic fermions from Eq. (5.2) can then

be written as [246]

$$H = \frac{1}{g^{00}(m_\alpha)}\underline{\gamma}^0\underline{\gamma}^i\sqrt{\frac{m_R}{m_I}}\,p_i\,c + i\hbar\Gamma_0 + \frac{1}{g^{00}(m_\alpha)}\underline{\gamma}^0\,m_R\,c^2\ . \tag{5.24}$$

From the above, one can obtain the modified Dirac equation in curved space-time (see Appendix D.1), which is used to determine the corresponding modified Dirac Lagrangian in curved space-time [246]

$$\mathcal{L} = \overline{\Psi}\left(i\hbar\underline{\gamma}^\mu\tilde{D}_\mu - m_R\,c\right)\Psi\ , \tag{5.25}$$

where $\tilde{D}_\mu = \left(\frac{1}{c}D_0, \sqrt{\frac{m_R}{m_I}}\mathbf{D}\right)$ (see Appendix D.2). The above Lagrangian can be used to test QEP with fermions in the framework of QFT in curved space-time.

As seen in the case for bosons, one needs to promote m_α to quantum operators, $m_\alpha \longrightarrow \mathcal{M}_\alpha$, and the metric gets promoted to a quantum operator in the same manner, $g^{\mu\nu}(m_\alpha) \longrightarrow \mathfrak{g}^{\mu\nu}(\mathcal{M}_\alpha)$. Considering $m_\alpha \gg \langle H_{int,\alpha}\rangle/c^2$ and using Eq. (5.6), the Hamiltonian from Eq. (5.24) reads as

$$\begin{aligned} H = &\sqrt{\frac{m_R}{m_I}}\frac{1}{\mathfrak{g}^{00}(\mathcal{M}_\alpha)}\underline{\gamma}^0\underline{\gamma}^i\,p_i\,c + i\hbar\Gamma_0 + \frac{1}{\mathfrak{g}^{00}(\mathcal{M}_\alpha)}\underline{\gamma}^0\,m_R\,c^2 \\ &+ \frac{1}{2\sqrt{m_R\,m_I}\,c^2}\frac{1}{\mathfrak{g}^{00}(\mathcal{M}_\alpha)}\underline{\gamma}^0\underline{\gamma}^i\,H_{int,R}\,p_i\,c - \frac{m_R^{1/2}}{2\,m_I^{3/2}\,c^2}\frac{1}{\mathfrak{g}^{00}(\mathcal{M}_\alpha)}\underline{\gamma}^0\underline{\gamma}^i\,H_{int,I}\,p_i\,c \\ &+ \frac{1}{\mathfrak{g}^{00}(\mathcal{M}_\alpha)}\underline{\gamma}^0\,H_{int,R}\ , \end{aligned} \tag{5.26}$$

where the additional terms with $H_{int,\alpha}$ represent first order corrections due to internal quantum effects of a composite fermion. They allow to make predictions to test such effects and probe QEP. Note that terms with $H_{int,G}$ are implicit in $\mathfrak{g}^{\mu\nu}(m_\alpha)$, $\underline{\gamma}^\mu$ and Γ_μ, and depend on the given space-time. Note that inverses of quantum operators are part of Eq. (5.26) as well. Applying this formalism to concrete physical problems, may present the same computational challenge as in the case of bosons.

Considering the weak field space-time, given by the metric in Eq. (5.14), one can see that the vanishing off-diagonal terms do not explicitly change the form of the Dirac Hamiltonian in Eq. (5.24), as is the case for bosons. Since $\phi/c^2 \ll 1$, one can again expand $\mathfrak{g}^{00}(\mathcal{M}_\alpha)$ as a power series to first order in ϕ/c^2. Eq. (5.26) in a weak gravitational field then reads as

$$\begin{aligned} H = & \sqrt{\frac{m_R}{m_I}}\,\gamma^0\gamma^i\,p_i\,c + \gamma^0\,m_R\,c^2 + \gamma^0\,m_G\,\phi + 2\,\frac{m_G}{\sqrt{m_R\,m_I}}\,\gamma^0\gamma^i\,\frac{\phi}{c^2}\,p_i\,c + \gamma^0\,H_{int,R} \\ & + \gamma^0\,H_{int,G}\,\frac{\phi}{c^2} + \frac{1}{2\,\sqrt{m_R\,m_I}\,c^2}\,\gamma^0\gamma^i\,H_{int,R}\,p_i\,c - \frac{m_R^{1/2}}{2\,m_I^{3/2}\,c^2}\,\gamma^0\gamma^i\,H_{int,I}\,p_i\,c \\ & + \frac{2}{\sqrt{m_R\,m_I}\,c^2}\,\gamma^0\gamma^i\,H_{int,G}\,\frac{\phi}{c^2}\,p_i\,c - \frac{m_G}{m_R^{3/2}\,m_I^{1/2}\,c^2}\,\gamma^0\gamma^i\,H_{int,R}\,\frac{\phi}{c^2}\,p_i\,c \\ & - \frac{m_G}{m_R^{1/2}\,m_I^{3/2}\,c^2}\,\gamma^0\gamma^i\,H_{int,I}\,\frac{\phi}{c^2}\,p_i\,c\ , \end{aligned} \tag{5.27}$$

which corresponds to a relativistic fermion in a weak gravitational field. To obtain a Hamiltonian for a non-relativistic fermion, one must diagonalize the the above operator, represented as a 4×4 matrix, and expand the obtained square root in a power series, up to terms of $O(1/c^2)$, since $\langle p^2\rangle \ll m_I^2\,c^2$ in the non-relativistic limit. The obtained Hamiltonian then reads as Eq. (5.23).

The non-relativistic boson and fermion cases in a weak gravitational field show that the generalization of the QEP formalism in this chapter is necessary and sufficient to obtain the earlier results of Ref. [238] as a special case for weak gravitational fields and non-relativistic velocities.

5.3 Experimental Proposals

Although QEP is intrinsically quantum in nature, any violations are expected to leave traces in the classical Lorentz transformation $\Lambda^\mu_\nu(\mathbf{v}, m_\alpha)$, as well as in the classical curved space-time metric $g^{\mu\nu}(m_\alpha)$. They appear as averaged deviations of mass ratios from unity, given by the expectation values $\langle \mathcal{M}_\alpha/\mathcal{M}_{\alpha'}\rangle$. In principle, this can provide measurable ef-

fects. There are several ways in which QEP can be tested. The most common tests can be performed in Earth-based experiments, which correspond to non-relativistic particle speeds and a weak gravitational field (see Eq. (5.23)). These include the neutron interferometer experiment by Colella, Overhauser and Werner (COW) [255] to test the WEP and the proposals mentioned in Ref. [238] to test the LLI and the LPI. The COW experiment can be used to measure the effective gravitational mass $\langle \mathcal{M}_G \rangle$ of the neutron, since the violation of the QEP modifies the phase shift to [246]

$$\Delta\Phi = \frac{m_G\, g A}{\hbar\, v} + \frac{E_{int,G}\, g A}{\hbar\, c^2\, v} \,, \tag{5.28}$$

where g is the gravitational acceleration, $A = lh$ the area, l the length and h the height of the interferometer, v is the velocity of the neutron in the lower branch and $E_{int,G} = \langle H_{int,G} \rangle$ is the deviation, obtained from the precision of measuring $\Delta\Phi$, which is $\sim 10^{-3}$ [256]. The effective inertial mass of the neutron corresponds to the accepted value of the mass of the neutron, since it is measured kinematically. Comparing the obtained effective masses provides an upper bound of $\sim 10^{-3}$ for the deviation of m_G/m_I from unity. Promoting the above masses to quantum operators and considering the semi-classical limit, the above bound corresponds to the upper bound on the difference of eigenvalues $(E_{int,G} - E_{int,I})/mc^2$. This provides a test for the WEP. See Ref. [3] for more similar tests.

To test the QEP at relativistic speeds in the absence of a gravitational field, one can, for example, consider the mean lifetime τ of a particle in a cosmic ray shower, which is given by

$$\tau = \gamma \tau_0 \,, \tag{5.29}$$

where τ_0 is the mean lifetime of the particle in its rest frame and γ is Lorentz factor, defined in Eq. (5.9), containing the mass ratio m_I/m_R. Considering a charged pion decay, the mean lifetime in its rest frame is $\tau_0 = (26.0231 \pm 0.0050)\,\text{ns}$ [257]. It can be shown that this

measurement provides a speed dependent upper bound[5] of [246]

$$\delta < 3.84 \times 10^{-4} \left(\frac{c^2}{v^2} - 1 \right) \tag{5.30}$$

for the deviation of m_I/m_R from unity. One can see that the upper bound becomes smaller as the speed of the pion increases. Pions with the highest measurable energies travel with speeds close to the speed of light $v = 0.9999996\,c$ (inferred from Ref. [258]). For such pions the above upper bound is $\delta < 3.33 \times 10^{-10}$. Promoting the above masses to quantum operators and considering the semi-classical limit, the above bound corresponds to the upper bound on the difference of eigenvalues $\delta = (E_{int,I} - E_{int,R})/mc^2$, where $E_{int,I} = \langle H_{int,I} \rangle$ and $E_{int,R} = \langle H_{int,R} \rangle$. This provides a test of the LLI. Other tests of the LLI, using electromagnetic radiation, have been done in the past [3]. However, the results provided here are the first test of LLI for a massive particle to one's knowledge.

To test the QEP in strong gravitational fields and at relativistic speeds, one can, for example, consider the perihelion precession of planets. Following the procedure outlined in Ref. [236] (p. 194-200) and using the metric from Eq. (5.16), it turns out that the perihelion precession during one orbit gets modified by the relevant mass ratio as [246]

$$\Delta\varphi = 6\pi \frac{m_G}{m_R} \frac{GM}{c^2 a (1 - e^2)} \,, \tag{5.31}$$

where a is the semimajor axis and e the eccentricity of the orbit. Considering a number of orbits N around the central object, the above expression is multiplied by N and the devia-

[5] One can write the relevant mass ratio as

$$\frac{m_I}{m_R} = 1 + \delta \,,$$

where $\delta \ll 1$ is the deviation of m_I/m_R from unity. By expanding γ over δ and comparing the obtained deviation with the measurement uncertainty of τ

$$\gamma \sigma_{\tau_0} \approx \gamma_0 \, \sigma_{\tau_0} = \gamma_0^3 \frac{v^2}{2c^2} \tau_0 \, \delta \,,$$

where $\gamma_0 = 1/\sqrt{1 - \frac{v^2}{c^2}}$, one obtains the deviation in Eq. (5.30).

tion should be detectable for a large enough N. It can be shown that the precision of the measured precession of the perihelion of Mercury, $\Delta\varphi_{Mercury} = (42.9799 \pm 0.0009)''/\text{cy}$ [259], provides an upper bound of 2.1×10^{-5} for the deviation of m_G/m_R from unity. Promoting the above masses to quantum operators and considering the semi-classical limit, the above bound corresponds to the upper bound on the difference of eigenvalues $(E_{int,G} - E_{int,R})/mc^2$. This provides a test for the LPI. See Ref. [3] for more similar tests.

5.4 Summary

In this chapter, a generalization of the applicability of QEP, introduced in Ref. [238], is proposed. Specifically, such that it is valid for arbitrary velocities, arbitrary curved space-times, and for bosonic and fermionic particles. The most important results that one obtains here are the modifications of the Lorentz symmetry and the curved space-time geometry. The modified Lorentz symmetry implies that particles with different masses have different "speeds of light", i.e., different maximum speed limits, in case of LLI violation. For multi-particle systems, this introduces the soccer-ball problem, which commonly emerges in candidate theories of QG. On the other hand, the curved space-time geometry probed by a test particle, e.g., via the geodesic motion that it follows, depends on the ratios of masses m_α/m'_α of the test particle. In other words, the geometry experienced by an observer is no longer just a function of the curved space-time metric, but also depends on the properties of the observer itself, unless QEP holds exactly. A violation of QEP causes deviations of the mass ratios from unity, which are expected to be very small. Therefore, no such violations have been observed so far. However, with ever increasing precision of measurements, QEP violations should eventually be observed. On the other hand, if QEP is preserved in Nature, all mass ratios equal unity, and one would not be able to measure any such effects.

The generalization, introduced here, must hold for any choice of curved space-time $g^{\mu\nu}$, which turns out to be a quantum operator in general. The way it appears in the relevant equations of motion, may present a significant computational challenge. Applying the

formalism to concrete physical problems remains the central problem in calculating exact dynamics of relativistic quantum particles in strong gravitational fields. One way out is to consider the semi-classical limit, where there is no need to obtain the eigenfunctions related to internal particle dynamics, and their eigenvalues become classical physical quantities.

Chapter 6

Conclusions

> "I think it's much more interesting to live not knowing than to have answers which might be wrong."
>
> *Richard P. Feynman*

It is not unreasonable to expect that there will be a single theory, which describes the Universe from the smallest to the largest scales. Such a theory is called a theory of Quantum Gravity. Currently, there are two successful theories, separately describing small and large scales, namely QT and GR, respectively. In Chapter 1 it was shown that there is no simple way to construct a consistent theory of QG, since formalisms of QT and GR are not fully compatible, due to differences in treating space-time and particle descriptions. Such a theory of QG should be able to quantize gravitational interactions of particles, as well as describe the fundamental nature space-time. So far, several attempts have been made to provide a theory of QG. Among others, ST and LQG are the best studied candidate theories of QG, while DSR is considered as a certain limit of QG (see Section 1.1). Since such theories assume that QG effects manifest at energies around E_P and scales around ℓ_P, while current experimental capabilities can achieve energies $E_{exp} \ll E_P$ and scales $\ell_{EW} \gg \ell_P$, it is currently not possible to directly test them.

Most candidate theories of QG agree on the existence of a minimum measurable length $\ell_{min} \propto \ell_P$. However, since there is no fundamental reason why the proportionality factor between ℓ_{min} and ℓ_P to be of the order $O(1)$, one can parameterize ℓ_{min} to be anywhere

between ℓ_P and ℓ_{EW}. This brings detection of QG effects within the reach of low energy Earth-based experiments, as well as in cosmological observations, and gives rise to the field of QGP (see Chapter 2). It turns out that the existence of ℓ_{min} implies a modification of the Heisenberg Uncertainty Principle (see Section 2.1). Such a modification is called the Generalized Uncertainty Principle, which can take different forms as shown in Eqs. (2.35), (2.36), (2.37) and (2.42) (see Section 2.2). GUP is a central tool in QGP, which is used to provide predictions of QG signatures at low energies in Earth-based experiments (see Chapter 3), and to provide explanations of anomalous phenomena in cosmological observations (see Chapter 4). In this work (Chapters 3 and 4), the ADV model of GUP from Eq. (2.42) is used, due to it being one of the most general forms of GUP, while other GUP models correspond to special cases of this model. Note that the GUP parameters are currently bound by the electroweak scale $\alpha_0, \sqrt{\beta_0} < \alpha_{EW} = 10^{17}$, which means that QG signatures are expected to be observed below this bound. As part of this work, QGP is also explored from a different angle, where one proposes and explores novel concepts, such as the Quantum Equivalence Principle (see Chapter 5), which may lead towards a formulation of a consistent theory of QG.

6.1 Earth-based Experiments

QGP in Earth-based experiments (see Chapter 3) is one of the most important approaches towards QG. It makes predictions of QG effects, which can be tested under controlled conditions, and compared to other effects of other origin, for the purpose of falsification. In the case, where such experiments detect no QG signatures, one can constrain GUP parameters, which sets an upper bound on their true value, and provides stricter conditions for future QGP considerations. Note that all bounds on GUP parameters, obtained by QGP in Earth-based experiments, depend on the precision of the considered experiment. Since experimental precision increases with time, the upper bound on GUP parameters decreases. This suggests that detection of QG signatures is only a question of time. In this work, QG

signatures in two specific natural phenomena, testable in Earth-based experiments, were explored in detail, namely Bose-Einstein condensates (see Section 3.1) and Larmor frequencies of atoms in an external magnetic field, measured in a magnetometer experiment (see Section 3.2).

6.1.1 Bose-Einstein Condensate

Bose-Einstein condensation is an interesting phenomenon, which has a variety of theoretical and experimental implications. For a BEC experiment with a high enough measurement precision, signatures of extra compact dimensions and QG effects, motivated by GUP, can be observable. Such signatures are predicted through respective modifications of the critical temperature T_c and the fraction of bosons in the ground state f_0 (see Section 3.1).

The predicted signatures which arise from the presence of extra compact dimensions are many orders of magnitude smaller than the current experimental capabilities. However, they imply interesting bounds on the sizes of such compact spaces. If such high precisions were to be achieved, one obtains an upper bound R_1, as well as the lower bound R_2 for the radius of compact dimensions, given the topology $\mathbb{R}^d \times S^N$ of the underlying spatial part of the manifold. This is shown in Fig. 3.1, for $d = 3$ and $N = 1$. It turns out that the lower bound is not useful in this context, since it is of the order $R_2 \sim 1\,\mathrm{m}$ [130]. However, these results can have far-reaching implications in the search for extra compact dimensions, which is an important ingredient in certain candidate theories of QG, such as ST.

The QG signatures, motivated by GUP, have been explored for three distinct cases of BECs, namely non-relativistic, neutral relativistic and charged relativistic BECs. Their respective QG modified observables are given by Eqs. (3.26), (3.40) and (3.41) for T_c, and by Eqs. (3.28), (3.44) and (3.45) for f_0. In all cases, increasing the number density n of a boson gas, influences the magnitude of the QG corrections, and for sufficiently high densities, this increase may be by one or more orders of magnitude. This is shown in Figs. 3.2 and 3.4 for T_c, while the same holds for f_0, since the maximum of its QG correction

is $\Delta f_0 \propto T_c$. Furthermore, the range of Δf_0 increases with increasing T_c. In obtaining the above QG modifications, linear and quadratic corrections were considered separately. If both are considered simultaneously, the calculations would be notably more complicated, but one would learn nothing new, since the results in Eqs. (3.26), (3.40), (3.41), (3.28), (3.44) and (3.45) would change only by a numerical factor of order $\sim O(1)$ in the quadratic correction term [130].

Currently, the only case that can be experimentally realized is a non-relativistic BEC. Although a relativistic BEC has not been experimentally realized so far, the provided theoretical predictions will be applicable to test QG as soon as such a state is finally achieved. The current experimental precision in BECs provide the GUP parameters bounds $\alpha_0 < 10^{19}$ and $\beta_0 < 10^{46}$ from T_c measurement precision (see Fig. 3.2), and $\alpha_0 < 10^{25}$ and $\beta_0 < 10^{52}$ from f_0 measurement precision (see Fig. 3.3) [130]. Compared to the attainable electroweak scale α_{EW}, one can conclude that QG signatures are not expected to be observed within the current BEC experiments. However, as experimental precisions increase, one expects to observe QG signatures in BECs in the future.

6.1.2 Magnetometer Experiment

Magnetometers are highly advanced experimental apparatuses, which can be designed to measure Larmor frequencies of atoms in an external magnetic field, with unprecedented precision. This makes a magnetometer experiment an ideal candidate to search for QG signatures. Such signatures are predicted through GUP motivated QG modifications of the Larmor frequency of an atom in an external magnetic field [48]. A specific experimental proposal is considered, where the Larmor frequency of ^{129}Xe atoms in an external magnetic field $B = 1\,\mathrm{T}$ is measured (see Section 3.2) [149].

Given the formulation of QG modifications of the Larmor frequency, it is proposed that such modifications manifest through relative velocities of individual atoms. A natural way to induce such velocities is to consider a thermalized ensemble of atoms. This means they

follow a certain velocity distribution at a given temperature. It turns out that the Maxwell-Boltzmann distribution is the relevant velocity distribution for the proposed experiment. This gives rise to a QG induced distribution of Larmor frequencies of an ensemble of atoms, given by Eq. (3.70). Such a distribution causes a deviation of the average Larmor frequency from its standard prediction, given by Eq. (3.72) (see also Fig. 3.6). Furthermore, it causes a distribution of deviations from the standard prediction, which implies a width of the QG signature, described by the standard deviation or the FWHM, given by Eqs. (3.82) and (3.83), respectively (see also Figs. 3.7 and 3.9).

On the other hand, velocities of atoms can also be induced by non-thermal methods. One of such methods is using convection currents. In this case, a gas of atoms is passed through a duct at a controlled velocity. For the proposed experiment, a square duct is considered and a velocity distribution of an incompressible, viscous fluid is assumed. Since the experiment can be designed to measure the Larmor frequency either in a line through the cross section of the duct, or the whole cross section of the duct, one can predict the corresponding QG signatures, given by Eqs. (3.92) and (3.93), respectively (see also Fig. 3.10).

The projected precision of the proposed magnetometer experiment suggests that QG signatures in Larmor frequency measurements can be observable for $\alpha_0 \approx 10^8$ (see Figs. 3.6 and 3.7 and 3.10) [149]. In the above, one assumes $\beta_0 = \alpha_0^2$. Since this estimate is well below α_{EW}, there is a strong chance to detect QG signatures for the first time. In case no such signatures are observed, an unprecedented bound of $\alpha_0 < 10^8$ will be set.

6.2 Cosmology

Cosmology (see Chapter 4) has proven to be an important arena for QGP research. It provides a range of unique phenomena, which cannot be recreated in Earth-based experiments. Furthermore, several cosmological observations contradict predictions, given by frameworks of QT and GR. This suggests that there must be some kind of unknown funda-

mental mechanism, which accounts for such anomalies. It turns out that a likely explanation is QG, since it is believed to affect the evolution of the early Universe. Although QGP in cosmology can be used to constrain GUP parameters through predicting deviations from well understood phenomena, it can also be used to estimate the GUP parameters from the observed anomalies, thus effectively explaining them. In this work, viable explanations of two observed cosmological anomalies were provided, namely the EDGES anomaly (see Section 4.1) and the observed Baryon Asymmetry in the Universe (see Section 4.2). Note that the EDGES anomaly was considered in a more general QGP context, i.e., through Modified Dispersion Relations.

6.2.1 The EDGES Anomaly

The EDGES collaboration has discovered an anomalous absorption signal in the CMB radiation spectrum. This signal is larger by about a factor of 2 with respect to the expected value (assuming that the background is described by the ΛCDM model), i.e., the EDGES anomaly. A proposal that MDRs can account for the EDGES anomaly, was explored in detail (see Section 4.1). The results indicate that considered MDRs (cases 1-3 in Section 4.1.1), originating from existing candidate theories of QG and thought experiments with ℓ_{min}, can provide a viable mechanism which explains the EDGES anomaly, through modifying the thermal spectrum of photons, in two different scenarios. In the first scenario, MDR parameters are not constant, i.e., they are functions of redshift z (or scale) (see Figs. 4.1, 4.2, 4.3, 4.4 and 4.5). In the second scenario, it is proposed that a consistent theory of QG predicts non-trivial deformation parameters (see Figs. 4.6, 4.7 and 4.8).

In the first scenario, it was shown that the above MDRs lead to the estimation of the MDR parameters $(\eta, \alpha_0, \sqrt{\beta_0}, \alpha, \lambda')\big|_{z=z_E} \approx 10^{32}$. This estimation is outside the bound provided by the electroweak scale, i.e., $(\eta, \alpha_0, \sqrt{\beta_0}, \alpha, \lambda')\big|_{z=z_E} \gg \alpha_{EW}$. On the other hand, given the precision with which the CMB temperature in the current epoch, $z = 0$, was measured, one obtains a constraint $(\eta, \alpha_0, \sqrt{\beta_0}, \alpha, \lambda')\big|_{z=0} < 10^{28}$, which is consistent

with the observed CMB black body spectrum. The above suggests that the MDR parameters are functions of redshift z and as such provide an explanation of the EDGES anomaly. The time evolution of MDR parameters in the later stages of the Universe must be slow or nearly constant, since the same physics can be observed at redshifts in the range of the observable Universe, between $z \approx 13$ to $z = 0$ [260]. However, in the earlier stages of the Universe, it could have been faster, as the EDGES anomaly suggests. This can provide an idea of the redshift dependence, and can point towards a phase transition of some sort.

In the second scenario, one lets the deformation parameters ω, γ and δ vary, in order to explain the EDGES anomaly. One sets η, α_0, $\sqrt{\beta_0}$, α, $\lambda' = \alpha_{EW}$ and fits the MDR modified thermal spectrum of photons to the anomaly, from which the bounds of the deformation parameters ω, γ and δ follow. Similar results were found in Ref. [174]. However, MDRs with non-trivial power dependencies require further research to better understand their relevance to QG. It will be interesting to study the consequences of such deformation parameters in various contexts, such as Earth-based experiments and Gamma Ray Burst physics [101].

6.2.2 Baryon Asymmetry in the Universe

One can explain the observed baryon asymmetry in the Universe through a mechanism, which satisfies the three Sakharov conditions. It has been shown that such a mechanism can indeed be constructed in the context of QG effects in the early Universe (in the radiation-dominated era, where the baryon asymmetry froze-in), applied through GUP (see Section 4.2). The baryon number B violating interactions are considered in the context of GUTs, since the energies in the radiation-dominated era correspond to those in GUTs [227]. The CP symmetry is broken by considering coupling between the derivative of the Ricci scalar and the baryon current, i.e., coupling between space-time and matter, given by a Lagrangian interaction term from Eq. (4.41). And finally, the thermal equilibrium is broken by QG effects, introduced through GUP. Therefore, such a mechanism satisfies all three Sakharov conditions. The first two Sakharov conditions are simply implied by proposing Eq. (4.41)

at GUT energies, while the third is more involved.

It was shown that GUP modifies the apparent horizon area of a black hole (see Eq. (4.27)), which in turn modifies the Bekenstein-Hawking entropy of a black hole (see Eq. (4.32)). The holographic principle then ensures this entropy is valid for the apparent horizon of the observable Universe. By using the first law of thermodynamics and the continuity equation, one obtains the QG modified Friedmann equations (see Eqs. (4.36) and (4.37)), which break thermal equilibrium. This ensures that the third Sakharov condition is met, which in turn produces a non-vanishing freeze-in of the baryon asymmetry in the early Universe (see Eq. (4.55)). It may be noted that the QG modified Friedmann Eqs. (4.36) and (4.37) are exact for the considered GUP model (ADV model from Eq. (2.42)). By comparing the prediction to the measured baryon asymmetry, it was possible to obtain estimates on the dimensionless GUP parameters $\alpha_0 \approx 10^5$ and $|\beta_0| \approx 10^9$, which determines the QG length scale $\ell_{min} \approx 10^{-30}\,\mathrm{m}$. This estimate is well within the bound, set by α_{EW}, and is one of the most stringent that has been obtained so far. Furthermore, it may also reflect the true QG scale. It is hoped that Earth-based experiments and observations in the near future may be able to detect QG signatures at such a scale. Note that the obtained values for the quadratic GUP parameter β_0 are close to the upper and lower bounds on the parameter found in a recent work (see Ref. [81]).

Finally, it should be mentioned that the baryon asymmetry results imply a negative value of the GUP parameter, i.e., $\beta_0 < 0$. This is commonly found in cosmological QGP considerations [54, 81, 152, 154, 157], and can arise from non-trivial structures of the space-time, such as the discreteness of space-time [66, 76, 261, 262, 263, 264, 265]. A similar result follows also in the context of a crystal lattice [153]. This suggests that at the fundamental level, space-time can have a lattice or granular structure.

6.3 The Quantum Equivalence Principle

A precise formulation of QEP is a necessary step towards formulating a fully consistent theory of QG, since in such a theory, gravity would be an intrinsically quantum interaction. Based on the formulation from Ref. [238], a generalization was proposed. It extends to bosonic and fermionic particles with arbitrary velocities and in generic curved space-times (see Chapter 5). Relativistic descriptions of bosons and fermions in curved space-times (see Eqs. (5.1) and (5.2)) were used as the starting point in formulating such a generalization. The inertial, gravitational and rest masses of the test particle, m_I, m_G and m_R (m_α, where $\alpha = I, G, R$ for short), respectively, were distinguished between each other, and identified in these descriptions (see Eqs. (5.19) and (5.24)).

Such a generalization implies modifications of the Lorentz symmetry and curved space-time geometries, which turn out to depend on ratios m_α/m'_α, in case of QEP violation. In other words, for such a violation, the Lorentz symmetry and curved space-time geometries depend on properties of the particle itself. While it may be argued that such observer dependence of measurable physical quantities is already a feature of standard QT, one can note that the observer dependence in the context of QEP manifests even at the purely classical level. Although seemingly counter-intuitive, there is nothing intrinsically impermissible about it. One can interpret modifications of the Lorentz symmetry and curved space-time geometries, effectively, as modifications of the speed of light $c' = c\sqrt{m_R/m_I}$ and the universal gravitational constant $G' = Gm_G/m_I$, respectively. This also implies a modification of constant κ from the Einstein equations (see Appendix D.4). Note that such modifications cannot be used to simply redefine the above constants for a general case, since they are different for different species of test particles.

For modifications in GR, three examples of curved space-times have been considered, namely the weak gravitational field space-time, the Schwarzschild space-time and the Kerr space-time. It turns out that all of them depend on m_G and m_R, while only the Kerr metric additionally depends on m_I, due to the rotation of the central object. From this, one may be

tempted to conjecture that if any gravitating central object causes inertial frame dragging in its vicinity, then m_I will affect the metric as well.

Promoting masses m_α to quantum operators, i.e., $m_\alpha \longrightarrow \mathcal{M}_\alpha$, gives rise to additional terms with $H_{int,\alpha}$, in the equations of motion (see Eqs. (5.21) and (5.26)), describing effects due to internal dynamics of the test particle. In Ref. [238], the additional terms with $H_{int,\alpha}$ describe first order corrections to internal dynamics of the test particle, corresponding to special relativistic time dilation and gravitational time dilation. On the other hand, the above generalization, provides exact corrections of such effects. This formulation must hold for any choice of curved space-time, described by metric $g^{\mu\nu}$. Note that in the non-relativistic and weak gravitational limits, one obtains the results from Ref. [238], which suggests that such a generalization is indeed correct.

Applying such a generalized formalism to concrete physical problems may present a significant computational challenge, because the modified curved space-time metric becomes a quantum operator, $g^{\mu\nu}(m_\alpha) \longrightarrow \mathfrak{g}^{\mu\nu}(\mathcal{M}_\alpha)$, when $m_\alpha \longrightarrow \mathcal{M}_\alpha$. For phenomenological considerations, one can consider the semi-classical limit, where the eigenvalues of $H_{int,\alpha}$ become classical physical quantities $E_{int,\alpha}$. This allows one to test QEP in a novel way, using high-energy Earth-based experiments, such as particle accelerators, and strong gravitational fields, such as near stars and black holes.

A handful of examples of experimental test of QEP were described in Section 5.3. The bounds on deviations of the mass ratios from unity, obtained through QEP considerations are $\lesssim 10^{-3}$ for WEP, $\lesssim 10^{-10}$ for LLI and $\lesssim 10^{-5}$ for LPI, and bounds obtained through standard methods are $\lesssim 10^{-15}$ for WEP [242], $\lesssim 10^{-19}$ for LLI [243] and $\lesssim 10^{-7}$ for LPI [244]. One can see that bounds obtained through QEP considerations are not as promising as the ones, obtained through standard methods. However, the approach through QEP is fairly new, and only a handful of test were considered. Considerations in other, more precise tests may provide unprecedented bounds, or even detect QEP violations.

6.4 Future Prospects

At this point, no QG signatures or QEP violations have been detected in Earth-based experiments, while explanations of observed anomalies in terms of QG effects in cosmology require further verification and understanding. There are also several theoretical issues which need to be dealt with appropriately, such as the soccer-ball problem and conservation laws in both, GUP and QEP considerations. However, the future of QGP looks promising. There is an abundance of phenomenological considerations, which provide a variety of predictions of QG signatures for different types of Earth-based experiments. Many of these predictions are yet to be tested. Since the experimental precision is ever increasing, it is expected that QG effects are detected in Earth-based experiments in the future. On the other hand, cosmological QG considerations already provide estimates, which determine ℓ_{min}. However, QEP violations have not been studied extensively, since it is a fairly new proposal. Therefore, it is necessary to explore QEP in detail, in order to stringently test its implications, and verify its relevance to the formulation of a consistent theory of QG.

The QGP considerations, discussed in this work, are only a small fraction of research, which is required to test QG and its foundations. Attempts to observe QG effects and to formulate candidate theories of QG are currently only in their initial stages. While one anticipates experimental precisions to increase with time, further theoretical research is necessary to learn as much as possible about the role and implications of QG in physics within current experimental capabilities. Such theoretical research will be put under scrutiny, once QG is experimentally confirmed. In the following, possible extensions and applications of results, obtained in this work, are proposed.

6.4.1 Statistical Mechanics

Considering QG effects in BECs (see Section 3.1), one finds that QG signatures increase with increasing n, while no upper bound on n was taken into account, allowing arbitrary magnitudes of QG signatures. However, experimental realizations of BECs use low num-

ber densities of bosons $n \in (10^{19}, 10^{21})\,\mathrm{m}^{-3}$, in order to decrease the probability of them colliding and forming molecules, thus ensuring a stable BEC state [123]. It will be interesting to extend the analysis to include a maximum allowed number density n_{max}, which will provide a more strict constraint on the magnitude of QG signatures.

In the above BEC considerations, also a QG modified density of states $g(\varepsilon)$ was obtained for cases of non-relativistic and relativistic particles (see Eqs. (3.24) and (3.37), respectively). They are valid for both types of particles, bosons and fermions. It turns out that all observables Y in statistical mechanics can be evaluated by ensemble averages, given in terms of phase space integrals

$$\langle Y \rangle = \int_0^\infty Y(\varepsilon)\, g(\varepsilon)\, f_{BE(FD)}(\varepsilon)\, \mathrm{d}\varepsilon \,, \tag{6.1}$$

where the density of states is essential in their construction (see Appendix A.1 for details). This implies that the QG modified densities of states can be used throughout statistical mechanics considerations, thus providing a rich QGP in this field. For example, one can obtain a QG modified neutron degeneracy pressure and apply it to neutron stars, which can provide constraints and insights on the neutron star equation of state. Other QGP applications of densities of states range from condensed matter physics, interstellar and intergalactic gases and early universe cosmology.

6.4.2 Nuclear Physics

In the magnetometer experiment considerations (see Section 3.2), it was shown that a QG modification of the Larmor frequency can be extended to the nucleus of an atom. In doing so, the implicit form of a QG modified Schrödinger equation of an atomic nucleus was obtained as

$$i\hbar \frac{\partial}{\partial t} \psi_N(\mathbf{r},t) = H_{0N}^{QG}\, \psi_N(\mathbf{r},t) \,, \tag{6.2}$$

where H_{0N}^{QG} is the relevant QG modified Hamiltonian of the nucleus (see Eq. (3.54)). It turned out that the above was not relevant in the context of Larmor frequencies. However, it can provide a framework to explore QG effects in nuclear physics. Specifically, one can explore QG effects in the nuclear shell model.

6.4.3 Cosmology

The results, obtained in explaining the EDGES anomaly in terms of MDRs (see Section 4.1), on one hand suggest the MDR parameters (including GUP parameters) must be redshift (scale) dependent, to account for the observations. Similar results were obtained in a work, where Dark Matter effects in rotational curves of galaxies are proposed to arise as a consequence of QG, motivated by GUP [151]. Also, other cosmological considerations provide a negative value for the quadratic GUP parameter $\beta_0 < 0$, while Earth-based experiments provide $\beta_0 > 0$. Such results imply that the Planck length ℓ_P can indeed be scale dependent. The only reasonable source of such a dependence can only be through the universal gravitational constant $G \propto \ell_P^2$. Such a dependence of G was proposed by authors of Ref. [266], which attribute Dark Matter and Dark Energy effects solely to gravity on different scales. Therefore, one can provide a connection between the results, found in such works and explore the scale dependence of G, or equivalently ℓ_P.

On the other hand, a viable explanation of the EDGES anomaly was proposed also in terms of non-trivial deformation parameters. Proposals of such MDRs are fairly new and need further exploration to understand their relevance to QG. They can be tested in other cosmological scenarios, such as explaining the observed baryon asymmetry in the Universe and BBN, and precise Earth-based experiments, such as particle accelerators and magnetometers. This will provide a clear comparison between this and the usual MDR models, and point out any possible inconsistencies.

One of the results, obtained in the baryon asymmetry considerations (see Section 4.2), is the QG modification of Friedmann equations (see Eqs. (4.36) and (4.37)). Since Friedmann

equations, which are central in the standard model of cosmology, govern the dynamics of the Universe, the QG modified Friedmann equations can provide a rich QGP in cosmology. They can be applied to practically all cosmological considerations. For example, the BBN, where GUP parameters can be bound from measurements of primordial abundances, frozen in at the freeze-out temperature T_f as

$$\frac{\delta T}{T_f} = \alpha_0 \frac{\pi^{3/2} G}{3\hbar c^5} \sqrt{\frac{g_*}{1620}} k_B^2 T_{0f}^2 - \beta_0 \frac{\pi^3 g_* G^2}{135\hbar^2 c^{10}} k_B^4 T_{0f}^4 \,. \tag{6.3}$$

Note that the BBN measurements do not manifest any anomalies at the current measurement precision. Therefore, only upper bounds on GUP parameters can be obtained. Another interesting application of QG modified Friedmann equations would be at the inflationary epoch of the Universe, where one expects strong QG effects.

6.4.4 The Quantum Equivalence Principle

QEP presents a novel approach to QG. It is believed to be the foundation of a consistent theory of QG. Therefore, it needs to be rigorously tested, before it is accepted as fundamental concept of Nature. In this work, a generalization of its applicability was introduced for the first time, which provides a general framework, where QEP can be tested in a range of different scenarios, namely weak gravitational fields, strong gravitational fields, non-relativistic speeds, relativistic speeds and everything in between, for either bosons or fermions. This provides a rich ground for QGP in the context of QEP. One can propose separate tests for WEP, LLI and LPI in Earth-based experiments and in cosmological or astronomical observations. For example, one can test the WEP in specifically designed magnetometer experiments, the LLI in scattering cross sections, measured in particle colliders and the LPI in galactic centres or quasars. On the other hand, one can attempt to find exact solutions of particle dynamics for Eqs. (5.21) and (5.26).

6.5 Final Remarks

In the last 150 years, physics has developed at an unprecedented rate, compared to its relatively long history, when classical mechanics was thought to be a complete description of Nature. As new discoveries could no longer be explained in terms of classical mechanics, it was clear that Nature is fundamentally more complex and requires a better description. The introduction of QT has changed the concepts of position and velocity of a particle in terms of the Heisenberg Uncertainty Principle, while the introduction of GR has changed the notion of space and time in terms of a single entity known as space-time, which can change its geometry in response to mass. Research in these fields has greatly advanced the understanding of fundamental mechanisms of Nature. However, there is still a lot more to be uncovered.

Considering the limits of QT and GR, one can find that both fail to consistently describe certain scenarios, expected to be found in Nature, such as centres of black holes and the beginning of the Universe. Similarly as in the advent of QT and GR, there is strong evidence that a better description of Nature is required. A description which includes QT, GR and more, i.e., a theory of QG, which implies the existence of a minimum measurable length and a quantum description of gravity. However, it has been proven difficult to formulate a consistent theory of QG. There have been several attempts to achieve this, such as ST and LQG. It turns out that they do not address all questions that arise in approaches to QG and in fact, give rise to new conceptual problems in their current forms. Compared to the advent of QT and GR, when there was clear evidence of new phenomena, which could not be accounted for by classical mechanics, the path to formulating a theory of QG today does not have such a privilege. One must rely on properties, which are believed to be generic predictions of QG, such as the existence of the minimum measurable length, and search for signatures of such properties in Earth-based experiments and in astronomical or cosmological observations.

One can find that QGP is a practical approach towards the QG problem, since it does

not depend on any candidate theory of QG, and the diversity of applications can narrow down the list of potential theories. Also, a new conceptual approach to QG is emerging, in which fundamental concepts, such as the Quantum Equivalence Principle, which should be a necessary ingredient for a consistent theory of QG, are put to the test.

Bibliography

[1] Charles Singer. *A Short History Of Science To The Nineteenth Century*. Oxford University Press, Oxford, UK, 1941.

[2] Anton Zeilinger. Experiment and the foundations of quantum physics. *Rev. Mod. Phys.*, 71:S288–S297, 1999.

[3] Clifford M. Will. The Confrontation between General Relativity and Experiment. *Living Rev. Rel.*, 17:4, 2014.

[4] Leonard E. Parker and D. Toms. *Quantum Field Theory in Curved Spacetime: Quantized Field and Gravity*. Cambridge Monographs on Mathematical Physics. Cambridge University Press, 8 2009.

[5] L. Parker. One Electron Atom as a Probe of Space-time Curvature. *Phys. Rev. D*, 22:1922–1934, 1980.

[6] Edward Witten. Reflections on the fate of space-time. *Phys. Today*, 49N4:24–30, 1996.

[7] Giovanni Amelino-Camelia. Quantum-Spacetime Phenomenology. *Living Rev. Rel.*, 16:5, 2013.

[8] Saurya Das and Elias C. Vagenas. Universality of Quantum Gravity Corrections. *Phys. Rev. Lett.*, 101:221301, 2008.

[9] K. S. Stelle. Renormalization of Higher Derivative Quantum Gravity. *Phys. Rev. D*, 16:953–969, 1977.

[10] B. Zwiebach. *A First Course in String Theory*. Cambridge University Press, Cambridge, UK, 2009.

[11] M. B. Green, J. H. Schwarz, and E. Witten. *Superstring Theory*. Cambridge University Press, New York, USA, 2012.

[12] J. Polchinski. *String Theory*. Cambridge University Press, New York, USA, 1998.

[13] K. Becker, M. Becker, and J. Schwarz. *String Theory adn M-Theory*. Cambridge University Press, New York, USA, 2007.

[14] Stephen P. Martin. A Supersymmetry primer. *Adv. Ser. Direct. High Energy Phys.*, 18:1–98, 1998.

[15] D. Amati, M. Ciafaloni, and G. Veneziano. Superstring Collisions at Planckian Energies. *Phys. Lett. B*, 197:81, 1987.

[16] Lee Smolin. An Invitation to loop quantum gravity. In *3rd International Symposium on Quantum Theory and Symmetries*, pages 655–682, 8 2004.

[17] Thomas Thiemann. Loop Quantum Gravity: An Inside View. *Lect. Notes Phys.*, 721:185–263, 2007.

[18] Carlo Rovelli. Loop quantum gravity. *Living Rev. Rel.*, 11:5, 2008.

[19] Martin Bojowald. Loop quantum gravity as an effective theory. *AIP Conf. Proc.*, 1483(1):5–30, 2012.

[20] Abhay Ashtekar and Jorge Pullin, editors. *Loop Quantum Gravity: The First 30 Years*, volume 4 of *100 Years of General Relativity*. World Scientific, 2017.

[21] Abhay Ashtekar and Eugenio Bianchi. A short review of loop quantum gravity. *Rept. Prog. Phys.*, 84(4):042001, 2021.

[22] Hermann Nicolai, Kasper Peeters, and Marija Zamaklar. Loop quantum gravity: An Outside view. *Class. Quant. Grav.*, 22:R193, 2005.

[23] Soren Holst. Barbero's Hamiltonian derived from a generalized Hilbert-Palatini action. *Phys. Rev. D*, 53:5966–5969, 1996.

[24] Joseph Samuel. Comment on Holst's Lagrangian formulation. *Phys. Rev. D*, 63:068501, 2001.

[25] A. Sen. Gravity as a Spin System. *Phys. Lett. B*, 119:89–91, 1982.

[26] Carlo Rovelli and Lee Smolin. Discreteness of area and volume in quantum gravity. *Nucl. Phys. B*, 442:593–622, 1995. [Erratum: Nucl.Phys.B 456, 753–754 (1995)].

[27] Giovanni Amelino-Camelia. Testable scenario for relativity with minimum length. *Phys. Lett. B*, 510:255–263, 2001.

[28] Joao Magueijo and Lee Smolin. Lorentz invariance with an invariant energy scale. *Phys. Rev. Lett.*, 88:190403, 2002.

[29] Giovanni Amelino-Camelia. Doubly special relativity: First results and key open problems. *Int. J. Mod. Phys. D*, 11:1643, 2002.

[30] Jerzy Kowalski-Glikman. Doubly special relativity: Facts and prospects. pages 493–508, 3 2006.

[31] S. Majid and H. Ruegg. Bicrossproduct structure of kappa Poincare group and noncommutative geometry. *Phys. Lett. B*, 334:348–354, 1994.

[32] Jerzy Lukierski, Henri Ruegg, Anatol Nowicki, and Valerii N. Tolstoi. Q deformation of Poincare algebra. *Phys. Lett. B*, 264:331–338, 1991.

[33] Giovanni Amelino-Camelia, Lee Smolin, and Artem Starodubtsev. Quantum symmetry, the cosmological constant and Planck scale phenomenology. *Class. Quant. Grav.*, 21:3095–3110, 2004.

[34] Giovanni Amelino-Camelia. Quantum gravity phenomenology: Status and prospects. *Mod. Phys. Lett. A*, 17:899–922, 2002.

[35] Joao Magueijo and Lee Smolin. Generalized Lorentz invariance with an invariant energy scale. *Phys. Rev. D*, 67:044017, 2003.

[36] P. Kosinski, J. Lukierski, P. Maslanka, and J. Sobczyk. The Classical basis for kappa deformed Poincare (super)algebra and the second kappa deformed supersymmetric Casimir. *Mod. Phys. Lett. A*, 10:2599–2606, 1995.

[37] J. Kowalski-Glikman and S. Nowak. Doubly special relativity theories as different bases of kappa Poincare algebra. *Phys. Lett. B*, 539:126–132, 2002.

[38] Jerzy Kowalski-Glikman and Sebastian Nowak. Noncommutative space-time of doubly special relativity theories. *Int. J. Mod. Phys. D*, 12:299–316, 2003.

[39] Jerzy Lukierski, Henri Ruegg, and Wojciech J. Zakrzewski. Classical quantum mechanics of free kappa relativistic systems. *Annals Phys.*, 243:90–116, 1995.

[40] Joao Magueijo and Lee Smolin. Gravity's rainbow. *Class. Quant. Grav.*, 21:1725–1736, 2004.

[41] Giovanni Amelino-Camelia. Relativity in space-times with short distance structure governed by an observer independent (Planckian) length scale. *Int. J. Mod. Phys. D*, 11:35–60, 2002.

[42] Sabine Hossenfelder. The Soccer-Ball Problem. *SIGMA*, 10:074, 2014.

[43] Luca Bombelli, Joohan Lee, David Meyer, and Rafael Sorkin. Space-Time as a Causal Set. *Phys. Rev. Lett.*, 59:521–524, 1987.

[44] Jan Ambjorn, Jerzy Jurkiewicz, and Charlotte F. Kristjansen. Quantum gravity, dynamical triangulations and higher derivative regularization. *Nucl. Phys. B*, 393:601–632, 1993.

[45] M. Reuter. Nonperturbative evolution equation for quantum gravity. *Phys. Rev. D*, 57:971–985, 1998.

[46] Michael R. Douglas and Nikita A. Nekrasov. Noncommutative field theory. *Rev. Mod. Phys.*, 73:977–1029, 2001.

[47] Saurya Das and Elias C. Vagenas. Reply to 'Comment on 'Universality of Quantum Gravity Corrections' '. *Phys. Rev. Lett.*, 104:119002, 2010.

[48] Pasquale Bosso and Saurya Das. Generalized Uncertainty Principle and Angular Momentum. *Annals Phys.*, 383:416–438, 2017.

[49] DaeKil Park and Eylee Jung. Generalized uncertainty principle and point interaction. *Phys. Rev. D*, 101(6):066007, 2020.

[50] Luca Buoninfante, Gaetano Lambiase, Giuseppe Gaetano Luciano, and Luciano Petruzziello. Phenomenology of GUP stars. *Eur. Phys. J. C*, 80(9):853, 2020.

[51] Joao Magueijo. Could quantum gravity be tested with high intensity lasers? *Phys. Rev. D*, 73:124020, 2006.

[52] Marcilio M. Dos Santos, Teodora Oniga, Andrew S. Mcleman, Martin Caldwell, and Charles H. T. Wang. Towards quantum gravity measurement by cold atoms. *J. Plasma Phys.*, 79:437, 2013.

[53] Ippei Danshita, Masanori Hanada, and Masaki Tezuka. Creating and probing the Sachdev-Ye-Kitaev model with ultracold gases: Towards experimental studies of quantum gravity. *PTEP*, 2017(8):083I01, 2017.

[54] Luca Buoninfante, Giuseppe Gaetano Luciano, and Luciano Petruzziello. Generalized Uncertainty Principle and Corpuscular Gravity. *Eur. Phys. J. C*, 79(8):663, 2019.

[55] Massimo Blasone, Gaetano Lambiase, Giuseppe Gaetano Luciano, Luciano Petruzziello, and Fabio Scardigli. Heuristic derivation of Casimir effect in minimal length theories. *Int. J. Mod. Phys. D*, 29(02):2050011, 2020.

[56] Simon A. Haine. Searching for Signatures of Quantum Gravity in Quantum Gases. *New J. Phys.*, 23(3):033020, 2021.

[57] Thomas W. van de Kamp, Ryan J. Marshman, Sougato Bose, and Anupam Mazumdar. Quantum Gravity Witness via Entanglement of Masses: Casimir Screening. *Phys. Rev. A*, 102(6):062807, 2020.

[58] Michele Maggiore. A Generalized uncertainty principle in quantum gravity. *Phys. Lett. B*, 304:65–69, 1993.

[59] Michele Maggiore. The Algebraic structure of the generalized uncertainty principle. *Phys. Lett. B*, 319:83–86, 1993.

[60] Michele Maggiore. Quantum groups, gravity and the generalized uncertainty principle. *Phys. Rev. D*, 49:5182–5187, 1994.

[61] Fabio Scardigli. Generalized uncertainty principle in quantum gravity from micro - black hole Gedanken experiment. *Phys. Lett. B*, 452:39–44, 1999.

[62] S. Capozziello, G. Lambiase, and G. Scarpetta. Generalized uncertainty principle from quantum geometry. *Int. J. Theor. Phys.*, 39:15–22, 2000.

[63] Achim Kempf, Gianpiero Mangano, and Robert B. Mann. Hilbert space representation of the minimal length uncertainty relation. *Phys. Rev. D*, 52:1108–1118, 1995.

[64] Fabio Scardigli and Roberto Casadio. Generalized uncertainty principle, extra dimensions and holography. *Class. Quant. Grav.*, 20:3915–3926, 2003.

[65] Saurya Das and Elias C. Vagenas. Phenomenological Implications of the Generalized Uncertainty Principle. *Can. J. Phys.*, 87:233–240, 2009.

[66] Ahmed Farag Ali, Saurya Das, and Elias C. Vagenas. Discreteness of Space from the Generalized Uncertainty Principle. *Phys. Lett. B*, 678:497–499, 2009.

[67] Ahmed Farag Ali, Saurya Das, and Elias C. Vagenas. The Generalized Uncertainty Principle and Quantum Gravity Phenomenology. In *12th Marcel Grossmann Meeting on General Relativity*, pages 2407–2409, 1 2010.

[68] Ahmed Farag Ali, Saurya Das, and Elias C. Vagenas. A proposal for testing Quantum Gravity in the lab. *Phys. Rev. D*, 84:044013, 2011.

[69] Igor Pikovski, Michael R. Vanner, Markus Aspelmeyer, M. S. Kim, and Caslav Brukner. Probing Planck-scale physics with quantum optics. *Nature Phys.*, 8:393–397, 2012.

[70] Fabio Scardigli and Roberto Casadio. Gravitational tests of the Generalized Uncertainty Principle. *Eur. Phys. J. C*, 75(9):425, 2015.

[71] Fabio Scardigli, Gaetano Lambiase, and Elias Vagenas. GUP parameter from quantum corrections to the Newtonian potential. *Phys. Lett. B*, 767:242–246, 2017.

[72] S. P. Kumar and M. B. Plenio. Quantum-optical tests of Planck-scale physics. *Phys. Rev. A*, 97(6):063855, 2018.

[73] D. Amati, M. Ciafaloni, and G. Veneziano. Can Space-Time Be Probed Below the String Size? *Phys. Lett. B*, 216:41–47, 1989.

[74] Kenichi Konishi, Giampiero Paffuti, and Paolo Provero. Minimum Physical Length and the Generalized Uncertainty Principle in String Theory. *Phys. Lett. B*, 234:276–284, 1990.

[75] Spyros Basilakos, Saurya Das, and Elias C. Vagenas. Quantum Gravity Corrections and Entropy at the Planck time. *JCAP*, 09:027, 2010.

[76] Ashmita Das, Saurya Das, and Elias C. Vagenas. Discreteness of Space from GUP in Strong Gravitational Fields. *Phys. Lett. B*, 809:135772, 2020.

[77] Gaetano Lambiase and Fabio Scardigli. Lorentz violation and generalized uncertainty principle. *Phys. Rev. D*, 97(7):075003, 2018.

[78] Alfredo Iorio, Gaetano Lambiase, Pablo Pais, and Fabio Scardigli. Generalized Uncertainty Principle in three-dimensional gravity and the BTZ black hole. *Phys. Rev. D*, 101(10):105002, 2020.

[79] Luciano Petruzziello. Generalized uncertainty principle with maximal observable momentum and no minimal length indeterminacy. *Class. Quant. Grav.*, 38(13):135005, 2021.

[80] Giuseppe Gaetano Luciano and Luciano Petruzziello. Generalized uncertainty principle and its implications on geometric phases in quantum mechanics. *Eur. Phys. J. Plus*, 136(2):179, 2021.

[81] Vijay Nenmeli, S. Shankaranarayanan, Vasil Todorinov, and Saurya Das. Maximal momentum GUP leads to quadratic gravity. *Phys. Lett. B*, 821:136621, 2021.

[82] Michael Bishop, Joey Contreras, and Douglas Singleton. A Subtle Aspect of Minimal Lengths in the Generalized Uncertainty Principle. *Universe*, 8(3):192, 2022.

[83] Michael Bishop, Joey Contreras, and Douglas Singleton. "The more things change the more they stay the same" Minimum lengths with unmodified uncertainty principle and dispersion relation. *Int. J. Mod. Phys. D*, 31(14):2241002, 2022.

[84] Michael Bishop, Joey Contreras, Peter Martin, and Douglas Singleton. Comments on the cosmological constant in generalized uncertainty models. *Front. Astron. Space Sci.*, 9:978898, 2022.

[85] Tom Banks, W. Fischler, S. H. Shenker, and Leonard Susskind. M theory as a matrix model: A Conjecture. *Phys. Rev. D*, 55:5112–5128, 1997.

[86] Nathan Seiberg and Edward Witten. String theory and noncommutative geometry. *JHEP*, 09:032, 1999.

[87] M. M. Sheikh-Jabbari. Open strings in a B field background as electric dipoles. *Phys. Lett. B*, 455:129–134, 1999.

[88] Juan Martin Maldacena and J. G. Russo. Large-N limit of noncommutative gauge theories. *Class. Quant. Grav.*, 17:1189–1203, 2000.

[89] Ali H. Chamseddine and Mikhail S. Volkov. NonAbelian vacua in D = 5, N=4 gauged supergravity. *JHEP*, 04:023, 2001.

[90] Chong-Sun Chu, Brian R. Greene, and Gary Shiu. Remarks on inflation and noncommutative geometry. *Mod. Phys. Lett. A*, 16:2231–2240, 2001.

[91] Achim Kempf. Mode generating mechanism in inflation with cutoff. *Phys. Rev. D*, 63:083514, 2001.

[92] Akikazu Hashimoto and N. Itzhaki. Traveling faster than the speed of light in noncommutative geometry. *Phys. Rev. D*, 63:126004, 2001.

[93] Stephon Alexander, Robert Brandenberger, and Joao Magueijo. Noncommutative inflation. *Phys. Rev. D*, 67:081301, 2003.

[94] Richard Easther, Brian R. Greene, William H. Kinney, and Gary Shiu. Inflation as a probe of short distance physics. *Phys. Rev. D*, 64:103502, 2001.

[95] Achim Kempf and Jens C. Niemeyer. Perturbation spectrum in inflation with cutoff. *Phys. Rev. D*, 64:103501, 2001.

[96] Massimo Blasone, Gaetano Lambiase, Giuseppe Gaetano Luciano, Luciano Petruzziello, and Luca Smaldone. Time-energy uncertainty relation for neutrino oscillations in curved spacetime. *Class. Quant. Grav.*, 37(15):155004, 2020.

[97] Robert H. Brandenberger and Jerome Martin. The Robustness of inflation to changes in superPlanck scale physics. *Mod. Phys. Lett. A*, 16:999–1006, 2001.

[98] Jerome Martin and Robert H. Brandenberger. The TransPlanckian problem of inflationary cosmology. *Phys. Rev. D*, 63:123501, 2001.

[99] V. Alan Kostelecky and Stuart Samuel. Spontaneous Breaking of Lorentz Symmetry in String Theory. *Phys. Rev. D*, 39:683, 1989.

[100] Gerard 't Hooft. Quantization of point particles in (2+1)-dimensional gravity and space-time discreteness. *Class. Quant. Grav.*, 13:1023–1040, 1996.

[101] G. Amelino-Camelia, John R. Ellis, N. E. Mavromatos, Dimitri V. Nanopoulos, and Subir Sarkar. Tests of quantum gravity from observations of gamma-ray bursts. *Nature*, 393:763–765, 1998.

[102] Rodolfo Gambini and Jorge Pullin. Nonstandard optics from quantum space-time. *Phys. Rev. D*, 59:124021, 1999.

[103] Giovanni Amelino-Camelia and Shahn Majid. Waves on noncommutative space-time and gamma-ray bursts. *Int. J. Mod. Phys. A*, 15:4301–4324, 2000.

[104] Sean M. Carroll, Jeffrey A. Harvey, V. Alan Kostelecky, Charles D. Lane, and Takemi Okamoto. Noncommutative field theory and Lorentz violation. *Phys. Rev. Lett.*, 87:141601, 2001.

[105] Petr Horava. Quantum Gravity at a Lifshitz Point. *Phys. Rev. D*, 79:084008, 2009.

[106] Petr Horava. Spectral Dimension of the Universe in Quantum Gravity at a Lifshitz Point. *Phys. Rev. Lett.*, 102:161301, 2009.

[107] Giovanni Amelino-Camelia. Doubly-Special Relativity: Facts, Myths and Some Key Open Issues. *Symmetry*, 2:230–271, 2010.

[108] S. W. Hawking. Particle Creation by Black Holes. *Commun. Math. Phys.*, 43:199–220, 1975. [Erratum: Commun.Math.Phys. 46, 206 (1976)].

[109] S. W. Hawking and G. F. R. Ellis. *The Large Scale Structure of Space-Time*. Cambridge Monographs on Mathematical Physics. Cambridge University Press, Cambridge, UK, 2 2011.

[110] H. A. Kramers and G. H. Wannier. Statistics of the two-dimensional ferromagnet. Part 1. *Phys. Rev.*, 60:252–262, 1941.

[111] T. Thiemann. A Length operator for canonical quantum gravity. *J. Math. Phys.*, 39:3372–3392, 1998.

[112] Abhay Ashtekar, Jerzy Lewandowski, and Hanno Sahlmann. Polymer and Fock representations for a scalar field. *Class. Quant. Grav.*, 20:L11–1, 2003.

[113] Maite Dupuis, James P. Ryan, and Simone Speziale. Discrete gravity models and Loop Quantum Gravity: a short review. *SIGMA*, 8:052, 2012.

[114] Dah-Wei Chiou. Loop Quantum Gravity. *Int. J. Mod. Phys. D*, 24(01):1530005, 2014.

[115] Nirmalya Kajuri. Path Integral representation for Polymer Quantized Scalar Fields. *Int. J. Mod. Phys. A*, 30(34):1550204, 2015.

[116] Masooma Ali and Sanjeev S. Seahra. Natural Inflation from Polymer Quantization. *Phys. Rev. D*, 96(10):103524, 2017.

[117] Salman Sajad Wani, Behnam Pourhassan, Mir Faizal, and Ahmed Jellal. Low Energy Consequences of Loop Quantum Gravity. *Int. J. Geom. Meth. Mod. Phys.*, 18(03):03, 2021.

[118] J. L. Cortes and J. Gamboa. Quantum uncertainty in doubly special relativity. *Phys. Rev. D*, 71:065015, 2005.

[119] Pasquale Bosso. Position in Minimal Length Quantum Mechanics. *Universe*, 8(1):17, 2021.

[120] F. Briscese, M. Grether, and M. de Llano. Planck-scale effects on Bose-Einstein condensates. *EPL*, 98(6):60001, 2012.

[121] F. Briscese. Trapped Bose-Einstein condensates with Planck-scale induced deformation of the energy-momentum dispersion relation. *Phys. Lett. B*, 718:214–217, 2012.

[122] J. I. Rivas, A. Camacho, and E. Goklu. Bogoliubov space of a Bose–Einstein condensate and quantum spacetime fluctuations. *Class. Quant. Grav.*, 29:165005, 2012.

[123] R. K. Pathria and P. D. Beale. *Statistical mechanics - third edition*. Butterworth-Heinemann, Oxford, UK, 2011.

[124] Kiyoshi Shiraishi. Bose-Einstein Condensation in Compactified Spaces. *Prog. Theor. Phys.*, 77:975–982, 1987.

[125] A. B. Acharyya and M. Acharyya. Bose-Einstein Condensation in arbitrary dimensions. *Acta Phys. Polon. B*, 43:1805–1810, 2012.

[126] Shay Leizerovitch and Benni Reznik. Kaluza-Klein tower of masses in compactified Bose-Einstein condensates. 10 2017.

[127] M. Grether, M. de Llano, and George A. Baker, Jr. Bose-Einstein Condensation in the Relativistic Ideal Bose Gas. *Phys. Rev. Lett.*, 99:200406, 2007.

[128] P. N. Pandita. Critical Behavior of a Relativistic Bose Gas. *Phys. Rev. E*, 89(3):032110, 2014.

[129] D. C. Wood. *The Computation of Polylogarithms, Technical Report **15-92***. University of Kent Computing Laboratory, Canterbury, UK, 1992.

[130] Saurya Das and Mitja Fridman. Test of quantum gravity in statistical mechanics. *Phys. Rev. D*, 104(2):026014, 2021.

[131] Jack Ekin. *Experimental Techniques for Low-Temperature Measurements: Cryostat Design, Material Properties and Superconductor Critical-Current Testing*. Oxford University Press, 10 2006.

[132] J. L. Basdevant. *Lectures on Quantum Mechanics, p. 74*. Springer Science+Business Media, LLC, New York, USA, 2007.

[133] Pasquale Bosso. On the quasi-position representation in theories with a minimal length. *Class. Quant. Grav.*, 38(7):075021, 2021.

[134] Pedro Alberto, Saurya Das, and Elias C. Vagenas. Relativistic particle in a box: Klein–Gordon versus Dirac equations. *Eur. J. Phys.*, 39(2):025401, 2018.

[135] M. G. Fuda. Feshbach-Villars Formalism and Pion Nucleon Scattering. *Phys. Rev. C*, 21:1480–1497, 1980.

[136] Herman Feshbach and Felix Villars. Elementary relativistic wave mechanics of spin 0 and spin 1/2 particles. *Rev. Mod. Phys.*, 30:24–45, 1958.

[137] M. H. Anderson, J. R. Ensher, M. R. Matthews, C. E. Wieman, and E. A. Cornell. Observation of Bose-Einstein condensation in a dilute atomic vapor. *Science*, 269:198–201, 1995.

[138] J. L. Roberts, N. R. Claussen, S. L. Cornish, E. A. Donley, E. A. Cornell, and C. E. Wieman. Controlled collapse of a bose-einstein condensate. *Phys. Rev. Lett.*, 86:4211–4214, May 2001.

[139] Fang F. Marti G. et al. Olf, R. Thermometry and cooling of a bose gas to 0.02 times the condensation temperature. *Nature Phys.*, 11:720–723, 2015.

[140] D. Budker and D. F. Jackson Kimball, editors. *Optical Magnetometry*. Cambridge University Press, Cambridge, UK, 2013.

[141] W. Demtröder. *Laser Spectroscopy*. Springer Berlin, Heidelberg, Heidelberg, DE, 2003.

[142] Gil Porat. Private communication.

[143] National Institute of Standards and Technology (NIST). Atomic spectroscopy - different coupling schemes, 9. notations for different coupling schemes. https://www.nist.gov/pml/atomic-spectroscopy-compendium-basic-ideas-notation-data-and-formulas/atomic-spectroscopy-2node095. Accessed: 2023-03-17.

[144] Emily Altiere, Eric R. Miller, Tomohiro Hayamizu, David J. Jones, Kirk W. Madison, and Takamasa Momose. High-resolution two-photon spectroscopy of a $5p^5 6p \leftarrow 5p^6$ transition of xenon. *Phys. Rev. A*, 97:012507, Jan 2018.

[145] K. S. Krane. *Introductory Nuclear Physics*. Wiley India, 2008.

[146] L. D. Landau and E. M. Lifshitz. *Statistical Physics*, volume 5. Pergamon Press, Oxford, UK, 1980. 3rd Ed.

[147] Włodzimierz Makulski. 129xe and 131xe nuclear magnetic dipole moments from gas phase nmr spectra. *Magnetic Resonance in Chemistry*, 53(4):273–279, 2015.

[148] Pasquale Bosso. Rigorous Hamiltonian and Lagrangian analysis of classical and quantum theories with minimal length. *Phys. Rev. D*, 97(12):126010, 2018.

[149] Gil Porat, James Maldaner, Lindsay LeBlanc, Mitja Fridman, Pasquale Bosso, and Saurya Das. Work in progress. 2023.

[150] R. K. Shah and A. L. London. *Laminar Flow Forced Convection in Ducts*. Academic Press, New York, US, 1978. 1st Ed.

[151] Pasquale Bosso, Mitja Fridman, and Giuseppe Gaetano Luciano. Dark matter as an effect of a minimal length. *Front. Astron. Space Sci.*, 9:932276, 2022.

[152] Yen Chin Ong. Generalized Uncertainty Principle, Black Holes, and White Dwarfs: A Tale of Two Infinities. *JCAP*, 09:015, 2018.

[153] Petr Jizba, Hagen Kleinert, and Fabio Scardigli. Uncertainty Relation on World Crystal and its Applications to Micro Black Holes. *Phys. Rev. D*, 81:084030, 2010.

[154] Petr Jizba, Gaetano Lambiase, Giuseppe Gaetano Luciano, and Luciano Petruzziello. Decoherence limit of quantum systems obeying generalized uncertainty principle: New paradigm for Tsallis thermostatistics. *Phys. Rev. D*, 105(12):L121501, 2022.

[155] Adel Awad and Ahmed Farag Ali. Minimal Length, Friedmann Equations and Maximum Density. *JHEP*, 06:093, 2014.

[156] Saurya Das, Mitja Fridman, Gaetano Lambiase, Antonio Stabile, and Elias C. Vagenas. Modified dispersion relations and a potential explanation of the EDGES anomaly. *Eur. Phys. J. C*, 82(8):720, 2022. [Erratum: Eur.Phys.J.C 82, 816 (2022)].

[157] Saurya Das, Mitja Fridman, Gaetano Lambiase, and Elias C. Vagenas. Baryon asymmetry from the generalized uncertainty principle. *Phys. Lett. B*, 824:136841, 2022.

[158] Zhong-Wen Feng, Xia Zhou, and Shi-Qi Zhou. Higher-order generalized uncertainty principle applied to gravitational baryogenesis. *JCAP*, 06(06):022, 2022.

[159] Giuseppe Gaetano Luciano. Primordial big bang nucleosynthesis and generalized uncertainty principle. *Eur. Phys. J. C*, 81(12):1086, 2021.

[160] Rong-Gen Cai, Li-Ming Cao, and Ya-Peng Hu. Corrected Entropy-Area Relation and Modified Friedmann Equations. *JHEP*, 08:090, 2008.

[161] Tao Zhu, Ji-Rong Ren, and Ming-Fan Li. Influence of Generalized and Extended Uncertainty Principle on Thermodynamics of FRW universe. *Phys. Lett. B*, 674:204–209, 2009.

[162] Serena Giardino and Vincenzo Salzano. Cosmological constraints on the Generalized Uncertainty Principle from modified Friedmann equations. *Eur. Phys. J. C*, 81(2):110, 2021.

[163] Jonathan R. Pritchard and Abraham Loeb. 21-cm cosmology. *Rept. Prog. Phys.*, 75:086901, 2012.

[164] Judd D. Bowman, Alan E. E. Rogers, Raul A. Monsalve, Thomas J. Mozdzen, and Nivedita Mahesh. An absorption profile centred at 78 megahertz in the sky-averaged spectrum. *Nature*, 555(7694):67–70, 2018.

[165] Ahmed Farag Ali and Mohammed M. Khalil. A Proposal for Testing Gravity's Rainbow. *EPL*, 110(2):20009, 2015.

[166] Cheng-Zhou Liu and Jian-Yang Zhu. Hawking radiation and black hole entropy in a gravity ' *s* rainbow. *Gen. Rel. Grav.*, 40:1899–1911, 2008.

[167] Carlos Leiva, Joel Saavedra, and Jose Villanueva. The Geodesic Structure of the Schwarzschild Black Holes in Gravity's Rainbow. *Mod. Phys. Lett. A*, 24:1443–1451, 2009.

[168] Huarun Li, Yi Ling, and Xin Han. Modified (A)dS Schwarzschild black holes in Rainbow spacetime. *Class. Quant. Grav.*, 26:065004, 2009.

[169] Remo Garattini and Gianluca Mandanici. Particle propagation and effective spacetime in Gravity's Rainbow. *Phys. Rev. D*, 85:023507, 2012.

[170] Adel Awad, Ahmed Farag Ali, and Barun Majumder. Nonsingular Rainbow Universes. *JCAP*, 10:052, 2013.

[171] John D. Barrow and Joao Magueijo. Intermediate inflation from rainbow gravity. *Phys. Rev. D*, 88(10):103525, 2013.

[172] Ahmed Farag Ali. Black hole remnant from gravity's rainbow. *Phys. Rev. D*, 89(10):104040, 2014.

[173] Ahmed Farag Ali, Mir Faizal, and Barun Majumder. Absence of an Effective Horizon for Black Holes in Gravity's Rainbow. *EPL*, 109(2):20001, 2015.

[174] Michele Arzano and Gianluca Calcagni. What gravity waves are telling about quantum spacetime. *Phys. Rev. D*, 93(12):124065, 2016. [Addendum: Phys.Rev.D 94, 049907 (2016)].

[175] G. Amelino-Camelia, John R. Ellis, N. E. Mavromatos, and Dimitri V. Nanopoulos. Distance measurement and wave dispersion in a Liouville string approach to quantum gravity. *Int. J. Mod. Phys. A*, 12:607–624, 1997.

[176] Bibhas Ranjan Majhi and Elias C. Vagenas. Modified Dispersion Relation, Photon's Velocity, and Unruh Effect. *Phys. Lett. B*, 725:477–480, 2013.

[177] Ashmita Das, Saurya Das, Noor R. Mansour, and Elias C. Vagenas. Bounds on GUP parameters from GW150914 and GW190521. *Phys. Lett. B*, 819:136429, 2021.

[178] Stephon Alexander and Joao Magueijo. Noncommutative geometry as a realization of varying speed of light cosmology. In *13th Rencontres de Blois on Frontiers of the Universe*, pages 281–297, 2004.

[179] J. Caniou. *Passive Infrared Detection: Theory and Applications*. Springer-Verlag US, Boston, MA, USA, 1999.

[180] E. A. Sharkov. *Passive Microwave Remote Sensing of the Earth*. Springer-Verlag Berlin Heidelberg, Berlin, DE, 2003.

[181] Rennan Barkana. Possible interaction between baryons and dark-matter particles revealed by the first stars. *Nature*, 555(7694):71–74, 2018.

[182] Steven Furlanetto, S. Peng Oh, and Frank Briggs. Cosmology at Low Frequencies: The 21 cm Transition and the High-Redshift Universe. *Phys. Rept.*, 433:181–301, 2006.

[183] N. Fornengo, R. Lineros, M. Regis, and M. Taoso. Possibility of a Dark Matter Interpretation for the Excess in Isotropic Radio Emission Reported by ARCADE. *Phys. Rev. Lett.*, 107:271302, 2011.

[184] D. J. Fixsen et al. ARCADE 2 Measurement of the Extra-Galactic Sky Temperature at 3-90 GHz. *Astrophys. J.*, 734:5, 2011.

[185] Laura Lopez-Honorez, Olga Mena, Ángeles Moliné, Sergio Palomares-Ruiz, and Aaron C. Vincent. The 21 cm signal and the interplay between dark matter annihilations and astrophysical processes. *JCAP*, 08:004, 2016.

[186] D. Aristizabal Sierra and Chee Sheng Fong. The EDGES signal: An imprint from the mirror world? *Phys. Lett. B*, 784:130–136, 2018.

[187] J. Colin Hill and Eric J. Baxter. Can Early Dark Energy Explain EDGES? *JCAP*, 08:037, 2018.

[188] Maxim Pospelov, Josef Pradler, Joshua T. Ruderman, and Alfredo Urbano. Room for New Physics in the Rayleigh-Jeans Tail of the Cosmic Microwave Background. *Phys. Rev. Lett.*, 121(3):031103, 2018.

[189] Takeo Moroi, Kazunori Nakayama, and Yong Tang. Axion-photon conversion and effects on 21 cm observation. *Phys. Lett. B*, 783:301–305, 2018.

[190] Gaetano Lambiase and Subhendra Mohanty. Hydrogen spin oscillations in a background of axions and the 21-cm brightness temperature. *Mon. Not. Roy. Astron. Soc.*, 494(4):5961–5966, 2020.

[191] Marco Chianese, Pasquale Di Bari, Kareem Farrag, and Rome Samanta. Probing relic neutrino radiative decays with 21 cm cosmology. *Phys. Lett. B*, 790:64–70, 2019.

[192] D. J. Fixsen. The Temperature of the Cosmic Microwave Background. *Astrophys. J.*, 707:916–920, 2009.

[193] D. J. Fixsen, E. S. Cheng, J. M. Gales, John C. Mather, R. A. Shafer, and E. L. Wright. The Cosmic Microwave Background spectrum from the full COBE FIRAS data set. *Astrophys. J.*, 473:576, 1996.

[194] John C. Mather, D. J. Fixsen, R. A. Shafer, C. Mosier, and D. T. Wilkinson. Calibrator design for the COBE far infrared absolute spectrophotometer (FIRAS). *Astrophys. J.*, 512:511–520, 1999.

[195] B. Ryden. *Introduction to Cosmology 2nd Edition*. Cambridge University Press, New York, USA, 2017.

[196] Pasquale Bosso, Saurya Das, Igor Pikovski, and Michael R. Vanner. Amplified transduction of Planck-scale effects using quantum optics. *Phys. Rev. A*, 96(2):023849, 2017.

[197] Laurent Canetti, Marco Drewes, and Mikhail Shaposhnikov. Matter and Antimatter in the Universe. *New J. Phys.*, 14:095012, 2012.

[198] A. D. Sakharov. Violation of CP Invariance, C asymmetry, and baryon asymmetry of the universe. *Pisma Zh. Eksp. Teor. Fiz.*, 5:32–35, 1967.

[199] J. Dunkley et al. Five-Year Wilkinson Microwave Anisotropy Probe (WMAP) Observations: Likelihoods and Parameters from the WMAP data. *Astrophys. J. Suppl.*, 180:306–329, 2009.

[200] W. M. Yao et al. Review of Particle Physics. *J. Phys. G*, 33:1–1232, 2006.

[201] Andrew G. Cohen and David B. Kaplan. SPONTANEOUS BARYOGENESIS. *Nucl. Phys. B*, 308:913–928, 1988.

[202] Stephon Haigh-Solom Alexander, Michael E. Peskin, and Mohammad M. Sheikh-Jabbari. Leptogenesis from gravity waves in models of inflation. *Phys. Rev. Lett.*, 96:081301, 2006.

[203] Gerard 't Hooft. Dimensional reduction in quantum gravity. *Conf. Proc. C*, 930308:284–296, 1993.

[204] Leonard Susskind. The World as a hologram. *J. Math. Phys.*, 36:6377–6396, 1995.

[205] Ted Jacobson. Thermodynamics of space-time: The Einstein equation of state. *Phys. Rev. Lett.*, 75:1260–1263, 1995.

[206] A. J. M. Medved and Elias C. Vagenas. When conceptual worlds collide: The GUP and the BH entropy. *Phys. Rev. D*, 70:124021, 2004.

[207] Ronald J. Adler, Pisin Chen, and David I. Santiago. The Generalized uncertainty principle and black hole remnants. *Gen. Rel. Grav.*, 33:2101–2108, 2001.

[208] D. Christodoulou. Reversible and irreversible transforations in black hole physics. *Phys. Rev. Lett.*, 25:1596–1597, 1970.

[209] D. Christodoulou and R. Ruffini. Reversible transformations of a charged black hole. *Phys. Rev. D*, 4:3552–3555, 1971.

[210] S. W. Hawking. Gravitational radiation from colliding black holes. *Phys. Rev. Lett.*, 26:1344–1346, 1971.

[211] Patrick J. Coles, Mario Berta, Marco Tomamichel, and Stephanie Wehner. Entropic uncertainty relations and their applications. *Rev. Mod. Phys.*, 89:015002, Feb 2017.

[212] Jacob D. Bekenstein. Black holes and entropy. *Phys. Rev. D*, 7:2333–2346, 1973.

[213] S. W. Hawking. Black Holes and Thermodynamics. *Phys. Rev. D*, 13:191–197, 1976.

[214] T. Kugo and S. Uehara. Improved Superconformal Gauge Conditions in the $N = 1$ Supergravity Yang-Mills Matter System. *Nucl. Phys. B*, 222:125–138, 1983.

[215] T. Kugo and S. Uehara. $N = 1$ Superconformal Tensor Calculus: Multiplets With External Lorentz Indices and Spinor Derivative Operators. *Prog. Theor. Phys.*, 73:235, 1985.

[216] Hooman Davoudiasl, Ryuichiro Kitano, Graham D. Kribs, Hitoshi Murayama, and Paul J. Steinhardt. Gravitational baryogenesis. *Phys. Rev. Lett.*, 93:201301, 2004.

[217] Nadeem Azhar, Abdul Jawad, and Shamaila Rani. Impact of f(G,T) and f(R,G) on gravitational baryogenesis and observational bounds. *Phys. Dark Univ.*, 32:100815, 2021.

[218] Hooman Davoudiasl. Gravitationally Induced Dark Matter Asymmetry and Dark Nucleon Decay. *Phys. Rev. D*, 88:095004, 2013.

[219] S. D. Odintsov and V. K. Oikonomou. Loop Quantum Cosmology Gravitational Baryogenesis. *EPL*, 116(4):49001, 2016.

[220] S. D. Odintsov and V. K. Oikonomou. Gauss–Bonnet gravitational baryogenesis. *Phys. Lett. B*, 760:259–262, 2016.

[221] V. K. Oikonomou and Emmanuel N. Saridakis. $f(T)$ gravitational baryogenesis. *Phys. Rev. D*, 94(12):124005, 2016.

[222] Snehasish Bhattacharjee and P. K. Sahoo. Baryogenesis in $f(Q,\mathcal{T})$ gravity. *Eur. Phys. J. C*, 80(3):289, 2020.

[223] E. H. Baffou, M. J. S. Houndjo, D. A. Kanfon, and I. G. Salako. $f(R,T)$ models applied to baryogenesis. *Eur. Phys. J. C*, 79(2):112, 2019.

[224] M. P. L. P. Ramos and J. Páramos. Baryogenesis in Nonminimally Coupled $f(R)$ Theories. *Phys. Rev. D*, 96(10):104024, 2017.

[225] Mitsuhiro Fukushima, Shuntaro Mizuno, and Kei-ichi Maeda. Gravitational Baryogenesis after Anisotropic Inflation. *Phys. Rev. D*, 93(10):103513, 2016.

[226] H. Mohseni Sadjadi. A Note on Gravitational Baryogenesis. *Phys. Rev. D*, 76:123507, 2007.

[227] Edward W. Kolb and Michael S. Turner. *The Early Universe*, volume 69. 1990.

[228] William H. Kinney, Edward W. Kolb, Alessandro Melchiorri, and Antonio Riotto. Inflation model constraints from the Wilkinson Microwave Anisotropy Probe three-year data. *Phys. Rev. D*, 74:023502, 2006.

[229] James M. Cline. Baryogenesis. In *Les Houches Summer School - Session 86: Particle Physics and Cosmology: The Fabric of Spacetime*, 9 2006.

[230] A. D. Dolgov. CP violation in cosmology. In *163rd Course of International School of Physics 'Enrico Fermi': CP Violation: From Quarks to Leptons*, pages 407–438, 11 2005.

[231] Antonio Riotto. Theories of baryogenesis. In *ICTP Summer School in High-Energy Physics and Cosmology*, pages 326–436, 7 1998.

[232] Antonio Riotto and Mark Trodden. Recent progress in baryogenesis. *Ann. Rev. Nucl. Part. Sci.*, 49:35–75, 1999.

[233] M. Yoshimura. Baryogenesis and thermal history after inflation. *J. Korean Phys. Soc.*, 29:S236, 1996.

[234] Gaetano Lambiase, Subhendra Mohanty, and Aragam R. Prasanna. Neutrino coupling to cosmological background: A review on gravitational Baryo/Leptogenesis. *Int. J. Mod. Phys. D*, 22:1330030, 2013.

[235] Lucien Hardy. Implementation of the Quantum Equivalence Principle. In *Progress and Visions in Quantum Theory in View of Gravity: Bridging foundations of physics and mathematics*, 3 2019.

[236] Steven Weinberg. *Gravitation and Cosmology: Principles and Applications of the General Theory of Relativity*. John Wiley and Sons, New York, 1972.

[237] Voisin, G., Cognard, I., Freire, P. C. C., Wex, N., Guillemot, L., Desvignes, G., Kramer, M., and Theureau, G. An improved test of the strong equivalence principle with the pulsar in a triple star system. *A&A*, 638:A24, 2020.

[238] Magdalena Zych and Časlav Brukner. Quantum formulation of the Einstein Equivalence Principle. *Nature Phys.*, 14(10):1027–1031, 2018.

[239] Michael E. Peskin and Daniel V. Schroeder. *An Introduction to quantum field theory*. Addison-Wesley, Reading, USA, 1995.

[240] G. Cognola, L. Vanzo, and S. Zerbini. Relativistic Wave Mechanics of Spinless Particles in a Curved Space-time. *Gen. Rel. Grav.*, 18:971–982, 1986.

[241] E. A. Tagirov. Field-theoretical approach to quantum mechanics in curved space-times. *Class. Quant. Grav.*, 16:2165–2185, 1999.

[242] Pierre Touboul et al. Space test of the Equivalence Principle: first results of the MICROSCOPE mission. *Class. Quant. Grav.*, 36(22):225006, 2019.

[243] Eli Megidish, Joseph Broz, Nicole Greene, and Hartmut Häffner. Improved Test of Local Lorentz Invariance from a Deterministic Preparation of Entangled States. *Phys. Rev. Lett.*, 122(12):123605, 2019.

[244] Steven Peil, Scott Crane, James L. Hanssen, Thomas B. Swanson, and Christopher R. Ekstrom. Tests of local position invariance using continuously running atomic clocks. *Phys. Rev. A*, 87:010102, Jan 2013.

[245] S. Baessler, Blayne R. Heckel, E. G. Adelberger, J. H. Gundlach, U. Schmidt, and H. E. Swanson. Improved Test of the Equivalence Principle for Gravitational Self-Energy. *Phys. Rev. Lett.*, 83:3585, 1999.

[246] Saurya Das, Mitja Fridman, and Gaetano Lambiase. The Quantum Equivalence Principle. *Work in progress*, 2023.

[247] Jonathan Hackett. Asymptotic flatness in rainbow gravity. *Class. Quant. Grav.*, 23:3833–3842, 2006.

[248] Yi Ling, Song He, and Hong-bao Zhang. The Kinematics of particles moving in rainbow spacetime. *Mod. Phys. Lett. A*, 22:2931–2938, 2007.

[249] K. Atazadeh. Matter and antimatter asymmetry in a rainbow universe. *Annals Phys.*, 446:169133, 2022.

[250] A. B. Bilim, O. Aydogdu, M. Salti, and K. Sogut. Particle production in a rainbow background. *Annals Phys.*, 449:169200, 2023.

[251] Eric Poisson. *A Relativist's Toolkit: The Mathematics of Black-Hole Mechanics*. Cambridge University Press, 2004.

[252] Philip K. Schwartz and Domenico Giulini. Post-Newtonian Hamiltonian description of an atom in a weak gravitational field. *Phys. Rev. A*, 100(5):052116, 2019.

[253] Subrahmanyan Chandrasekhar. *The mathematical theory of black holes*. Oxford University Press, New York, USA, 1983.

[254] A. Papapetrou. *Lectures on General Relativity*. D. Reidel Publishing Company, Dordrecht, NL, 1974.

[255] R. Colella, A. W. Overhauser, and S. A. Werner. Observation of gravitationally induced quantum interference. *Phys. Rev. Lett.*, 34:1472–1474, 1975.

[256] K. C. Littrell, B. E. Allman, and S. A. Werner. Two-wavelength-difference measurement of gravitationally induced quantum interference phases. *Phys. Rev. A*, 56:1767–1780, 1997.

[257] T. Numao, J. A. Macdonald, Glen M. Marshall, A. Olin, and M. C. Fujiwara. A New pi+ lifetime measurement. *Phys. Rev. D*, 52:4855–4859, 1995.

[258] G. Brooke, M. A. Meyer, and A. W. Wolfendale. The energy spectrum of cosmic ray pions near sea level in the range 0.7-150 gev. *Proceedings of the Physical Society (1960)*, 83(5):871–877, 1964.

[259] R. S. et al Park. Precession of Mercury's Perihelion from Ranging to the MESSENGER Spacecraft. *Astron. J.*, 153:121, 2017.

[260] Yuichi Harikane, Akio K. Inoue, Ken Mawatari, Takuya Hashimoto, Satoshi Yamanaka, Yoshinobu Fudamoto, Hiroshi Matsuo, Yoichi Tamura, Pratika Dayal, L. Y. Aaron Yung, Anne Hutter, Fabio Pacucci, Yuma Sugahara, and Anton M. Koekemoer. A search for h-dropout lyman break galaxies at z 12–16. *The Astrophysical Journal*, 929(1):1, apr 2022.

[261] Elias C. Vagenas, Lina Alasfar, Salwa M. Alsaleh, and Ahmed Farag Ali. The GUP and quantum Raychaudhuri equation. *Nucl. Phys. B*, 931:72–78, 2018.

[262] S. Aghababaei, H. Moradpour, and Elias C. Vagenas. Hubble tension bounds the GUP and EUP parameters. *Eur. Phys. J. Plus*, 136(10):997, 2021.

[263] T. Kanazawa, G. Lambiase, G. Vilasi, and A. Yoshioka. Noncommutative Schwarzschild geometry and generalized uncertainty principle. *Eur. Phys. J. C*, 79(2):95, 2019.

[264] Saurya Das, Elias C. Vagenas, and Ahmed Farag Ali. Discreteness of Space from GUP II: Relativistic Wave Equations. *Phys. Lett. B*, 690:407–412, 2010. [Erratum: Phys.Lett.B 692, 342–342 (2010)].

[265] Soumen Deb, Saurya Das, and Elias C. Vagenas. Discreteness of Space from GUP in a Weak Gravitational Field. *Phys. Lett. B*, 755:17–23, 2016.

[266] Saurya Das and Sourav Sur. Gravitational lensing and missing mass. *Phys. Open*, 15:100150, 2023.

[267] Matias Zaldarriaga, Steven R. Furlanetto, and Lars Hernquist. 21 Centimeter fluctuations from cosmic gas at high redshifts. *Astrophys. J.*, 608:622–635, 2004.

[268] P. A. R. Ade et al. Planck 2015 results. XIII. Cosmological parameters. *Astron. Astrophys.*, 594:A13, 2016.

[269] Robert C. Hilborn. Einstein coefficients, cross sections, f values, dipole moments, and all that. *Am. J. Phys.*, 50:982–986, 1982.

[270] Rong-Gen Cai and Sang Pyo Kim. First law of thermodynamics and Friedmann equations of Friedmann-Robertson-Walker universe. *JHEP*, 02:050, 2005.

[271] Rong-Gen Cai, Li-Ming Cao, and Ya-Peng Hu. Hawking Radiation of Apparent Horizon in a FRW Universe. *Class. Quant. Grav.*, 26:155018, 2009.

[272] Sean A. Hayward. Unified first law of black hole dynamics and relativistic thermodynamics. *Class. Quant. Grav.*, 15:3147–3162, 1998.

Appendix A

Statistical Mechanics

A.1 Mathematical Tools

When a prediction of any physical observable in statistical mechanics is made, one needs to compute averages, because in systems with many particles, one can only measure macroscopic observables of the whole system, such as temperature, pressure and volume. To compute an ensemble average of a physical, single particle quantity Y over the whole energy range $\varepsilon \in [0,\infty)$, for a gas of bosons or fermions, the ensemble average is used

$$\langle Y \rangle = \int_0^\infty Y(\varepsilon)\, g(\varepsilon)\, f_{BE(FD)}(\varepsilon)\, \mathrm{d}\varepsilon \,, \tag{A.1}$$

where

$$g(\varepsilon) = \frac{V d\, \Omega_d\, 2^{d/2-1}\, m^{d/2}\, \varepsilon^{d/2-1}}{(2\pi\hbar)^d} \tag{A.2}$$

is the d-dimensional density of states for non-relativistic particles,

$$g(\varepsilon) = \frac{V d\, \Omega_d\, \varepsilon \left(\varepsilon^2 - m^2c^4\right)^{d/2-1}}{(2\pi\hbar c)^d} \tag{A.3}$$

is the d-dimensional density of states for relativistic particles, where $\Omega_d = \pi^{d/2}/\Gamma(d/2+1)$, and

$$f_{BE(FD)}(\varepsilon) = \frac{1}{e^{\beta_T(\varepsilon-\mu)} \mp 1} \,, \tag{A.4}$$

is the BE distribution $(-)$ or FD distribution $(+)$. In the above, $\beta_T = 1/k_B T$, ε the energy of the particle and μ the chemical potential. For any single particle quantity $Y(\varepsilon)$, all integrals given by Eq. (A.1), which are calculated using the BE distribution from Eq. (A.4) (which corresponds to the $-$ sign), are of the following form

$$I_\nu(\beta_T, \beta_T\mu) = \int_0^\infty \frac{\varepsilon^\nu}{e^{\beta_T(\varepsilon-\mu)} - 1}\, \mathrm{d}\varepsilon = \frac{\Gamma(\nu+1)}{\beta_T^{\nu+1}}\, Li_{\nu+1}(e^{\beta_T\mu}) \,, \tag{A.5}$$

where ν is the power of the energy in the integral, $\Gamma(\nu+1)$ is the gamma function evaluated at $\nu+1$ and

$$Li_\nu(x) = \sum_{k=1}^{\infty} \frac{x^k}{k^\nu} \tag{A.6}$$

is the polylogarithm function. For $x = 1$, which corresponds to the case $\mu = 0$, the polylogarithm function in Eq. (A.6) reduces to the well known Riemann zeta function

$$\zeta(\nu) = \sum_{k=1}^{\infty} \frac{1}{k^{\nu}} \, . \tag{A.7}$$

On the other hand, all integrals, which are calculated using the FD distribution from Eq. (A.4) (corresponding to the + sign), are of the following form

$$J_{\nu}(\beta_T, \beta_T \mu) = \int_0^{\infty} \frac{\varepsilon^{\nu}}{e^{\beta_T(\varepsilon-\mu)}+1} \, d\varepsilon = -\frac{\Gamma(\nu+1)}{\beta_T^{\nu+1}} Li_{\nu+1}(-e^{\beta_T \mu}) \, . \tag{A.8}$$

For $x = -1$, corresponding to $\mu = 0$, the polylogarithm function in Eq. (A.6) reduces to

$$Li_{\nu}(-1) = -\eta(\nu) \, , \tag{A.9}$$

where

$$\eta(\nu) = \sum_{k=1}^{\infty} \frac{(-1)^{k-1}}{k^{\nu}} \tag{A.10}$$

is the Dirichlet eta function. The values for the Riemann zeta and Dirichlet eta, as a function of ν, where defined, can be found numerically.

As the simplest example, one can obtain the number of particles in a gas of bosons, contained in a volume V, using the BE distribution and Eqs. (A.1) and (A.2), where $Y = 1$, as

$$\begin{aligned} N_{BE} &= \int_0^{\infty} g(\varepsilon) \, f_{BE}(\varepsilon) \, d\varepsilon \\ &= \frac{V d \, \Omega_d \, 2^{d/2-1} \, m^{d/2}}{(2\pi\hbar)^d} \int_0^{\infty} \frac{\varepsilon^{d/2-1}}{e^{\beta_T(\varepsilon-\mu)}-1} \, d\varepsilon \\ &= \frac{V d \, \Omega_d \, 2^{d/2-1} \, m^{d/2}}{(2\pi\hbar)^d} \, (k_B T)^{d/2} \, \Gamma\left(\tfrac{d}{2}\right) \, Li_{d/2}(e^{\beta_T \mu}) \\ &\overset{d=3}{=} \frac{V}{8\hbar^3} \left(\frac{2 m k_B T}{\pi}\right)^{3/2} Li_{3/2}(e^{\beta_T \mu}) \, , \end{aligned} \tag{A.11}$$

where Eq. (A.5) was used to evaluate the integral in line two. As the temperature approaches T_c, the chemical potential vanishes $\mu \longrightarrow 0$, which reduces the polylogarithm function in Eq. (A.11) to the Riemann zeta function $\zeta(3/2) \simeq 2.612$. This is the regime where the Bose-Einstein condensation begins to occur.

In the same manner one can obtain the number of particles in a gas of fermions, contained in a volume V, using the FD distribution and Eqs. (A.1) and (A.2), where $Y = 1$, as

$$
\begin{aligned}
N_{FD} &= \int_0^\infty g(\varepsilon)\, f_{FD}(\varepsilon)\, \mathrm{d}\varepsilon \\
&= \frac{V d\, \Omega_d\, 2^{d/2-1}\, m^{d/2}}{(2\pi\hbar)^d} \int_0^\infty \frac{\varepsilon^{d/2-1}}{e^{\beta_T(\varepsilon-\mu)}+1}\, \mathrm{d}\varepsilon \\
&= -\frac{V d\, \Omega_d\, 2^{d/2-1}\, m^{d/2}}{(2\pi\hbar)^d} (k_B T)^{d/2}\, \Gamma\left(\tfrac{d}{2}\right) Li_{d/2}(-e^{\beta_T \mu}) \\
&\overset{d=3}{=} -\frac{V}{8\hbar^3} \left(\frac{2 m k_B T}{\pi}\right)^{3/2} Li_{3/2}(-e^{\beta_T \mu})\,,
\end{aligned}
\tag{A.12}
$$

where Eq. (A.8) was used to evaluate the integral in line two. The above is an exact solution for a Fermi gas at temperature T. In the case, when $T \longrightarrow 0$, the FD distribution reduces to $f_{FD}(\varepsilon) = 1$, and one obtains a finite, so-called Fermi energy E_f, as an upper limit to the integral, since this is the maximal energy a fermion can have in such conditions. This would represent a degenerate fermion gas.

A.2 Linear GUP Operator

To evaluate the eigenvalues, corresponding to the linear GUP term, one must consider the operator $p_0 = \sqrt{p_{0k}\, p_{0k}}$, where $p_{0i} = -i\hbar\partial_{x_{0i}}$. Note that p_0 is a scalar operator, and obtaining its eigenvalues was considered a difficult computational problem. In the following, a solution to this problem, including its proof, is introduced. Explicitly, p_0 can be written as

$$
p_0 = \sqrt{-\hbar^2 \left(\frac{\partial^2}{\partial x_0^2} + \frac{\partial^2}{\partial y_0^2} + \frac{\partial^2}{\partial z_0^2}\right)} = \sqrt{-\hbar^2 \nabla_0^2} = \hbar \left(-\nabla_0^2\right)^{1/2}\,. \tag{A.13}
$$

Without loss of generality, one can write the above as

$$
p_0 = \frac{\hbar}{\ell} \left(1 - \ell^2 \nabla_0^2 - 1\right)^{1/2}\,, \tag{A.14}
$$

where ℓ is a non-zero constant and a $0 = 1 - 1$ has been added inside the parenthesis. One can interpret ℓ as a length scale, and therefore assume it to be positive and non-vanishing. This also ensures that the eigenvalues of p_0 are positive. One can see that the above is of the form $(1+x)^{1/2}$, where $x = -\ell^2 \nabla_0^2 - 1$, and can be represented as a Taylor series

$$
(1+x)^{1/2} = \sum_{m=0}^{\infty} c_m x^m\,. \tag{A.15}
$$

In the above, the expansion coefficients c_m correspond to those of $(1+x)^{1/2}$ and their exact values are not required for the remainder of the proof. Using the above Taylor series, one

can write Eq. (A.14) as

$$p_0 = \frac{\hbar}{\ell} \sum_{m=0}^{\infty} c_m \left(-\ell^2 \nabla_0^2 - 1\right)^m \ . \tag{A.16}$$

In the above, the parenthesis on the right hand side, can be expanded in terms of the binomial theorem

$$(a+b)^m = \sum_{q=0}^{m} \binom{m}{q} a^{m-q} b^q \quad \text{with} \quad a, b \in \mathbb{R} \ , \tag{A.17}$$

where

$$\binom{m}{q} = \frac{m!}{(m-q)!\, q!} \ . \tag{A.18}$$

Using the above binomial theorem, one can rewrite Eq. (A.16) as

$$p_0 = \frac{\hbar}{\ell} \sum_{m=0}^{\infty} c_m \sum_{q=0}^{m} \binom{m}{q} \left(-\ell^2 \nabla_0^2\right)^{m-q} (-1)^q \ . \tag{A.19}$$

Since the identity operator commutes with every other operator, i.e., $[1, \left(\nabla_0^2\right)^r] = 0$ in this case, where $r \in \mathbb{N} \cup \{0\}$, one can rewrite Eq. (A.19) as

$$p_0 = \frac{\hbar}{\ell} \sum_{m=0}^{\infty} c_m \sum_{q=0}^{m} \binom{m}{q} (-1)^q \left(\ell^2\right)^{m-q} \left(-\nabla_0^2\right)^{m-q} . \tag{A.20}$$

In the BEC considerations, eigenfunctions of a three dimensional particle in a box $|\psi_{\mathbf{n}}\rangle$ are considered, where the eigenvalues of the operator $-\nabla_0^2$ turn out as

$$-\nabla_0^2 |\psi_{\mathbf{n}}\rangle = k_{\mathbf{n}}^2 |\psi_{\mathbf{n}}\rangle \ , \tag{A.21}$$

where $k_{\mathbf{n}}^2 = k_{n_x}^2 + k_{n_y}^2 + k_{n_z}^2 = \frac{\pi^2}{L^2}(n_x^2 + n_y^2 + n_z^2)$. Therefore, by squaring the operator $-\nabla_0^2$, one obtains

$$\begin{aligned} \left(-\nabla_0^2\right)^2 |\psi_{\mathbf{n}}\rangle &= \left(-\nabla_0^2\right)\left(-\nabla_0^2\right)|\psi_{\mathbf{n}}\rangle \\ &= \left(-\nabla_0^2\right) k_{\mathbf{n}}^2 |\psi_{\mathbf{n}}\rangle \\ &= k_{\mathbf{n}}^2 \left(-\nabla_0^2\right)|\psi_{\mathbf{n}}\rangle \\ &= k_{\mathbf{n}}^2 k_{\mathbf{n}}^2 |\psi_{\mathbf{n}}\rangle \\ &= \left(k_{\mathbf{n}}^2\right)^2 |\psi_{\mathbf{n}}\rangle \ . \end{aligned} \tag{A.22}$$

Similarly, for all other powers $r \in \mathbb{N} \cup \{0\}$ of the operator $-\nabla_0^2$, it can be proven by induction, that

$$\left(-\nabla_0^2\right)^r |\psi_{\mathbf{n}}\rangle = \left(k_{\mathbf{n}}^2\right)^r |\psi_{\mathbf{n}}\rangle \ . \tag{A.23}$$

Having all necessary ingredients, one can now use the operator from Eq. (A.20) on the eigenfunction $|\psi_{\mathbf{n}}\rangle$, in order to obtain its eigenvalue as

$$\begin{aligned}
p_0|\psi_{\mathbf{n}}\rangle &= \frac{\hbar}{\ell}\sum_{m=0}^{\infty} c_m \sum_{q=0}^{m}\binom{m}{q}(-1)^q\left(\ell^2\right)^{m-q}\left(-\nabla_0^2\right)^{m-q}|\psi_{\mathbf{n}}\rangle \\
&= \frac{\hbar}{\ell}\sum_{m=0}^{\infty} c_m \sum_{q=0}^{m}\binom{m}{q}(-1)^q\left(\ell^2\right)^{m-q}\left(k_{\mathbf{n}}^2\right)^{m-q}|\psi_{\mathbf{n}}\rangle \\
&= \frac{\hbar}{\ell}\sum_{m=0}^{\infty} c_m \sum_{q=0}^{m}\binom{m}{q}\left(\ell^2 k_{\mathbf{n}}^2\right)^{m-q}(-1)^q|\psi_{\mathbf{n}}\rangle \\
&= \frac{\hbar}{\ell}\sum_{m=0}^{\infty} c_m \left(\ell^2 k_{\mathbf{n}}^2-1\right)^m|\psi_{\mathbf{n}}\rangle \\
&= \frac{\hbar}{\ell}\left(1+\ell^2 k_{\mathbf{n}}^2-1\right)^{1/2}|\psi_{\mathbf{n}}\rangle \\
&= \frac{\hbar}{\ell}\left(\ell^2 k_{\mathbf{n}}^2\right)^{1/2}|\psi_{\mathbf{n}}\rangle \\
&= \hbar\left(k_{\mathbf{n}}^2\right)^{1/2}|\psi_{\mathbf{n}}\rangle\,. \qquad \text{(A.24)}
\end{aligned}$$

To compute the eigenvalue of the operator p_0^3, found in the linear term in GUP, one uses operators p_0 and p_0^2 consecutively on the state $|\psi_{\mathbf{n}}\rangle$. It reads as

$$\begin{aligned}
p_0^3|\psi_{\mathbf{n}}\rangle &= p_0^2\, p_0|\psi_{\mathbf{n}}\rangle \\
&= p_0^2\,\hbar\left(k_{\mathbf{n}}^2\right)^{1/2}|\psi_{\mathbf{n}}\rangle \\
&= \hbar\left(k_{\mathbf{n}}^2\right)^{1/2} p_0^2|\psi_{\mathbf{n}}\rangle \\
&= \hbar\left(k_{\mathbf{n}}^2\right)^{1/2}\left(-\hbar^2\nabla_0^2\right)|\psi_{\mathbf{n}}\rangle \\
&= \hbar\left(k_{\mathbf{n}}^2\right)^{1/2}\left(\hbar^2 k_{\mathbf{n}}^2\right)|\psi_{\mathbf{n}}\rangle \\
&= \hbar^3\left(k_{\mathbf{n}}^2\right)^{3/2}|\psi_{\mathbf{n}}\rangle\,. \qquad \text{(A.25)}
\end{aligned}$$

To the best of one's knowledge, this is the first time that the eigenfunctions of the p_0^3 operator in three spatial dimensions have been found by the above method, thereby providing a simple solution for future research in QGP involving a linear GUP.

A.3 GUP Corrections

The QG corrected density of states is obtained in a similar way as it is obtained in standard theory. In the standard theory, one considers the continuum limit and the dispersion relation $\varepsilon(p)$ (classical or relativistic). The number of particles, and by extension the density of states in three dimensions, are then obtained as

$$\sum_{\mathbf{n}} \approx \int \mathrm{d}^3 n = \frac{V}{(2\pi\hbar)^3}\int_0^\infty \mathrm{d}^3 p = \frac{V}{2\pi^2}\int_0^\infty k^2\,\mathrm{d}k = \int_0^\infty g(\varepsilon)\,\mathrm{d}\varepsilon\,, \qquad \text{(A.26)}$$

where $p = \hbar k$ and $\mathrm{d}^3 p = 4\pi p^2 \mathrm{d}p$ were used. In the last equality one uses the relevant dispersion relation to obtain the corresponding density of states. By using the modified dispersion relations from Eqs. (3.23) and (3.36), one obtains the QG corrected density of states for non-relativistic and relativistic particles, respectively. Both, k^2 and $\mathrm{d}k$ are modified, by expressing k in terms of the particle energy ε from Eq. (3.23) for the non-relativistic case, and from Eq. (3.36) for the relativistic case, in the continuum limit ($k_{\mathbf{n}} \longrightarrow k$ and $\varepsilon_{\mathbf{n}} \longrightarrow \varepsilon$). For convenience, the linear and quadratic GUP corrections were considered separately. Considering both contributions simultaneously would make the results change by a numerical factor of $O(1)$ in front of the quadratic term.

A.3.1 Quadratic GUP

For the quadratic QG corrections ($\alpha = 0$), k is obtained from Eqs. (3.23) and (3.36), by solving a quadratic equation for $k^2(\varepsilon)$. The solutions read as

$$k_{1,2}^2 = \begin{cases} \dfrac{1}{10\beta\hbar^2}\left[-1 \pm \sqrt{1+40\beta m\varepsilon}\right] & , \quad \text{non-relativistic,} \\ \dfrac{1}{10\beta\hbar^2}\left[-1 \pm \sqrt{1+20\beta\left(\dfrac{\varepsilon^2}{c^2} - m^2c^2\right)}\right] & , \quad \text{relativistic.} \end{cases} \tag{A.27}$$

Each of the above cases gives rise to 4 solutions. However, in the following, only physically relevant solutions are considered. Namely, $k_{1,2} \in \mathbb{R}$ *and* $k_{1,2} > 0$, since it is the radius of a sphere in $k-$space. This reduces the number of solutions to just 1 for each case.

To obtain the quadratic QG corrected measure $\mathrm{d}k$, one computes the derivatives of Eqs. (3.23) and (3.36) (for $\alpha = 0$) with respect to k, and expresses $\mathrm{d}k$ as

$$\mathrm{d}k = \begin{cases} \dfrac{\mathrm{d}\varepsilon}{\frac{\hbar^2 k}{m} + \frac{10\beta\hbar^4 k^3}{m}} & , \quad \text{non-relativistic,} \\ \dfrac{\varepsilon\,\mathrm{d}\varepsilon}{\hbar^2 c^2 k + 10\beta\hbar^4 c^2 k^3} & , \quad \text{relativistic.} \end{cases} \tag{A.28}$$

To obtain the density of states with quadratic QG corrections, one plugs the solution for k from Eq. (A.27) in Eq. (A.28), such that the measure is now completely dependent on ε. Finally, one plugs Eqs. (A.27) and (A.28) in Eq. (A.26) to obtain the quadratic QG corrected densities of states from Eqs. (3.24) and (3.37) (for $\alpha = 0$) for non-relativistic and relativistic particles, respectively. Note that a perturbative approach was necessary to obtain the quadratic QG corrected densities of states, where terms of order equal to or higher than $O(\beta^2)$ were ignored.

A.3.2 Linear GUP

To obtain the linear GUP corrections to the density of states, a procedure, similar as for quadratic GUP corrections, was followed. For the linear QG corrections ($\beta = 0$), k is obtained from Eqs. (3.23) and (3.36), by solving cubic equations for $k(\varepsilon)$. This gives rise

to 3 solutions for each, the non-relativistic case and the relativistic case, which read as

$$k = \begin{cases} \frac{1}{6\alpha\hbar}\left[1-\cos\left(\varphi(\alpha)\right)+\sqrt{3}\sin\left(\varphi(\alpha)\right)\right], \\ \frac{1}{6\alpha\hbar}\left[1-\cos\left(\varphi(\alpha)\right)-\sqrt{3}\sin\left(\varphi(\alpha)\right)\right], \\ \frac{1}{6\alpha\hbar}\left[1+2\cos\left(\varphi(\alpha)\right)\right], \end{cases} \tag{A.29}$$

where

$$\varphi(\alpha) = \begin{cases} \frac{1}{3}\arctan\left(\frac{6\sqrt{6}\alpha\sqrt{m\varepsilon}\sqrt{1-54\alpha^2 m\varepsilon}}{1-108\alpha^2 m\varepsilon}\right) & , \text{ non-relativistic,} \\ \frac{1}{3}\arctan\left(\frac{2\sqrt{27}\alpha\sqrt{\frac{\varepsilon^2}{c^2}-m^2c^2}\sqrt{1-27\alpha^2\left(\frac{\varepsilon^2}{c^2}-m^2c^2\right)}}{1-54\alpha^2\left(\frac{\varepsilon^2}{c^2}-m^2c^2\right)}\right) & , \text{ relativistic.} \end{cases} \tag{A.30}$$

Out of the above 3 solutions of Eq. (A.29), only the first is physically relevant, since the second solution is negative, and the third solution diverges in the limit $\alpha \longrightarrow 0$, implying large QG effects, which are not observed. This reduces the number of solutions to just 1 for each case.

To obtain the linear QG corrected measure dk, one computes the derivatives of Eqs. (3.23) and (3.36) (for $\beta = 0$) with respect to k, and expresses dk as

$$\mathrm{d}k = \begin{cases} \frac{\mathrm{d}\varepsilon}{\frac{\hbar^2 k}{m}-\frac{3\alpha\hbar^3k^2}{m}} & , \text{ non-relativistic,} \\ \frac{\varepsilon\,\mathrm{d}\varepsilon}{\hbar^2c^2k-3\alpha\hbar^3c^2k^2} & , \text{ relativistic.} \end{cases} \tag{A.31}$$

To obtain the density of states with linear QG corrections, one plugs the solution for k from Eq. (A.29) in Eq. (A.31), such that the measure is now completely dependent on ε. Finally, one plugs Eqs. (A.29) and (A.31) in Eq. (A.26) to obtain the linear QG corrected densities of states from Eqs. (3.24) and (3.37) (for $\beta = 0$) for non-relativistic and relativistic particles, respectively. Note that also here a perturbative approach was necessary to obtain the linear QG corrected densities of states, where terms of order equal to or higher than $O(\alpha^2)$ were ignored.

A.4 Example of an Alternative Derivation of QG Corrections

Due to the complexity of the approach to obtain the density of states in Ref. [123], only quadratic QG corrections ($\alpha = 0$) for the non-relativistic case are considered in the following. For a particle in a box in standard theory, one can define a dimensionless energy

variable ε^* as

$$\varepsilon^* \equiv n^2 = n_x^2 + n_y^2 + n_z^2 = \frac{2mL^2\varepsilon}{\hbar^2\pi^2} \ . \tag{A.32}$$

To introduce QG corrections in the above, one must solve the quadratic equation, from Eq. (3.23) ($\alpha = 0$) for $n^2 \equiv n_x^2 + n_y^2 + n_z^2$ (see also the non-relativistic case from Eq. (A.27)). The solutions read as

$$n_{1,2}^2 = \frac{L^2}{10\beta\pi^2\hbar^2}\left(-1 \pm \sqrt{1+40\beta m\varepsilon_{\mathbf{n}}}\right) . \tag{A.33}$$

In what follows, only the physically relevant $+$ solution is considered. For the $-$ solution, the right hand side of Eq. (A.33) is negative, and hence n imaginary, whereas it is required that $n_x, n_y, n_z \in \mathbb{Z}$.

The dimensionless energy in standard theory for a gas of N such particles is a sum of single particle dimensionless energies ε^*, given by n_r^2, where $r \in (x, y, z)$, and reads as

$$\sum_{r=1}^{3N} n_r^2 = \frac{2mL^2E}{\hbar^2\pi^2} \equiv E^* \ , \tag{A.34}$$

where $E = \varepsilon_{\mathbf{n}_1} + \varepsilon_{\mathbf{n}_2} + \cdots + \varepsilon_{\mathbf{n}_N}$ is the sum of all single particle energies and $E^* = \varepsilon_1^* + \varepsilon_2^* + \cdots + \varepsilon_N^*$ the sum of all single particle dimensionless energies. One follows the same procedure, using the QG corrected dimensionless energy from Eq. (A.32). It turns out that a perturbative approach is necessary, where a Taylor expansion up to second order $\sqrt{1+x} \approx 1 + x/2 - x^2/8$ is used. The sum from Eq. (A.34) then reads as

$$\sum_{r=1}^{3N} n_r^2 = \frac{2mV^{2/3}E}{\hbar^2\pi^2} - \frac{20\beta m^2 V^{2/3}E_s^2}{\hbar^2\pi^2} = E^* \ , \tag{A.35}$$

where $E_s^2 = \varepsilon_{\mathbf{n}_1}^2 + \varepsilon_{\mathbf{n}_2}^2 + \cdots + \varepsilon_{\mathbf{n}_N}^2$ is the sum of squares of all single particle energies and $V^{2/3} = L^2$. E_s is related to the total energy E through $E^2 = E_s^2 + 2E_m^2 = \varepsilon_{\mathbf{n}_1}^2 + \varepsilon_{\mathbf{n}_2}^2 + \cdots + \varepsilon_{\mathbf{n}_N}^2 + 2\varepsilon_{\mathbf{n}_1}\varepsilon_{\mathbf{n}_2} + 2\varepsilon_{\mathbf{n}_1}\varepsilon_{\mathbf{n}_3} + \cdots + 2\varepsilon_{\mathbf{n}_2}\varepsilon_{\mathbf{n}_3}\cdots$, where E_m^2 is the sum of all mixed terms.

To compute the number of microstates up to some arbitrary energy, one makes use of the formula for a volume of a d-dimensional sphere

$$V_d(R) = \frac{\pi^{d/2}}{\Gamma\left(\frac{d}{2}+1\right)} R^d \ , \tag{A.36}$$

and applies it to E^* space. One considers $n^2 \geq 0$, so just the upper half of a sphere remains. Each degree of freedom of each particle (spatial degrees of freedom have been already integrated out in V), contributes one dimension in the dimensionless energy phase space. Therefore, $d = 3N$ and $R = \sqrt{E^*}$, and the number of microstates turns out as

$$\Sigma_N(E^*) = \left(\frac{1}{2}\right)^{3N} \left[\frac{\pi^{\frac{3N}{2}}}{\Gamma\left(\frac{3N}{2}+1\right)} E^{*\frac{3N}{2}}\right] \ . \tag{A.37}$$

One then plugs Eq. (A.35) in the above to obtain

$$\Sigma(N,V,E) = \left(\frac{1}{2}\right)^{3N} \left[\frac{\pi^{\frac{3N}{2}}}{\Gamma\left(\frac{3N}{2}+1\right)} \left(\frac{2mV^{2/3}E}{\hbar^2\pi^2} - \frac{20\beta m^2 V^{2/3} E_s^2}{\hbar^2\pi^2} \right)^{\frac{3N}{2}} \right] . \tag{A.38}$$

The number of microstates in a spherical shell of thickness Δ is obtained as

$$\begin{aligned} \Gamma(N,V,E;\Delta) &= \frac{\partial\Sigma(N,V,E)}{\partial E}\Delta \\ &= \frac{\Delta}{E} \frac{\pi^{\frac{3N}{2}}}{\left(\frac{3N}{2}-1\right)!} \frac{V^N}{2^{3N}\pi^{3N}\hbar^{3N}} \\ &\quad \times \left[2mE - 20\beta m^2 \left(E^2 - 2E_m^2\right) \right]^{\frac{3N}{2}} \frac{1 - 20\beta m\left(E - 2E_m \frac{\partial E_m}{\partial E}\right)}{1 - 10\beta m\left(E - 2\frac{E_m^2}{E}\right)} . \end{aligned} \tag{A.39}$$

On the other hand, one can obtain the number of microstates in an energy shell with thickness Δ, by using the phase space integral $\Gamma(N,V,E) = \omega/\omega_0$, where ω_0 is the normalization of the phase space, which is of main interest of this consideration, and

$$\begin{aligned} \omega &= \int \mathrm{d}^{3N}x \int \mathrm{d}^{3N}p = V^N \int_{2m\left(E-\frac{1}{2}\Delta\right) \le \sum_{i=1}^{3N} y_i^2 \le 2m\left(E+\frac{1}{2}\Delta\right)} \cdots \int \mathrm{d}^{3N}y \\ &= V^N \frac{\Delta}{E} \frac{(2\pi mE)^{\frac{3N}{2}}}{\left(\frac{3N}{2}-1\right)!} = \Gamma(N,V,E)\,\omega_0 . \end{aligned} \tag{A.40}$$

One then compares Eqs. (A.39) and (A.40) to obtain

$$\omega_0 = \frac{(2\pi\hbar)^{3N}}{\left[1 - 10\beta m\left(E - 2\frac{E_m^2}{E}\right)\right]^{\frac{3N}{2}-1} \left[1 - 20\beta m\left(E - 2E_m\frac{\partial E_m}{\partial E}\right)\right]} , \tag{A.41}$$

which is valid for an arbitrary number of particles N. In the thermodynamic limit, where $N \longrightarrow \infty$, Eq. (A.41) reduces to $\omega_0 = (2\pi\hbar)^{3N}$. In the case of a BEC, the relevant case is $N = 1$, where

$$\omega_0 = \frac{(2\pi\hbar)^3}{1 - 25\beta m\varepsilon} , \tag{A.42}$$

where ε is again a single particle energy. It turns out that $\Gamma(N=1,V,\varepsilon) = g(\varepsilon)$ Note that the density of states, derived using the modified normalization of the phase space integral, is identical to that, obtained by using the method in Appendix A.3 for quadratic GUP.

Appendix B

21-cm Cosmology

B.1 Standard Theory

In this Appendix, the main features of the 21-cm cosmology are briefly reviewed. First, note that the 21-cm line is associated with the relative orientation of electron and proton spins (anti-parallel for the singlet level with lower energy $E_{\uparrow\downarrow}$ and parallel for the triplet level with higher energy $E_{\uparrow\uparrow}$). This gives rise to a hyperfine energy splitting between the two energy levels of the $1S$ ground state of the hydrogen atom. The corresponding energy gap $E_{21} \equiv E_{\uparrow\uparrow} - E_{\uparrow\downarrow}$ is measured at $E_{21} = 5.87\,\mu\text{eV}$, that of the absorbed or emitted photons in consideration, which corresponds to a wavelength $\lambda_{21}^{rest} = 21\,\text{cm}$, or frequency $\nu_{21}^{rest} = 1420\,\text{MHz}$. Due to this 21-cm transition, neutral hydrogen after the epoch of recombination, with redshift $z \lesssim z_{rec}$, can act as a detector of the background photons that have been produced at higher redshifts. In the ΛCDM model, such a photon background is produced by thermal radiation of the CMB, with temperature $T_{CMB}(z) = T_{CMB,0}\,(1+z)$, where $T_{CMB,0} = 2.725\,\text{K} \simeq 2.35 \times 10^{-4}\,\text{eV}/k_B$.

The frequency of the 21-cm transition falls in the Rayleigh-Jeans tail, where the intensity $I_\nu \propto T$, since $E_{21} \ll k_B T_{CMB}(z)$ for $z \lesssim z_{rec}$. To study absorption and emission of light, one can therefore use the integrated radiative transfer equation (in a rest frame) written in terms of temperature [163, 267]

$$T_b(\tau_\nu) = T_S\left(1 - e^{-\tau_\nu}\right) + T_\gamma\, e^{-\tau_\nu}\,, \tag{B.1}$$

where $T_b(\tau_\nu)$ is the observed absolute brightness temperature, T_S the so-called *spin temperature*, defined by the ratio of the atomic population in the excited state n_2 and the ground state state n_1, given by

$$\frac{n_2}{n_1} \equiv \frac{g_2}{g_1}\, e^{-\frac{E_{21}}{k_B T_S}}\,, \tag{B.2}$$

where $g_2/g_1 = 3$ indicates the ratio of the statistical degeneracy factors of the two hydrogen hyperfine levels and τ_ν is the optical depth, defined as [182, 163]

$$\tau_\nu = \int \mathrm{d}s\, \sigma_{21}\left(1 - e^{-\frac{E_{21}}{k_B T_S}}\right)\phi(\nu)\, n_0 \approx \sigma_{21}\left(\frac{h\nu}{k_B T_S}\right)\left(\frac{N_{\text{HI}}}{4}\right)\phi(\nu) \tag{B.3}$$

in the case of a hydrogen cloud. In the above, $\phi(\nu)$ is the line profile, which is, in general, described by a Voigt function, normalized as $\int \phi(\nu)\,\mathrm{d}\nu = 1$, $\mathrm{d}s$ is the line element between

the source and the observer, n_0 is the number density of neutral hydrogen, $N_{\rm HI} = \int \mathrm{d}s\, n_0$ is the column density of neutral hydrogen and σ_{21} is the absorption cross-section for the 21-cm transition. The latter is defined as [182]

$$\sigma_{21} = \frac{3\,c^2 A_{21}}{8\,\pi \nu^2}\ , \tag{B.4}$$

where A_{21} is the Einstein coefficient for spontaneous emission. A relevant quantity in context of the 21-cm cosmology is the brightness temperature, defined as [163, 182, 267]

$$\begin{aligned} T_{21}(z) \equiv \delta T_b(z) &= \frac{T_S(z) - T_\gamma(z)}{1+z}\,(1 - e^{-\tau_\nu}) \simeq \frac{T_S(z) - T_\gamma(z)}{1+z}\,\tau_\nu \\ &\simeq 23\,\mathrm{mK}\,(1+\delta_B)\,x_{HI}(z) \left(\frac{\Omega_B h^2}{0.02}\right) \left(\frac{0.15}{\Omega_m h^2}\right)^{1/2} \left(\frac{1+z}{10}\right)^{1/2} \left[1 - \frac{T_\gamma(z)}{T_S(z)}\right]\ , \end{aligned} \tag{B.5}$$

where $\Omega_B h^2 = 0.02226$ is the baryon abundance, $\Omega_m h^2 = 0.1415$ the matter abundance [268], δ_B the baryon overdensity, x_{HI} the fraction of neutral hydrogen and $T_\gamma(z)$ the effective temperature of the photon background radiation at frequency $\nu_{21}(z) = \nu_{21}^{rest}/(1+z)$. In the ΛCDM model $T_\gamma(z)$ coincides with $T_{CMB}(z)$. The above 21-cm brightness temperature $T_{21}(z)$ is expressed relatively to the photon background at redshift z and can therefore be negative as well. The spin temperature T_S is related to the kinetic temperature of the gas T_{gas} as

$$1 - \frac{T_\gamma}{T_S} \simeq \frac{x_c + x_\alpha}{1 + x_c + x_\alpha} \left(1 - \frac{T_\gamma}{T_{\rm gas}}\right)\ . \tag{B.6}$$

In the above, the coefficients x_c and x_α describe the coupling between the hyperfine levels and the gas. They are characterized by the fact, that for $x_c + x_\alpha \gg 1$ (limit of strong coupling), it follows $T_S = T_{\rm gas}$, while for $x_\alpha = x_c = 0$ (no coupling), it follows $T_S = T_\gamma$, which implies that there is no signal.

B.2 MDR Modifications of the Einstein Coefficients

Considering a gas of atoms, MDR modifications of absorption, spontaneous emission, and induced emission are explored. Such processes occur when background radiation with specific frequency passes through the gas. This in turn provides a mechanism to explore MDR modifications of the optical depth τ_ν. In the subsequent considerations, the procedure outlined in Ref. [269] is followed.

If there are N_2 atoms in the higher energy state with E_2, the atoms will spontaneously decay to a lower energy state with E_1 and emit photons with a specific frequency $\nu = (E_2 - E_1)/h$. The transition rate for spontaneous emission is then written as

$$W_{21}^s = A_{21} N_2\ , \tag{B.7}$$

where A_{21} is the Einstein coefficient for spontaneous emission. Note that here 1 and 2 refer to the lower and higher energy states of the atomic transition, respectively, and not as a subscript for 21-cm.

On the other hand, if there are N_1 atoms in the lower energy state, and they are exposed

to radiation, which follows a MDR modified thermal spectrum, given by $\rho_{MDR}(\nu) = \rho(\nu) R$ (see Eq. (4.7)), photons with frequency ν will be absorbed, and a fraction of these atoms will transition to the higher energy state. The transition rate for such induced absorption is

$$W_{12} = B_{12} N_1 \rho(\nu) R \,, \tag{B.8}$$

where B_{12} is the Einstein coefficient for induced absorption and R the MDR modification of the thermal spectrum.

There is also a third possibility. If there are N_2 atoms in the higher energy state, and they are exposed to radiation, which follows a MDR modified thermal spectrum, given by $\rho_{MDR}(\nu)$, photons with ν will induce emission of new photons with the same frequency, originating from the induced transition of a fraction of these atoms to a lower energy state. It turns out that such photons travel in the same direction as the incident radiation. The transition rate for such induced emission is

$$W_{21}^{i} = B_{21} N_2 \rho(\nu) R \,, \tag{B.9}$$

where B_{21} is the Einstein coefficient for induced emission. The total transition rate for emission is the sum of the spontaneous and induced emission transition rates

$$W_{21} = W_{21}^{s} + W_{21}^{i} = N_2 \left(A_{21} + B_{21} \rho(\nu) R\right) \,. \tag{B.10}$$

The principle of detailed balance states that in thermal equilibrium, the emission and absorption rates are equal, i.e., $W_{21} = W_{12}$. Using this, as well as Eqs. (B.2), (4.8) and $E = h\nu$, one obtains the ratio of the Einstein coefficients

$$\frac{A_{21}}{B_{21}} = \frac{8\pi h \nu^3}{c^3} R \,, \tag{B.11}$$

and the ratio of induced absorption and emission coefficients

$$\frac{B_{12}}{B_{21}} = \frac{g_2}{g_1} \,. \tag{B.12}$$

From Eq. (B.11), one can see that while the ratio of the Einstein coefficients is modified, it does not provide explicit information on how the individual coefficients are modified. However, Eqs. (B.7), (B.8) and (B.9) suggest that only the B coefficients are modified by R, and that the A coefficient remains unmodified, since

$$B_{12} \propto B_{21} \propto \frac{1}{R} \quad \text{and} \quad A_{21} \not\propto f(R) \,. \tag{B.13}$$

In the following, it is shown that the absorption cross-section σ_{21} does not depend on R as well. The driving equation to describe absorption and emission of radiation in a gas, is the radiative transfer equation, written in the differential form as

$$\frac{\mathrm{d}I_\nu}{\mathrm{d}s} = -\alpha(\nu) I_\nu \,, \tag{B.14}$$

where $I_\nu = c\,\rho(\nu)\,R = I_{0\nu}\,R$ is the spectral intensity, $I_{0\nu}$ the unmodified spectral intensity and $\alpha(\nu)$ the absorption coefficient. The emission term, expected in Eq. (B.14), is omitted, since only information on absorption is required to obtain σ_{21}. The absorption coefficient $\alpha(\nu)$ is related to the absorption cross-section σ_{21} as

$$\alpha(\nu) = n_1\,\sigma_{21}\,\phi(\nu)\ , \tag{B.15}$$

where n_1 is the number density of atoms in the lower energy state. By plugging $I_\nu = I_{0\nu}\,R$ in Eq. (B.14), one finds that the same radiative transfer equation holds also for $I_{0\nu}$, since $R \neq f(s)$, and reads as

$$\frac{\mathrm{d}I_{0\nu}}{\mathrm{d}s} = -\,\alpha(\nu)\,I_{0\nu}\ . \tag{B.16}$$

The power of the incident beam with frequencies between ν and $\nu + \mathrm{d}\nu$ is absorbed by N_1 atoms, and reads as

$$-\Delta P = h\nu\,W_{12}\,\phi(\nu)\,\mathrm{d}\nu = h\nu\,B_{12}\,N_1\,\rho(\nu)\,R\,\phi(\nu)\,\mathrm{d}\nu\ , \tag{B.17}$$

where $h\nu$ is the energy of the absorbed photon, W_{12} the absorption transition rate, given by Eq. (B.8), and $\phi(\nu)$ the line profile defined in Eq. (B.3). Writing the number of atoms in the ground state as $N_1 = n_1\,A\,\Delta s$ (confined inside a volume $A\,\Delta s$), and the thermal spectrum $\rho(\nu)$ in terms of spectral intensity I_ν, one obtains

$$-\Delta P = \frac{h\nu}{c}\,B_{12}\,n_1\,A\,\Delta s\,I_{0\nu}\,R\,\phi(\nu)\,\mathrm{d}\nu\ . \tag{B.18}$$

By the definition of the spectral intensity, it is known that $\frac{\Delta P}{A\,\mathrm{d}\nu\,\Delta s} \implies \frac{\mathrm{d}I_{0\nu}}{\mathrm{d}s}$. Therefore one can rewrite Eq. (B.18) as

$$\frac{\mathrm{d}I_{0\nu}}{\mathrm{d}s} = -\frac{h\nu}{c}\,n_1\,B_{12}\,R\,\phi(\nu)\,I_{0\nu}\ . \tag{B.19}$$

Comparing the above equation with Eqs. (B.16) and (B.15), one obtains the absorption cross-section, which reads as

$$\sigma_{21} = \frac{h\nu}{c}\,B_{12}\,R\ . \tag{B.20}$$

By using Eqs. (B.12) and (B.11) in the above, one can see that the factor R cancels, and the final expression for the absorption cross-section reads as

$$\sigma_{21} = \frac{3\,c^2\,A_{21}}{8\,\pi\,\nu^2}\ , \tag{B.21}$$

which is identical to Eq. (B.4). One can see that the above absorption cross-section does not depend on R and therefore, MDRs do not modify the optical depth τ_ν.

Appendix C

Friedmann Equations

C.1 Derivation

In the following, a detailed derivation of the Friedmann equations is provided, and follows the steps from Ref. [125]. The main assumptions of the holographic principle are that the entropy of the apparent horizon is that, given by Eq. (4.29), while the temperature of the apparent horizon is given by [270, 271]

$$T = \frac{\kappa \hbar c}{2\pi k_B} \,, \tag{C.1}$$

where $\kappa = (1/2\sqrt{-h})\,\partial_c(\sqrt{-h}\,h^{cd}\,\partial_b\tilde{r}) = -(1/\tilde{r}_A)(1-(\dot{\tilde{r}}_A/2H\,\tilde{r}_A))$ is the surface gravity of the apparent horizon, $h = \det(h^{cd})$ and $\tilde{r}_A$ the radius of the apparent horizon. The location of the apparent horizon is obtained from $h^{cd}\,\partial_c\tilde{r}\,\partial_d\tilde{r} = 0$, and reads as [270]

$$\tilde{r}_A = \frac{c}{\sqrt{H^2 + \frac{kc^2}{a^2}}} \,, \tag{C.2}$$

where $H = \dot{a}/a$ is the Hubble parameter. As usual, one assumes that the matter in the Universe is a perfect fluid, and is described by the energy-momentum tensor, which reads as

$$T_{\mu\nu} = \left(\rho + \frac{p}{c^2}\right) u_\mu u_\nu + p\, g_{\mu\nu} \,, \tag{C.3}$$

where u_μ is the four velocity, ρ the matter density, p the pressure and $g_{\mu\nu}$ the space-time metric of the $(n+1)$-dimensional FLRW model (see Eq. (4.33)). The energy conservation law, i.e., $T^{\mu\nu}_{\ ;\nu} = 0$, for a perfect fluid gives rise to the continuity equation

$$\dot{\rho} + nH\left(\rho + \frac{p}{c^2}\right) = 0 \,. \tag{C.4}$$

The Friedmann equations, in context of the holographic principle, are obtained by considering the first law of thermodynamics for the matter content inside the apparent horizon, which reads as

$$\mathrm{d}E = T\mathrm{d}S + W\mathrm{d}V \,, \tag{C.5}$$

where E is the total energy inside the apparent horizon, given by $E = \rho c^2 V$ (here, V is the volume of an n-dimensional sphere, given by $V = \Omega_n \tilde{r}_A^n$, with $\Omega_n = \pi^{n/2}/\Gamma(n/2+1)$ and an area $A = n\Omega_n \tilde{r}_A^{n-1}$) and W the work density, defined as [272]

$$W = -\frac{c^2}{2} T^{cd} h_{cd} = \frac{1}{2}\left(\rho c^2 - p\right) . \tag{C.6}$$

Given the above information, one can obtain the first Friedmann equation, by explicitly writing all the terms from Eq. (C.5). Using Eq. (C.4), one can write the energy differential as

$$\mathrm{d}E = n\Omega_n \tilde{r}_A^{n-1} \rho c^2 \,\mathrm{d}\tilde{r}_A - n\Omega_n \tilde{r}_A^n (\rho c^2 + p) H \,\mathrm{d}t , \tag{C.7}$$

where $\mathrm{d}V = n\Omega_n \tilde{r}_A^{n-1} \mathrm{d}\tilde{r}_A$ has been used. The second term in Eq. (C.5) can be written using Eqs. (4.30) and (C.1), and reads as

$$T\mathrm{d}S = -\frac{\hbar c}{2\pi k_B \tilde{r}_A}\left(1 - \frac{\dot{\tilde{r}}_A}{2H\tilde{r}_A}\right)\frac{k_B c^3 f'(A)}{4\hbar G} n(n-1)\Omega_n \tilde{r}_A^{n-2}\,\mathrm{d}\tilde{r}_A . \tag{C.8}$$

Finally, the third term in Eq. (C.5) can be written using Eq. (C.6), and reads as

$$W\mathrm{d}V = \frac{1}{2} n\Omega_n \tilde{r}_A^{n-1}(\rho c^2 - p)\,\mathrm{d}\tilde{r}_A . \tag{C.9}$$

By plugging Eqs. (C.7), (C.8) and (C.9) in Eq. (C.5), one obtains the first Friedmann equation, which reads as

$$-\frac{8\pi G}{n-1}\left(\rho + \frac{p}{c^2}\right) = \left(\dot{H} - \frac{kc^2}{a^2}\right) f'(A) . \tag{C.10}$$

To correctly derive the above Friedmann equation, one must consider $\dot{\tilde{r}}_A = 0$, since the apparent horizon radius is assumed to be fixed in an infinitesimal time interval, which constrains the possible equation of state to $p \simeq -\rho c^2$. This must also be taken into account for terms including $(\rho c^2 - p)$. By integrating the first Friedmann equation, given by Eq. (C.10), while using the continuity equation, as given in Eq. (C.4), one obtains the second Friedmann equation, which reads as

$$-\frac{8\pi G}{n(n-1)}\rho = \frac{c^2 (n\Omega_n)^{\frac{n+1}{n-1}}}{n(n-1)\Omega_n}\int f'(A)\frac{\mathrm{d}A}{A^{\frac{n+1}{n-1}}} . \tag{C.11}$$

The Friedmann equations, obtained in Eqs. (C.10) and (C.11), are presented in the main text as Eqs. (4.34) and (4.35).

After plugging $f'(A)$ from Eq. (4.31) in Eqs. (C.10) and (C.11) for $n = 3$ spatial dimensions, one obtains the QG modified Friedmann equations, which read as

$$-4\pi G\left(\rho + \frac{p}{c^2}\right) = \left(\dot{H} - \frac{kc^2}{a^2}\right)\frac{\beta^*}{2}\frac{1}{A + \alpha^* A^{1/2} - \sqrt{A^2 + 2\alpha^* A^{3/2} + (\alpha^{*2} - \beta^*)A}} \tag{C.12}$$

and

$$\begin{aligned}\frac{8\pi G}{3}\rho &= -4\pi c^2 \int \frac{\beta^*}{2A^2}\frac{\mathrm{d}A}{\left(A+\alpha^* A^{1/2}-\sqrt{A^2+2\alpha^* A^{3/2}+(\alpha^{*2}-\beta^*)A}\right)} \\ &= 2\pi c^2\Bigg[\frac{1}{A}+\alpha^*\frac{2}{3}\frac{1}{A^{3/2}}+\Bigg(\frac{2}{3}\frac{1}{A}+\frac{\alpha^*}{3(\alpha^{*2}-\beta^*)}\frac{1}{A^{1/2}}-\underbrace{\frac{3\alpha^{*2}-2(\alpha^{*2}-\beta^*)}{3(\alpha^{*2}-\beta^*)^2}}_{\frac{\alpha^{*2}+2\beta^*}{3(\alpha^{*2}-\beta^*)^2}}\Bigg) \\ &\qquad\times\sqrt{1+2\alpha^*\frac{1}{A^{1/2}}+(\alpha^{*2}-\beta^*)\frac{1}{A}} \\ &\quad+\frac{\alpha^*\beta^*}{(\alpha^{*2}-\beta^*)^{5/2}}\ln\Bigg(\alpha^*+(\alpha^{*2}-\beta^*)\frac{1}{A^{1/2}} \\ &\qquad+\sqrt{\alpha^{*2}-\beta^*}\sqrt{1+2\alpha^*\frac{1}{A^{1/2}}+(\alpha^{*2}-\beta^*)\frac{1}{A}}\Bigg)\Bigg] \\ &\quad+C\,,\end{aligned} \tag{C.13}$$

where C is an integration constant. C is determined by considering the boundary conditions in the vacuum energy (dark energy) dominated era, where the energy density goes to $\rho = \rho_{vac} = \Lambda$, as the area of the apparent horizon of the universe goes to $A \longrightarrow \infty$, and reads as

$$C = \frac{8\pi G}{3}\Lambda + 2\pi c^2\left[\frac{\alpha^{*2}+2\beta^*}{3(\alpha^{*2}-\beta^*)^2}-\frac{\alpha^*\beta^*}{(\alpha^{*2}-\beta^*)^{5/2}}\ln\left(\alpha^*+\sqrt{\alpha^{*2}-\beta^*}\right)\right]\,. \tag{C.14}$$

C.2 Classical Limit

In the following, the limit for vanishing GUP parameters, i.e., $\alpha^*, \beta^* \longrightarrow 0$ is considered, in order to verify if the standard Friedmann equations can be obtained. For this, one takes the truncated (for $x \ll 1$) Taylor expansions $\sqrt{1+x} \approx 1 + x/2 - x^2/8$ and $\ln(1+x) \approx x - x^2/2$, i.e., up to second order, as required. By second order, one means of course that all terms up to those $\propto \alpha^{*2}$ and $\propto \beta^*$ are retained and higher order terms are ignored. Here, both GUP parameters are considered small simultaneously, as they are proportional to Planck length and its square respectively, and therefore in the limit $\ell_P \longrightarrow 0$, which is required to obtain standard results, they both approach zero concurrently. In this limit, the first QG modified Friedmann equation from Eq. (4.36) reduces to

$$\begin{aligned}&-4\pi G\left(\rho+\frac{p}{c^2}\right) \approx \left(\dot{H}-\frac{kc^2}{a^2}\right) \\ &\times\frac{\beta^*}{8\pi c^2}\frac{\left(H^2+\frac{kc^2}{a^2}\right)}{\cancel{1}+\frac{\alpha^*}{(4\pi)^{1/2}c}\left(H^2+\frac{kc^2}{a^2}\right)^{1/2}-\cancel{1}-\frac{\alpha^*}{(4\pi)^{1/2}c}\left(H^2+\frac{kc^2}{a^2}\right)^{1/2}-\frac{\cancel{(\alpha^{*2}}-\beta^*)}{8\pi c^2}\left(H^2+\frac{kc^2}{a^2}\right)}\cdots\end{aligned}$$

$$\cdots \cancel{+\frac{\alpha^{*2}}{8\pi c^2}\left(H^2+\frac{kc^2}{a^2}\right)} + O(\alpha^{*3},\beta^{*2})$$

$$= \left(\dot{H}-\frac{kc^2}{a^2}\right)\frac{\cancel{\beta^*}}{\cancel{8\pi c^2}}\frac{\cancel{8\pi c^2}}{\cancel{\beta^*}}\frac{\cancel{\left(H^2+\frac{kc^2}{a^2}\right)}}{\cancel{\left(H^2+\frac{kc^2}{a^2}\right)}} = \dot{H}-\frac{kc^2}{a^2}\,, \tag{C.15}$$

while the second GUP-modified Friedmann equation from Eq. (4.37) reduces to

$$\begin{aligned}
\frac{8\pi G}{3}(\rho-\Lambda) \approx{}& \frac{1}{2}\left(H^2+\frac{kc^2}{a^2}\right)+\frac{\alpha^*}{3(4\pi)^{1/2}c}\left(H^2+\frac{kc^2}{a^2}\right)^{3/2}+\frac{2\pi c^2(\alpha^{*2}+2\beta^*)}{3(\alpha^{*2}-\beta^*)^2}\\
&+\left[\frac{1}{3}\left(H^2+\frac{kc^2}{a^2}\right)+\frac{(4\pi)^{1/2}c\,\alpha^*}{6(\alpha^{*2}-\beta^*)}\left(H^2+\frac{kc^2}{a^2}\right)^{1/2}-\frac{2\pi c^2(\alpha^{*2}+2\beta^*)}{3(\alpha^{*2}-\beta^*)^2}\right]\\
&\quad\times\left(1+\frac{\alpha^*}{(4\pi)^{1/2}c}\left(H^2+\frac{kc^2}{a^2}\right)^{1/2}+\frac{(\alpha^{*2}-\beta^*)}{8\pi c^2}\left(H^2+\frac{kc^2}{a^2}\right)\right.\\
&\quad\left.-\frac{\alpha^{*2}}{8\pi c^2}\left(H^2+\frac{kc^2}{a^2}\right)+O(\alpha^{*3},\beta^{*2})\right)\\
&+\frac{2\pi c^2\alpha^*\beta^*}{(\alpha^{*2}-\beta^*)^{5/2}}\left[\frac{(\alpha^{*2}-\beta^*)}{(4\pi)^{1/2}c\,(\alpha^*+\sqrt{\alpha^{*2}-\beta^*})}\left(H^2+\frac{kc^2}{a^2}\right)^{1/2}\right.\\
&\quad+\frac{\sqrt{\alpha^{*2}-\beta^*}}{\alpha^*+\sqrt{\alpha^{*2}-\beta^*}}\left(\frac{\alpha^*}{(4\pi)^{1/2}c}\left(H^2+\frac{kc^2}{a^2}\right)^{1/2}\right.\\
&\quad\left.\left.+\frac{(\alpha^{*2}-\beta^*)}{8\pi c^2}\left(H^2+\frac{kc^2}{a^2}\right)-\frac{\alpha^{*2}}{8\pi c^2}\left(H^2+\frac{kc^2}{a^2}\right)+O(\alpha^{*3},\beta^{*2})\right)\right.\\
&\quad\left.-\frac{2(\alpha^{*2}-\beta^*)^{3/2}\alpha^*+2\alpha^{*4}-3\alpha^{*2}\beta^*+\beta^{*2}}{8\pi c^2(2\alpha^{*2}+2\alpha^*\sqrt{\alpha^{*2}-\beta^*}-\beta^*)}\left(H^2+\frac{kc^2}{a^2}\right)\right.\\
&\quad\left.+O(\alpha^{*3},\beta^{*2})\right]\\
={}&\cancel{\frac{2\pi c^2(\alpha^{*2}+2\beta^*)}{3(\alpha^{*2}-\beta^*)^2}}-\cancel{\frac{2\pi c^2(\alpha^{*2}+2\beta^*)}{3(\alpha^{*2}-\beta^*)^2}}\\
&+\pi^{1/2}\left[\frac{\cancel{(\alpha^{*3}-\alpha^*\beta^*)\left(\alpha^*+\sqrt{\alpha^{*2}-\beta^*}\right)}}{3(\alpha^{*2}-\beta^*)^2\left(\alpha^*+\sqrt{\alpha^{*2}-\beta^2}\right)}\cdots\right.\\
&\qquad\left.\cdots\frac{-\cancel{(\alpha^{*3}-\alpha^*\beta^*)\left(\alpha^*+\sqrt{\alpha^{*2}-\beta^*}\right)}}{}\right]\left(H^2+\frac{kc^2}{a^2}\right)^{1/2}
\end{aligned}$$

$$
\begin{aligned}
&+\left[\frac{5}{6}+\frac{\cancel{\left(\alpha^{*2}-\beta^{*}\right)^{5/2}\left(2\alpha^{*2}+2\alpha^{*}\sqrt{\alpha^{*2}-\beta^{*}}-\beta^{*}\right)}}{6\cancel{\left(\alpha^{*2}-\beta^{*}\right)^{5/2}\left(2\alpha^{*2}+2\alpha^{*}\sqrt{\alpha^{*2}-\beta^{*}}-\beta^{*}\right)}}\right]\left(H^{2}+\frac{kc^{2}}{a^{2}}\right)\\
&+O(\alpha^{*},\beta^{*})\\
&\approx H^{2}+\frac{kc^{2}}{a^{2}}\,. \qquad \text{(C.16)}
\end{aligned}
$$

One arrives to the last line in the above, after some straightforward but tedious algebra. To obtain first order GUP corrections in α^{*} and β^{*} to the Friedmann equations, one must use the Taylor expansion up to fourth order to gather all required terms.

Appendix D

Quantum Equivalence Principle

D.1 Details on Particle Statistics

In the following, a derivation of the Klein-Gordon equation in curved space-time, from the effective Hamiltonian for bosons in curved space-time in the Feshbach-Villars formalism (see Eq. (5.1)), is presented. The eigenstates of this Hamiltonian are represented by a pair of scalar functions φ and χ as

$$\Psi = \begin{bmatrix} \varphi \\ \chi \end{bmatrix} . \tag{D.1}$$

The Hamiltonian from Eq. (5.1) and the above wave function satisfy a Schrödinger-like equation

$$H\Psi = i\hbar\,\partial_0\Psi . \tag{D.2}$$

In the above, the partial derivative with respect to time is identical to the covariant derivative, i.e., $\partial_0\Psi = \nabla_0\Psi$, since Ψ consists of scalar functions. This identity is taken into account in the following steps.

The Klein-Gordon field in this formalism is defined as $\Phi = \varphi + \chi$. To see that the above formalism indeed represents the Klein-Gordon equation in curved space-time, one plugs Eqs. (5.1) and (D.1) in Eq. (D.2), in order to obtain two coupled differential equations, which read as

$$g^{ij}\frac{\hbar^2\nabla_i\nabla_j}{2m}\Phi + g^{0i}\frac{\hbar^2\nabla_0\nabla_i}{mc}\Phi + mc^2\varphi = i\hbar\sqrt{g^{00}}\,\nabla_0\varphi , \tag{D.3}$$

and

$$-g^{ij}\frac{\hbar^2\nabla_i\nabla_j}{2m}\Phi - g^{0i}\frac{\hbar^2\nabla_0\nabla_i}{mc}\Phi - mc^2\chi = i\hbar\sqrt{g^{00}}\,\nabla_0\chi . \tag{D.4}$$

The above pair of equations represent a coupled system of equations for φ and χ. However, it is required to obtain the equation of motion for Φ, since it is defined as the Klein-Gordon field. To achieve this, Eqs. (D.3) and (D.4) can be used to obtain additional relations between φ and χ. Eqs. (D.3) and (D.4) may then be added together and derived over time

to obtain a useful identity, which reads as

$$m c^2(\varphi-\chi) = i\hbar\sqrt{g^{00}}\,\nabla_0\Phi \quad\longrightarrow\quad m c^2(\nabla_0\varphi-\nabla_0\chi) = i\hbar\sqrt{g^{00}}\,\nabla_0\nabla_0\Phi\,. \tag{D.5}$$

In the above, the identity $\nabla_\alpha\, g^{\mu\nu}=0$ has been used. Furthermore, subtracting Eq.(D.4) from (D.3), one obtains another useful identity, which reads as

$$g^{ij}\,\frac{\hbar^2\nabla_i\nabla_j}{m}\,\Phi + 2\,g^{0i}\,\frac{\hbar^2\nabla_0\nabla_i}{mc}\,\Phi + m c^2\,\Phi = i\hbar\sqrt{g^{00}}\,(\nabla_0\varphi-\nabla_0\chi)\,. \tag{D.6}$$

By plugging Eq. (D.5) in Eq. (D.6) and after a bit of algebraic manipulation, one obtains the Klein-Gordon equation in curved space-time as [4]

$$\left(g^{\mu\nu}\,\nabla_\mu\nabla_\nu + \frac{m^2c^2}{\hbar^2}\right)\Phi = 0\,. \tag{D.7}$$

As expected, in the non-relativistic limit and in flat space-time, the standard quantum mechanical results are obtained. This shows that Eq. (5.1) is indeed the right Hamiltonian for a bosonic particle in an arbitrary curved space-time.

By identifying masses m_α in the Hamiltonian from Eq. (5.1), and following the above procedure, one obtains a modified Klein-Gordon equation in curved space-time, which reads as

$$\left(g^{\mu\nu}(m_\alpha)\,\tilde{\nabla}_\mu\tilde{\nabla}_\nu + \frac{m_R^2c^2}{\hbar^2}\right)\Phi = 0\,, \tag{D.8}$$

where $\tilde{\nabla}_\mu = ((1/c)\,\nabla_0,\,\sqrt{m_R/m_I}\,\boldsymbol{\nabla})$, which is consistent with the quantum version of Eq. (D.14), when multiplied by $i\hbar$.

The Hamiltonian from Eq. (5.2) satisfies the Schrödinger-like equation

$$H\Psi = i\hbar\,\partial_0\Psi\,, \tag{D.9}$$

where Ψ is the Dirac spinor wave function for fermions in this case. By plugging Eq. (5.2) in the above, multiplying both sides by $\underline{\gamma}^0$ and using $\underline{\gamma}^0\underline{\gamma}^0 = g^{00}$ from Eq. (5.4), after a bit of algebraic manipulation, one obtains the Dirac equation in curved space-time, which reads as [5]

$$\left(i\hbar\underline{\gamma}^\mu D_\mu - mc\right)\Psi = 0\,. \tag{D.10}$$

It again follows that in the non-relativistic limit and in flat space-time, the standard quantum mechanical results are obtained.

By identifying masses m_α in the Hamiltonian from Eq. (5.2), and following the above procedure, one obtains a modified Dirac equation in curved space-time, which reads as

$$\left(i\hbar\underline{\gamma}^\mu \tilde{D}_\mu - m_R c\right)\Psi = 0\,, \tag{D.11}$$

where $\tilde{D}_\mu = ((1/c)\,D_0,\, \sqrt{m_R/m_I}\,\boldsymbol{D})$.

The above demonstrates that both the Klein-Gordon and the Dirac equations, relevant for spin 0 and spin $1/2$ particles, respectively, can be written as effective Hamiltonians for Schrödinger-like equations.

D.2 Modification of Special Relativity

One first considers the relativistic dispersion relation and its non-relativistic limit. From the non-relativistic limit of the energy-momentum dispersion relation one finds

$$E = \sqrt{p^2 c^2 + m^2 c^4} \approx m c^2 + \frac{p^2}{2m} \quad \longrightarrow \quad m_R c^2 + \frac{p^2}{2 m_I} \,, \tag{D.12}$$

where one identifies the m_I and m_R as seen in Ref. [238]. One can trace back the steps, and in a straightforward manner identify where masses m_α enter the standard relativistic energy-momentum dispersion relation, which then reads as

$$E^2 = \frac{m_R}{m_I}\, p^2 c^2 + m_R^2 c^4 \,. \tag{D.13}$$

Note that the form of Eq. (D.13) is necessary to obtain the non-relativistic limit of Eq. (D.12). Since there is no corresponding non-relativistic relation for massless particles, there is no equivalent of Eq. (D.13) for photons. Therefore, the issues related to the equivalence principle and its quantum counterpart do not apply to massless particles. To satisfy Eq. (D.13) and the Lorentz scalar for the four-momenta $p^\mu p_\mu = m_R^2 c^2$, the four-momentum must take the form of

$$p^\mu = \left(\frac{E}{c}, \sqrt{\frac{m_R}{m_I}}\, \mathbf{p} \right) \,, \tag{D.14}$$

where $\mathbf{p} = m_I\, \mathbf{v}\, \gamma$ is the relativistic momentum, γ the Lorentz factor and $E = m_R c^2 \gamma$ the relativistic energy of a particle, equivalent to Eq. (D.13). By using the definitions of E and $\mathbf{p}$ containing the Lorentz factor γ, and plugging them in the Lorentz scalar product for four-momenta $p^\mu p_\mu = m_R^2 c^2$, one can immediately see that the Lorentz factor γ also contains a ratio of inertial and rest masses, and reads as

$$\gamma = \frac{1}{\sqrt{1 - \frac{m_I}{m_R}\frac{v^2}{c^2}}} \,. \tag{D.15}$$

The above modified Lorentz factor can be interpreted in terms of a modification to the time dilation and length contraction of a relativistic particle, and implies the modified Lorentz boost transformation from Eq. (5.10).

To define the four-velocity, one can write the four-momentum from Eq. (D.14) in terms

of the four-velocity as

$$p^\mu = \sqrt{m_R m_I}\, c \left(\sqrt{\frac{m_R}{m_I}}\, \gamma, \frac{\mathbf{v}}{c}\gamma \right) = \sqrt{m_R m_I}\, c \left(\frac{1}{c}\frac{c\,\mathrm{d}t}{\mathrm{d}\tau}, \sqrt{\frac{m_I}{m_R}}\frac{1}{c}\frac{\mathrm{d}\mathbf{x}}{\mathrm{d}\tau} \right) = \sqrt{m_R m_I}\, c\, u^\mu \,, \tag{D.16}$$

where τ represents the proper time. In the above, factoring out the masses appears as such that $u^\mu u_\mu = m_R/m_I$ is satisfied. From the above, one can read out the zeroth component of the four-velocity as

$$\frac{1}{c}\frac{c\,\mathrm{d}t}{\mathrm{d}\tau} = \sqrt{\frac{m_R}{m_I}}\,\gamma \quad \Longrightarrow \quad \left(\frac{c\,\mathrm{d}t}{\mathrm{d}\tau}\right)^2 = \frac{m_R}{m_I}c^2\gamma^2 \,. \tag{D.17}$$

Using the modified Lorentz transformation from Eq. (5.10) with the four-velocity defined above, for a particle moving in the x-direction, one finds the composition law for velocities

$$v' = \frac{v_0 - v}{1 - \frac{m_I}{m_R}\frac{v_0 v}{c^2}} \,, \tag{D.18}$$

where v_0 is the particle velocity in the initial inertial frame, v is the velocity of the boosted inertial frame and v' is the particle velocity as measured in the boosted inertial frame.

D.3 Weak Gravitational Field and the Schwarzschild Metric

In the following, the formulation of the equivalence principle is generalized to curved space-times, using masses m_α. In GR, the motion of a particle in a background space-time is described by the geodesic equation [253]

$$\frac{\mathrm{d}^2 x^\mu}{\mathrm{d}\tau^2} + \Gamma^\mu_{\rho\sigma}\frac{\mathrm{d}x^\rho}{\mathrm{d}\tau}\frac{\mathrm{d}x^\sigma}{\mathrm{d}\tau} = 0 \,. \tag{D.19}$$

In the case of the weak field limit of GR, when $g_{\mu\nu} = \eta_{\mu\nu} + h_{\mu\nu}$ and $|h_{\mu\nu}| \ll 1$, and the Newtonian limit for which $\mathrm{d}x^i/\mathrm{d}\tau \ll c\,\mathrm{d}t/\mathrm{d}\tau$, one has $\Gamma^i_{00} = -\partial_i h_{00}/2$, and the above geodesic equation reduces to

$$\frac{\mathrm{d}^2 x^i}{\mathrm{d}\tau^2} \approx \frac{\mathrm{d}^2 x^i}{\mathrm{d}t^2} = -\frac{1}{2}\,\partial_i h_{00}\left(\frac{c\,\mathrm{d}t}{\mathrm{d}\tau}\right)^2 \,. \tag{D.20}$$

To obtain the modified h_{00}, one must identify masses m_α in $\mathrm{d}^2x^i/\mathrm{d}t^2$ and $c\,\mathrm{d}t/\mathrm{d}\tau$ in the non-relativistic limit. For the former, one considers Newton's second law applied to gravity, with identified m_I and m_G, which reads as

$$m_I\,\mathbf{a} = -m_G \nabla\phi \,, \tag{D.21}$$

where $\mathbf{a}$ is the particle acceleration, ϕ the gravitational potential and $\mathbf{g} = -\nabla\phi$ the gravitational acceleration. The acceleration $\mathbf{a}$ can be rewritten in component form as

$$\frac{\mathrm{d}^2 x^i}{\mathrm{d}t^2} = -\frac{m_G}{m_I}\,\partial_i \phi\ . \tag{D.22}$$

The modified ${}^{c\,\mathrm{d}t}/_{\mathrm{d}\tau}$ factor is given by Eq. (D.17). In the non-relativistic limit $\gamma \approx 1$, since $v^2 \ll c^2$. To evaluate the small deviation (in this case of the 00 component) of the metric from the flat Minkowski space-time, due to a weak gravitational field, one plugs Eqs. (D.17) and (D.22) in Eq. (D.20) to obtain

$$h_{00} = 2\frac{m_G}{m_R}\frac{\phi}{c^2} \quad \Longrightarrow \quad g_{00} = 1 + h_{00} = 1 + 2\frac{m_G}{m_R}\frac{\phi}{c^2}\ . \tag{D.23}$$

One obtains the modifications for other components of the metric by relating them to h_{00}. Because the equations in QEP considerations use a contravariant metric $g^{\mu\nu}$, one must obtain the inverse of $g_{\mu\nu}$. In the case of a diagonal metric, the inverse simply inverts the diagonal elements. Therefore,

$$g^{00} = \frac{1}{g_{00}} = \frac{1}{1 + 2\frac{m_G}{m_R}\frac{\phi}{c^2}} \approx 1 - 2\frac{m_G}{m_R}\frac{\phi}{c^2}\ , \tag{D.24}$$

since $\phi \ll c^2$. These results are then used to obtain the weak field metric in Eq. (5.14). It turns out that every p^2 obtains a factor $1/m_I$ in front (or equivalently, every v^2 obtains a m_I in front), every ϕ obtains a factor m_G in front and every c^2 obtains a factor of m_R in front, which can be used as a rule of thumb to identify masses m_α in equations.

For a strong gravitational field, described by a Schwarzschild space-time, the general solution for a covariant metric, before evaluating the integration constant K, can be written as

$$g_{\mu\nu} = \begin{bmatrix} \left(1 + \frac{K}{r}\right) & 0 & 0 & 0 \\ 0 & -\left(1 + \frac{K}{r}\right)^{-1} & 0 & 0 \\ 0 & 0 & -r^2 & 0 \\ 0 & 0 & 0 & -r^2 \sin^2\theta \end{bmatrix}\ . \tag{D.25}$$

The constant K is obtained in the asymptotic limit, where $r \longrightarrow \infty$ and the gravitational field is weak. This is exactly the weak field metric, considered earlier. Therefore, one can use the result from Eq. (D.23) to compare to the g_{00} component of the above Schwarzschild metric. It follows that

$$K = 2\frac{m_G}{m_R}\frac{\phi}{c^2}\,r = -\frac{m_G}{m_R}\frac{2GM}{c^2}\ . \tag{D.26}$$

The inverse of the metric from Eq. (D.25), using the above constant, exactly corresponds to the modified Schwarzschild metric in Eq. (5.16). Note that in the weak field limit of the geodesic equation from Eq. (D.19) for the above metric, one obtains the second Newton's law from Eq. (D.21).

D.4 Kerr metric

To obtain the additional integration constant L, due to the rotation of the central object, the steps from Ref. [254] are followed. The general form of a covariant Kerr metric, before evaluating constants K and L, can be written as [253]

$$g_{\mu\nu} = \begin{bmatrix} \left(1+\frac{Kr}{\rho^2}\right) & 0 & 0 & -\frac{KLr}{\rho^2}\sin^2\theta \\ 0 & -\frac{\rho^2}{\Delta} & 0 & 0 \\ 0 & 0 & -\rho^2 & 0 \\ -\frac{KLr}{\rho^2}\sin^2\theta & 0 & 0 & -\left(r^2+L^2-\frac{KL^2 r\sin^2\theta}{\rho^2}\right)\sin^2\theta \end{bmatrix}, \tag{D.27}$$

where $\Delta = r^2 + Kr + L^2$ and $\rho^2 = r^2 + L^2\cos^2\theta$. Since the procedure in Ref. [254] uses Cartesian coordinates, it is convenient to write the above metric in Cartesian coordinates as a line element [253]

$$\begin{aligned} \mathrm{d}s^2 = &\left(1+\frac{Kr^3}{r^4+L^2z^2}\right)c^2\,\mathrm{d}t^2 - \left(1-\frac{Kr^3}{(r^4+L^2z^2)(r^2+L^2)^2}(Ly-rx)^2\right)\mathrm{d}x^2 \\ &- \left(1-\frac{Kr^3}{(r^4+L^2z^2)(r^2+L^2)^2}(Lx+ry)^2\right)\mathrm{d}y^2 - \left(1-\frac{Krz^2}{r^4+L^2z^2}\right)\mathrm{d}z^2 \\ &+ \frac{2Kr^3}{(r^4+L^2z^2)(r^2+L^2)}(Ly-rx)\,c\,\mathrm{d}t\,\mathrm{d}x - \frac{2Kr^3}{(r^4+L^2z^2)(r^2+L^2)}(Lx+ry)\,c\,\mathrm{d}t\,\mathrm{d}y \\ &- \frac{2Kr^2z}{r^4+L^2z^2}\,c\,\mathrm{d}t\,\mathrm{d}z - \frac{2Kr^3}{(r^4+L^2z^2)(r^2+L^2)^2}(Ly-rx)(Lx+ry)\,\mathrm{d}x\,\mathrm{d}y \\ &- \frac{2Kr^2z}{(r^4+L^2z^2)(r^2+L^2)}(Ly-rx)\,\mathrm{d}x\,\mathrm{d}z + \frac{2Kr^2z}{(r^4+L^2z^2)(r^2+L^2)}(Lx+ry)\,\mathrm{d}y\,\mathrm{d}z\,, \end{aligned} \tag{D.28}$$

where $x = (r\cos\varphi + L\sin\varphi)\sin\theta$, $y = (r\sin\varphi - L\cos\varphi)\sin\theta$, $z = r\cos\theta$ and $r^4 - r^2(x^2+y^2+z^2-L^2) - L^2z^2 = 0$. Note that the choice of the coordinate system in the above is such that the rotational axis corresponds to the z-axis.

Following the procedure outlined in Ref. [254], one obtains the metric of a rotating object in the asymptotic limit from the weak field Einstein equations (using $g_{\mu\nu} = \eta_{\mu\nu} + h_{\mu\nu}$ with $|h_{\mu\nu}| \ll 1$), which is later compared to the asymptotic limit of the metric in Eq. (D.28), to obtain constants K and L. The weak field Einstein equations turn out as [254]

$$\Box\gamma_{\mu\nu} = -2\kappa\,{}_0T_{\mu\nu}\,, \tag{D.29}$$

where

$$\gamma_{\mu\nu} = h_{\mu\nu} - \frac{1}{2}\eta_{\mu\nu}h\,, \quad h = \eta^{\rho\sigma}h_{\rho\sigma}\,, \tag{D.30}$$

κ is the Einstein constant and ${}_0T_{\mu\nu}$ is the special-relativistic energy-momentum tensor which describes the source of the gravitational field for a weak gravitational field. The Kerr metric is stationary, which means that the temporal derivative in Eq. (D.29) vanishes, and one

obtains

$$\nabla^2 \gamma_{\mu\nu} = 2\kappa \, {}_0T_{\mu\nu} \, . \tag{D.31}$$

The general solution of the above equation reads as [254]

$$\gamma_{\mu\nu}(\mathbf{x}) = -\frac{\kappa}{2\pi} \int \frac{1}{R} \, {}_0T_{\mu\nu}(\mathbf{X}) \, \mathrm{d}^3\mathbf{X} \, , \tag{D.32}$$

where $\mathbf{x}$ is an arbitrary location outside the gravitating object, $\mathbf{X}$ is the location inside the gravitating object, over which the integral is evaluated, and R is the distance between the two locations, defined as

$$R^2 = (x^i - X^i)^2 = r^2 - 2x^i X^i + X^i X^i \, , \tag{D.33}$$

where the Einstein summation rule is applied and $r^2 = x^i x^i$ is the square of the distance of the observer from the central object. Note that in this notation $x^1 = x$, $x^2 = y$, $x^3 = z$, and $X^1 = X$, $X^2 = Y$, $X^3 = Z$. Since all quantities must be evaluated in the asymptotic limit, where $X^i/r \ll 1$, one can write $1/R$ (as given in Eq. (D.32)) as

$$\frac{1}{R} = \frac{1}{\sqrt{r^2 - 2x^i X^i + X^i X^i}} \approx \frac{1}{r} + \frac{x^i X^i}{r^3} \, . \tag{D.34}$$

The energy-momentum tensor of a distribution of matter, also known as a dust distribution, is defined as ${}_0T_{\mu\nu} = \rho \, c^2 \, u_\mu \, u_\nu$, where $u_\mu = \eta_{\mu\nu} \, u^\nu$ is defined in Eq. (D.16). For the case of a rotating body, which rotates around the z-axis in a Cartesian coordinate system, the components of ${}_0T_{\mu\nu}$ turn out as

$$\begin{aligned}
{}_0T_{00} &= \rho \, \frac{m_R}{m_I} \, c^2 \, , \\
{}_0T_{01} &= \rho \sqrt{\frac{m_R}{m_I}} \, c \, v \sin\varphi \equiv \sqrt{\frac{m_R}{m_I}} \, {}^0_0T_{01} \, , \\
{}_0T_{02} &= -\rho \sqrt{\frac{m_R}{m_I}} \, c \, v \cos\varphi \equiv \sqrt{\frac{m_R}{m_I}} \, {}^0_0T_{02} \, ,
\end{aligned} \tag{D.35}$$

where ρ is the matter distribution density, v is the tangential velocity at the equator of the rotating central object, assumed to be small $v \ll c$, and ${}^0_0T_{01}$ and ${}^0_0T_{02}$ are the unmodified tensor components. Note that other tensor components vanish. Using the above energy-momentum tensor and Eq. (D.34), one can write the off-diagonal components of the solution from Eq. (D.32) as

$$\gamma_{01} = -\frac{\kappa}{2\pi} \, \frac{y}{r^3} \int Y \, {}_0T_{01} \, \mathrm{d}^3\mathbf{X} \quad \text{and} \quad \gamma_{02} = -\frac{\kappa}{2\pi} \, \frac{x}{r^3} \int X \, {}_0T_{02} \, \mathrm{d}^3\mathbf{X} \, , \tag{D.36}$$

where the axial symmetry of the system ensures that the $1/r$ terms and terms with other coordinate components vanish. By choosing the z-axis as the axis of rotation, the special

relativistic angular momentum reads

$$J^z = \frac{1}{c}\int \left(X\,{}^0_0T^{02} - Y\,{}^0_0T^{01}\right) \mathrm{d}^3\mathbf{X}\,. \tag{D.37}$$

The axial symmetry of the system also relates the two terms in the above definition as

$$\int X\,{}^0_0T^{02}\,\mathrm{d}^3\mathbf{X} = -\int Y\,{}^0_0T^{01}\,\mathrm{d}^3\mathbf{X} = \frac{c}{2}J^z\,. \tag{D.38}$$

Note that the energy-momentum tensor components in the definition of the angular momentum are contravariant. To make this consistent with the previous steps, it is easy to show the relations with the covariant energy-momentum tensor components ${}^0_0T^{01} = -{}^0_0T_{01}$ and ${}^0_0T^{02} = -{}^0_0T_{02}$. Using these relations, the second and third expressions from Eq. (D.35), and Eq. (D.38), the solutions from Eq. (D.36) turn out as

$$\gamma_{01} = -\frac{\kappa c y}{4\pi r^3}\sqrt{\frac{m_R}{m_I}}\,J^z \quad \text{and} \quad \gamma_{02} = \frac{\kappa c x}{4\pi r^3}\sqrt{\frac{m_R}{m_I}}\,J^z\,. \tag{D.39}$$

What remains is to evaluate is the Einstein constant κ. To do this, one must first consider the first integral of the geodesic equation

$$g_{\mu\nu}\frac{\mathrm{d}x^\mu}{\mathrm{d}s}\frac{\mathrm{d}x^\nu}{\mathrm{d}s} = 1\,, \tag{D.40}$$

where, in this case, $g_{\mu\nu}$ is the exact Kerr solution from Eq. (D.27), for which one wants to evaluate the constants. To obtain constant K, one compares the above result with the Newtonian limit, all terms $(1/r)^2$ and higher in the above expression, are ignored. One considers a geodesic trajectory for a particle orbiting the central object in the $x-y$ plane. After some algebraic manipulation of Eq. (D.40) and differentiating it over φ (see Ref. [254], page 72 for more details), one obtains

$$\frac{\mathrm{d}^2}{\mathrm{d}\varphi^2}\left(\frac{1}{r}\right) + \frac{1}{r} = -\frac{K}{2\ell^2}\,, \tag{D.41}$$

where $\ell \equiv r^2\,\mathrm{d}\varphi/\mathrm{d}s$ is a constant of motion, related to angular momentum, for an orbiting particle. According to Newtonian mechanics, the energy of an orbiting particle is constant for any distance from the central object r, and reads as

$$\frac{m_I\dot{r}^2}{2} - \frac{G m_G M}{r} = \text{const.}\,, \tag{D.42}$$

where one can clearly identify m_I and m_G. Assuming the particle is orbiting the central object in the $x-y$ plane, one can write the particle position vector as $\mathbf{r} = r(\cos\varphi, \sin\varphi)$ and its angular momentum as $\mathbf{J} = \mathbf{r}\times\mathbf{p} = \sqrt{m_R m_I}\,c\,\ell\,\hat{z}$, where $\mathbf{p}$ is the spatial part of Eq. (D.16). Using the above, one can write $\mathbf{J} = I\boldsymbol{\omega} = m_I r^2\,\mathrm{d}\varphi/\mathrm{d}t\,\hat{z}$ and differentiate it with respect

to φ, which turns out as

$$\frac{\mathrm{d}^2}{\mathrm{d}\varphi^2}\left(\frac{1}{r}\right)+\frac{1}{r}=\frac{m_G}{m_R}\frac{GM}{\ell^2 c^2}\,. \tag{D.43}$$

By comparing Eqs. (D.41) and (D.43), one can identify the constant K, which is exactly the same as in the Schwarzschild and weak field cases (see Eq. (D.26)). Note that the angular momentum, used to derive Eq. (D.43) corresponds to the angular momentum of a test particle orbiting the central object and is different from the angular momentum, defined in Eq. (D.37), which corresponds to the rotation of the central object.

To obtain κ, one uses the first expression in Eq. (D.35) with Eq. (D.31), which turns out as

$$\nabla^2\gamma_{00}=2\,\kappa\,\rho\,\frac{m_R}{m_I}c^2\,, \tag{D.44}$$

which corresponds to the Poisson's equation for the Newtonian gravitational potential, which reads as

$$\nabla^2\phi=4\pi G\rho\,. \tag{D.45}$$

Note that the above Poisson's equation does not get modified, since the m_G/m_I ratio would modify it on both sides in the same way, which would then cancel. By comparing the above two equations, one can see that

$$\gamma_{00}=\frac{m_R}{m_I}\frac{\kappa c^2}{2\pi G}\phi\,, \tag{D.46}$$

and by using the inverse relation of Eq. (D.30), the g_{00} component in the weak field approximation turns out as

$$g_{00}=1+\frac{m_R}{m_I}\frac{\kappa c^2}{4\pi G}\phi=1+\frac{K}{r}\,. \tag{D.47}$$

Precisely the same constant K appears in components g_{11}, g_{22} and g_{33} of the weak field approximation in the Cartesian coordinate system. Since the constant K and potential ϕ are known (see Eq. (D.26)), the modified Einstein constant κ can easily be identified as

$$\kappa=\frac{m_G m_I}{m_R^2}\frac{8\pi G}{c^4}\,, \tag{D.48}$$

thus effectively modifying the Einstein equations as

$$R_{\mu\nu}-\frac{1}{2}R\,g_{\mu\nu}=\frac{m_G m_I}{m_R^2}\frac{8\pi G}{c^4}T_{\mu\nu}\,. \tag{D.49}$$

By plugging the modified Einstein constant from Eq. (D.48) in the expressions from

Eq. (D.39) and using Eq. (D.30), one obtains

$$h_{01} = \gamma_{01} = -\frac{m_G m_I^{1/2}}{m_R^{3/2}} \frac{2G}{c^3} \frac{y}{r^3} J^z \quad \text{and} \quad h_{02} = \gamma_{02} = \frac{m_G m_I^{1/2}}{m_R^{3/2}} \frac{2G}{c^3} \frac{x}{r^3} J^z \,. \tag{D.50}$$

At this point one can define the constant $a \equiv J^z/Mc$. Using a and the above information, one can write the line element of the metric of a rotating object as

$$\begin{aligned} \mathrm{d}s^2 = &\left(1 - \frac{m_G}{m_R} \frac{2GM}{c^2 r}\right) c^2 \mathrm{d}t^2 - \left(1 - \frac{m_G}{m_R} \frac{2GM}{c^2}\right) (\mathrm{d}x^2 + \mathrm{d}y^2 + \mathrm{d}z^2) \\ &- \frac{m_G m_I^{1/2}}{m_R^{3/2}} \frac{4GM}{c^2} \frac{y}{r^3} a\, c\, \mathrm{d}t\, \mathrm{d}x + \frac{m_G m_I^{1/2}}{m_R^{3/2}} \frac{4GM}{c^2} \frac{x}{r^3} a\, c\, \mathrm{d}t\, \mathrm{d}y \,. \end{aligned} \tag{D.51}$$

Comparing the above line element with the asymptotic limit of the line element from Eq. (D.28), when $r \longrightarrow \infty$, one can identify the remaining constant L as

$$L = \sqrt{\frac{m_I}{m_R}}\, a \,. \tag{D.52}$$

The obtained constants K and L are then plugged in the metric from Eq. (D.27), which is then inverted to obtain the contravariant Kerr metric as seen in Eq. (5.18).